



**HAL**  
open science

## High impact polypropylene: structure evolution and impact on reaction

Aarón José Cancelas Sanz

► **To cite this version:**

Aarón José Cancelas Sanz. High impact polypropylene: structure evolution and impact on reaction. Chemical engineering. Université de Lyon, 2017. English. NNT : 2017LYSE1210 . tel-01630759

**HAL Id: tel-01630759**

**<https://theses.hal.science/tel-01630759>**

Submitted on 8 Nov 2017

**HAL** is a multi-disciplinary open access archive for the deposit and dissemination of scientific research documents, whether they are published or not. The documents may come from teaching and research institutions in France or abroad, or from public or private research centers.

L'archive ouverte pluridisciplinaire **HAL**, est destinée au dépôt et à la diffusion de documents scientifiques de niveau recherche, publiés ou non, émanant des établissements d'enseignement et de recherche français ou étrangers, des laboratoires publics ou privés.

N°d'ordre NNT : 2017LYSE1210



## **THESE de DOCTORAT DE L'UNIVERSITE DE LYON**

opérée au sein de  
**l'Université Claude Bernard Lyon 1**

**Ecole Doctorale N° ED206**  
**Chimie de Lyon**

**Spécialité de doctorat : Polyolefins Reaction Engineering**  
**Discipline : Chemical Engineering**

Soutenue publiquement le 06/10/2017, par :

**Aarón José**

**CANCELAS SANZ**

---

# **HIGH IMPACT POLYPROPYLENE: STRUCTURE EVOLUTION AND IMPACT ON REACTION**

---

Devant le jury composé de :

Moreno, Jovita Professeure/Universidad Rey Juan Carlos (ESPAÑA)	Rapporteure
Soares, João B. P. Professeur/ Donadeo Innovation Centre for Engineering (CANADA)	Rapporteur
Beyou, Emmanuel Professeur/ Laboratoire IMP (Ingénierie des Matériaux Polymères)	Examineur
Sheibat-Othman, Nida Chargée de Recherches/ Laboratoire d'Automatique et de Génie des Procédés	Examinatrice
Deslman, Erik Staff Scientist/SABIC, Geleen, The Netherlands	Examineur
McKenna, Timothy F.L. Professeur/ Laboratory of Chemistry, Catalysis, Polymers and Process	Directeur Thèse
Monteil, Vincent Professeur/ Laboratory of Chemistry, Catalysis, Polymers and Process	Co-directeur Thèse



# UNIVERSITE CLAUDE BERNARD - LYON 1

## **Président de l'Université**

Président du Conseil Académique

Vice-président du Conseil d'Administration

Vice-président du Conseil Formation et Vie Universitaire

Vice-président de la Commission Recherche

Directrice Générale des Services

**M. le Professeur Frédéric FLEURY**

M. le Professeur Hamda BEN HADID

M. le Professeur Didier REVEL

M. le Professeur Philippe CHEVALIER

M. Fabrice VALLÉE

Mme Dominique MARCHAND

## ***COMPOSANTES SANTE***

Faculté de Médecine Lyon Est – Claude Bernard

Faculté de Médecine et de Maïeutique Lyon Sud – Charles Mérieux

Faculté d'Odontologie

Institut des Sciences Pharmaceutiques et Biologiques

Institut des Sciences et Techniques de la Réadaptation

Département de formation et Centre de Recherche en Biologie Humaine

Directeur : M. le Professeur G.RODE

Directeur : Mme la Professeure C. BURILLON

Directeur : M. le Professeur D. BOURGEOIS

Directeur : Mme la Professeure C. VINCIGUERRA

Directeur : M. X. PERROT

Directeur : Mme la Professeure A-M. SCHOTT

## ***COMPOSANTES ET DEPARTEMENTS DE SCIENCES ET TECHNOLOGIE***

Faculté des Sciences et Technologies

Département Biologie

Département Chimie Biochimie

Département GEP

Département Informatique

Département Mathématiques

Département Mécanique

Département Physique

UFR Sciences et Techniques des Activités Physiques et Sportives

Observatoire des Sciences de l'Univers de Lyon

Polytech Lyon

Ecole Supérieure de Chimie Physique Electronique

Institut Universitaire de Technologie de Lyon 1

Ecole Supérieure du Professorat et de l'Education

Institut de Science Financière et d'Assurances

Directeur : M. F. DE MARCHI

Directeur : M. le Professeur F. THEVENARD

Directeur : Mme C. FELIX

Directeur : M. Hassan HAMMOURI

Directeur : M. le Professeur S. AKKOUCHE

Directeur : M. le Professeur G. TOMANOV

Directeur : M. le Professeur H. BEN HADID

Directeur : M. le Professeur J-C PLENET

Directeur : M. Y.VANPOULLE

Directeur : M. B. GUIDERDONI

Directeur : M. le Professeur E.PERRIN

Directeur : M. G. PIGNAULT

Directeur : M. le Professeur C. VITON

Directeur : M. le Professeur A. MOUGNIOTTE

Directeur : M. N. LEBOISNE





This research forms part of the research programme of DPI, project #785

DPI, P.O. Box 902, 5600 AX Eindhoven, the Netherlands



## Acknowledgements

For all the people who have convoyed me during my PhD in the past four years and have been involved in this work, I want to express my deep gratitude.

First and foremost, I want to thank my main supervisor Prof. Dr. Timothy F. L. McKenna for giving me the fantastic opportunity to work on a fascinating field of research — polyolefins reaction engineering— with his full support. Discussions with him have always been motivating and inspiring, while at the same time filled my head with innovative ideas—after every meeting I rushed to my desk to jot down everything. Thanks for showing me that it was up to me what I've learnt during my PhD.

I want to thank my secondary supervisor Dr. Vincent Monteil for his guidance on my studies. I consider his advices and thorough attention to details of immense importance in my work. Thank you for proving me that good ideas are more important than equipment. Along with Dr. McKenna, I am grateful for their trust in my competence and skills, and letting me learn from them. I consider them the architects of my new way of thinking.

I would like to express my gratitude to Dutch Polymer Institute (DPI) for the financial support of this project. Specially, I would like to thank Dr. Erik Delsman and Dr. Markus Gahleitner, whose invaluable expert opinion in this PhD greatly helped in shaping it. The “HIPSTER” project partners, Prof. Dr. Michael Bartke and Don Miguel A. Plata also deserve some big thanks from me, for their aid with the Sorption Magnetic Balance (SMB) and their hospitality in Halle (Saale). I would also like to thank to Dr. M. Podivinská and Prof. Dr. J. Kosek for more results from their SMB.

This dissertation would not have happened without persistent support of the permanent staff at C2P2, that is Dr. Norsic —Seb—, Mr. Dugas —PY—, Mme. Manel Taam, Mme. Jouglard —Nath—, Mr. Olivier Boyron, Dr. Franck Collas and Dr. Damien Montarnal. I am thankful for their assistances, and for having a lot patience with my French. Knowing that I would use it to talk with you made me learn it faster.

Motivation for this accomplishment also came from other lab colleagues. Namely, Dr. Montree Namkajorn —ขอบคุณ for all the turbosphere secrets—, Dr. M. Ahsan Bashir —شکریہ for transmitting me the pride of being a PO guy—, Ms. Ana R. Martins, Dr. Goond Hongmanee and Mr. Brian Zhong —Thanks for your high interest and motivation—, Ms.

Fabiana N. Andrade —Obrigado for helping with the lab organization— and Dr. Arne Wolpers —Danke for the passion in document formatting—.

I want to thank all the past and present LCPP fellows including Dr. Bárbara Rezende, Dr. Thiago Guimarães, Dr. Thaissa Chaparro, Dr. Bastian Ebeling, Dr. Ming Koh, Dr. Edgar Espinosa, Mr. José Carlos Mendoza, Dr. Ana C. Méndez, Dr. Solmaz Aryafar, Ms. Rita Alves, Ms. Amel Ben-Mrad, Dr. Arthur Zarrouki, Ms. Yashmin Blazzio, Dr. Anderson Medeiros, Dr. Lionel Bosco, Ms. Lucie Griveau and many more for the friendly, supportive, and comfortable atmosphere, which I consider an crucial factor for fruitful research. Special thanks to those who were going with me on every weekend at Flanigan's.

Muchas gracias a Doña Elena Díez López, por su apoyo, atender a mis presentaciones (aunque a veces el sueño venciera), y, en general, *estar siempre ahí*. Soy muy afortunado de poder tenerte, mi sol.

Finalmente quiero agradecer a mi familia — Don José L. Cancelas, Doña M. Julia Sanz, Doña Noemí Cancelas, Don Diego Sánchez, Doña Elara Cancelas, Doña Danae Cancelas, Doña Vega Sanz, Don Marco Cancelas y Don Tomás A. Sanz—por su absoluto apoyo y confianza en mí.

## Abstract

Isotactic Polypropylene (iPP) homopolymers have higher stiffness than polyethylene (PE), but also limited toughness, especially at lower temperatures. This can be overcome by incorporating an elastomeric copolymer of ethylene and propylene directly in the semi-crystalline iPP matrix. Such in situ reactor blends are well-known, and their production requires a multi-step reaction process. Very briefly, an industrial process for high impact polypropylene (hiPP) products involves 2 reaction zones (each zone can be composed of one or more reactors). iPP is made in the first zone, the still active powders are then degassed and sent to a second zone in which an elastomer (usually a copolymer of propylene and ethylene referred to as Ethylene-Propylene Rubber (EPR)) is made. The iPP homopolymer can be produced in the gas phase or slurry phase, whereas the EPR must be made in a gas phase reactor. In the current thesis, our focus was on an “all gas phase” process.

Therefore, the morphology of hiPP will be greatly dependent on that of the intermediate iPP, which in turn, will depend on the precatalyst morphology. However, the same precatalyst can lead to different iPP morphologies, depending on the injection protocol followed. Therefore, catalyst injection is a critical aspect while producing hiPP. Such aspect has been studied by performance of a designed set of propylene polymerization reaction experiments. Commercially available supported Ziegler-Natta (ZN) catalysts along with a lab-scale stirred-bed reactor and a gas phase stopped flow reactor have been used. It is understood why prepolymerization and wetting the catalyst with hydrocarbon before being charged to the reactor ensure high activity and quality morphology while producing iPP.

During the production of hiPP, sorption thermodynamics of the gas phase have a big impact on propylene homopolymerization and copolymerization kinetics. For instance, higher hydrocarbons enhance the propylene solubility in polymer (which is known as “co-solubility” phenomenon) which leads to an activity increase. In addition, the solubility and diffusivity of the different monomers used to produce hiPP (propylene, ethylene and ethylene/propylene mixtures) in the powders depend on the temperatures and pressures which the process is conducted at. Experimental data of these quantities was obtained and semi-empirical models generally used in the polyolefin industry were used to understand their dependence on the process conditions.

Finally, several hiPP powders were made in the lab-scale stirred-bed reactor with a supported ZN catalyst, following the “all gas phase” route. The morphology of the iPP matrix and conditions during copolymerization such as amount of copolymer, temperature, pressure, relative amount of ethylene to propylene and the presence of hydrogen have been systematically varied to comprehend their impact on the rubber distribution among the PP matrix. The aforementioned factor is, in turn, crucial for (1) a correct industrial process operation, and (2) the mechanical properties sought-after in hiPP.

## Résumé

Les homopolymères à base de polypropylène isotactique (iPP en anglais) ont une rigidité plus élevée que le polyéthylène (PE), mais aussi une dureté limitée, en particulier à températures plus basses. Ceci peut être surmonté en incorporant un élastomère copolymère d'éthylène et de propylène directement dans la matrice semi-cristalline de iPP. De tels mélanges obtenus in situ dans des réacteurs successifs sont bien connus, et leur production nécessite un procédé multi-étapes. De façon succincte, un procédé industriel pour la synthèse de PP choc (hiPP, high impact PP en anglais) implique 2 zones de réaction (chaque zone peut être composée d'un ou plusieurs réacteurs). L'iPP est fabriqué dans la première zone. Les poudres encore actives sont ensuite dégazées et envoyées dans une seconde zone dans laquelle est incorporé un élastomère (généralement un copolymère de propylène et d'éthylène appelé caoutchouc éthylène-propylène (ethylene-propylene rubber (EPR) en anglais). L'homopolymère iPP peut être produit en phase gaz ou en suspension (slurry en anglais) dans un hydrocarbure, alors que l'EPR doit être fabriqué dans un réacteur en phase gaz. Dans la thèse actuelle, nous nous sommes concentrés sur les procédés intégralement en phase gaz.

Par conséquent, la morphologie du polypropylène choc (hiPP) dépendra fortement de celle de l'iPP intermédiaire, qui, à son tour, dépendra de la morphologie du précatalyseur. Cependant, le même précatalyseur peut conduire à différentes morphologies d'iPP, selon le protocole d'injection suivi. L'injection de catalyseur est donc un aspect critique de la production du hiPP. Cet aspect a été étudié grâce à la réalisation d'un plan d'expériences de polymérisation du propylène. On a utilisé des catalyseurs supportés Ziegler-Natta (ZN), disponibles commercialement, dans un réacteur à cuve agitée et un réacteur phase gaz à flux stoppé. On a mis en évidence pourquoi la prépolymérisation et le mouillage du catalyseur par un hydrocarbure avant d'être introduits dans le réacteur assurent de hautes activités et un contrôle de la morphologie des particules de polymère tout en produisant l'iPP.

Au cours de la production de l'hiPP, la thermodynamique de sorption de la phase gaz a un impact important sur la cinétique d'homopolymérisation et de copolymérisation du propylène. Par exemple, les hydrocarbures supérieurs améliorent la solubilité du propylène dans le polymère (phénomène de «co-solubilité») ce qui conduit à une augmentation de l'activité. De plus, la solubilité et la diffusivité des différents monomères (et de leurs

mélanges) utilisés pour produire l'hiPP (propylène, éthylène et mélange éthylène / propylène) dans les poudres dépendent des températures et des pressions auxquelles le procédé est conduit. Les données expérimentales de ces quantités ont été obtenues et des modèles semi-empiriques généralement utilisés dans l'industrie des polyoléfinés ont été utilisés pour comprendre leur dépendance à l'égard des conditions du procédé.

Finalement, plusieurs poudres d'hiPP ont été obtenues dans le réacteur à cuve agitée avec un catalyseur ZN supporté, en suivant la voie intégrale phase gaz. La morphologie de la matrice iPP et les conditions de la copolymérisation telles que la quantité de copolymère, la température, la pression, la quantité relative d'éthylène par rapport au propylène et la présence d'hydrogène ont été systématiquement variées pour comprendre leur impact sur la répartition du caoutchouc dans la matrice PP. Ce facteur est, à son tour, crucial pour (1) un fonctionnement du procédé industriel optimal, et (2) les propriétés mécaniques recherchées de l'hiPP.

## Table of Contents: Chapters

1	General Introduction.....	17
1.1	Introduction to Isotactic Polypropylene.....	17
1.2	From iPP to High Impact Polypropylene (hiPP) .....	18
1.3	High Impact Polypropylene Manufacturing Processes.....	19
1.3.1	Gas-Phase Processes.....	20
1.3.2	The importance of powder morphology .....	23
1.4	Thermodynamics of Sorption .....	25
1.4.1	Thermodynamic models to predict solubility in polymer systems.....	25
1.4.2	Mass Transport .....	27
1.5	Outline of this thesis .....	27
1.6	References.....	30
2	Impact of Catalyst Injection Conditions on the Gas Phase Polymerisation of Propylene.....	33
2.1	Introduction.....	33
2.2	Experimental Section.....	36
2.2.1	Chemicals .....	36
2.2.2	Semi-Batch Polymerization.....	37
2.2.3	Gas Phase Stopped-Flow Polymerization .....	39
2.2.4	Polymer Characterization .....	41
2.2.5	Lists of Experiments.....	41
2.2.6	Kinetic Model.....	42
2.3	Results and Discussion .....	43
2.3.1	Comparison of Dry vs Wet Injection in the Gas Phase Polymerization of Propylene.....	43
2.3.2	Comparison of the Influence of Temperature during Slurry and Gas Phase.	

2.4	Conclusions.....	65
2.5	References.....	66
3	Thermodynamics of Sorption in the Gas Phase Polymerization of Propylene.....	71
3.1	The Impact of the Presence of Alkanes and Hydrogen on the Gas Phase Polymerization of Propylene .....	73
3.1.1	Introduction .....	73
3.1.2	Experimental Section.....	74
3.1.3	Results and Discussion .....	79
3.1.4	Conclusions for Objective 1: Impact of alkanes and hydrogen.....	85
3.2	Solubility and Diffusivity of Propylene, Ethylene, and Propylene–Ethylene mixtures in Polypropylene.....	86
3.2.1	Introduction .....	86
3.2.2	Experimental Section.....	88
3.2.3	Results and Discussion .....	94
3.2.4	Conclusions for Objective 2: Sorption .....	111
3.2.5	References .....	112
4	The Effect of Reactor Conditions on High-Impact Polypropylene Properties and Gas Phase Polymerization Kinetics .....	117
4.1	Introduction.....	117
4.2	Experimental Section.....	119
4.2.1	Chemicals .....	119
4.2.2	Semibatch Polymerization.....	119
4.2.3	Polymer Characterization .....	123
4.2.4	List of Experiments .....	127
4.3	Results and Discussion .....	128
4.3.1	Kinetic Profiles .....	128
4.3.2	Polymer Fractionation .....	133
4.3.3	Powder Flowability .....	135

4.3.4	Crystallisable Copolymers of Ethylene and Propylene .....	137
4.3.5	Mechanical Properties .....	142
4.3.6	Powder Morphology with Increasing Copolymer Content.....	145
4.3.7	AFM analyses .....	148
4.4	Conclusions.....	157
4.5	References.....	159
5	Conclusions and Perspectives.....	163
5.1	Conclusions.....	163
5.2	Perspectives .....	166

## **Table of Contents: Appendices**

A.	Sanchez-Lacombe equation of state (SL EoS) .....	169
A.1.	Description of SL EoS model .....	169
A.2.	Example: Solution methodology for a vapor-liquid system at equilibrium with SL-EoS .....	171
A.2.1.	Gas phase.....	172
A.2.2.	Liquid phase .....	173
A.3.	References.....	174
B.	Impact of Precatalyst and Cocatalyst/External Electron Donor Precontacting in the Gas Phase Polymerization of Propylene.....	177
B.1.	Introduction.....	177
B.2.	Experimental Conditions .....	178
B.2.1.	Chemicals .....	178
B.2.2.	Semi-batch Polymerization.....	178
B.2.3.	Polymer Characterization .....	179
B.3.	Results and Discussion .....	180
B.3.1.	Kinetic Study .....	180
B.3.2.	Sorption measurements .....	183

B.4.	Conclusions.....	185
B.5.	References.....	186
C.	Mass Transfer Resistance to Ethylene in Very High Impact Polypropylene .....	189
C.1.	Introduction.....	189
C.2.	Experimental Section.....	189
C.2.1.	Chemicals .....	189
C.2.2.	Semibatch Polymerisation Methods .....	190
C.2.3.	Polymer Characterization .....	190
C.3.	Results and Discussion .....	190
C.3.1.	Resistance to the mass transfer of ethylene in very hiPP .....	190
C.4.	Conclusions.....	191
C.5.	References.....	192

## 1 General Introduction

### 1.1 Introduction to Isotactic Polypropylene

By virtue of their broad range of applications, polyolefins account for the most common plastics of everyday life. Their remarkable success (160 million tons of polyolefins produced in 2012<sup>1</sup>) is due to their wide range of properties, extending from liquid-like materials to rigid solids. However, chemically speaking, they are only composed of carbon and hydrogen, since they are polymers of alkenes with the general formula  $C_nH_{2n}$ . They are generally classified into very broad families of material: polyethylene (PE) and polypropylene (PP). Both terms include not only the homopolymers of ethylene or of propylene, but also their copolymers with other  $\alpha$ -olefins. Traditionally, PE is further subdivided per its density, into three types: high density polyethylene (HDPE), linear low density polyethylene (LLDPE), and low density polyethylene (LDPE). However, PP is subdivided based on the *stereospecificity* of the polymerization. The monomer unit of PP is asymmetrical, and the way these molecules are bound to the polymer backbone will determine the macromolecular tacticity. The three kinds of macromolecules in polypropylene are classified according to their stereospecificity (tacticity) as exhibited in Figure 1.1.

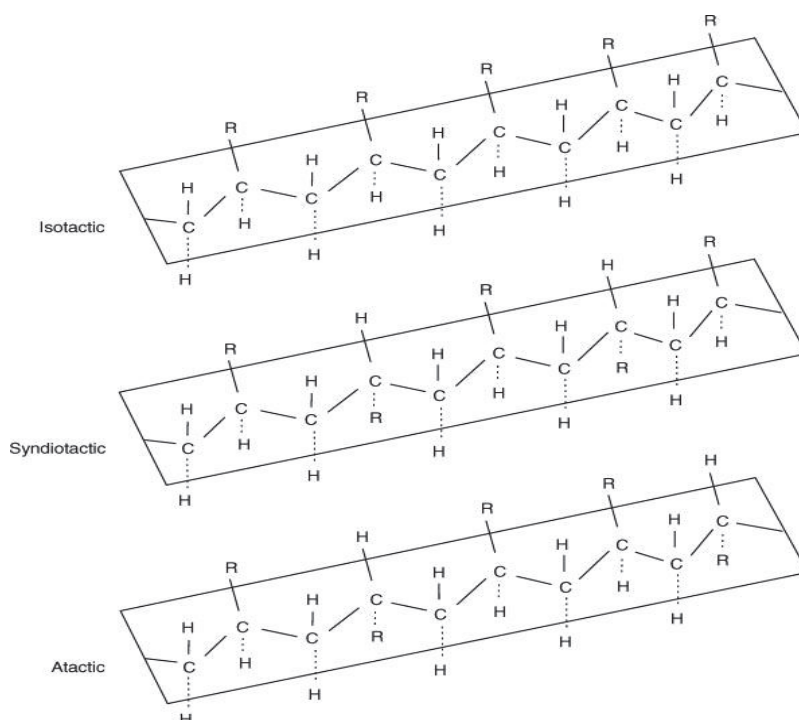


**Figure 1.1.** Classification of polypropylene polymers conforming to their tacticity: (a) isotactic, (b) syndiotactic, and (c) atactic. Reproduced with permission.<sup>2</sup> Copyright 2017, John Wiley and Sons.

Isotactic polypropylene (iPP) is composed of highly isotactic macromolecules, where all the methyl groups of the propylene units are mainly located on the same side. In syndiotactic macromolecules, the methyl groups have mainly alternating positions along the chain, and atactic ones have them randomly placed along the chain.<sup>3</sup> Fully atactic polypropylene (aPP) is amorphous and has almost no commercial value. Both isotactic and syndiotactic polypropylene (sPP) present high melting temperatures due to their semicrystalline nature. Compared to sPP, iPP dominates the market because it is less expensive to produce (production is almost entirely based on high activity heterogeneous Ziegler-Natta (ZN) catalysts) than sPP, but offers an attractive properties/price ratio. sPP is commercially almost nonexistent, since it can only be polymerized with specialized metallocenes, resulting in a fairly more expensive production, and any gain in materials properties is far outweighed by the overall product cost.<sup>4</sup>

While PE macromolecules crystallise in a linear manner, iPP macromolecules loop into a helical shape shown in Figure 1.2. These “springs” then line up next to one another to form the crystals. The crystal regions are, unlike those of PE, only slightly denser than the amorphous ones. Most of its sought-after properties are a direct consequence of this chain conformation and crystallinity. For instance, in comparison to PE, iPP presents lower density, a better resistance to fatigue, less thermal expansion, higher melting point, higher stiffness and many more advantages.<sup>5,6</sup>

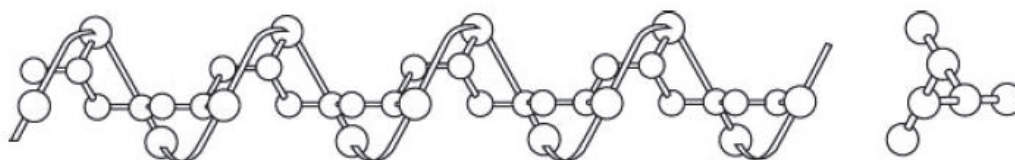


**Figure 1.2.** Chain conformation of an iPP macromolecule. Reproduced with permission.<sup>2</sup> Copyright 2017, John Wiley and Sons.

## 1.2 From iPP to High Impact Polypropylene (hiPP)

These differences in physical structure mean that iPP is more rigid than PE, but less tough and with a worse impact resistance, especially at lower temperatures, since polypropylene glass transition temperature ( $T_g$ ) is about 0 °C.<sup>7</sup> Below its  $T_g$  iPP becomes very brittle, which prevents its application in freezing environments. One proposed method to improve its toughness and impact resistance has been the incorporation of an elastomer of ethylene-propylene (EPR). Adding a certain amount as a dispersed phase within an iPP semicrystalline matrix serves to tailor the final properties of the resulting material which is

referred to as high impact polypropylene (hiPP). The inclusions of the amorphous EPR stop the possible crack propagation originated in the crystalline matrix and absorb the impacts energy, while iPP provides stiffness to the material. This balance among toughness and rigidity will be a function of the final percentage of rubber in the material.

Until the mid 1960s this bi-phasic material was done by compounding, in which iPP homopolymers were mixed with different quantities of externally produced elastomers. However, it is well known that physical mixing of two polymers is thermodynamically unfavorable, so intimate mixing, and at best adequate mechanical properties were obtained in this manner. Back then polymerizations were commonly executed in slurry phase processes, that is, the use of inert hydrocarbons (typically a C<sub>4</sub>-C<sub>6</sub> alkane) as the reacting medium. However, copolymers of propylene with low crystallinity are soluble in liquid hydrocarbons, and hence, it was not until gas phase processes appeared that the production of hiPP started to be done in two (or more) reaction steps: (1) first propylene homopolymerisation, mostly carried out in liquefied monomer (bulk) or gas phase, and (2) the in-situ hybridisation with EPR, always done in vapor phase. The resulting products from these multi-stage processes have a complex microstructure, since they are more heterogenous in terms of their composition as compared to the compounded ones. For instance, in addition to the two original phases they can also have crystalline copolymers (EPC), having both PP and PE crystallisable segments, which plays a key role in the interfacial adhesion between the matrix and the amorphous phase. Thus, multi-stage process resulted in a more effective impact-modified PP. Furthermore, in-reactor design (defined by the capabilities of the catalyst and the polymerization process) allowed the development of a whole new range of hiPP polymers, capable of covering wide application areas. More information about the development history, in-reactor design and post-reactor modification of this industrially relevant material class can be found in Gahleitner *et al.*<sup>7</sup> review.

### 1.3 High Impact Polypropylene Manufacturing Processes

Consequently, polyolefin reaction engineering has developed several PP reactor configurations that are able to produce a wide range of products, like propylene homopolymer, random propylene/ethylene copolymers (which is a copolymer of propylene/ethylene or a terpolymer propylene/ethylene/ $\alpha$ -olefin with a limited comonomer content of up to 8% wt), and heterophasic impact copolymers (hiPP). Table 1.1 summarizes

the PP process that can be found in industry.

**Table 1.1.** Industrial polypropylene manufacture processes <sup>a 4,8,9</sup>

Phase	Process	Developer	Owner	Reactor type		Prepoly
				PP	EPR	
Gas	Unipol	Union Carbide	W.R. Grace & Co	FBR (Condensed)	FBR	No
Gas	Sumitomo	Sumitomo Chemical	Sumitomo Chemical	FBR (Condensed)	2 FBR	No
Gas	Novolen	BASF	CB&I	VSBR (Condensed)	VSBR	No
Gas	Innovene	Amoco Chisso	Ineos	HSBR (Condensed)	HSBR	No
Gas	Horizone	Amoco Chisso	Japan PP Corp.	HSBR (Condensed)	HSBR	No
Hybrid	Spheripol	Montell	Lyondell-Basell	2 Loop	FBR	Yes, continuous
Hybrid	Spherizone	Lyondell-Basell	Lyondell-Basell	2 Loop	CBR	Yes, continuous
Hybrid	Hypol	Mitsui Sekka	Mitsui Chemicals	SAR/Loop	SBR	Yes, batch
Hybrid	El Paso	-	Rexene	SBR	SBR	-
Hybrid	Borstar	Borealis	Borealis	Main Loop	FBR	Yes, continuous

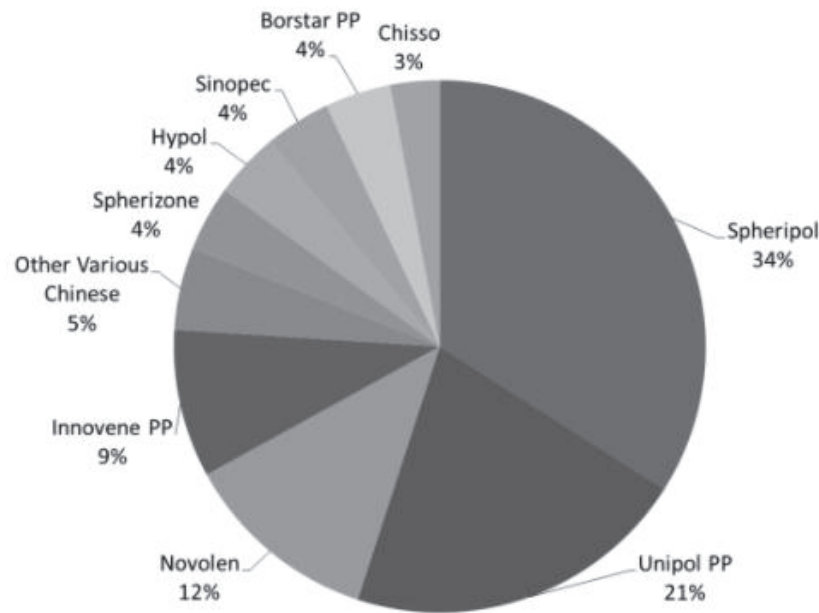
<sup>a</sup>FBR, VSBR, HSBR, CBR stand for Fluidized, Vertical Stirred, Horizontal Stirred, Circular + Bed Reactor, respectively. SAR is Stirred Autoclave Reactor.

Table 1.1 shows nine of the major licensors of PP technology in the world. While different, each of these processes offers unique variations of the two basic production processes: all gas phase (both homo and copolymerization are done in gas phase) and hybrid (propylene homopolymerization is carried out in liquid propylene). Currently, Spheripol has the largest share of installed capacity, followed by Unipol PP and Novolen, as Figure 1.3 shows.

All this process for PP rely exclusively on Ziegler-Natta catalysts with the exceptions of Novolen and Spheripol, that can also employ metallocenes.<sup>10</sup> In the coming subsections, we will briefly describe the main industrial gas phase process for PP.

### 1.3.1 Gas-Phase Processes

As Table 1.1 shows, the reactor configuration of Sumitomo and Horizone processes resemble those of Unipol and Innovene, respectively. Thus, industrially, there are three clearly different configurations for PP gas phase process, here represented by Unipol, Novolen, and Innovene.



Source: Townsend Solutions

**Figure 1.3.** Top 10 global PP technology exploitation by 2015 capacity. From ref. <sup>9</sup>

As indicated in Table 1.1, condensed mode is used in the first reactor (for propylene homopolymerization or random copolymers) of all gas phase processes. Recycle propylene is partially fed as a liquid, and upon vaporization, helps to efficiently remove the heat of polymerization. The cooling that is provided by the vaporization of the liquid quench greatly increases monomer conversion per pass, as compared to pure gas phase processes that rely solely on the heat capacity of the gas for heat removal.

A scheme of the Unipol process is exhibited in Figure 1.4. Propylene homopolymerization or random polymerization are implemented in a large fluidized bed gas-phase reactor (FBR). The second reactor for impact copolymer production is also a FBR but run in pure gas phase. It is smaller because copolymerization reaction is faster, (although in this case is performed at lower pressures and temperatures) and since we make more polymer a shorter residence in the second reactor is possible.

The Novolen process was one of the first gas-phase processes for PP and it is still used today owing to the simplicity of the reactor design and operation. Figure 1.5 demonstrates how the process counts on two vertical stirred bed reactors (VSB) that can operate either in cascade to make impact copolymers or in parallel to increase homopolymers and random copolymers production. The different components of the catalyst formulation are injected

at several points of the first reactor to avoid rapid activation, which would lead to overheating.<sup>12</sup>

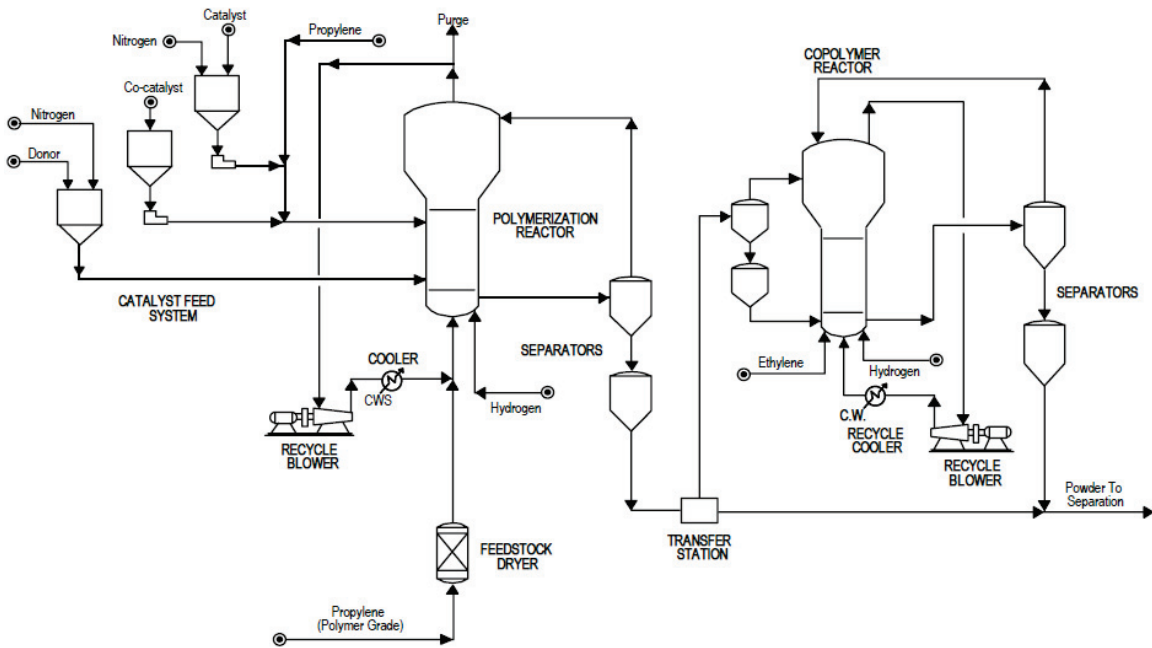


Figure 1.4. Schematical representation of Unipol process<sup>11</sup>

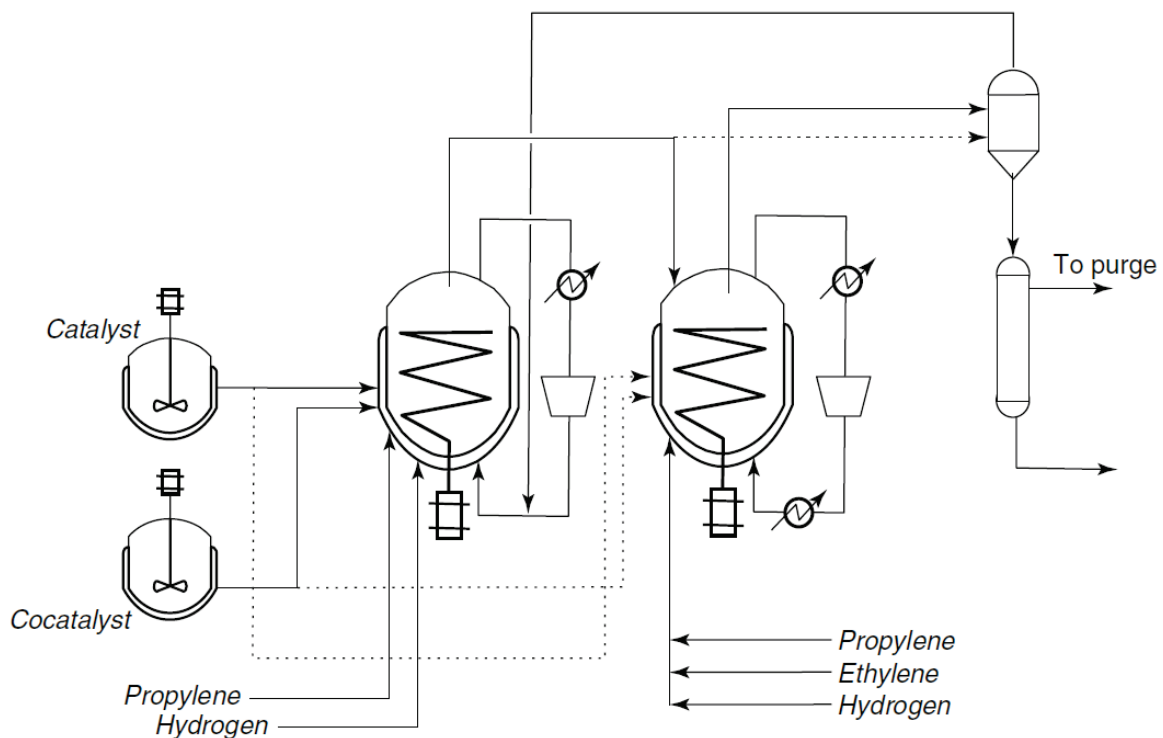
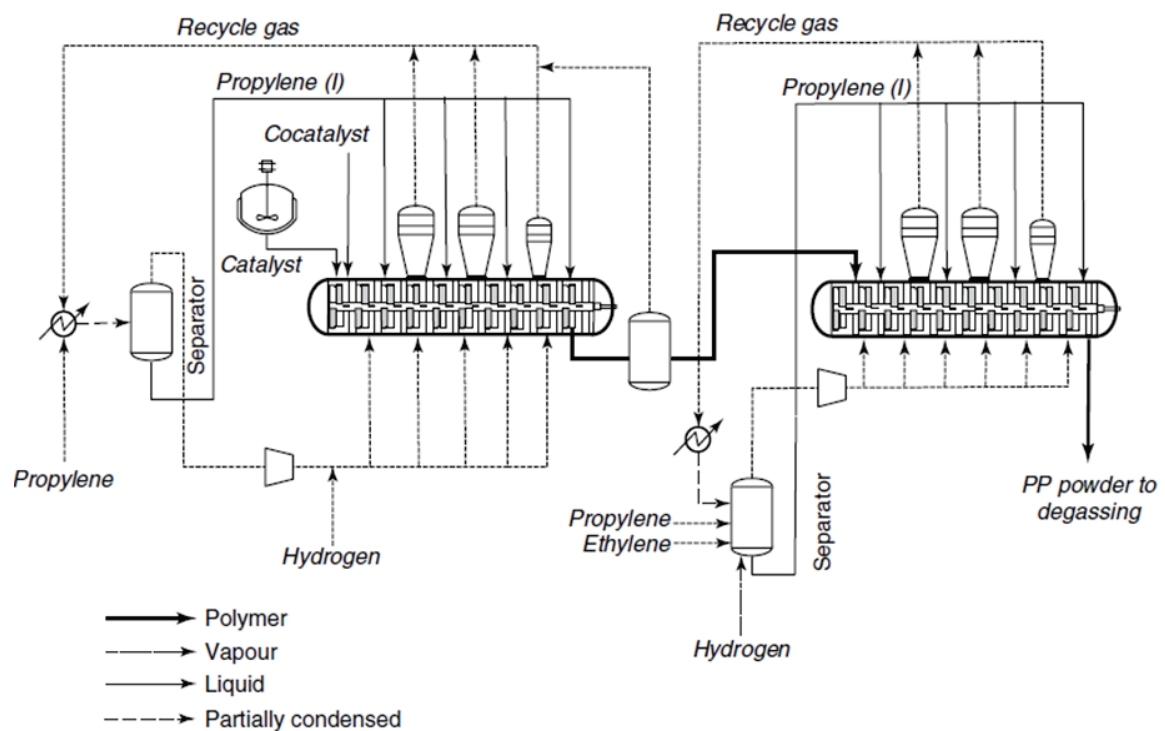


Figure 1.5. Process flow diagram of the Novolen process in cascade mode (hiPP). Broken lines show the configuration for parallel mode operation. Reproduced with permission.<sup>4</sup> Copyright 2017, John Wiley and Sons.

As stated in Figure 1.3, the third gas phase technology in terms of available capacity is the

Innovene process. It is based on two horizontal stirred bed reactors (HSBR), as displayed in Figure 1.6. Like the other gas phase processes, catalyst is not prepolymerized, but injected in a specific manner designed to steadily activate it directly in the reactor. It is claimed that it is important to inject the catalyst and cocatalyst at a well-defined separation distance since this facilitates the gradual activation of the catalyst by thoroughly mixing it with the polymer material within the reactor vessel. The big advantage of the Innovene process is the fine control possible to exert over polymer properties, thanks to the plug-flow-like reactor characteristics. Preliminary tracer studies done by Amoco Chemical Company indicated that its residence time distribution (RTD) ranges from 3 to 5 equivolume continuous stirred tank reactors in series (CSTR).<sup>13</sup> This allows fast grade polymer transitions.



**Figure 1.6.** Flow sheet of Innovene and Horizone processes. Reproduced with permission.  
<sup>4</sup> Copyright 2017, John Wiley and Sons.

The detailed description about these or other polypropylene manufacture processes and polyolefin reactors in general, can be found in ref.<sup>4</sup>

### 1.3.2 The importance of powder morphology

Industrial process for propylene polymerization pay special attention to the first instants of the catalyst life. As earlier mentioned, in gas phase process co-catalyst and precatalyst are

injected at separated points to the reactor to gradually activate the catalyst. On the other hand, as indicated in Table 1.1, hybrid processes can include prepolymerization. This consists of polymerizing the catalyst under mild reacting conditions before sending it to the main reactor at high T and P. Prepolymerization thus promotes a gentler growth, ensuring a correct fragmentation (we will talk about this below) of the heterogeneous catalyst.

In one way or another, with these practices it is intended to yield polymer particles with the correct morphology, which should be a replica of the catalyst shape. This replication phenomenon is illustrated in Figure 1.7 for a iPP particle resulting from magnesium dichloride supported Ziegler–Natta catalysts.

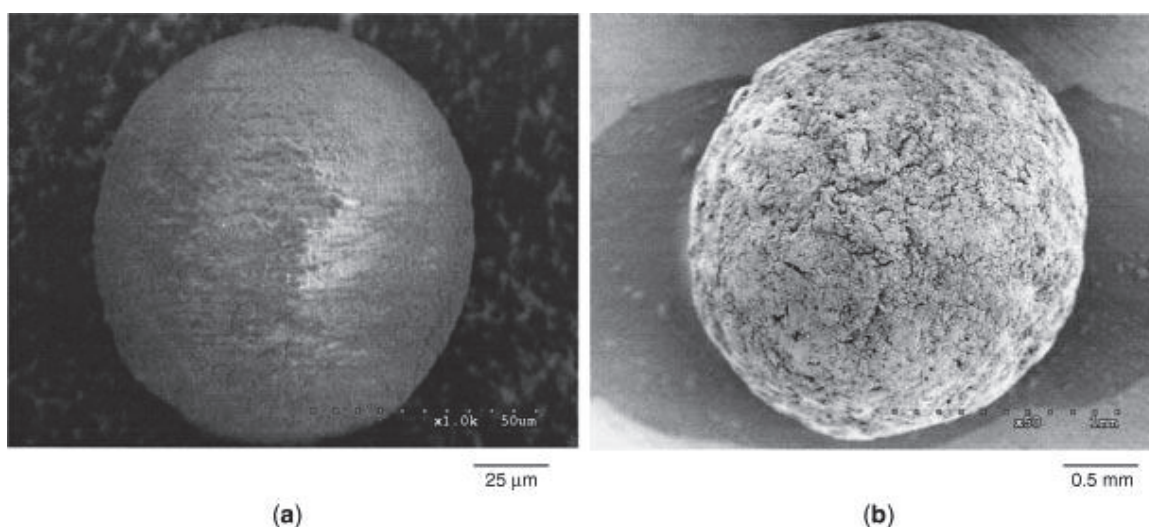


**Figure 1.7.** Ziegler–Natta catalyst particle (a) and corresponding polymer particle (b). Reproduced with permission.<sup>2</sup> Copyright 2017, John Wiley and Sons.

While important for all the polymer resulting from heterogeneous catalyst, obtaining a good morphology of iPP particles is especially crucial for hiPP. The way rubber is distributed within iPP depends tremendously on its internal structure. This, in turn, will affect the product performance, and, among other aspects, can significantly alter reactor throughput. The evolution of a catalyst particle into a hiPP particle is represented schematically in Figure 1.8.

In addition, obtaining a regular hiPP powder morphology and an homogeneous distribution of EPR phase in iPP matrix relies upon the quantity and the physical properties of the rubber itself. In this context, detailed data about this complex interaction between process conditions and powder/product properties is required.

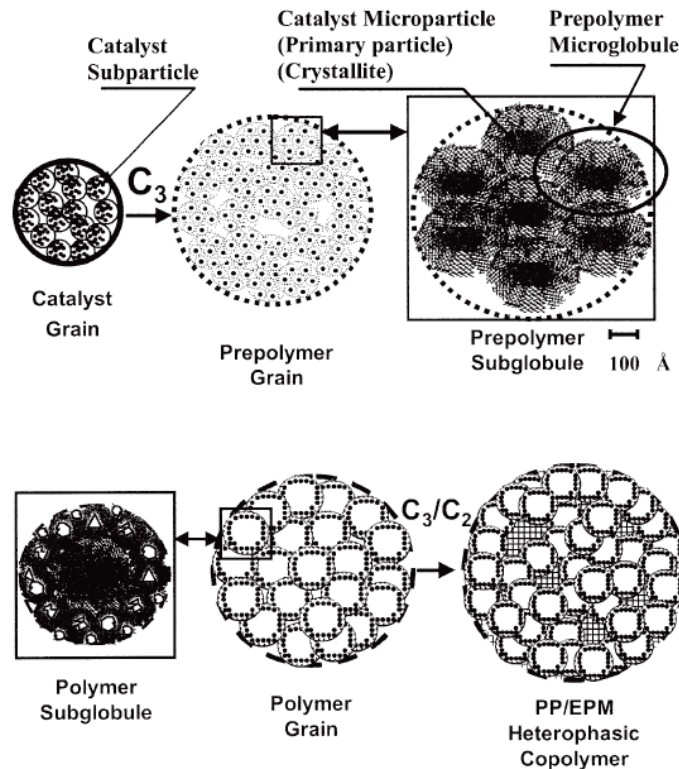


**Figure 1.8.** Particle growth of a hiPP particle over a  $\text{MgCl}_2/\text{TiCl}_4$  catalyst: pre-polymerization, iPP matrix polymerization and ethylene/propylene copolymerization. Reproduced with permission.<sup>7,14</sup> Copyright 2017, John Wiley and Sons.

#### 1.4 Thermodynamics of Sorption

To enhance the quality of the produced resins it is important to develop a full understanding of the kinetics of this process. In the literature dealing with the polymerization of olefins over heterogeneous catalysts, it is recognized that the concentration of monomer in the active sites will determine the rate of reaction.<sup>15–17</sup> For the very first instants of polymerizations conducted in the gas phase, the monomer concentration in the active sites of the catalyst will be identical as in the bulk. However, as the polymerization proceeds, active sites will be surrounded with amorphous polymer. At this point, the rate of reaction will be primarily determined by the concentration of monomer in the amorphous phase of the semi-crystalline PP and the rate at which the monomer diffuses through the polymer particle.

##### 1.4.1 Thermodynamic models to predict solubility in polymer systems

During hiPP production different gases coexist in the reactor, especially during rubber production, but also throughout propylene homopolymerization, due to the presence of inert condensed hydrocarbons used to control reactor temperature or to transport the

different catalyst components. Consequently, the solubility in the polymer of the corresponding monomer will depend on the gas phase composition. The correct prediction of this aspect is, therefore, of great importance. Solubility data can be gained experimentally, to confirm after theoretical predictions done with well-known thermodynamic models.

Henry's law is unable to predict the solubility of a gas phase as a mixture of components in polymer. In consequence, a superior thermodynamic model is needed to this, and related quantities. Among the equations of state (EoS) models, the polymer industry has made extensive use of two: (1) PC-SAFT (perturbed-chain statistical associating fluid theory), and (2) the Sanchez Lacombe equation of state (SL-EoS). Since they correctly predict the equilibrium monomer solubility in polymers they are widely employed in the polymer industry.

PC-SAFT was proposed by Gross and Sadowski in 2001,<sup>18</sup> and it is a variant of the SAFT family (statistical associating fluid theory). It is designed for modelling mixtures of all types of substances: gases, solvents and polymers. Its simple formulation facilitates its incorporation into commercial software, where it is widely used for phase equilibria calculation.<sup>19</sup> More information about the different developed versions of SAFT family and PC-SAFT can be found in the literature.<sup>18–21</sup>

The well-known Sanchez Lacombe equation of state (SL-EoS) is based on lattice theory, and states that fluids are composed of mixtures of molecules and holes, confined to sites in a lattice. The SL EoS can be considered as a continuation of the Flory Huggins (FH) theory. The inherent improvement of the SL EoS over FH theory is the introduction of holes into the lattice. The hypothetical lattice can be considered compressible and density variations can be accounted for.<sup>22–25</sup>

The SL EoS, has been shown to describe and predict the solubility of a gas phase, either as individual components or as a mixture of multiple, in amorphous polymer. For instance, Kanellopoulos *et al.*<sup>26</sup> fitted this theoretical model to available solubility measurements of different binary systems (consisting of a single gas phase component and a polymer) under various conditions of pressure and temperature with a single adjustable parameter,  $k_{ij}$ .

However, predicting behavior of multicomponent mixtures is more complex, partially because of interactions between the different species in the system. An example of this is

the co-solubility effect where, in a mixture of solutes in polymer, the solubility of the lighter species increases due to the presence of a heavier one (and that of the heavier one is decreased by the lighter species). Recently, Bashir *et al.*<sup>27</sup> extended the SL-EoS to successfully describe the solubility of two gas solute components in polyolefins, using two adjustable interaction parameters to account for the co-solubility phenomenon. Therefore, to adapt the same approach to describe the solubility of (a) propylene and a vaporized inert hydrocarbon in iPP and (b) ethylene and propylene mixtures in iPP/hiPP will be of great importance in the context of hiPP industrial processes.

#### 1.4.2 Mass Transport

During polymerization, mass transport can become the reaction rate limiting factor if monomer does not diffuse from the gas phase through the polymer to the active sites as fast as it is converted into polymer. In the context of in situ rubber production in iPP, propylene is about 5 times more soluble in hiPP than ethylene,<sup>26</sup> and, for most of the ZN catalyst systems, ethylene is roughly two times more reactive than propylene. As a consequence, it seems reasonable to think that during the copolymerization step in hiPP production, ethylene might be subject to mass transfer resistance in certain cases, especially in dense particles. In this sense, precise knowledge of how to obtain iPP matrixes that ease monomer diffusion would be convenient.

In addition, in the context of these circumstances, to develop an improved understanding of the diffusivity and co-diffusivity of the multi-component gas phase in iPP particles under industrially relevant conditions, in terms of pressure, temperature and composition of the gas phase, will be tremendously useful.

#### 1.5 Outline of this thesis

The aim of this project is to study the evolution of the properties of hiPP particles during its production in the gas phase, studying the influence that the morphology of the initial PP matrix and the localization of the rubber on it, at different rubber loadings and with rubber of different properties, have on the final polymers. This aim is achieved by studying the process illustrated in Figure 1.9. This thesis is subdivided in three chapters that describe in progress made against our objectives focused on different aspects of this process. Through combined modelling and experimental efforts, and from a reaction engineering perspective, a global understanding of the full process is developed, by assembling the enlightened

pieces of the whole puzzle.

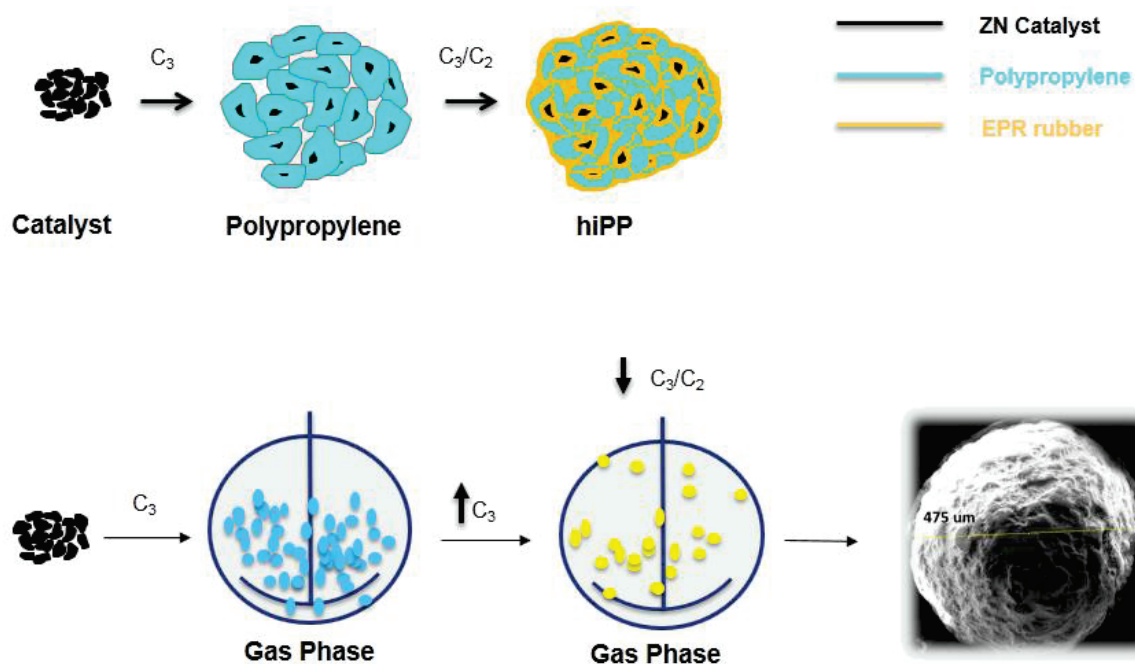


**Figure 1.9.** Schematic representation of the steps followed to produce hiPP in the gas phase in this thesis.

As represented in Figure 1.9, the morphology of hiPP will be greatly dependent on that of the intermediate PP, which in turn, will depend on the precatalyst morphology. However, the same catalyst can lead to different iPP morphologies, depending on the injection protocol followed. Therefore, catalyst injection is a critical aspect while producing hiPP. In Chapter 2, the impact of catalyst injection conditions on various aspects of the homopolymerization of propylene is studied. Propylene is polymerized in the gas phase in a 2.5 L semibatch reactor (as illustrated in Figure 1.9) using two commercially available supported Ziegler–Natta (ZN) catalyst. The mode of injection (dry, as received, or wetted with a commercially available paraffinic mineral oil), and the impact of including a prepolymerization step, are systematically investigated in terms of their influence on the instantaneous polymerization rate and morphology.

The third chapter is divided in two parts, since its goal is twofold. The first one is to investigate how different gas phase compositions affect kinetics and MWD during propylene homopolymerization. Thus, propylene was polymerized in the gas phase with a supported Ziegler–Natta catalyst. The composition of the gas phase has been systematically varied to investigate its influence on the experimentally measured reaction rates, which were fitted with a kinetic model. The monomer concentration in the polymer was calculated

with the Sanchez–Lacombe Equation of State.

The second objective of the third chapter is to study the solubility of propylene, ethylene and ethylene/propylene mixtures in iPP, and how they diffuse into the polymer powder. Thus, the measured gas solubilities for propylene, ethylene, and propylene-ethylene equimolar mixtures in isotactic polypropylene (iPP) obtained with a high-pressure sorption balance at different temperatures and pressures are shown. The resulting experimental sorption isotherms of both binary systems (propylene-iPP and ethylene-iPP) were fitted with the Sanchez-Lacombe Equation of State (SL EoS).

Diffusivities of the gases (individual or mixed) in iPP powders were also studied. For the desorption rates, the effective diffusion coefficient increases with pressure (or penetrant concentration in the polymer) and temperature. In the case of sorption experiments, diffusion of gas ethylene-propylene mixtures has always been lower as compared to both individual gases, which diffused into the polymer at similar rates.

In Chapter 4 several hiPP powders were obtained in the 2.5L gas phase reactor with a supported Ziegler-Natta catalyst, according to the schematic representation shown in Figure 1.9. Initially, the iPP matrix was kept constant. However, conditions during copolymerization such as amount of copolymer, temperature, pressure, relative amount of ethylene to propylene and the presence of hydrogen were systematically varied to study their impact on the experimentally measured reaction rates, powders stickiness, chemical composition of the polymers, mechanical properties and powders morphology. Along with other discoveries, evidence for a resistance to the mass transfer of ethylene during copolymerization was found. To understand this phenomenon 4 hiPP samples were microtomed and analyzed by atomic microscopy techniques (AFM). 3 of them had equal iPP matrix but different copolymer compositions, in terms of ethylene/propylene ratios. Contrarily, the 4<sup>th</sup> sample had a singular iPP matrix made of smaller meso-particles, easing monomer diffusion, but the same copolymer composition as one of the previous three samples. After cryo-microtomed, the hiPP samples were stored at -21°C to avoid rubber migration to the surface, preserving the original morphology. The goal is to understand the influence of PP morphology and copolymer properties on rubber distribution

In the Appendix A, firstly the Sanchez-Lacombe equation of state is briefly described. Then, an example of a vapor liquid system in equilibrium is solved step by step.

Tangential investigations not fitting within the body of the thesis were also done and are shown in appendices B and C. Appendix B depicts the importance that (1) precontacting the precatalyst and cocatalyst/External electron donor and (2) the hydrocarbon injected along the precatalyst have on the gas phase polymerization of propylene, in terms of activity and morphology. Finally, in appendix C it is investigated the incorporation of ethylene during semibatch copolymerization of hiPP in the smallest and biggest particles.

Chapters 2 to 4 and Appendix B have been submitted as publications and can be read independently from other chapters. The introduction of each chapter includes a specific bibliographic review. Reiteration of general information has therefore possibly occurred.

## 1.6 References

1. Petrochemical Analysis: Global Market Reports - Platts. Available at: <http://www.platts.com/products/petchem-analytics-global-polyolefins-outlook>. (Accessed: 28th October 2015)
2. Lieberman, R. & Stewart, C. Propylene polymers. *Encycl. Polym. Sci. Technol.* (2004).
3. *Compendium of polymer terminology and nomenclature: IUPAC Recommendations 2008 ; issued by the polymer division.* (RSC Publ, 2009).
4. Soares, J. B. P. & McKenna, T. F. L. *Polyolefin Reaction Engineering.* (Wiley-VCH, 2013).
5. Kaiser, W. in *Kunststoffchemie für Ingenieure I–XXXII* (Carl Hanser Verlag GmbH & Co. KG, 2011). doi:10.3139/9783446430495.fm
6. Maier, C. & Calafut, T. *Polypropylene: The Definitive User's Guide and Databook.* (Elsevier Science, 2008).
7. Gahleitner, M., Tranninger, C. & Doshev, P. Heterophasic copolymers of polypropylene: Development, design principles, and future challenges. *J. Appl. Polym. Sci.* **130**, 3028–3037 (2013).
8. Pater, J. T. M. Prepolymerization and morphology. Study on the factors determining powder morphology in propylene polymerization. (2001).

9. Technology\_22May2016\_PPTechnologyReview. Available at: [http://www.townsendolutions.com/technology\\_22may2016\\_pptechologyreview](http://www.townsendolutions.com/technology_22may2016_pptechologyreview). (Accessed: 14th May 2017)
10. Expertise Beyond Borders - Business and Technology Management Advisory for the global Chemical and Materials Industries. Available at: <http://www.jansz-ebb.com/>. (Accessed: 5th August 2016)
11. Nexant | Reimagine tomorrow. Available at: <http://www.nexant.com/>. (Accessed: 24th October 2016)
12. Hans-Georg, T., Wolfgang, R., Theodor, J. & Helmut, P. Polymerization of Propylene with Ziegler Catalysts in a Stirred Gas Phase Reactor. (1972).
13. Caracotsios, M. Theoretical modelling of Amoco's gas phase horizontal stirred bed reactor for the manufacturing of polypropylene resins. *Chem. Eng. Sci.* **47**, 2591–2596 (1992).
14. Cecchin, G., Marchetti, E. & Baruzzi, G. On the Mechanism of Polypropene Growth over MgCl<sub>2</sub>/TiCl<sub>4</sub> Catalyst Systems. *Macromol. Chem. Phys.* **202**, 1987–1994 (2001).
15. Kanellopoulos, V., Dompazis, G., Gustafsson, B. & Kiparissides, C. Comprehensive analysis of single-particle growth in heterogeneous olefin polymerization: the random-pore polymeric flow model. *Ind. Eng. Chem. Res.* **43**, 5166–5180 (2004).
16. Yiagopoulos, A., Yiannoulakis, H., Dimos, V. & Kiparissides, C. Heat and mass transfer phenomena during the early growth of a catalyst particle in gas-phase olefin polymerization : the effect of prepolymerization temperature and time. *Chem. Eng. Sci.* **56**, 3979–3995 (2001).
17. Floyd, S., Choi, K. Y., Taylor, T. W. & Ray, W. H. Polymerization of olefins through heterogeneous catalysis. III. Polymer particle modelling with an analysis of intraparticle heat and mass transfer effects. *J. Appl. Polym. Sci.* **32**, 2935–2960 (1986).
18. Gross, J. & Sadowski, G. Perturbed-Chain SAFT: An Equation of State Based on a Perturbation Theory for Chain Molecules. *Ind. Eng. Chem. Res.* **40**, 1244–1260 (2001).
19. Dominik, A. & Chapman, W. G. Thermodynamic Model for Branched Polyolefins

- Using the PC-SAFT Equation of State. *Macromolecules* **38**, 10836–10843 (2005).
20. PC-SAFT - Thermodynamik - Fakultät Bio- und Chemieingenieurwesen - TU Dortmund. Available at: <https://www.th.bci.tu-dortmund.de/cms/de/Forschung/PC-SAFT/index.html>. (Accessed: 17th May 2017)
  21. Wei, Y. S. & Sadus, R. J. Equations of state for the calculation of fluid-phase equilibria. *AIChE J.* **46**, 169–196 (2000).
  22. Alizadeh, A. Study of sorption, heat and mass transfer during condensed mode operation of gas phase ethylene polymerization on supported catalyst. (Université Claude Bernard-Lyon I; Queen's university at Kingston, 2014).
  23. Sanchez, I. C. & Lacombe, R. H. An elementary molecular theory of classical fluids. Pure fluids. *J. Phys. Chem.* **80**, 2352–2362 (1976).
  24. Khare, N. P. Predictive Modeling of Metal-Catalyzed Polyolefin Processes. (2003).
  25. Bashir, M. A. *et al.* The Effect of Pure Component Characteristic Parameters on Sanchez-Lacombe Equation-of-State Predictive Capabilities. *Macromol. React. Eng.* **7**, 193–204 (2013).
  26. Kanellopoulos, V., Mouratides, D., Pladis, P. & Kiparissides, C. Prediction of Solubility of  $\alpha$ -Olefins in Polyolefins Using a Combined Equation of State Molecular Dynamics Approach. *Ind. Eng. Chem. Res.* **45**, 5870–5878 (2006).
  27. Bashir, M. A., Al-haj Ali, M., Kanellopoulos, V. & Seppälä, J. Modelling of multicomponent olefins solubility in polyolefins using Sanchez–Lacombe equation of state. *Fluid Phase Equilibria* **358**, 83–90 (2013).

## 2 Impact of Catalyst Injection Conditions on the Gas Phase Polymerisation of Propylene

*Parts of this chapter have been published in three different publications:*

Cancelas, A. J., Monteil, V. & McKenna, T. F. L. Impact of catalyst injection conditions on the gas phase polymerization of propylene. *React. Chem. Eng.* **2**, 75–87 (2017).

Cancelas, A. J. et al. A Comparison of the Influence of Temperature During Slurry and Gas Phase Propylene Polymerization on Ziegler-Natta Catalyst. *Macromol. Symp.* **370**, 41–51 (2016).

Martins, A. R., Cancelas, A. J. & McKenna, T. F. L. A Study of the Gas Phase Polymerization of Propylene: The Impact of Catalyst Treatment, Injection Conditions and the Presence of Alkanes on Polymerization and Polymer Properties. *Macromol. React. Eng.* **11**, n/a-n/a (2017).

### 2.1 Introduction

As mentioned in the General Introduction of this thesis (Chapter 1, Page 17), polypropylene (PP) is the second most widely produced polymer in the world after polyethylene,<sup>1</sup> and an important part of PP production is high impact polypropylene (hiPP) polymers. During the production of hiPP, an initial stage of the production process is used to make an isotactic homopolymer of propylene (iPP), and a second copolymerization step is used to form an ethylene-propylene rubber (EPR) elastomeric phase inside the still-reactive homopolymer particles. This second step must be carried out in the gas phase, since the amorphous EPR component is soluble in any organic solvent, including liquefied monomer. One of the process-related challenges in hiPP production is to obtain the most controlled possible morphology (i.e., regular particle shape, narrow particle size distribution) during the homopolymerization step. This helps to avoid problems associated such as stickiness, lump formation, reactor fouling and several other problems.

iPP kinetics and particle morphology are greatly influenced during the initial instants when fragmentation takes place. These moments are especially crucial for gas phase processes because of the sensitivity of PP catalysts to thermal degradation,<sup>2–4</sup> and the well-known limitations of heat removal in gas state. It is to be expected that if we can better control the polymerisation during the initial instants, it should proceed more favorably during its later stages. Therefore, in the current chapter, we will study the impact of different operating parameters that can influence the rate of reaction and particle growth during the initial

moments of the reaction, which are the most critical part of the reaction for polymerization on solid catalysts.<sup>5,6</sup>

The use of a prepolymerisation step for olefin polymerization has been patented in the past,<sup>7,8</sup> and its advantages have been demonstrated both experimentally<sup>2,9-11</sup> and via modelling studies.<sup>12</sup> It is well known that prepolymerizing ZN catalyst particles before the main polymerization reaction helps to control the growth of the polymer particle and avoids overheating during the initial reaction times, especially when the catalyst is highly active. Prepolymerization takes place under mild conditions, which allows the fragmentation step to take place in a controlled manner. This has the double effect of both ensuring more appropriate particle morphology, and increasing the surface area of the growing polymer particle that is available for heat transfer.

In an industrial context, many commercially available technologies make use of prepolymerization reactors for PP, usually in liquid propylene.<sup>13</sup> Very few investigations into the impact of prepolymerization for polypropylene have been reported in the literature. Monji *et al.*<sup>14</sup> studied prepolymerization in hexane-slurry phase polymerization, and concluded that a combination of isothermal and non-isothermal prepolymerization methods (INM), especially at low temperature, gave better particle morphology than other prepolymerization methods. Samson *et al.*<sup>2</sup> stated that performance of a prepolymerization for a few minutes in either liquid propylene or pentane slurry at ambient temperature increased the reaction rates and yields of the gas-phase polymerizations by about 15%, due to lower thermal runaway of the prepolymerized particles as compared to the normal procedure. Pater *et al.*<sup>15</sup> polymerized liquid propylene and indicated that the particle morphology is determined by the initial reaction rate experienced by the particle, since it affects the fragmentation of the catalyst support as well. However, these works used a slurry phase prepolymerization step. To the best of our knowledge, only Meier *et al.*<sup>16</sup> investigated prepolymerization in the gas phase for PP. They prepolymerized a heterogeneous metallocene catalyst and saw a higher reaction rate for the main polymerization reaction. Furthermore, we only located one patent<sup>8</sup> that discloses the use of a gas phase prepolymerization step in a fluidized-bed reactor and/or one fitted with a mechanical stirrer. A reduced amount of sheeting and agglomerates was observed when this prepolymer, which was contacted with antistatic agents, was used in a (co)polymerization medium. In the current chapter, we will study the impact of using a gas

phase prepolymerization step on kinetics profiles and powder morphology obtained from gas phase semibatch polymerization reactions.

While a prepolymerization step presents certain advantages, it also increases the complexity and final costs of the whole process. Alternatives to this kind of step would be useful. Several patents<sup>7,17</sup> reveal the possibility of adding a small amount of hydrocarbon to the catalyst prior to its injection in the reactor. It was found that this method improves polymer morphology, reducing the level of fines associated with the final polymer. As a way of testing the influence of catalyst injection, two systems were studied: solid-solid with NaCl salt and solid-liquid with mineral oil. While the first method is a common approach used in literature for gas phase processes,<sup>16,18</sup> mineral oil is commonly used in PP processes as a protective catalyst carrier.<sup>19</sup> In both cases, the suspending medium can absorb some of the reaction heat, improving heat transfer between catalyst particles and surrounding environment. In the case of wet injection, the oil fills the pores (at least the macropores) of the catalyst. It is possible that this can slow the diffusion of monomer to the active sites, and cause the polymerization to occur more slowly than it would in the case of a “dry” injection. After some moments of reaction, probably after fragmentation, this liquid is displaced from the pores, which enables the monomer to enter freely in the active sites.

Clearly the initial instants of a polymerization on supported ZN catalyst are extremely important in the development of the polymer particles. Standard reactors such as the semi-batch stirred bed reactors used to polymerize olefins at fixed pressures are ill-adapted to studying very short reaction times, so a gas phase stopped flow reactor was developed by our group to study the initial instants of gas phase ethylene polymerization.<sup>20–25</sup> Here, this same tool is used for the first time to investigate systematically the polymerization of propylene. It has also been found that the use of an approximate energy balance around the stopped flow reactor can give a better estimate of the relationship between the polymerization rate and the particle temperature than is possible in a standard stirred powder bed reactor.<sup>20,21</sup> This approach is used to investigate the temperature rise of pre-wetted and dry ZN catalysts during the initial moments of propylene polymerization. This will allow us to determine whether temperature excursions at short times can be correlated with lower long-time yields. Furthermore, analyses of the resultant polymers explain the morphological and activity differences observed.

## 2.2 Experimental Section

### 2.2.1 Chemicals

Two precatalyst systems were used. Both were a commercial Ziegler-Natta polypropylene catalyst,  $\text{MgCl}_2$  supported titanium fourth generation, one of them with titanium content of 2.02%, which was called “A” and the other one with 2.8%, here called “B”. The particle size distribution of the catalysts is shown in Figure 2.1. While A precatalyst is showing a narrow distribution and an average size of 21.1  $\mu\text{m}$ , B precatalyst has a wider distribution and an average size of about 10.6  $\mu\text{m}$ .

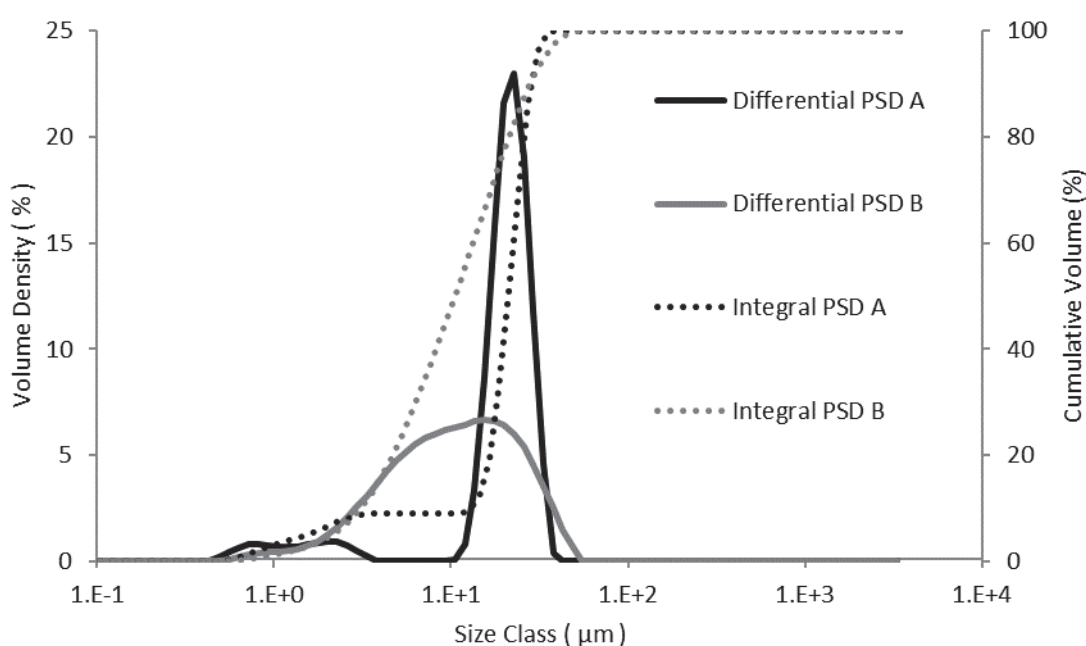


**Figure 2.1.** Differential (solid lines) and integral (dashed lines) particle size distributions of “A” and “B” precatalysts.

All heptane used was pre-treated on 3Å molecular sieves. Mineral oil Primol 352,<sup>19</sup> a medicinal grade white mineral oil, was purchased from Fisher Scientifics. It is an inert and protective carrier commonly used industrially for polypropylene processes, and its main properties are summarized in Table 2.1. Before use, it was degassed cold under vacuum to eliminate any trace of oxygen and then kept under argon atmosphere at room temperature. Sodium chloride (purity > 99.5 %) was obtained from Acros Organics, France, and then dried under vacuum ( $10^{-3}$  bar) at 200 °C for 5 hours and kept under argon atmosphere. Propylene and propane with a minimum purity of 99.5 % and hydrogen with minimum purity of 99.99% were purchased from Air Liquide (France). Propylene was purified with

a three-stage system of columns before use: a first one filled with BASF R3-16 catalyst (CuO on alumina), a second one filled with molecular sieves (13X, 3A, Sigma-Aldrich), and a last one filled with Selexsorb COS (Alcoa). Argon provided by Air Liquide, France, with a minimum purity of 99.5 %, was used to keep the reaction free of oxygen.

**Table 2.1.** Main Properties of the oil used for wetting the precatalyst particles in this work

OIL Primol 352	
Appearance	Clear and Bright
Density @ 20 °C, kg/m <sup>3</sup>	865
Flash Point, °C	240
Average Molecular Weight	480
Paraffinic / Naphthenic / Aromatic	66 / 34 / 0

### 2.2.2 Semi-Batch Polymerization

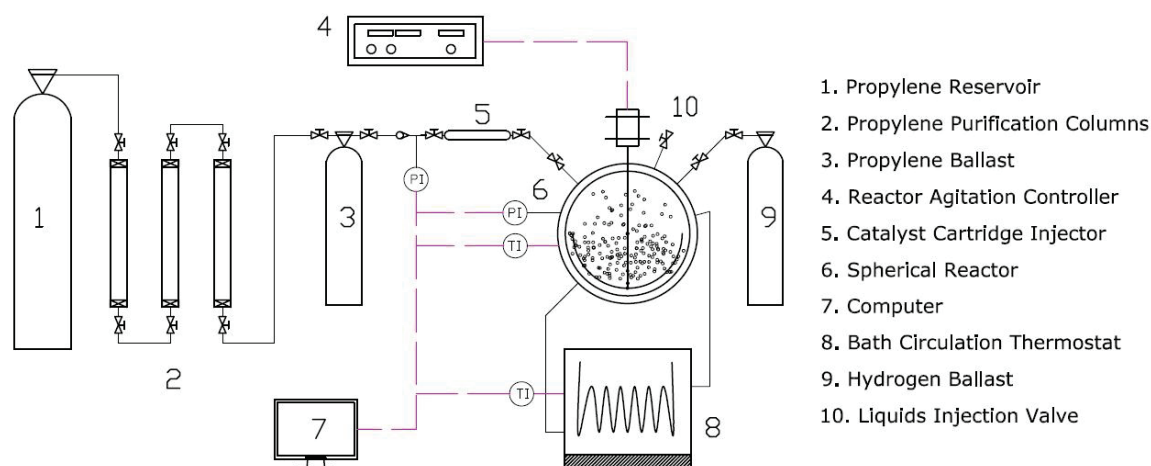


**Figure 2.2.** A schematic representation of the experimental set-up used to study gas phase propylene polymerization on the supported catalyst.

Two different kinds of reactors were used to analyze the effect of the injection conditions on the gas phase polymerisation of propylene: semi-batch and stopped flow reactors. The experimental set-up for experiments in semi-batch mode is shown in the schema in Figure 2.2. Gas phase and slurry phase polymerizations were done in a 2.5 L spherical stirred-bed reactor (turbosphere), equipped with injection valves for the catalyst and monomer feeds. The system was kept under isothermal conditions (except if prepolymerization step was used – see below). A pressure reducer was used to maintain constant pressure. Continuous measurements of the monomer pressure in the ballast were interpreted using the Soave-Redlich-Kwong equation of state (SRK-EOS)<sup>26</sup> to obtain the productivity as a function of time. With the derivative of the pressure drop the reaction rate is determined. Another possibility was to close every five minutes the reactor inlet and to measure the time for a

determined pressure difference to drop.

For each precatalyst, two suspensions were prepared in a glovebox (Jacomex, France) under argon atmosphere. A solid-solid suspension of precatalyst in coarse NaCl salt (2.5 mg/g) was prepared for the protocol named “dry injection” hereafter. For the wet injection method precatalyst was suspended in mineral oil in a concentration of 60 mg·mL<sup>-1</sup>.

Prior to reaction, the turbosphere reactor was placed under vacuum and heated to the reaction temperature for one hour. Oxygen was further purged from the reaction environment by cycling vacuum and argon inside the reactor three times. TEA and DCPDMS were used as cocatalyst and external Lewis base (ELB) respectively. The procedure for gas phase reactions was the following: The required amount of 1M TEA/heptane solution was added before reaction to remove residual oxygen from the chamber and was stirred for 5 minutes (~300 rpm). Then, the required volume of the donor/heptane mixture (0.42 M) and 250 µL of the precatalyst suspension in mineral oil (15 mg of precatalyst) or 10 g (unless differently stated) of the precatalyst suspension in NaCl salt (25 mg of precatalyst) were injected under argon, for wet and dry protocols, respectively. A 100 cm<sup>3</sup> cartridge injector and a positive displacement micropipette were used to inject the respective suspensions of dry and wet methods. Note that precontacting of precatalyst and cocatalyst/external electron donor was done, since all the compounds were injected under argon stream. The impact of precontacting these compounds in the gas phase polymerization of propylene is studied in Appendix B. Reaction was started by pressurization with a monomer-hydrogen mixture in the desired ratio. Gas phase reactions were conducted at 7.5 bar propylene with 2% hydrogen for 1 h and 70 °C (this temperature was normally used unless otherwise stated). Al/Ti and Si/Ti were set to 190 and 10.

**For slurry phase polymerizations** (shown in Table 2.5 and Figure 2.22), the liquid mixture was prepared under argon. 30mg of catalyst were mixed with TEA (Al/Ti of 190) and external donor (Si/Ti of 10) in 1L volumetric flask under argon atmosphere with 500mL of heptane (Please note that precontacting was also done) The slurry was transferred to reactor with pressure of propylene slightly above atmospheric pressure and at low stirring rate. The reaction was conducted at 7.5 bar of propylene and 2 % of hydrogen for 1 h increasing stirring rate (~500 rpm).

The procedure for those **slurry experiments where the precatalyst was “baked”** varied

slightly (runs exhibited in Table 2.3 and Figure 2.14). 500 mL of heptane were injected along TEA to the turbosphere and were stirred at 400 rpm and 60 °C to scavenge potential impurities. The precatalyst suspension in mineral oil was pre-heated to the desired temperature (25, 80, 100 and 120 °C) by plunging it in a thermostated silicon oil bath. Note that the precatalyst suspension was only heated to the next temperature if all the experiments at a determined injection temperature were finished. 10 minutes after TEA injection ELB was injected under argon, and then, precatalyst suspension under propylene. Therefore, precontacting was not performed, and reaction started at the specific temperature at which precatalyst was pre-heated. Slurry phase reactions were conducted at 8 bar propylene and 2% hydrogen for 1 h at 60 °C. Al/Ti and Si/Ti were set to 260 and 20, respectively.

Once the reaction is finished (typically one hour) the monomer inlet is closed and the reactor is rapidly cooled down and depressurized. Polymer is recovered after filtration in the slurry case. For gas phase reactions, it is recovered directly from the reactor for the wet injection procedure, since no seedbed was used. NaCl salt was washed away with demineralized water for the dry injection case. Then PP was vacuum-dried for two hours at 90 °C to remove the remaining traces of water.

**Prepolymerization** was just performed in selected gas phase reactions. It was done at 3.5 bar of propylene pressure, without hydrogen, at 40 °C for 10 min. Then, the temperature was raised to 70 °C over the course of approximately 10 minutes (this is the upper limit at which the reactor can be heated). Thus, an isothermal/non-isothermal prepolymerization method is applied (INM).<sup>14</sup> For the sake of brevity the prepolymerization rate profiles are not shown, but the yields were always approximately 200 g·g<sup>-1</sup>. When prepolymerization wasn't used, all the reactants were injected once the reactor is at the temperature of main polymerization. Nevertheless, note that the catalyst is injected and then the polymerization is started by reactor pressurization, which is a slightly milder initiation compared to industrial conditions where monomer is already present.

### 2.2.3 Gas Phase Stopped-Flow Polymerization

A schematic view of the  $\pi$  mL fixed packed bed stopped flow reactor system is shown in Figure 2.3. The reactor and feed lines are plunged into a water bath to set the bed and feed temperatures. The inlet and outlet gas phase temperatures are measured with

thermocouples. The polymerization occurs when a pulse of gas from the second ballast in Figure 2.3 is fed to the reactor for a fixed time (range 0.01 to 100 seconds). For a more detailed description of the system and reactor technology, the reader is referred to previous publications.<sup>20 21</sup>

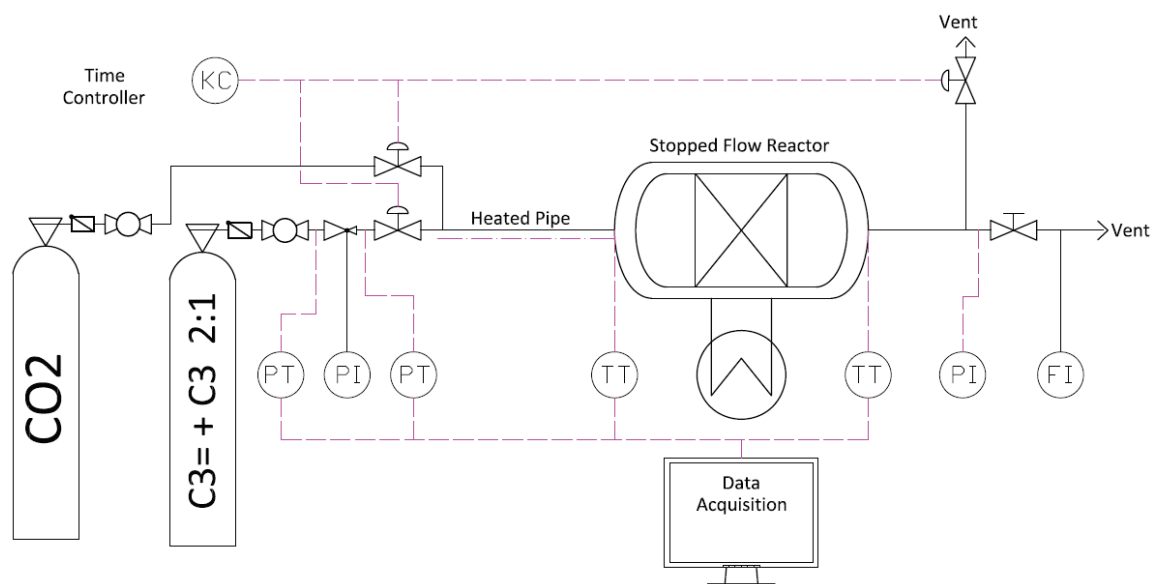


**Figure 2.3.** Stopped-flow reactor experimental setup and control system.

Reactors were prepared in a glovebox under argon atmosphere. Every reactor carried 15 mg of ZN precatalyst, either as a powder (dry method), or suspended in 250  $\mu\text{l}$  of mineral oil (wet method). In both cases, they were mixed and packed with 2 g of finely divided NaCl salt, consisting of single cubes of 5–10  $\mu\text{m}$  that are slightly agglomerated to give a final single object of around 30  $\mu\text{m}$ .<sup>20</sup> TEA (1 M, heptane solution) was added to the catalyst/salt bed in a molar ratio Al/Ti of 26. As compared to typical semibatch polymerizations Al/Ti ratio was diminished to avoid over-reduction, since a smaller volume will boost the local TEA concentration. The Si/Ti molar ratio was kept the same as semibatch reactions. Heptane from donor and cocatalyst solutions was removed by applying vacuum to the solid mixture holding the activated catalyst before the reaction was run. Otherwise, heptane and its vapourisation would affect the measurements. All reactions were run at 4.5 bar (gauge pressure) of a mixture propylene-propane (33% propane) at 70°C. The propylene was diluted with propane to improve heat transfer conditions inside the packed bed. Polymerizations were run at 1, 5, 10, 20, 40 and 75 seconds, always followed by degassing for 5 seconds and then 30 seconds of a CO<sub>2</sub> stream, to halt the reaction.

Reaction yield is measured by weighing the reactor before and after polymerization. It was considered that there were no losses of mineral oil during the process, because of its high

boiling point (240 °C). Afterwards salt was washed away with water and polymer recovered for further analysis.

#### 2.2.4 Polymer Characterization

The **bulk density** was determined by weighing a known loosely packed polypropylene powder. A recipient with a precisely known volume was filled with a known mass of polymer powder. The bulk density is indicated in gram polymer per milliliter volume

The **molecular weight distributions (MWD)** of polymer samples were characterized by HT-SEC (Viscotek-Malvern Instruments). The system was equipped with three detectors (a refractometer, a viscometer and light scattering) and with three columns (PSS POLEFIN analytical 1 000 - 100 000 - 1 000 000 Å). Analyses were performed in 1,2,4-trichlorobenzene stabilized with butylhydroxytoluol at 0.2 g L<sup>-1</sup> at 150°C at a flow rate of 1 mL min<sup>-1</sup>. Triple detection calculated the molecular weight distributions. Refractometer, viscometer, and light scattering signals were used to erase artifacts.

The **crystallinity** and **melting temperatures** of the polymer samples were measured by DSC (DSC 1 by Mettler Toledo). Two heating steps were performed from -80 to 200 °C at a heating rate of 10 °C min<sup>-1</sup> separated by a cooling from 200 to -80 °C at a rate of 10 °C min<sup>-1</sup>. The crystallinity of the samples was calculated using a value of 207 J g<sup>-1</sup> for a full crystalline polypropylene.<sup>27</sup> We considered data obtained during the second heating step.

**Nuclear magnetic resonance (NMR)** characterization was performed on a Bruker Avance III 400 spectrometer running at 100.6 MHz for <sup>13</sup>C NMR. <sup>13</sup>C NMR spectra were obtained with a 10 mm PA-SEX probe at 393 K. A volume mixture of o-C<sub>6</sub>H<sub>4</sub>Cl<sub>2</sub> (90%) and p-C<sub>6</sub>D<sub>4</sub>Cl<sub>2</sub> (10%) was used as solvent. Chemical shifts were measured in ppm using the resonance of polypropylene (T<sub>ββ</sub>, m-m-PPP) as internal reference at 28.65 ppm.<sup>28</sup>

#### 2.2.5 Lists of Experiments

There are two lists of the experiments which were performed in the current study. The first one is shown in Table 2.2, where the conditions and partial pressures of the components present in the gas phase is summarized. The experiments shown in this list were used to study the influence of prepolymerization and type of precatalyst injection (wet or dry).

Therefore, the name of the experiments is generally given by “X00-Y”, where “X” is the catalyst used (A or B), “00” is the temperature the catalyst is injected at (“40” when prepolymerization was performed and “70” when it was not), and finally “Y” is the type of injection (“W” or “D” for wet and dry injection, respectively).

The second list is Table 2.5, where the influence of temperature during slurry and gas phase (dry injection) propylene polymerization is compared.

### 2.2.6 Kinetic Model

A well-known semi-empirical model is used to describe the reaction rate for the semi-batch experiments. The instantaneous rate of propylene polymerization is calculated from the rate of pressure drop in the propylene feed ballast. To ensure that the results were reproducible, all polymerizations were repeated at least twice under a given set of operating conditions. For each experiment, the measured reaction rates have been fitted to the mathematic model shown in Equation 2.1 with lumped rate constants and 1<sup>st</sup> order deactivation (i.e. although it is known that ZN catalysts have different types of sites, we will simply look at an overall value). Fitting is done by minimizing the deviations between the experimental and model curves. Development of the equation can be found elsewhere.<sup>13</sup>

$$Rp = k_p C_0 \cdot C_m \cdot e^{-k_d \cdot t} \cdot \frac{1 - e^{-K_a \cdot \left(1 - \frac{k_d}{K_a}\right) \cdot t}}{1 - \frac{k_d}{K_a}} \quad 2.1$$

$k_p$ ,  $k_a$ , and  $k_d$  are the propagation, activation, and deactivation rate constants, respectively.  $K_a$  is the product of the activation rate constant and the cocatalyst concentration ( $K_a = k_a[Al]$ ). Since the cocatalyst is present in large excess,  $K_a$  is assumed to be constant.  $C_0$  is the initial amount of nonactivated catalyst and  $C_m$  is monomer concentration in the amorphous polymer at the active sites. Units were adapted to obtain reaction rate ( $Rp$ ) in  $\text{g} \cdot \text{gcat}^{-1} \text{h}^{-1}$ . Propene concentration ( $C_m$ ) at the active sites was considered equal to the solubility of propylene in amorphous polypropylene. At reaction conditions (70 °C and 7.5 bar of propylene pressure) is 34.5 g/L, according to our experimental data provided in the next chapter (Page 97). This data is consistent with that published by Sato *et al.*<sup>29</sup>

## 2.3 Results and Discussion

### 2.3.1 Comparison of Dry vs Wet Injection in the Gas Phase Polymerization of Propylene

The influence of type of injection and prepolymerization on the polymerization kinetics have been studied using the described kinetic model from Equation 2.1. The values obtained for the activation constant  $K_a$ , the deactivation constant  $k_d$ , and the kinetic parameter  $k_p \cdot C_0$  are used to analyze the various process parameters in a qualitative manner. Table 2.2 displays a summary of the semi-batch runs, side by side their respective process conditions and found kinetic parameters. Note that in the case prepolymerization was performed, the beginning of the reaction, time  $t = 0$  is defined as the moment where the reactor temperature reached 50 °C (during the heat up from 40 to 70 °C). The reason for this choice is that experience showed that the reaction rate began to increase quickly near this temperature for all runs. Therefore, at this point the pressure was increased to 7.5 bar and kinetic measurements were started. This was a way to ensure that all reactions after prepolymerization started at an equivalent time, ensuring the lowest possible level of catalyst deactivation and a similar amount of prepolymerization yield. Although values of  $K_a$  were calculated for all runs (and were constant at approximately  $8 \times 10^{-3}$  to  $10 \times 10^{-3} \text{ s}^{-1}$  for all prepolymerization runs) only those found for runs without prepolymerization are reported in Table 2.2 since conditions varied during the initial phase of the prepolymerization runs.

**Table 2.2.** Summary of semi-batch polymerization reactions designed and performed in the current study in the turbosphere reactor. <sup>a</sup>

Run	Type of Injection	Pre-Polymer	Precatalyst	$k_p \cdot C_0$ ( $\text{L} \cdot \text{g}_{\text{cat}}^{-1} \cdot \text{h}^{-1}$ )	$K_a \cdot 10^3$ ( $\text{s}^{-1}$ )	$k_d \cdot 10^4$ ( $\text{s}^{-1}$ )
A40-D	Dry	Yes	A	85	-	4
B40-D	Dry	Yes	B	67	-	3
B70-D	Dry	No	B	26.3	50	2.2
A40-W	Wet	Yes	A	128	-	2
B40-W	Wet	Yes	B	125	-	2
B70-W	Wet	No	B	97	28	2

<sup>a</sup> All reactions were conducted for 1 h at 70 °C in the gas phase, with 7.5, 0.15, and 1 bar of propylene, hydrogen, and argon, respectively.

Figure 2.4 shows the effect of prepolymerization of catalyst B on the reaction rate of

propylene polymerization for dry injection case, where the catalyst is suspended in salt. Kinetic parameter  $k_p \cdot C_0$  of experiments with prepolymerization (B40-D) was about 2.5 times than that of experiments with direct injection (B70-D).

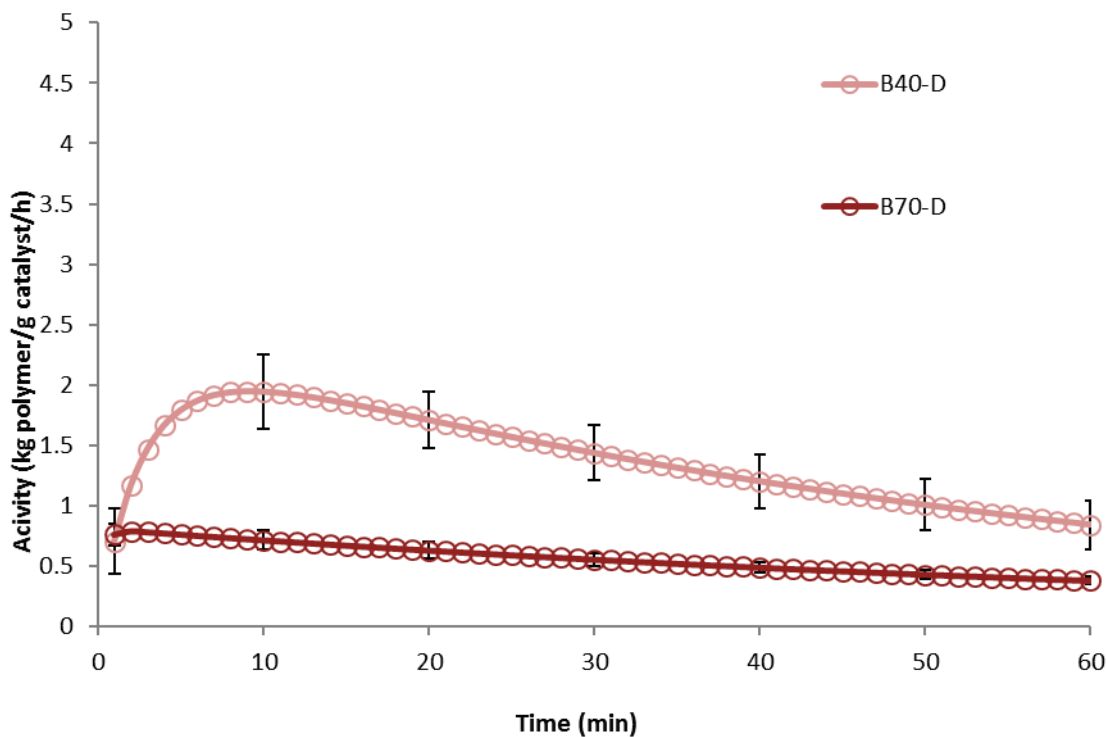


**Figure 2.4.** Instantaneous rate of propylene polymerization with non-prepolymerized (B70-D) and prepolymerized catalyst (B40-D) following dry injection protocol.

In dry injections, there is an absence of resistance to the arrival of monomer until the active sites during the first few seconds following catalyst injection into propylene atmosphere. This most likely provokes a higher initial reaction rate, with its subsequent over-heating due to exothermic reaction. As said in the introduction, first stages of reaction can be the most critical in terms of heat transfer for active catalysts. It is at this point that particles have smallest surface area (for evacuating heat) to amount of heat generated. The lower the surface, the higher the temperature rises for each catalyst particle. The latter combined with the high sensitivity of polypropylene catalysts to high temperatures<sup>2 3 4</sup> makes overheating a likely reason for the low instantaneous rate profiles observed for dry injection and no prepolymerization performed (B70-D). Achievement of higher activities when a prepolymerization is applied to the catalyst particles certainly supports this hypothesis of rapid thermal deactivation, even if they do not provide absolute proof.

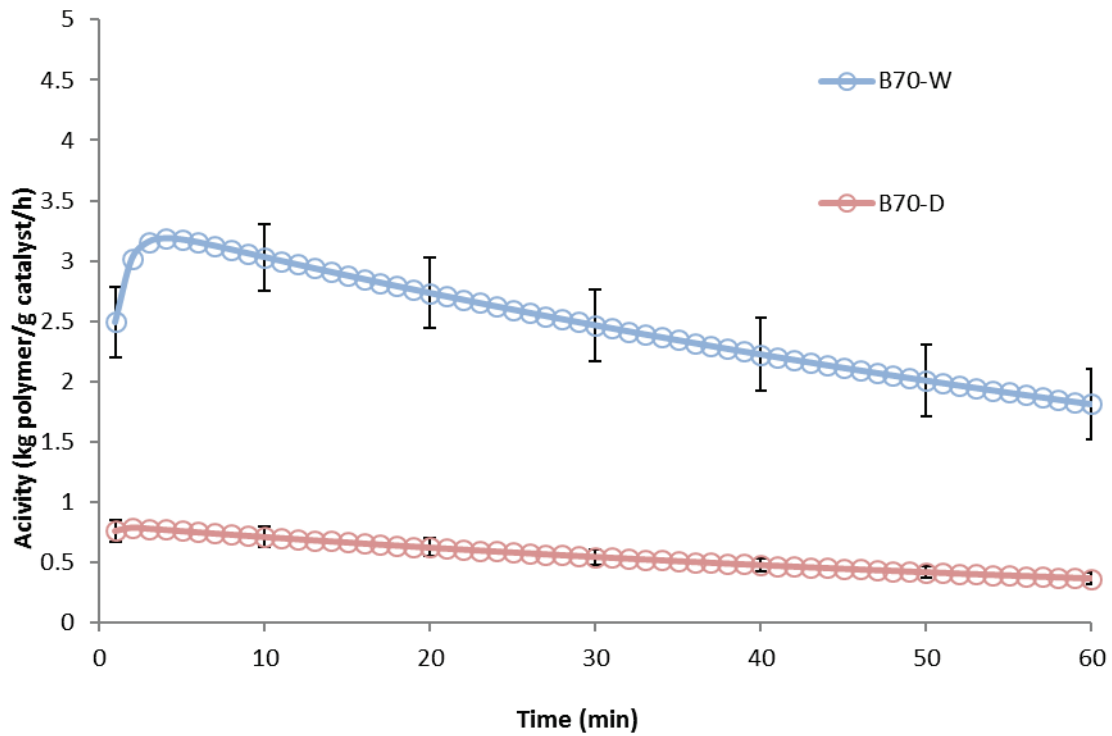


**Figure 2.5.** Instantaneous rate of propylene polymerization with non-prepolymerized B catalyst injected wet (B70-W) and dry (B70-D).

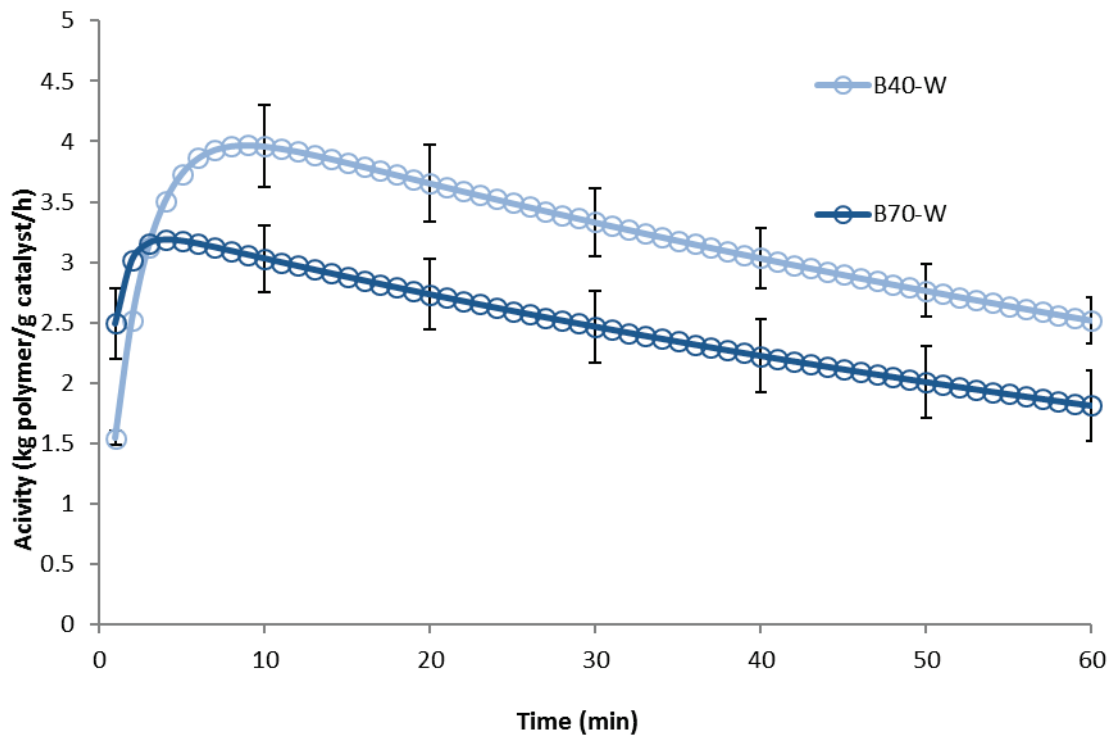


**Figure 2.6.** Instantaneous rate of propylene polymerization with non-prepolymerized (B70-D) and prepolymerized catalyst (B40-D) following wet injection protocol.

Figure 2.5 illustrates a comparison of runs without prepolymerization (B70-D and B70-W). When catalyst is pre-wetted with mineral oil,  $k_p \cdot C_0$  is about 3 times than if injected in a

solid-solid suspension with NaCl salt, as Table 2.2 exhibits. The general idea which explains this outcome being that if the oil blocks the pores of the catalyst particle, the diffusion process will slow down until the particle undergoes fragmentation. Therefore, the overall effect is in many ways like that of prepolymerization: Catalyst suffers less thermal degradation and the observed activity is higher.

On the other hand, when prepolymerization is applied, polymerization activity resulting from wet injection has a less significant enhancement, as compared to dry injection. As revealed in Table 2.2 and represented in Figure 2.6, kinetic parameter  $k_p \cdot C_0$  just showed an increase of 30%. This fact surely shows that mineral oil protects, at least partially, active sites from overheating. As a further proof, it should be considered that  $k_d$  is, in general, smaller for wet injected precatalyst than for dry injected ones.

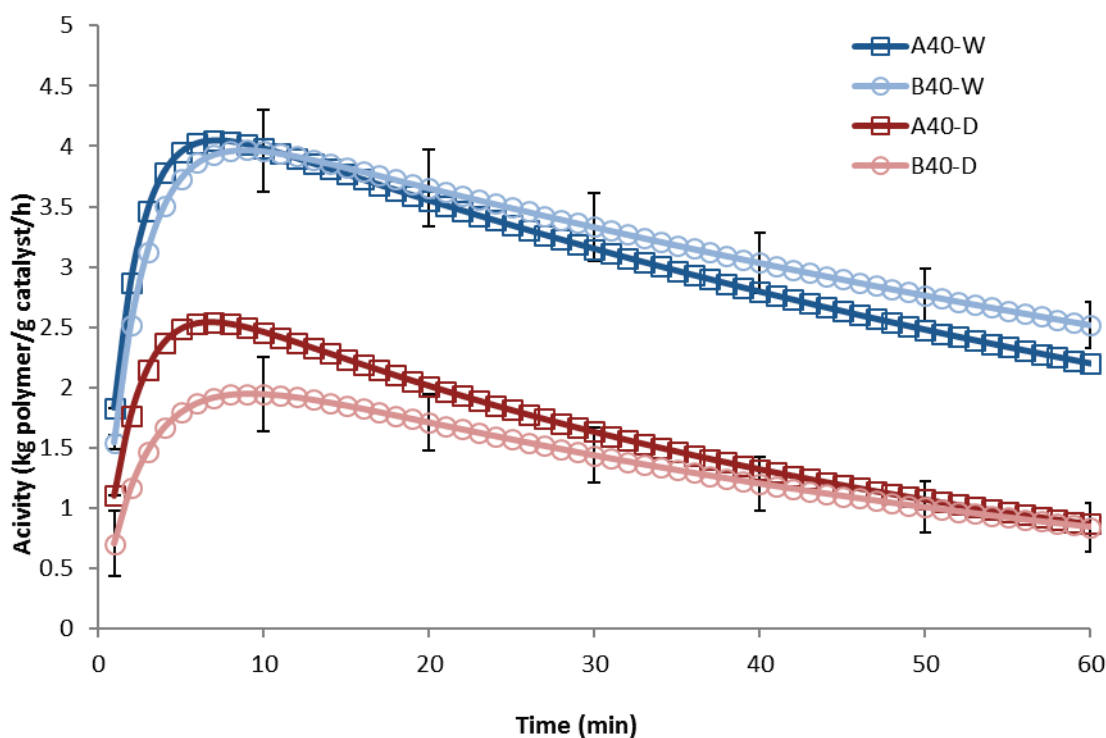


**Figure 2.7.** Instantaneous rate of propylene polymerization using two different types of catalyst injection and two ZN catalysts: A with wet injection (A40-W), B with wet injection (B40-W), A with dry injection (A40-D) and B with dry injection (B40-D).

Figure 2.7 exhibits effect of injection conditions of suspensions in mineral oil (wet) and in salt only (dry) on instantaneous rate of propylene polymerization for prepolymerized A and B catalysts.

It can be appreciated here a significant increase in activity for both catalysts when they are

pre-contacted with a mineral oil prior to injection. Based on results from Figure 2.7, lower activities obtained when polymerizing gas propylene on a dry supported ZN catalyst cannot be only explicated with thermal degradation, since, if our previous premise is correct, it should have been avoided through prepolymerization. Hence, it appears that mineral oil improves ZN catalyst activity by other means. In addition, a substantial impact on particle morphology is seen depending on the injection conditions. Figure 2.8 shows bulk density of PP powders resulting from Figure 2.7 experiments.

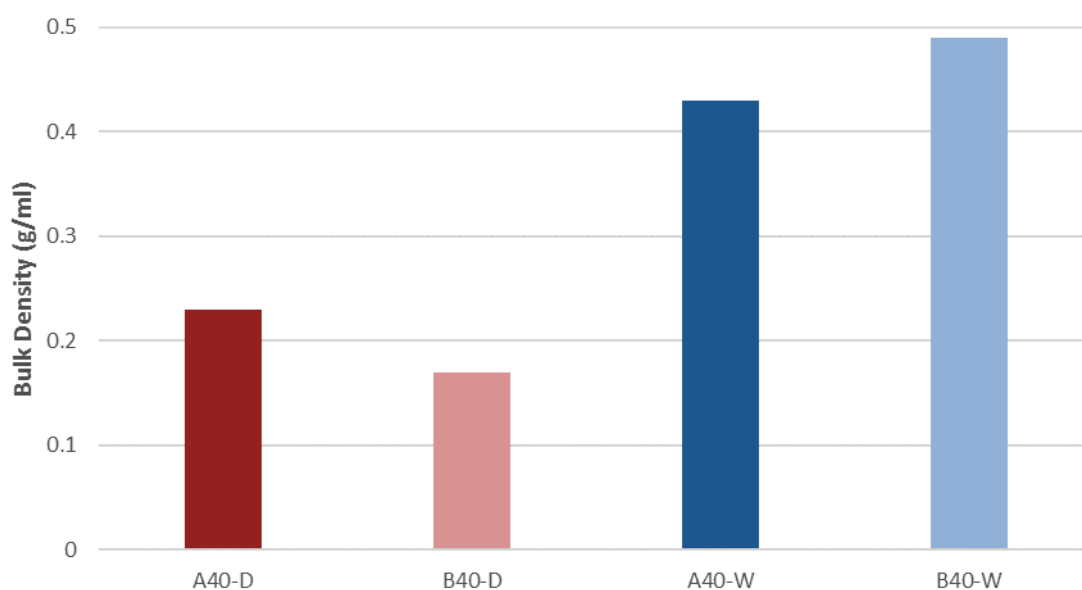


**Figure 2.8.** Bulk densities of PP powders resulting from wet (red) and dry (blue) catalyst injections protocols with prepolymerization.

It can be seen here that the bulk densities are much lower for the dry injection for both catalysts. As we mentioned above, oil does not block the pores of the catalyst/polymer particles in the case of dry injection, so mass transfer resistance is quite likely much lower and therefore the reaction can go faster, even with prepolymerization appliance. It is well known that rapid initial reactions are correlated with poor control of the particle morphology. For instance, Pater *et al.*<sup>15</sup> concluded that bulk densities are low when initial reaction rates are high. This certainly supports earlier hypothesis of local thermal runaways at particle scale, and its reduction with wet injection.

As Figure 2.9 exhibits dry injection produces expanded, big, flaky particles with a lot of fines, while particles made using wet injection are more spherical and replicate original catalyst shape. Figure 2.10 and Figure 2.11 further reflect this difference in morphology, where we can see the particle size distribution (PSD) of catalyst particles along resulting

polymer particles for both modes of injection for catalysts A and B respectively. Even with longer prepolymerization times this poor morphology was always found with dry-injected catalysts. It is possible that the oil plasticizes the polymer during the first phases with the wet injection protocol, since a more amorphous polymer would deform more easily during fragmentation, overheat less (and thus grow more uniformly) and thus help to keep the spherical shape of the catalyst particle and avoid fines formation during the polymerization reaction.

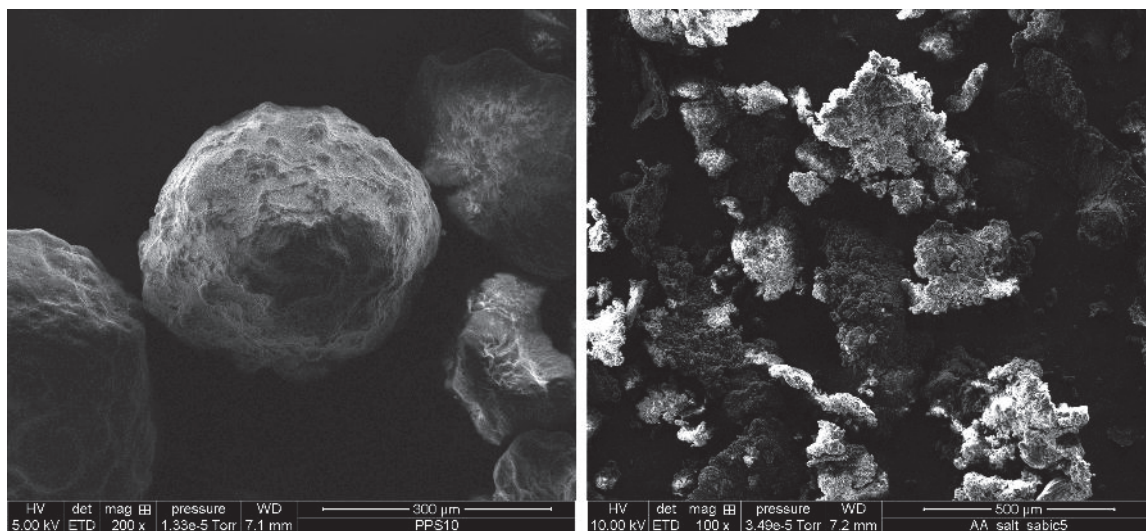


**Figure 2.9.** SEM micrographs of polymer particles produced using prepolymerized catalyst A, and injected wet (left) and dry (right).

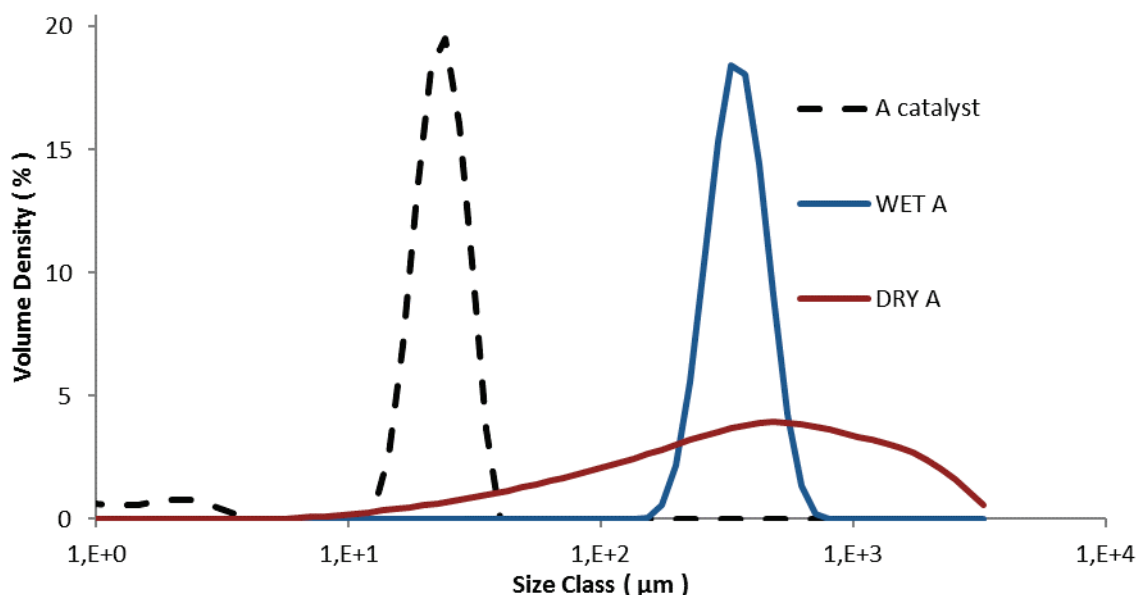


**Figure 2.10.** PSD of catalyst A (dashed line) and PP powders yielded with it, a prepolymerization step and wet or dry injection (continuous line).

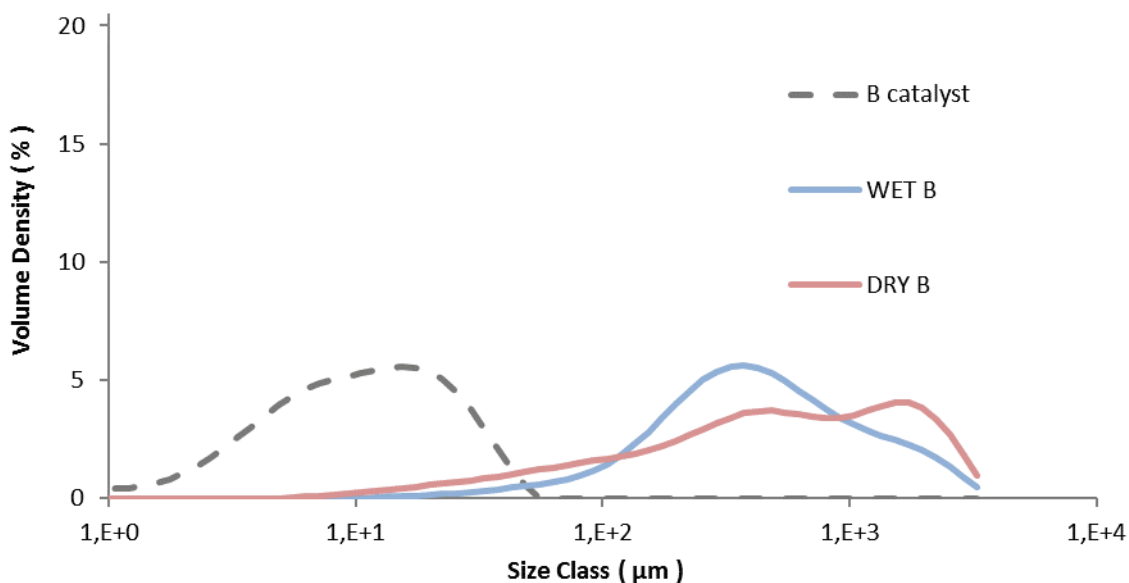


**Figure 2.11.** PSD of catalyst B (dashed line) and PP powders yielded with it, a prepolymerization step and wet or dry injection (continuous line).

It seems that the use of oil in PP production has a significant impact on the rate of production and morphology of the final polymer. As said in the introduction, these properties are greatly influenced during the first instants of reaction, when fragmentation takes place. For this reason, to understand the effect that injection conditions have on initial temperature profiles, nascent polymer properties and polymerization kinetics, gas phase reactions were conducted in a stopped flow reactor (whose scheme is displayed in Figure 2.3).

Initially, a series of runs using different injection conditions and a relative gas/particle velocity on the order of  $8.75 \text{ cm s}^{-1}$  were carried out to investigate the impact of wet vs. dry catalyst injection at short times. To ensure that results were reproducible, all polymerizations were repeated at least three times under a given set of operating conditions. The results are shown in Figure 2.12, where one can see the outlet gas temperature profiles as a function of time (the inlet temperature is constant at  $70 \text{ }^\circ\text{C}$ ) and estimates of the temperature of the solid particles in the bed at 5, 10, 20, 40 and 75 seconds of reaction versus time for both dry and wet methods. The average solid temperature of the bed (catalyst and salt,  $T_{\text{solid}}$ ) at the end of each reaction is calculated with Equation 2.2, derived by Tioni *et al.*<sup>20 21</sup> Here,  $T_0$  is the initial solid temperature ( $70 \text{ }^\circ\text{C}$ ) and  $m_{\text{solid}}$  and  $C_{p,\text{solid}}$  are the mass and heat capacity of the bed, respectively.

$$T_{solid} = T_0 + \frac{Q_{acc}}{m_{solid}C_{p,solid}} \quad 2.2$$

Note that Equation 2.2 represents a lower limit of the temperature of the catalyst particles, especially at very short times, since it assumes that the entire mass of the bed reaches the same average temperature almost instantaneously. It is entirely possible that the catalyst particles themselves are hotter than the salt particles and in particular for the first few seconds of the reaction. Nevertheless, this equation certainly gives one a better picture of the state of the catalyst particles than simply measuring the gas phase temperatures.

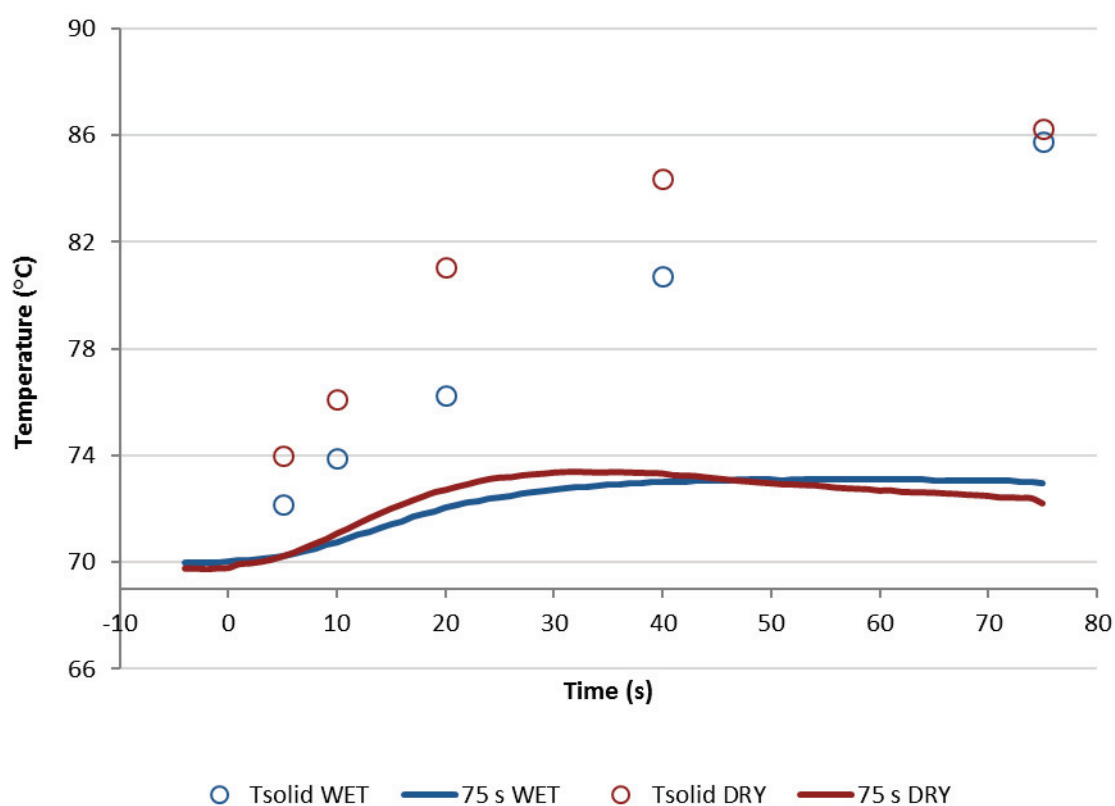


**Figure 2.12.** Outlet gas temperature profile and average calculated solid temperature ( $T_{solid}$ ) for 5, 10, 20, 40 and 75 s propylene homopolymerization using a linear gas velocity of  $8.75 \text{ cm s}^{-1}$  through the packed bed, at  $70 \text{ }^\circ\text{C}$  and 4.5 bar propylene/propane 2 : 1 molar mixture using supported ZN catalyst in wet and dry status. All polymerizations were done with Al/Ti and Si/Ti ratios of 26 and 10, respectively.

The wet and dry outlet temperature profiles showed in Figure 2.12 are quite similar, and if one only monitored the gas phase temperature it might be concluded that the reactions are similar for both methods. For the wet case, the outlet gas temperature increased by approximately  $3 \text{ }^\circ\text{C}$  within 50 s and remained constant, and in the dry case it raised by 3.5

°C in 25 s and afterwards started to decay. If we consider the solid temperatures, the story is somewhat different as  $T_{\text{solid}}$  is always higher than the observed outlet temperature for both cases. However, the packed bed (and in consequence catalyst particles) from the series of dry polymerizations overheats more than the runs using the wet protocol, which shows a slower, steadier increase of temperature. This is logically correlated with higher initial activities (5, 10, 20 and 40 s) for the dry mode, as shown in Figure 2.13.

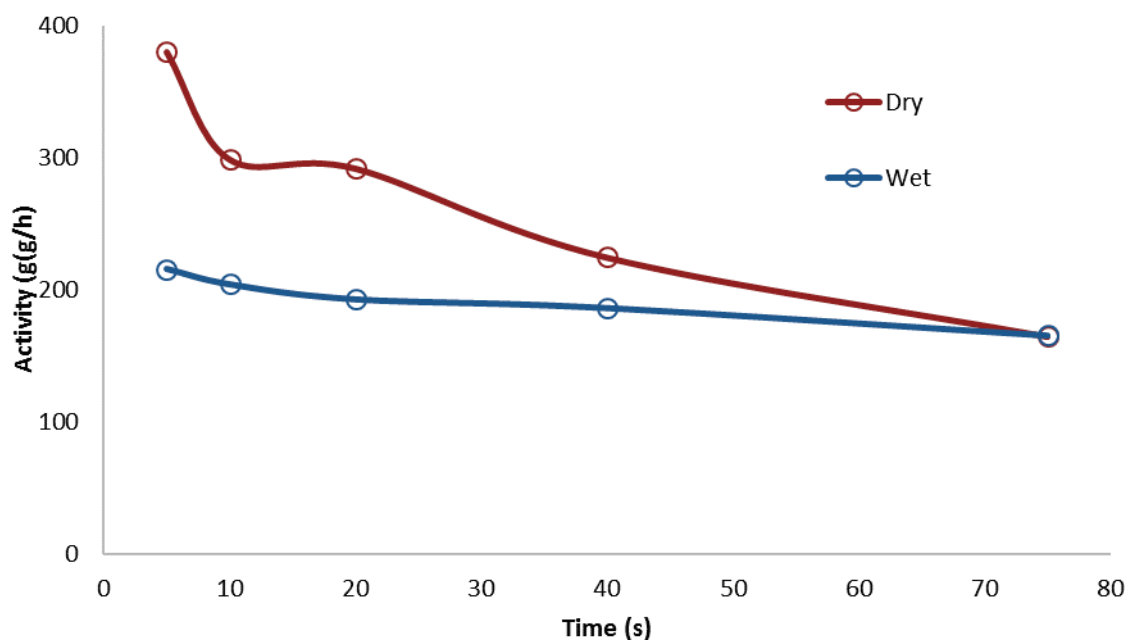


**Figure 2.13.** Activity for 5, 10, 20, 40 and 75 s propylene homopolymerization at 70 °C and 4.5 bar of propylene/propane 2:1 molar mixture using supported ZN catalyst in wet and dry status.

It is known that PP catalysts are somewhat more sensitive to thermal deactivation than those used in PE processes, and so will lose some activity at higher temperatures, which might be the cause for the faster deactivation seen in the dry instantaneous rate profile from Figure 2.13.

In order to investigate the possibility that the deactivation is due to overheating, a series of semibatch experiments was planned. Precatalyst was pre-heated to a determined temperature (in Table 2.3 referred as catalyst injection temperature) and then a slurry phase polymerization was conducted at 60 °C in the turbosphere reactor. As said in the introduction, it is not unreasonable to assume that slurry phase polymerizations provide much better heat transfer conditions as compared to gas phase ones. Therefore, overheating of the catalyst will be much less significant in slurry than in gas phase reactions, and any

difference in the final polymer yield can be attributed to the applied precatalyst pre-heating.

To ensure that the results were reproducible, all polymerizations were repeated twice under a given set of operating conditions. Table 2.3 and Figure 2.14 show the resulting yields for every reaction performed and the averaged activity profiles for each set of conditions, respectively.

Since the catalyst is injected into the semi-batch reactor before the propylene, there is a short period of time during which propylene from the feed ballast is consumed by both the polymerization and the equilibration of the propylene–heptane mixture until heptane is saturated with propylene. Since the reaction rate is measured directly from the pressure drop in the ballast, this makes the initial activity appear higher than its true value, and this should be taken into consideration when interpreting the results shown in Figure 2.14.

**Table 2.3.** Obtained PP yields for semibatch reactions designed and performed to test the hypothesis of catalyst thermal degradation. <sup>a</sup>

Injection Temperature (°C)	Run	Productivity (g)
25	1	31
	2	27.2
80	1	25.7
	2	17
100	1	21.5
	2	15.5
120	1	9.5
	2	7.2

<sup>a</sup> All reactions were conducted at 60 °C, with 500 mL of heptane, and 8, 0.2, and 1 bar of partial pressure of propylene, hydrogen and argon, respectively.

Based on the results from Figure 2.14 and Table 2.3, it seems that the precatalyst can be thermally deactivated for propylene polymerization due to pre-heating. In general, the higher the temperature the precatalyst is treated at, the lower its productivity is. The precatalyst treated at 80 °C is less active and less productive than that prepared at room temperature, and a big drop in productivity is found with the increase of pre-heating temperature from 100 °C to 120 °C. If the thermal shock required to deactivate the catalyst does not need to be particularly long, these results could explain in large part those obtained in Figure 2.5 (and Figure 2.12). The dry injection in Figure 2.5 probably has a higher initial temperature than the wet injection curve. Care should be taken when trying to compare the rate curves in Figure 2.5 and Figure 2.12 since the experiments in Figure 2.5 were run at

7.5 bar propylene rather than 3.3 (in Figure 2.12), and while TEA was added to the seed bed in the stopped-flow experiments, none was added to the gas fed to the reactor. This means that TEA can be rapidly blown out of the bed and that the Al/Ti ratios are different in the 2 sets of experiments. Nevertheless, the results presented in Figure 2.14 show that the catalyst is sensitive to overheating. Those in Figure 2.12 show that the dry catalyst overheats more than the wet injected catalyst, and those in Figure 2.5 show that the long-term activities of wet and dry catalyst are quite different.

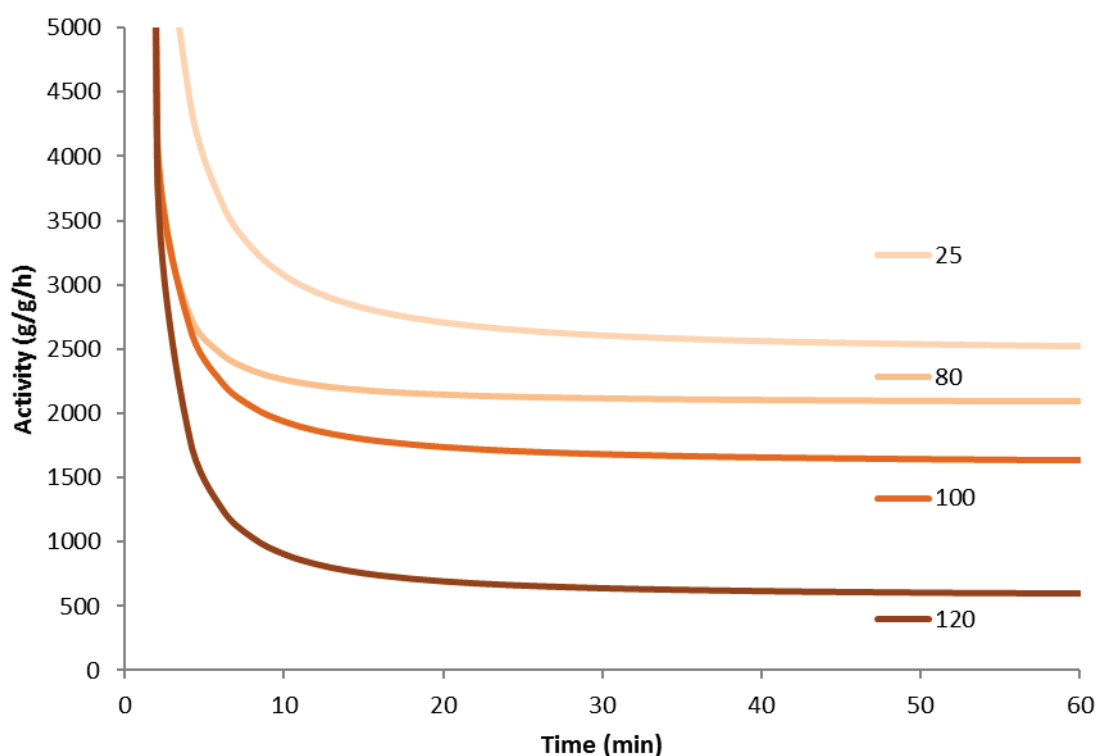


**Figure 2.14.** Instantaneous rate of propylene polymerization at 60 °C with 8 bars of propylene in slurry phase injecting precatalyst at 25, 80, 100 and 120 °C.

As further proof, consider the results in Figure 2.15 where the wet and dry series of runs were repeated but with a higher gas flow rate of  $17.5 \text{ cm s}^{-1}$ , which gives better heat transfer conditions. Here it can be seen that the wet and dry runs give very similar solid temperature profiles, especially during the initial 20 seconds. The dry method overheats slightly faster, but the difference is minimal. This is reflected in the activity curves seen in Figure 2.16.

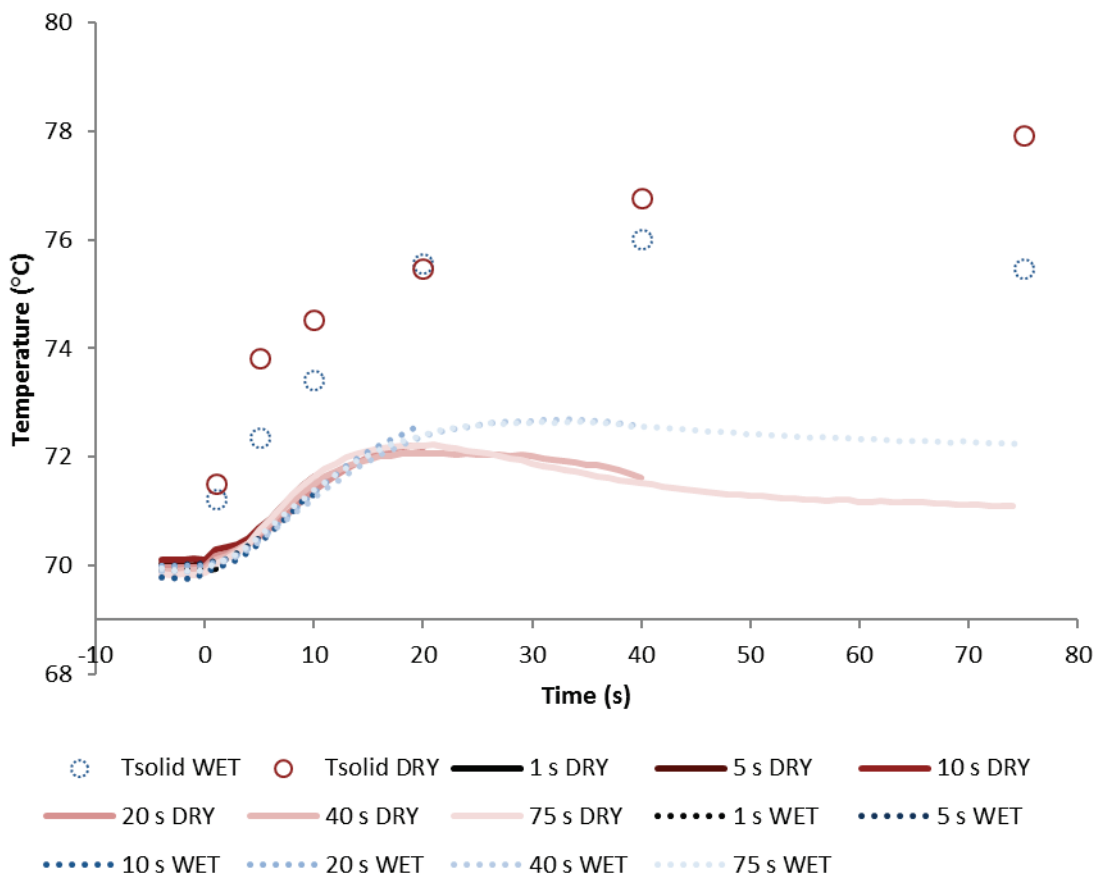


**Figure 2.15.** Outlet gas temperature profile and average calculated solid temperature ( $T_{solid}$ ) for 1, 5, 10, 20, 40 and 75 s propylene homopolymerization using a linear gas velocity through the packed bed of  $17.5 \text{ cm}\cdot\text{s}^{-1}$  at  $70 \text{ }^\circ\text{C}$  and 4.5 bar of propylene/propane 2:1 molar mixture using supported ZN catalyst in wet and dry status.

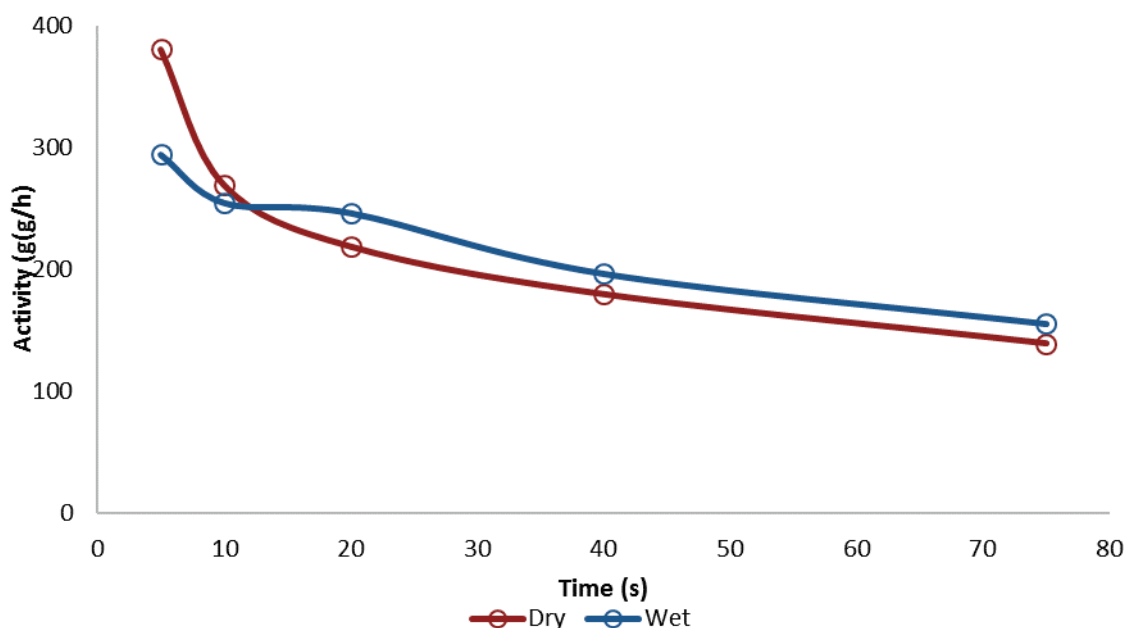


**Figure 2.16.** Activity for 5, 10, 20, 40 and 75 s propylene homopolymerization at  $70 \text{ }^\circ\text{C}$  and 4.5 bar of propylene/propane 2:1 molar mixture using supported ZN catalyst in wet and dry status.

and dry status.

The PP microstructure does not appear to be affected by wet injection. NMR studies were done for the stopped flow samples, showing isotacticity values ranging from 96 to 98% mm in any case. Therefore, in this sense polymer properties are the same as those of common commercialized iPP and earlier displayed semibatch samples, so withdrawn conclusions can be extrapolated.

Difference scanning calorimetry analyses were run on polymers obtained from Figure 2.15 experiments. Figure 2.17 and Figure 2.18 show the obtained thermograms for crystallization and melting curves, respectively.

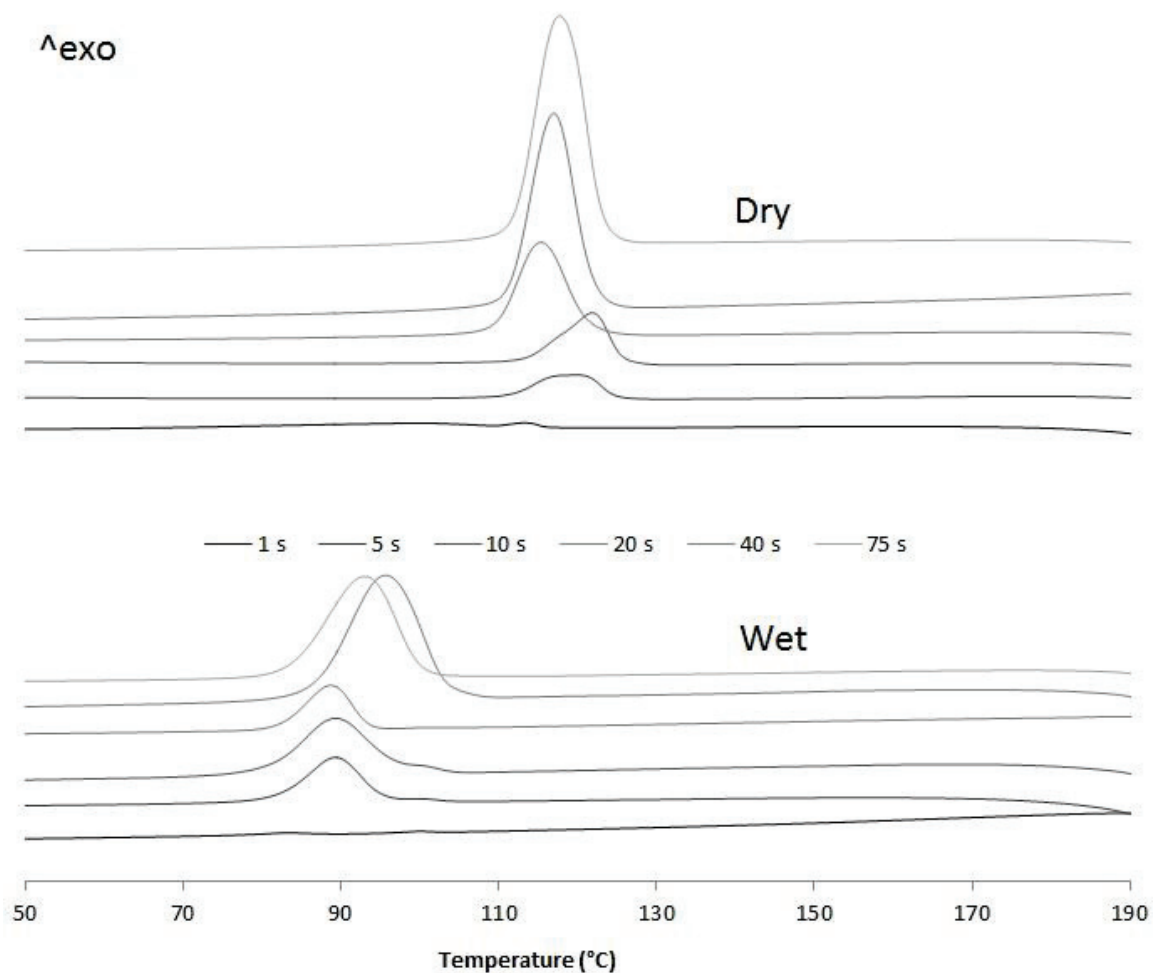


**Figure 2.17.** DSC crystallization curves of Dry and Wet samples from 1, 5, 10, 20, 40 and 75 seconds' reaction time.

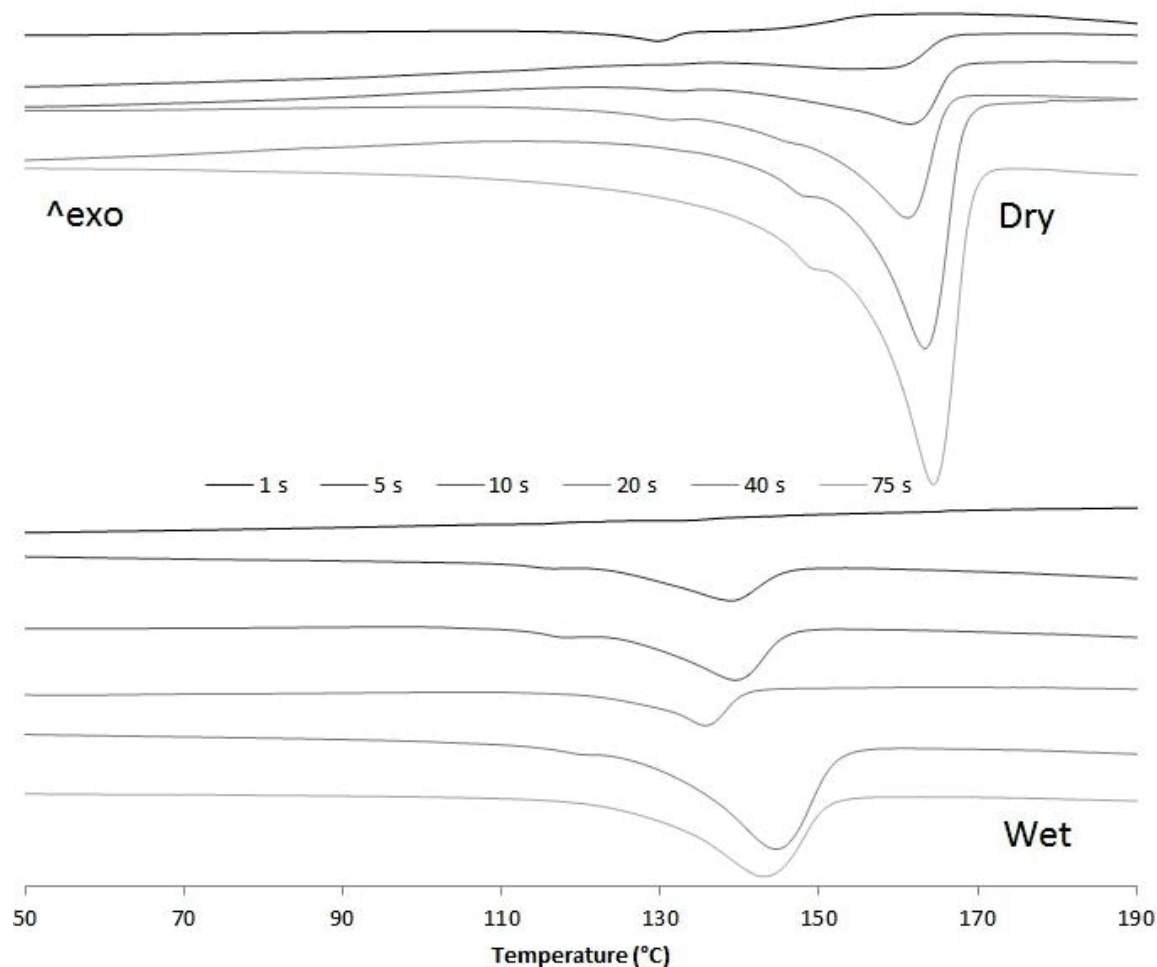


**Figure 2.18.** 2<sup>nd</sup> DSC melting curves of Dry and Wet samples from 1, 5, 10, 20, 40 and 75 seconds' reaction time.

Figure 2.17 and Figure 2.18 show how, in both cases, crystallization and melting temperatures ( $T_c$  and  $T_m$ , respectively) gradually increase with reaction time, and Figure 2.19 summarizes the evolution of the volume fraction of crystalline material for both runs. While polymer made with dry catalyst at 75 s nearly shows the same values as those typical for iPP (~30% crystallinity,  $T_c$  of 117 °C and  $T_m$  of 165 °C), polymer resulting from wet injection is still far from there (~13% crystallinity,  $T_c < 100$  °C and  $T_m < 150$  °C).

In fact, it can be seen in Figure 2.19 that the crystallinity of the nascent powders more than doubles in the dry samples than in the corresponding wet samples, essentially because the wet samples still hold some of the oil with which they were injected. (After washing them with water, PP particles contain about 60 wt% oil for 75 s reaction.) This means that not only does the oil impact the heat transfer conditions, but it also has a non-negligible impact on the physical properties of the polymer.

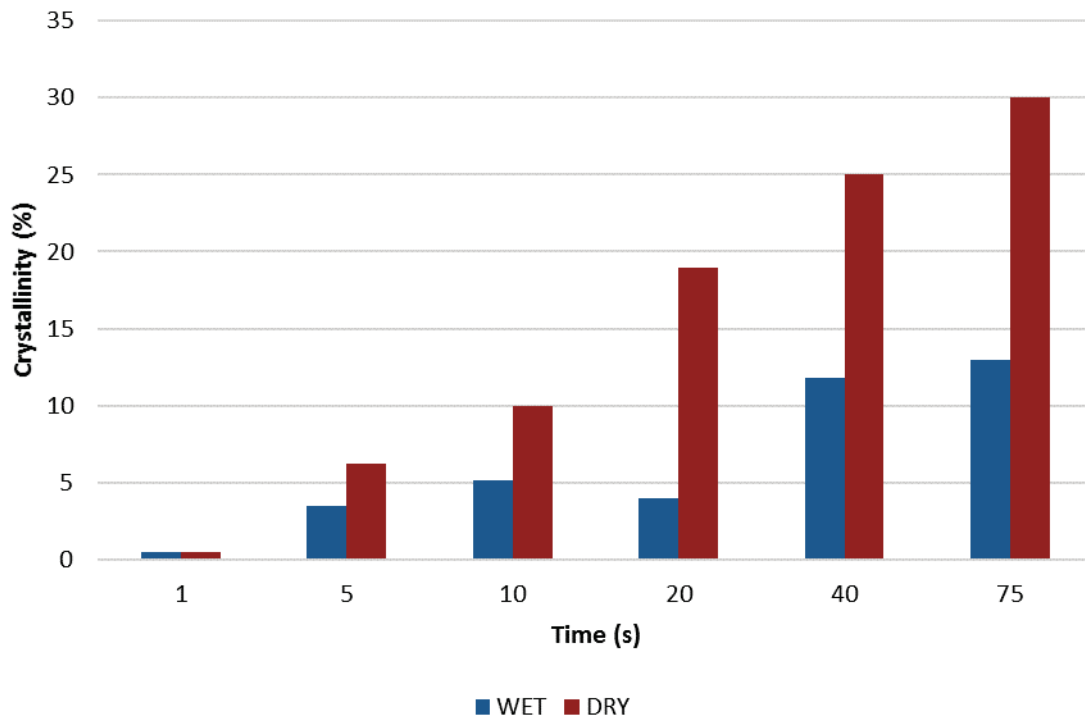


**Figure 2.19.** Evolution of crystallinity (2<sup>nd</sup> heating curve) with reaction time for PP powders produced by stopped flow reactor with dry or wet catalyst

Earlier it was observed that dry injection yields a broad PP particle size distribution mainly composed of flaky particles and fines, whereas the catalysts injected with the oil had a more regular structure (*cf.* Figure 2.9). A more crystalline polymer structure is more brittle and less flexible and it would have more probabilities of breaking apart during catalyst fragmentation, leading to fine formation. On the contrary, the wet injection protocol leads to a more amorphous structure (composed of iPP and mineral oil) which would deform more easily during fragmentation and thus help to keep the spherical shape of the catalyst particle and avoid formation of fines during the polymerization reaction.

As noted before, looking at Figure 2.17 and Figure 2.18, the  $T_c$  and  $T_m$  of newly formed PP seem to be influenced by the oil surrounding catalyst particles. To better understand this phenomenon, the melting (2<sup>nd</sup> pass) and crystallization temperatures of a series of physical mixtures of an iPP homopolymer (semi-batch gas phase polymerization) with Primol 352 oil are shown in Figure 2.20.

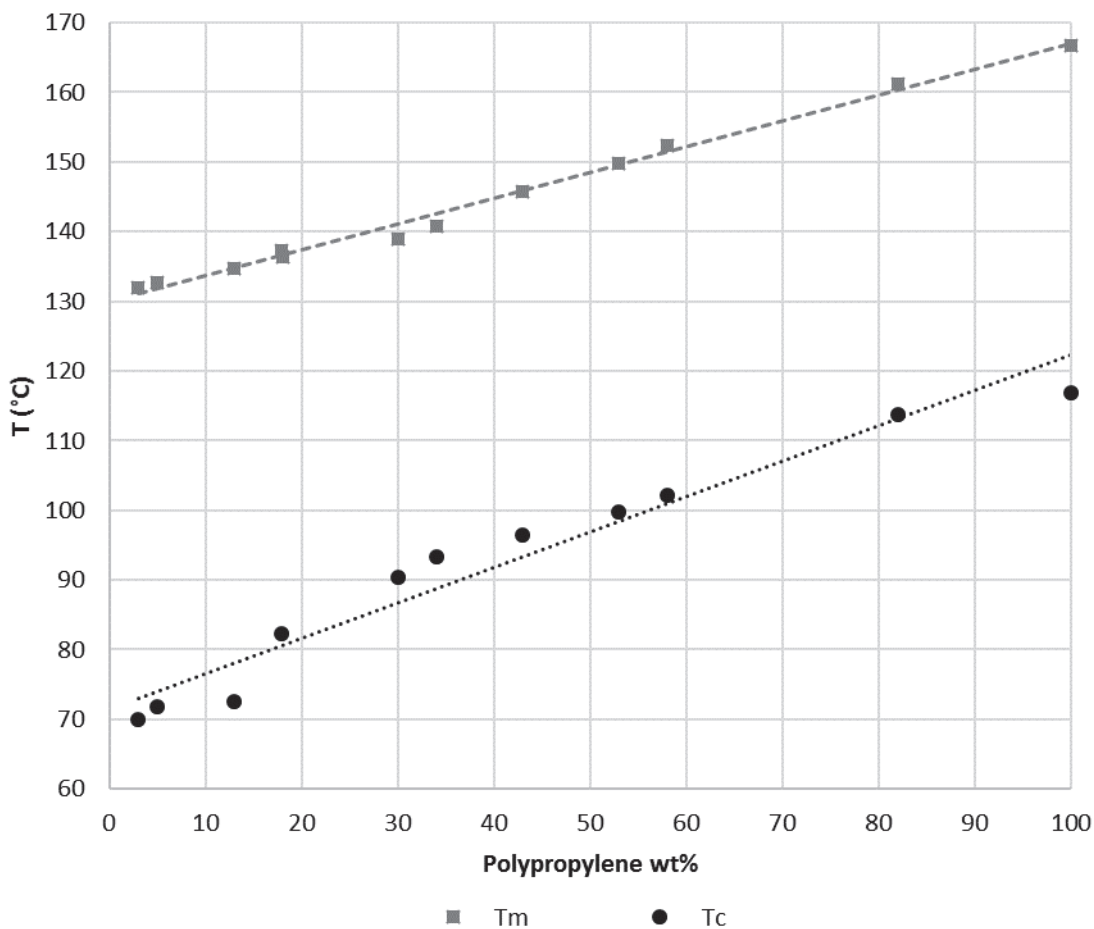


**Figure 2.20.** DSC study showing  $T_c$  and  $T_m$  of iPP depending on oil concentration.

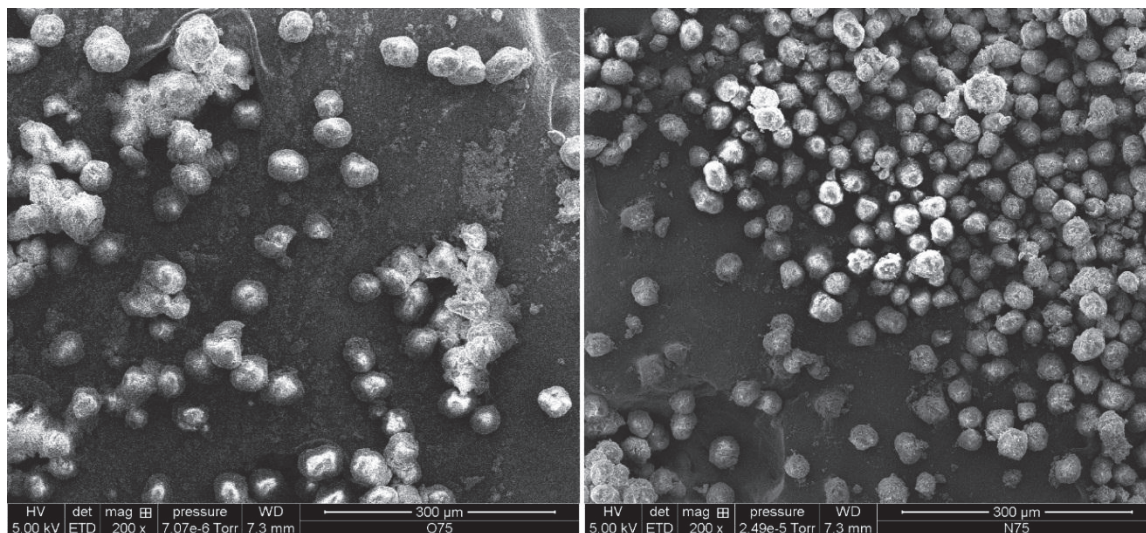


**Figure 2.21.** SEM micrographs of polymer particles produced using precatalyst injected wet (left) and dry (right) in a 75 s reaction with  $17.5 \text{ cm}\cdot\text{s}^{-1}$  of linear gas velocity.

Figure 2.20 shows how the  $T_c$  of iPP can decrease to as low as  $70 \text{ }^\circ\text{C}$  when the oil/iPP ratio is high enough. During the first instants of the gas propylene polymerization runs in the current work we will most certainly be in the same situation at  $70 \text{ }^\circ\text{C}$  and the initial PP

chains will not be able to crystallize if oil is present. In fact, in the current experiments, given that the temperature rises to 78–80 °C, the PP chains will not be able to crystallize until the polymer represents 20 weight percent of the mixture of polymer + oil. If one considers Figure 2.21, it can be seen that after 75 seconds of polymerization, the PP particles formed in the presence of oil have a significantly more spherical form than those injected dry. It is quite probable that this can, at least in part, explain the observed improvement of polymer morphology and reduced level of fines during gas phase propylene polymerization claimed in industrial patents when the catalyst is injected with oil instead of dry.<sup>7 18</sup>

Analysis of the SEM micrographs (and additional similar images not shown here for the sake of brevity) allowed us to compute the average particle size and standard deviation of the wet and dry powders shown in Figure 2.21. The values shown in Table 2.4 reveal that for a similar productivity (wet and dry runs were performed under favorable heat transfer conditions), the particles injected dry were smaller.

**Table 2.4.** Productivity and average length of the greatest dimension for all particles shown in Figure 22 for wet and dry injection respectively.

Run	Diameter (Max. Dimension)		Productivity (g per g <sub>catalyst</sub> )
	Average (µm)	Deviation (µm)	
Wet 75 s	52	7	3,2
Dry 75 s	37	6	2,9

Since productivities are similar for both cases, the observed trend of bigger particles seems to be attributable to the presence of the paraffinic oil, which would swell polymer particles (it is hard to say whether the bulk densities are different since there is so little polymer made during the experiments). It seems entirely possible that this difference will have also a significant impact on other reaction aspects. Firstly, particles will overheat less since the larger particles have a higher surface area (by a factor of 2 after 75 seconds). The higher surface area for the same quantity of active sites per particle means that it is easier to evacuate energy during this critical stage of the polymerisation. In addition, activity will be enhanced due to a higher solubility of propylene, caused by two factors: (1) a higher amorphous fraction and (2) the co-solubility effect caused by the mineral oil (which has an average molecular weight of 480 g mol<sup>-1</sup>, as shown in Table 2.1).<sup>19</sup> Specifically, this augmented solubility may be the reason for which one obtains better activity with wet injection even when early catalyst overheating is avoided through prepolymerization, as shown in Figure 2.7. In conclusion, it is the combination of all these factors which makes

the fact of pre-wetting catalyst particles with oil provoke an enhancement of polymerization rate and a better morphology control in the gas phase polymerization of propylene.

### 2.3.2 Comparison of the Influence of Temperature during Slurry and Gas Phase.

During this work, the ratio of mineral oil to precatalyst has been kept in 60 mg/mL, when wet injection protocol was conducted. Slurry phase polymerization can be looked upon as the extreme case scenario of wet injection, when practically an infinite amount of hydrocarbon is injected along with every mg of precatalyst. Therefore, the comparison of slurry (in heptane) and gas phase polymerizations at different temperatures will probably suppose a valuable contribution to the discussion developed throughout this chapter.

In this second subsection, the influence of reaction phase (gas vs. slurry), temperature and seedbed amount on the polymerization kinetics has been studied with the same semi-empirical model as previously (Equation 2.1). A summary of the runs performed and their corresponding results is shown in Table 2.5. Please note that the estimated reaction rate constants also englobe a number of physical factors —such as mass transfer rate— and therefore they should be considered as “pseudo” polymerization rate constants. Hence, these pseudo parameters might not behave as true kinetic constants when temperature is varied.

In this part of study propene concentration ( $C_m$ ) at the active sites is not constant as before, since it depends on temperature and phase of polymerization. Therefore, to understand how reaction phase, temperature and seedbed amount impact the reaction rate of propylene, it is essential to correctly estimate  $C_m$ . For gas phase reactions once more it has been considered equal to the solubility of propylene in polypropylene, and experimental data from Sato *et al.*<sup>29,30</sup> was used. However, for slurry polymerizations it is assumed to be in equilibrium with the propylene solubilized in the diluent. In this case, data was taken from Dashti *et al.*<sup>31</sup> Table 2.5 shows the used  $C_m$  values.

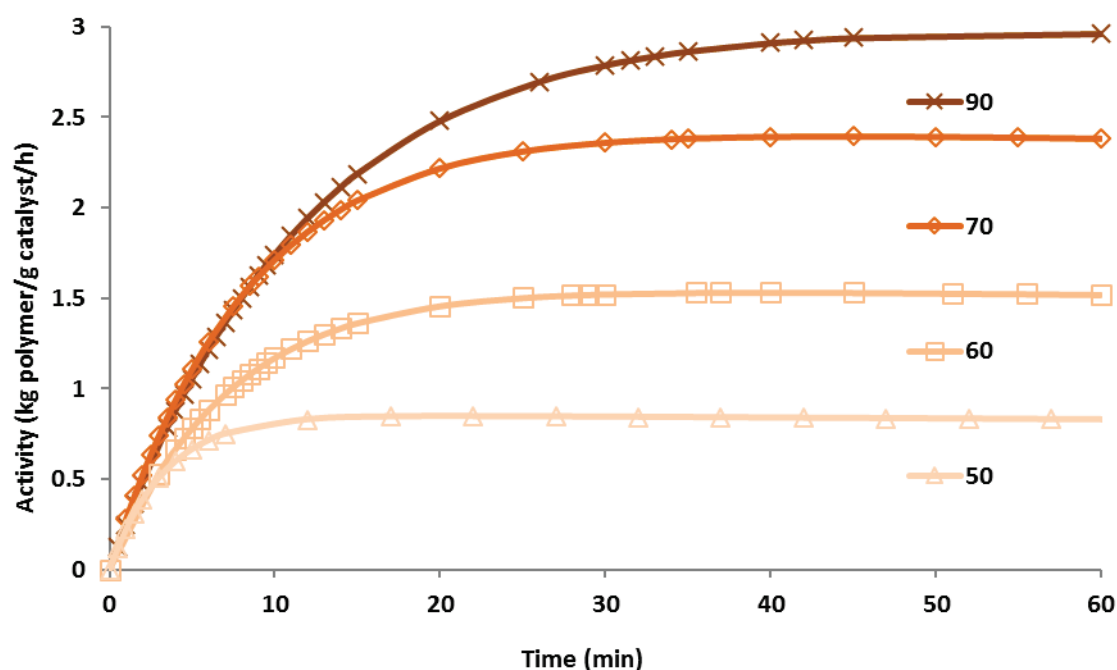
Figure 2.22 shows the influence of temperature on the activity in slurry phase with B supported ZN catalyst with 7.5 bar of propylene in the reaction environment. Please note that these slurry kinetic profiles are different to those shown in Figure 2.14 because in this case pressure drop was measured from the ballast and not directly in the reactor, so kinetic measurements were not started until the whole system was stabilized and heptane was saturated with propylene.

**Table 2.5.** Summary of semi-batch polymerization reactions designed to compare the influence of temperature during slurry and gas phase propylene polymerizations. <sup>a</sup>

Reaction Phase	Seed-bed (g NaCl)	Temp. (°C)	Average Activity (kgPP/gcat/h)	$k_p \cdot C_0$ (L·g <sub>cat</sub> <sup>-1</sup> ·h <sup>-1</sup> )	$K_a \cdot 10^3$ (s <sup>-1</sup> )	$k_d \cdot 10^4$ (s <sup>-1</sup> )	Cm (g·L <sup>-1</sup> )
Slurry	-	50	0,83	9,3	5	0,1	95
Slurry	-	60	1,38	19,3	2,3	0,1	81
Slurry	-	70	2,11	36,3	1,6	0,1	70
Slurry	-	90	2,47	52,8	1,4	0,1	58
Gas	10	50	0,67	20,4	50	2,8	53
Gas	10	60	0,75	41,9	50	5	39
Gas*	10	70	0,62	26,3	50	2,2	35
Gas	20	70	0,93	37,5	50	1,9	35

\* This run is the same as B70-D shown in Table 2.2

<sup>a</sup> B precatalyst was used for every experiment.

**Figure 2.22.** Instantaneous rate of propylene polymerization with 7.5 bars of propylene in slurry phase at 50, 60, 70 and 90 °C.

It can be seen here that activity profiles are build-up type for slurry phase polymerizations. The activity increased during the reaction until it reached a maximum, and remained constant for the duration of the reaction. Therefore, there is very little likelihood of overheating, since the activation is gradually done, and the catalyst particles undergo

through a process which we baptized as an “in-situ prepolymerization”.<sup>34</sup> The induction period is the time taken to reach the maximum rate, and it was extended by the increase of reaction temperature. At 50 °C, the induction period was within first 10 min of the reaction while there was around 40 min for 90 °C. The activation constant,  $K_a$ , can be used to quantify this effect, since this parameter stands for how fast reaction takes to reach maximum catalytic activity. As we see in Table 2.5, it decreased with increasing temperature. Monomer must pass several barriers for slurry polymerization to go on. In our three phases system (gas, liquid and solid) first monomer diffuses into heptane, then to the pores of the particle and gets sorbed in the polymer layer covering the active sites, where it reacts. With higher temperature propene solubility decreases, but monomer consumption rises. Therefore, while monomer flow decreases over the gas-liquid boundary, its driving force augments, making a greater resistance that controls monomer transport.<sup>32</sup> Thus, induction period augments (along with a  $K_a$  diminution) and equilibrium is reached later.

As exposed in Table 2.5, the catalytic activity at 70 °C was higher than that of 50 °C and it slightly increased at 90 °C. This trend was not exactly the same for the kinetic parameter  $k_p \cdot C_0$ , which showed an almost exponential increase with reaction temperature (as expected). Variations of propene concentration cause these dissimilarities. Additionally, in this set of experiments, the deactivation was not influenced by changing temperature as seen in constant  $k_d$  value in every temperature.

Figure 2.23 exhibits the influence of temperature (50, 60 and 70 °C) on the instantaneous rate of propylene polymerization in gas phase with a ZN catalyst with 7.5 bar of partial pressure of propylene in the reaction environment. They show rapid activation ( $K_a \rightarrow \infty$ ) followed by rapid deactivation. The run performed at a bulk temperature of 60 °C presented highest average activity, as well as greatest  $k_p \cdot C_0$ , whereas at same amount of salt the run performed at 70 °C produced the lowest amount of PP.

The reaction profiles from slurry and gas phase polymerizations clearly showed different trends even though the same catalyst was used in the reaction at the same bulk temperatures and the same pressures. In slurry phase reaction, the build-up type profile did not show deactivation within 1 h of reaction. These could be explained as the advantage of solvent. It has a significant role in adsorbing generated heat during the reaction and possible slowing the monomer arrival to active centers. Since there is no direct evidence of thermal deactivation, the temperature was most likely well controlled, and thus catalyst was not

harmful by overheating. On the other hand, gas-phase reaction showed a very rapid decay-type reaction profile. Interestingly, the highest rate of deactivation was coming from the highest rate of reaction, at 60 °C.

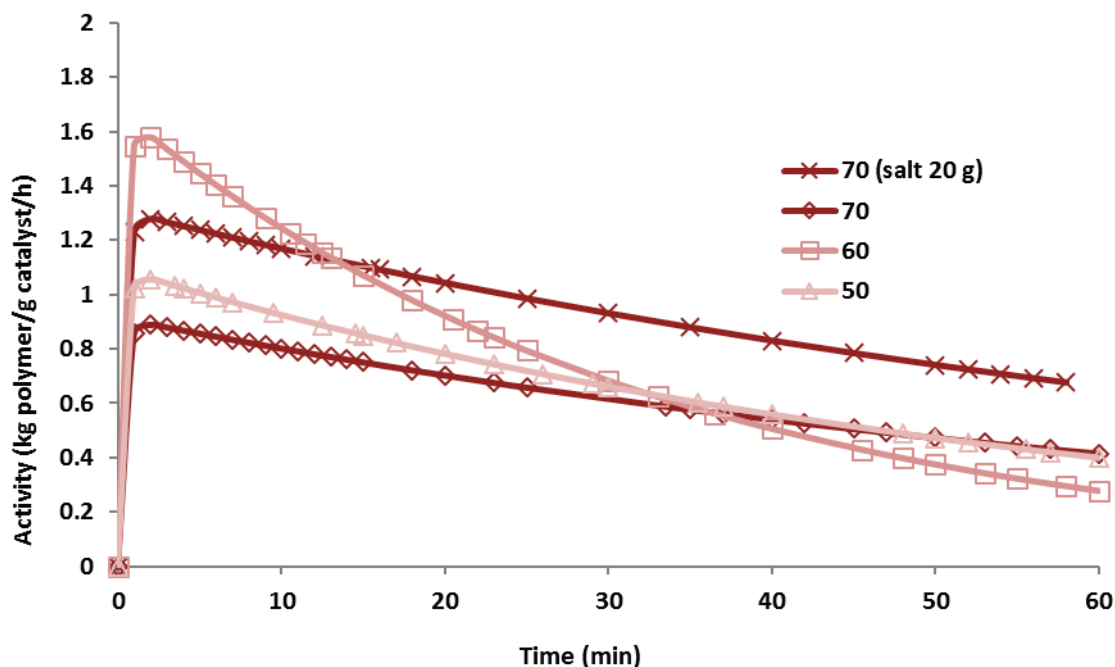


**Figure 2.23.** Instantaneous rate of propylene polymerization with 7.5 bars of propylene in gas phase at 50, 60 and 70 °C. For the last temperature two different amount of seedbed were used, 10 and 20 grams.

The possible explanation for these differences among slurry and gas reactions are in line with those previously exposed for the differences observed among wet and dry protocols. Since the diffusivity of the monomer is much higher in the gas phase than the slurry, the reaction began more quickly in the entire catalyst particle than for slurry.<sup>33</sup> This led to a rapid generation of a large amount of heat was generated as the result of an initial high rate of reaction. Since heat transfer is poorest right at the start of the reaction, coupled with the fact that the gas phase is a very poor heat sink with respect to slurry means that heat generated was not totally removed from the particle, and the local temperature went up. For a short period, this had a positive effect on the rate, however, since thermal deactivation is important for PP catalysts as earlier demonstrated, then this rapid overheating quickly leads to catalyst deactivation. The “optimal” value of 60°C for the reactor temperature (in terms of initial reaction rate) suggests that this value is a trade-off between the exothermic nature of the reaction, the fact that more heat generation leads to faster heat up and higher activity, yet also to faster deactivation.

As shown before, these problems can be overcome adding the catalyst together with solvent or mineral oil<sup>34</sup>. Figure 2.23 also shows another point suggestive of overheating as the explanation for the observed behaviour. All the reactions except one were run with a seed bed of 10 g of salt. Increasing the mass of the seedbed at the reaction temperature of 70 °C leads to an increase in the observed activity as well. Once again, we can attribute this to improved heat transfer during the nascent stages of the reaction as more salt will absorb more energy and decrease the likelihood of catalyst particles approaching each other. As shown in Table 1  $k_p \cdot C_0$  value increased while  $k_d$  decreased. Thus, temperature obviously affected early stage of reaction.

Previously it was shown that wet injection had a clear effect on the morphology of the produced powders. If heat transfer differences between both methods (slurry and gas phase) are related to the differences among wet and dry injection, the morphology of the obtained powder should be impacted in a similar way. Figure 2.24 shows the effect of reaction phase on bulk density of PP powders for a supported ZN catalyst.

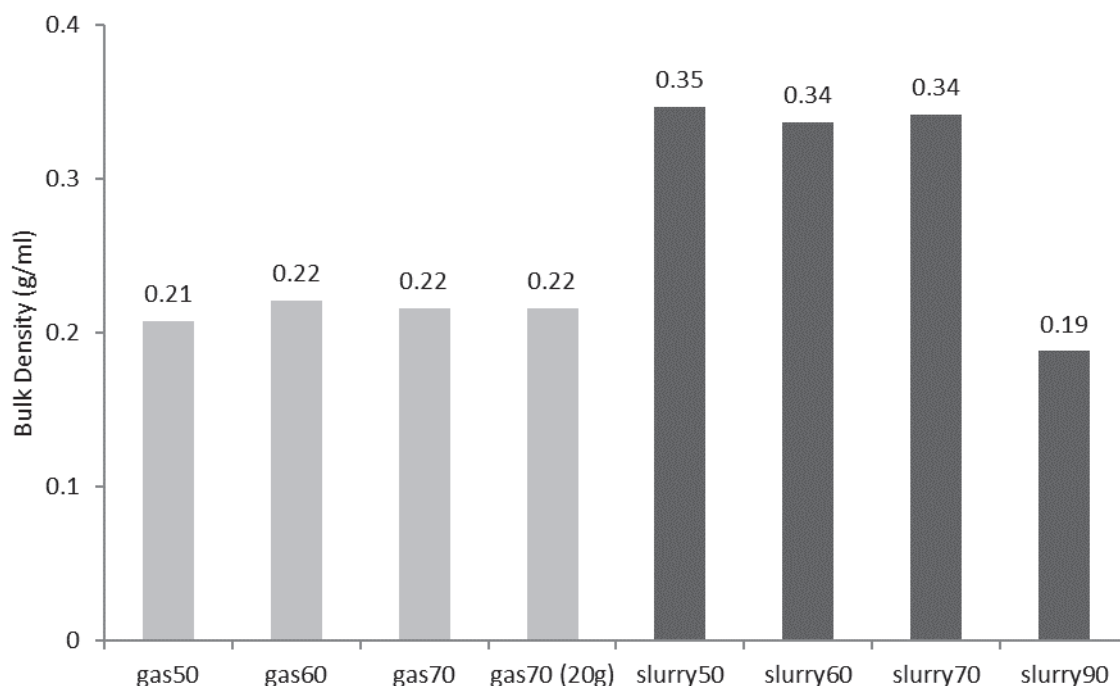


**Figure 2.24.** Bulk densities of polypropylene powders from runs shown in Table 2.5.

It is revealed here how bulk densities are lower for gas phase without dependence on seedbed amount, when compared to similar reaction temperature in slurry phase. While PP particles with regular and more or less spherical shape were being obtained from the slurry

polymerizations, (except reaction at 90 °C, which yielded big agglomerates of polymer) gas phase ones produced mainly fines with some flaky particles. Therefore, heat transfer differences between both methods (slurry and gas phase) are clearly related to those among wet and dry injection. In addition, the fragmentation process that catalyst suffers is obviously similar in gas (with wet injection) and slurry phases, and this might be in part the result not only of the presence of the solvent in the slurry reactions but also of better initial temperature control, as explained before.

## 2.4 Conclusions

Initially, propylene was polymerized in the gas phase in a 2.5 L semibatch reactor using two commercially available supported Ziegler–Natta (ZN) catalyst. The method of catalyst injection, and the use of a prepolymerization step have been systematically varied to investigate their influence on the experimentally measured reaction rates, which were fitted with a kinetic model.

The use of a gas phase prepolymerization step enhanced polymerization activity by 30%. It was argued that the lower reaction rates observed without prepolymerization are due to overheating, which would cause a certain degree of thermal deactivation during in the initial instants of reaction. In addition, a further, more significant enhancement of the polymerization rate was obtained when the catalyst was injected wet, i.e., suspended in mineral oil, than when it was injected dry. However, even when prepolymerization was applied to both cases activity was still twofold when precatalyst was injected wet. Therefore, this outcome cannot be credited to overheating. Furthermore, the original shape of the precatalyst was only replicated by the polymer wet-injected, while dry injection yielded in general a very bad morphology, either with or without prepolymerisation. Morphology is determined during catalyst fragmentation, which takes place during the first instants of reaction. Therefore, primary overheating and morphology evolution during the first instants of catalyst life were investigated in a stopped flow reactor.

The results from gas phase stopped flow reactor showed that when heat transfer limitations exist, dry particles overheat more rapidly, while wet particles show a steadier, slower increase of temperature. This is explained because of a more direct exposure to the monomer of the dry particles causing a faster reaction start in the entire catalyst particle, whereas in the second case better particle temperature control is obtained because of the

slower diffusion of the monomer in the oil blocked pores and the fact that the oil itself can also absorb some of the heat produced. In this way, thermal degradation is avoided, which explains the enhancement of propylene polymerization rate observed in ‘typical’ semibatch polymerizations. A series of runs where the precatalyst was heated at different temperatures clearly demonstrated that overheating the catalyst leads to thermal deactivation.

DSC analysis of the resulting polymers reveals that mineral oil provokes a decrease in crystallization temperature. A series of mixtures of an iPP homopolymer with the oil normally used for catalyst dosing were carried out, and it was found that the crystallization temperature of iPP can decrease to as low as 70 °C when the oil/iPP ratio is high enough. This absence of crystallinity during initial instants of life of the particles explains the better morphology observed by different patents and in ‘typical’ semibatch polymerizations when mineral oil is present. Another consequence is that the solubility of propylene is enhanced due to polymer swelling, a higher amorphous fraction and the co-solubility effect due to mineral oil. This provokes a further enhancement of the polymerization rate in the gas phase polymerization of propylene. A higher solubility of propylene elucidates why activity is double when precatalyst is injected wet as compared to dry-injected when prepolymerization is done in both cases.

Slurry phase polymerizations can be considered as a scale-up of “wet injection”. Build-up type profiles for slurry phase polymerizations showed that reaction started in a more gradual fashion. Build-up type profiles take place in slurry polymerizations because mass transfer is limited by the rate at which propylene is solubilized in the liquid hydrocarbon (heptane). These powders presented high bulk densities, like those resulting from wet injection. All these factors helped us to understand wet-injection, since the process which catalyst particles undergo during slurry phase polymerizations is related.

## 2.5 References

1. Petrochemical Analysis: Global Market Reports - Platts. Available at: <http://www.platts.com/products/petchem-analytics-global-polyolefins-outlook>. (Accessed: 28th October 2015)
2. Samson, J. J. C., van Middelkoop, B., Weickert, G. & Westerterp, K. R. Gas-phase polymerization of propylene with a highly active ziegler-natta catalyst. *AIChE J.* **45**, 1548–1558 (1999).

3. Spitz, R., Bobichon, C. & Guyot, A. Synthesis of polypropylene with improved MgCl<sub>2</sub>-supported Ziegler-Natta catalysts, including silane compounds as external bases. *Makromol. Chem.* **190**, 707–716 (1989).
4. Guastalla, G. & Giannini, U. The influence of hydrogen on the polymerization of propylene and ethylene with an MgCl<sub>2</sub> supported catalyst. *Makromol. Chem. Rapid Commun.* **4**, 519–527 (1983).
5. Floyd, S., Choi, K. Y., Taylor, T. W. & Ray, W. H. Polymerization of olefins through heterogeneous catalysis. III. Polymer particle modelling with an analysis of intraparticle heat and mass transfer effects. *J. Appl. Polym. Sci.* **32**, 2935–2960 (1986).
6. Hutchinson, R. A. & Ray, W. H. Polymerization of olefins through heterogeneous catalysis. VII. Particle ignition and extinction phenomena. *J. Appl. Polym. Sci.* **34**, 657–676 (1987).
7. Kimberley, B., Lacane, G. & Mastroianni, S. *Polymerisation Process*. (2005).
8. Daire, E. & Speakman, J. G. *Gas phase olefin polymerization process*. (Google Patents, 1994).
9. Hassan Nejad, M., Ferrari, P., Pennini, G. & Cecchin, G. Ethylene homo- and copolymerization over MgCl<sub>2</sub>-TiCl<sub>4</sub> catalysts: Polymerization kinetics and polymer particle morphology. *J. Appl. Polym. Sci.* **108**, 3388–3402 (2008).
10. Ruff, M. & Paulik, C. Controlling Polyolefin Properties by In-Reactor Blending: 2. Particle Design. *Macromol. React. Eng.* **7**, 71–83 (2013).
11. Pater, J. T., Weickert, G., Loos, J. & van Swaaij, W. P. High precision prepolymerization of propylene at extremely low reaction rates—kinetics and morphology. *Chem. Eng. Sci.* **56**, 4107–4120 (2001).
12. Yiagopoulos, A., Yiannoulakis, H., Dimos, V. & Kiparissides, C. Heat and mass transfer phenomena during the early growth of a catalyst particle in gas-phase olefin polymerization : the effect of prepolymerization temperature and time. *Chem. Eng. Sci.* **56**, 3979–3995 (2001).
13. Soares, J. B. P. & McKenna, T. F. L. *Polyolefin Reaction Engineering*. (Wiley-

VCH, 2013).

14. Monji, M., Abedi, S., Pourmahdian, S. & Taromi, F. A. Effect of prepolymerization on propylene polymerization. *J. Appl. Polym. Sci.* **112**, 1863–1867 (2009).
15. Pater, J. T. M., Weickert, G. & Swaaij, W. P. M. V. Polymerization of liquid propylene with a fourth-generation Ziegler–Natta catalyst: Influence of temperature, hydrogen, monomer concentration, and prepolymerization method on powder morphology. *J. Appl. Polym. Sci.* **87**, 1421–1435 (2003).
16. Meier, G. B., Weickert, G. & Van Swaaij, W. P. M. Gas-phase polymerization of propylene: Reaction kinetics and molecular weight distribution. *J. Polym. Sci. Part Polym. Chem.* **39**, 500–513 (2001).
17. Kim, Y.-K., Lo, K. & Kim, I.-S. *Prepolymerization method of  $\alpha$ -olefin*. (Google Patents, 2005).
18. Peters, E. F. *Catalyst feeding system*. (Google Patents, 1986).
19. Primol 352. Available at: [http://www.exxonmobil.com/Denmark-English/Specialties/PDS/GLXXENSPCEMPrimol\\_352.aspx](http://www.exxonmobil.com/Denmark-English/Specialties/PDS/GLXXENSPCEMPrimol_352.aspx). (Accessed: 30th July 2015)
20. Tioni, E., Spitz, R., Broyer, J. P., Monteil, V. & McKenna, T. Packed-bed reactor for short time gas phase olefin polymerization: Heat transfer study and reactor optimization. *AIChE J.* **58**, 256–267 (2012).
21. Tioni, E., Broyer, J. P., Monteil, V. & McKenna, T. Influence of Reaction Conditions on Catalyst Behavior during the Early Stages of Gas Phase Ethylene Homo- and Copolymerization. *Ind. Eng. Chem. Res.* **51**, 14673–14684 (2012).
22. Silva, F. M. *et al.* Investigation of Catalyst Fragmentation in Gas-Phase Olefin Polymerisation: A Novel Short Stop Reactor. *Macromol. Rapid Commun.* **26**, 1846–1853 (2005).
23. Machado, F., Lima, E. L., Pinto, J. C. & McKenna, T. F. Evaluation of the Initial Stages of Gas-Phase Ethylene Polymerizations with a SiO<sub>2</sub>-Supported Ziegler–Natta Catalyst. *Macromol. React. Eng.* **3**, 47–57 (2009).

24. Machado, F., Lima, E. L., Pinto, J. C. & McKenna, T. F. An experimental study on the early stages of gas-phase olefin polymerizations using supported Ziegler-Natta and metallocene catalysts. *Polym. Eng. Sci.* **51**, 302–310 (2011).
25. Olalla, B., Broyer, J.-P. & McKenna, T. F. L. Heat Transfer and Nascent Polymerisation of Olefins on Supported Catalysts. *Macromol. Symp.* **271**, 1–7 (2008).
26. Redlich, O. & Kwong, J. N. S. On the Thermodynamics of Solutions. V. An Equation of State. Fugacities of Gaseous Solutions. *Chem. Rev.* **44**, 233–244 (1949).
27. Bu, H.-S., Cheng, S. Z. D. & Wunderlich, B. Addendum to the thermal properties of polypropylene. *Makromol. Chem. Rapid Commun.* **9**, 75–77 (1988).
28. Masson, P., Llauro-darricades, M.-F., Spitz, R. & Cheng, H. N. A Study of the Dispersity of Catalytic Sites in Ethylene/Propylene Copolymerization Through Computer-Assisted <sup>13</sup>C NMR Analysis. *Int. J. Polym. Anal. Charact.* **2**, 379–393 (1996).
29. Sato, Y. *et al.* Vapor–liquid equilibrium ratios for hexane at infinite dilution in ethylene+impact polypropylene copolymer and propylene+impact polypropylene copolymer. *Fluid Phase Equilibria* **170**, 49–67 (2000).
30. Sato, Y., Yurugi, M., Yamabiki, T., Takishima, S. & Masuoka, H. Solubility of propylene in semicrystalline polypropylene. *J. Appl. Polym. Sci.* **79**, 1134–1143 (2001).
31. Dashti, A., Mazloumi, S. H., Bakhshi Ani, A. & Akbari, A. Experimental and Modeling of the Propene Solubility in the Heptane and Methylbenzene Solvents. *J. Chem. Eng. Data* **59**, 2258–2262 (2014).
32. Daftaribesheli, M. *Comparison of catalytic ethylene polymerization in slurry and gas phase.* (University of Twente [Host], 2009).
33. Wu, Q., Wang, H. & Lin, S. Gas-phase versus slurry copolymerization of ethylene with 1-butene over MgCl<sub>2</sub>-supported titanium catalysts after prepolymerization. *Macromol. Chem. Phys.* **197**, 155–163 (1996).
34. Cancelas, A. J., Monteil, V. & McKenna, T. F. L. Influence of Activation Conditions on the Gas Phase Polymerisation of Propylene. *Macromol. Symp.* **360**, 133–141 (2016).



### 3 Thermodynamics of Sorption in the Gas Phase Polymerization of Propylene

*The first part of this chapter has been published. The second part will be submitted for publication:*

Martins, A. R., Cancelas, A. J. & McKenna, T. F. L. A Study of the Gas Phase Polymerization of Propylene: The Impact of Catalyst Treatment, Injection Conditions and the Presence of Alkanes on Polymerization and Polymer Properties. *Macromol. React. Eng.* **11**, n/a-n/a (2017).

Cancelas, A. J., Plata, M. A., Bashir, M. A., Bartke, M., Monteil, V. & McKenna, T. F. L. Solubility and Diffusivity of Propylene, Ethylene, and Propylene–Ethylene mixtures in Polypropylene. To be submitted. (2017).

In the literature dealing with the polymerization of olefins over heterogeneous catalysts, it is generally recognized that the concentration of monomer in the active sites will determine the rate of reaction.<sup>1–3</sup> For the very first instants of polymerizations conducted in the gas phase, the monomer concentration in the active sites of the catalyst will be identical as in the bulk. However, as the polymerization proceeds, active sites will be surrounded with amorphous polymer. At this point, the rate of reaction will be function of two factors: (1) the concentration of monomer in the amorphous phase, and (2) the rate at which the monomer diffuses through the polymer particle.

As we saw in the general introduction, high impact polypropylene (hiPP) is prepared in (at least) two separate reaction steps. In the first step propylene is polymerized leading to the formation of an initial isotactic polypropylene matrix (iPP). In Chapter 2 (Page 58), we begin to elicit the impact of hydrocarbons on the physical properties of the nascent polymer (e.g. higher amorphous fraction, swelling...) and on the polymerization rate in the gas phase polymerization of propylene (mostly due to the co-solubility effect). Therefore, the inclusion of alkanes in the vapour phase might allow us to isolate their impact on the reaction rate, independently of the mass transfer issues that could eventually be associated if hydrocarbons would be in a liquid state.

While the gas phase in the first step is typically composed of propylene and hydrogen, during the second step propylene, ethylene and (optionally) hydrogen coexist in the reactor, which will form an ethylene–propylene rubber (EPR) elastomeric phase inside the still-reactive homopolymer particles. Therefore, understanding the way propylene or propylene/ethylene mixtures diffuse and precise knowledge of their solubilities in iPP/hiPP

is of great industrial importance, since they will ultimately determine the kinetics of each step of the process and the nature of the powders obtained.

Consequently, this chapter is divided in two subsections, since its focus is twofold: The first one is to investigate the impact of different gas phase compositions (varying the concentration of an alkane and hydrogen) on the kinetics of propylene homopolymerization and the properties of the final product. The second one is to study the solubility of propylene, ethylene and ethylene/propylene mixtures in iPP, and how they diffuse into the polymer powder under industrially relevant conditions.

### 3.1 The Impact of the Presence of Alkanes and Hydrogen on the Gas Phase Polymerization of Propylene

#### 3.1.1 Introduction

Along with polyethylene, polypropylene (iPP) is one of the most commercially important polyolefins in the world, and is one of the most versatile thermoplastic polymers available. Its wide-spread use is due in large part to the wide range of physical properties (low density, high stiffness, heat resistance, recyclability, etc.) and relatively low cost. Today's global PP production capacity is hovering near 60 million tonnes per year, and it is expected to reach nearly 75 million tonnes per year in 2022.<sup>4</sup> There is clearly a need to increase the productivity and space-time yield in existing processes, and to understand how to build more efficient units in the event that producers wish to install new capacity.

As shown in Chapter 2 (Page 53), thermal degradation severely affects the activity of propylene precatalysts. Industrially, a common approach to remove the heat in olefin polymerization is to inject a quench liquid into the reactor. In iPP the “quench” liquid is typically liquefied monomer, whereas it is an inert alkane (often referred to as an induced condensing agent, ICA) in the case of polyethylene. With the advent of copolymers of propylene and heavier monomers such as butene or hexene, it would also be possible to condense these monomers and inject them in liquid form in a gas phase process. If we want to understand how the injection of liquefied comonomers will influence the reaction rate, it is essential to be able to identify how these components influence solubility, transport, and other “physical” processes on the one hand, and impact they will have on the reaction on the other. For instance, Namkajorn *et al.*<sup>5</sup> observed that the instantaneous rate of ethylene polymerization was promoted in the presence of an ICA (they examined different isomers of pentane and hexane), and attributed it to the effect of the heavier hydrocarbon enhancing the local concentration of ethylene at the catalyst active sites. However, when the alkane is replaced by an analogous alkene, the effects are more complex.<sup>6</sup> Thermodynamically the alkenes and alkanes both enhance the rate of polymerisation of ethylene via co-solubility effect (the concentration of ethylene is higher in the presence of a heavier compound than it is with just ethylene). However, since the alkenes are also comonomers, they will also have a direct impact on the rate of reaction. It was found that at low concentrations they have a boosting on the rate of polymerization (the so-called comonomer effect), but they slowed the reaction down at higher concentrations despite the

co-solubility effect. We will therefore look at the thermodynamic impact of such components as a prelude to studying the impact of comonomers such as butene or hexene in the case of propylene polymerization. Since hydrocarbon solubility is higher in PP than in polyethylene (PE),<sup>4,5</sup> a greater impact over the instantaneous rate of propylene polymerization is expected.

Hydrogen is often used in olefin polymerization to control the molecular weight distribution, but it also has an activating effect on the reaction rate. Most olefin polymerization catalysts are highly regio-selective, favoring 1-2 insertions of propylene molecules. However, occasional 2,1 insertions give rise to “dormant sites”, often referred this way because of its lower reactivity towards further insertion. Several authors suggested that the activating effect of hydrogen can be ascribed to regeneration of the active sites following chain transfer with hydrogen at the dormant 2,1-inserted sites.<sup>7-10</sup> Therefore, increasing the hydrogen concentration in the reactor will lead to an increase in the rate of polymerization for PP and to a decrease in the average molecular weight. It has been shown that heavier components can influence the way hydrogen is absorbed in PE,<sup>5</sup> so we will also investigate this effect for propylene polymerization.

### 3.1.2 Experimental Section

#### 3.1.2.1 Chemicals

Commercial fourth generation  $MgCl_2$  supported titanium Ziegler-Natta with a titanium content of 2.8 % was used for polymerization. Its particle size distribution (PSD) was shown in the previous chapter, in Figure 2.1 at Page 36 (Precatalyst “B”). The B precatalyst has a broad distribution with a particle average size of 10.6  $\mu m$ . Iso-hexane with a minimum purity of 99% was obtained from Sigma-Aldrich (France). Triethylaluminium (TEA, Witco, Germany) was used as cocatalyst and scavenger at 1 M dilution in heptane. Dicyclopentyl dimethoxysilane (DCPDMS) was used as external electron donor, in 0.42 M solution in heptane. Two inert injection materials were used to suspend the catalyst: (1) sodium chloride (common coarse NaCl salt) with purity of 99.5% obtained from Acros Organics, France; and (2) Primol 352,<sup>11</sup> a medicinal grade white mineral oil which is a mixture of Paraffinic and Naphthenic cuts (64:36 wt%) often used as a plasticizer for food packaging and precatalyst carrier. It was bought from Fisher Scientific and its main properties were summarized in Table 2.1 (Chapter 2, Page 37). The salt was dried under

vacuum for 5 h at 200 °C to eliminate all the traces of water before use in order. Mineral oil and iso-hexane were degassed almost frozen under vacuum, to eliminate any trace of oxygen and then kept under argon atmosphere at room temperature, contacted with zeolite molecular sieves (type 3A) 24 h before use. The heptane was pre-treated on 3 Å molecular sieves before use.

Propylene with minimum purity of 99.5% and hydrogen with minimum purity of 99.99% were purchased from Air Liquide (France). The propylene was purified with a three-stage system of columns before use: a first column filled with BASF R3-16 catalyst (CuO on alumina), a second column filled with molecular sieves (13X, 3A, Sigma-Aldrich), and a third column filled with Selexsorb COS (Alcoa). Argon with minimum purity of 99.5% was obtained from Air Liquide, France, and was used in order to keep the reaction environment free of oxygen.

### 3.1.2.2 Polymerization Methods

Regardless of the method of injection, the precatalyst was prepared in a glovebox (Jacomex, France) under argon atmosphere. When the salt was used to inject the precatalyst, 25 mg of the latter were mixed with 10 grams of coarse NaCl in a 100 cm<sup>3</sup> cartridge injector (from now on this is referred to as “dry injection”). For the liquid suspension system, the mineral oil–precatalyst mixture was kept in suspension by permanent agitation, and a positive displacement micropipette was used to take the 250 µl, corresponding to 15 mg of precatalyst, and inject them into the turbosphere (From now on this method will be referred as “wet injection”). The precatalyst was not pre-activated before injection to the turbosphere reactor in either case.

Polymerization runs were carried out in a spherical laboratory scale 2.5 L semi-batch reactor. The detailed reactor set-up has been described in the previous chapter (Page 37). The reactor was purified by heating it up to 70 °C with at least three argon-vacuum cycles. When the system reached the desired initial temperature, the TEA/heptane mixture was injected into the reactor for scavenging all the remaining traces of water while also acting as the cocatalyst and agitation (300 rpm) was started. Subsequently, ≈5 min after the first injection, the donor/heptane mixture and (if needed) the specific amount of iso-hexane were injected under an argon stream. This was followed by the wet or dry precatalyst suspension injection. Note that the catalyst was activated under argon atmosphere, and thus,

precontacting was done (see Appendix B for more information about the impact that precontacting has). Then the reaction was started by pressurization with a mixture of monomer–hydrogen in the desired ratio. The Al/Ti and Si/Ti ratios were 190 and 10, correspondingly.

Recovery of the resulting polymer and prepolymerization (if applicable) were done as explained in the previous chapter (Page 37).

As an indication of the degree of control and the dynamics of a typical polymerization experiment, gas phase and bath temperatures (main axis) and reactor pressure (secondary axis) are shown in Figure 3.1. Note that the sudden pressure increase at about half of the prepolymerization is due to hydrogen injection.

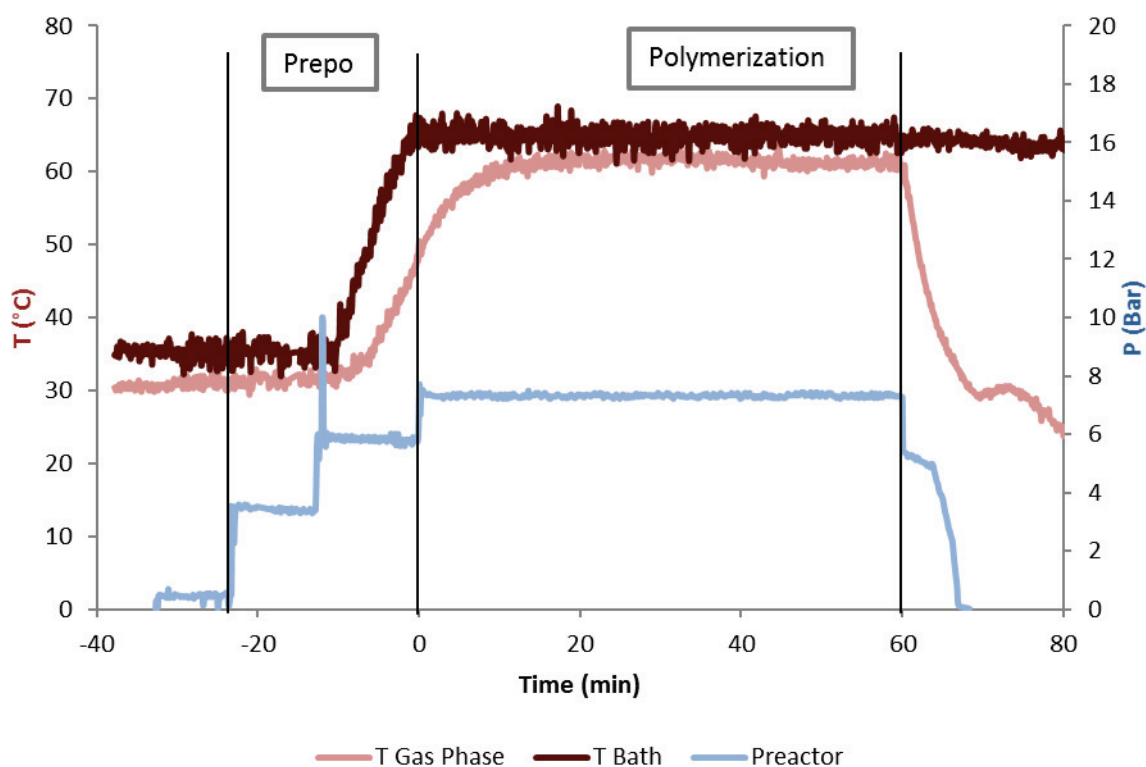


**Figure 3.1.** Gas phase and bath temperatures (main axis) and reactor pressure (secondary axis) during a representative run with prepolymerization (B40-100-4%). Note that reactor wall temperature can be considered equal to bath temperature.

As can be seen in Figure 3.1, there is an  $\approx 5$  °C difference between gas phase and bath temperature. Propylene expansion causes this difference as it enters the reactor.

To study the effect of iso-hexane in gas phase propylene polymerization, no liquid hexane

should be present in the reactor during the polymerization phase. Therefore, the desired amount of liquid iso-hexane was injected only once prepolymerization was finished and reactor temperature had reached full reaction conditions. Although it was liquid at room temperature, at full reaction conditions, the tiny amounts of added hexane are fully vaporized

### 3.1.2.3 Polymer Characterization

The molecular weight distribution (MWD) of polymer samples was characterized as explained in Chapter 2 (Page 41).

### 3.1.2.4 List of Experiments

**Table 3.1.** Summary of the polymerization conditions for the reactions designed and performed in the current study. All polymerizations were done at 343.2 K.

Run	Partial Pressure (bar)				Pre-po	Precatalyst Suspension
	Propylene	iso-Hexane	Hydrogen	Argon		
B40-0-2	7.50	0.00	0.15	1.00	Yes	Wet
B40-25-2	7.50	0.33	0.15	1.00	Yes	Wet
B40-50-2	7.50	0.67	0.15	1.00	Yes	Wet
B40-75-2	7.50	1.00	0.15	1.00	Yes	Wet
B40-100-2	7.50	1.33	0.15	1.00	Yes	Wet
B70-0-2	7.50	0.00	0.15	1.00	No	Wet
B70-25-2	7.50	0.33	0.15	1.00	No	Wet
B70-50-2	7.50	0.67	0.15	1.00	No	Wet
B70-75-2	7.50	1.00	0.15	1.00	No	Wet
B70-100-2	7.50	1.33	0.15	1.00	No	Wet
B40-0-0	7.50	0.00	0.00	1.00	Yes	Wet
B40-100-0	7.50	1.33	0.00	1.00	Yes	Wet
B40-0-1	7.50	0.00	0.08	1.00	Yes	Wet
B40-100-1	7.50	1.33	0.08	1.00	Yes	Wet
B40-0-4	7.50	0.00	0.30	1.00	Yes	Wet
B40-100-4	7.50	1.33	0.30	1.00	Yes	Wet
BDry-0-2	7.50	0.00	0.15	1.00	Yes	Dry
BDry-100-2	7.50	1.33	0.15	1.00	Yes	Dry

The list of the experiments performed in the current study with the conditions and partial pressures of the components present in the gas phase is summarized in Table 3.1. The name

of the experiments is generally given by “B00-Y-Z”: where “B” is the catalyst used, “00” is the temperature the catalyst is injected at (“40” or “Dry” when prepolymerization was performed and “70” when it was not) and the type of injection (“40” or “70” for wet injection and “Dry” for dry injection), “Y” is the quantity of iso-hexane relative to its saturation pressure at reaction conditions in percentage (i.e., 100% refers to a partial pressure of 1.33 of iso-hexane); and finally, “Z” is the hydrogen concentration.

### 3.1.2.5 Kinetic Model

The rate of polymerization can be described using Equation 2.1 (Page 42), described in Chapter 2. This helps one to quantify the complex physical and chemical effects on the performance of the catalyst without specifically using a multisite model for ZN catalysts. All reaction data were fitted using Equation 2.1 with 1<sup>st</sup> order deactivation for single site catalyst.

The monomer concentration in the amorphous polymer at the active sites ( $C_m$ ) is an input of Equation 2.1. For each set of polymerization conditions shown in Table 3.1, it was calculated with the Sanchez–Lacombe equation of state (SL-EoS).<sup>12</sup> The description of this EoS can be found in Appendix A (Page 169). First, two binary systems have to be studied to accurately determine the solubility of different propylene-hexane mixtures in iPP at 70 °C (343.2 K): Propylene- iPP and hexane-iPP. These two systems were experimentally studied by Sato *et al.*<sup>13</sup> We fitted our model to their empirical data, and the resulting fitted binary interaction parameters for each binary system are shown in Table 3.2.

**Table 3.2.** Binary interaction parameters ( $k_{ij}$ ) implemented in the ternary Sanchez–Lacombe EoS.

Ternary System	343,2 K
<i>Propylene (1) - Hexane (2) -iPP (3)</i>	
$k_{12}$	0
$k_{13}$	0,021
$k_{23}$	0,033

Although Sato *et al.*<sup>13</sup> studied the system hexane-hiPP and not hexane-iPP, here, due to the small variation of gas solubilities in these two polymers, this approximation was assumed to be valid.

The binary interaction parameters shown in Table 3.2 were implemented in the ternary

system and the solubility of propylene in iPP in the presence of hexane was determined. Figure 3.2 compares the propylene concentration in iPP with propylene concentration in iPP when different partial pressures of hexane are present in the system.

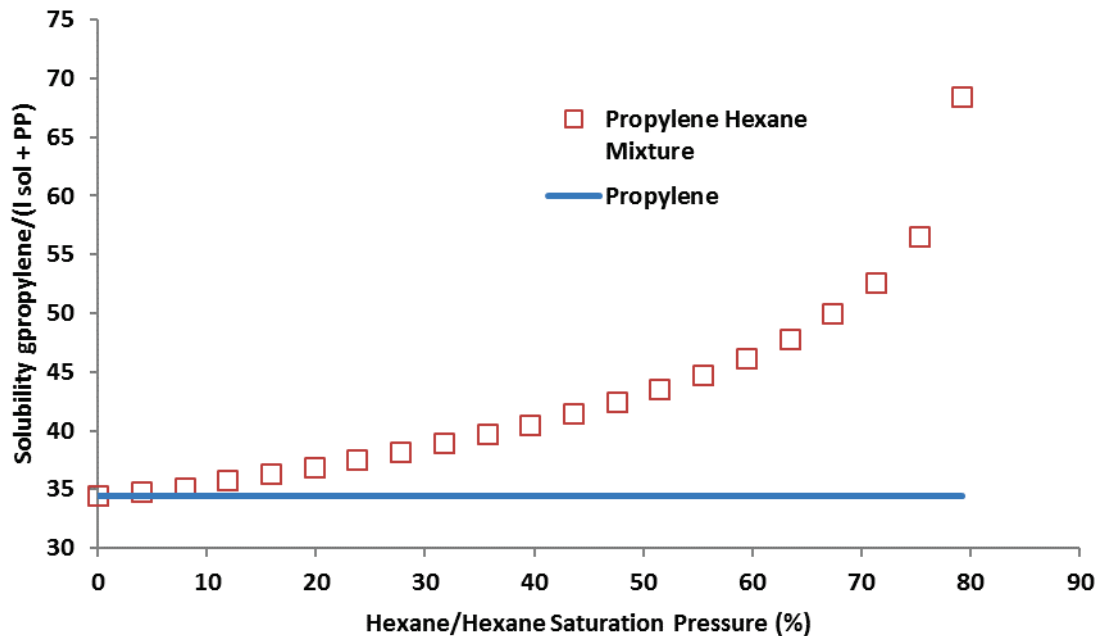


**Figure 3.2.** Propylene solubility in amorphous PP with the presence (red) and the absence (blue) of hexane in the system for every relative pressure of gas hexane to its saturation pressure for the conditions studied, 343.2 K and 7.5 bar of propylene.

No value is shown at 100% because the dew point of hexane propylene mixture is 343.2K, and the mixture starts to liquefy when hexane is at 80% of its saturation pressure. As we see in Figure 3.2, the concentration of propylene in PP increases dramatically as the dew point of the hexane–propylene mixture is approached.

### 3.1.3 Results and Discussion

The instantaneous rate of propylene polymerization is calculated from the rate of pressure drop in the propylene feed ballast. To ensure that the results were reproducible, all polymerizations were repeated at least twice under a given set of operating conditions. The influence of hexane pressure and hydrogen on the polymerization kinetics has been studied by using the described kinetic model from Equation 2.1 (Page 42). Fitting is done by minimizing the deviations between the experimental and model curves. The values obtained for the activation constant  $K_a$ , the deactivation constant  $k_d$ , and the kinetic parameter  $k_p \cdot C_0$  are used to analyze the various process parameters in a qualitative manner. Table 3.3 displays a summary of the semi-batch runs, side by side their respective process

conditions and found kinetic parameters. Note that in the case prepolymerization was performed, the beginning of the reaction, time  $t = 0$  is defined as the moment where the reactor temperature reached 50 °C (during the heat up from 40 to 70 °C). The reason for this choice is that experience showed that the reaction rate began to increase quickly near this temperature for all runs. Therefore, at this point pressure was increased to 7.5 bar and kinetic measurements were started. This was a way to ensure that all reactions after prepolymerization started at an equivalent time, ensuring the lowest possible level of catalyst deactivation and a similar amount of prepolymerization yield. Although values of  $K_a$  were calculated for all runs (and were constant at approximately  $8 \times 10^{-3}$  to  $10 \times 10^{-3} \text{ s}^{-1}$  for all prepolymerization runs) only those found for runs without prepolymerization are reported in Table 3.3 since conditions varied during the initial phase of the prepolymerization runs.

**Table 3.3.** Summary of the experiments: Kinetic constants and monomer concentration.

RUN	$k_p \cdot C_0$ ( $\text{L} \cdot \text{g}_{\text{cat}}^{-1} \cdot \text{h}^{-1}$ )	$K_a \cdot 10^3$ ( $\text{s}^{-1}$ )	$k_d \cdot 10^4$ ( $\text{s}^{-1}$ )	$C_m$ ( $\text{g} \cdot \text{L}^{-1}$ )
B40-0-2%	125	-	2	34
B40-25-2%	126	-	2	38
B40-50-2%	161	-	2	44
B40-75-2%	127	-	2	57
B40-100-2%	119	-	2	68
B70-0-2%	97	28	2	34
B70-25-2%	91	75	2	38
B70-50-2%	91	65	2	44
B70-75-2%	106	50	3	57
B70-100-2%	98	100	3	68
B40-0-0%	65	-	2	34
B40-100-0%	48	-	2	68
B40-0-1%	93	-	4	34
B40-100-1%	112	-	3	68
B40-0-4%	118	-	2	34
B40-100-4%	133	-	3	68
BDry-0-2%	67	-	3	34
BDry-100-2%	30	-	4	68

Figure 3.3 demonstrates the effect of the partial pressure of iso-hexane in the range of 0 bar

(B70-0-2 and B40-0-2), 0.33 bar (B70-25-2 and B40-25-2), 0.67 bar (B70-50-2 and B40-50-2), 1.00 bar (B70-75-2 and B40-75-2), and 1.33 bar (B70-100-2 and B40-100-2) on the instantaneous rate of propylene polymerization at 70 °C using supported catalyst for both non-prepolymerized and prepolymerized runs. Note that the gas phase composition of the last two experiments (B70-100-2 and B40-100-2) is such that the mixture is at a temperature slightly below its dew point so it is possible that small amounts of liquid alkane are present in the reactor.

As shown in Figure 3.3, the instantaneous rate of propylene polymerization increases in the presence of iso-hexane, therefore supporting the idea that heavier (or more soluble) components such as alkanes increase the solubility of propylene in PP, as has been seen for PE.<sup>5</sup> If one looks back at Table 3.3, it can be seen that the estimate of the value of  $k_p \cdot C_0$  is not significantly different from run to run if the correct monomer concentration is used during the parameter estimation step. In other words, the enhanced solubility of propylene is enough to explain the increase in the observed polymerization rates. It also points out the importance of correctly accounting for the thermodynamic conditions in the reactor when estimating kinetic constants. As an example, if we had used 34 g L<sup>-1</sup> as the concentration, then  $k_p \cdot C_0$  would increase with increasing hexane content, which makes no physical sense. This will be crucial when one wishes to make copolymers of propylene and other  $\alpha$ -olefins, since these components can influence the concentration at the active sites.<sup>14</sup>

At this point is important to remember that in a gas phase mixture of 1.05 bar of iso-hexane and 7.5 bar of propylene, the dew point is reached at 343.2 K. The small quantity of heptane injected along TEA and ELB, would lower it slightly more. This means that experiments B70-75-2, B70-100-2, B40-75-2, and B40-100-2 were done very close to (or at) the dew point of propylene–hexane–heptane mixture. It is therefore not unexpected that we observe the same enhancement in propylene concentration in PP.

Figure 3.4 shows the effect of different hydrogen concentrations in the gas-phase composition as 0% (B40-0-0 and B40-100-0), 1% (B40-0-1 and B40-100-1), 2% (B40-0-2 and B40-100-2), and 4% (B40-0-4 and B40-100-4) on the instantaneous rate of propylene polymerization at 70°C using supported catalyst prepolymerized, without and with iso-hexane present in the gas phase.

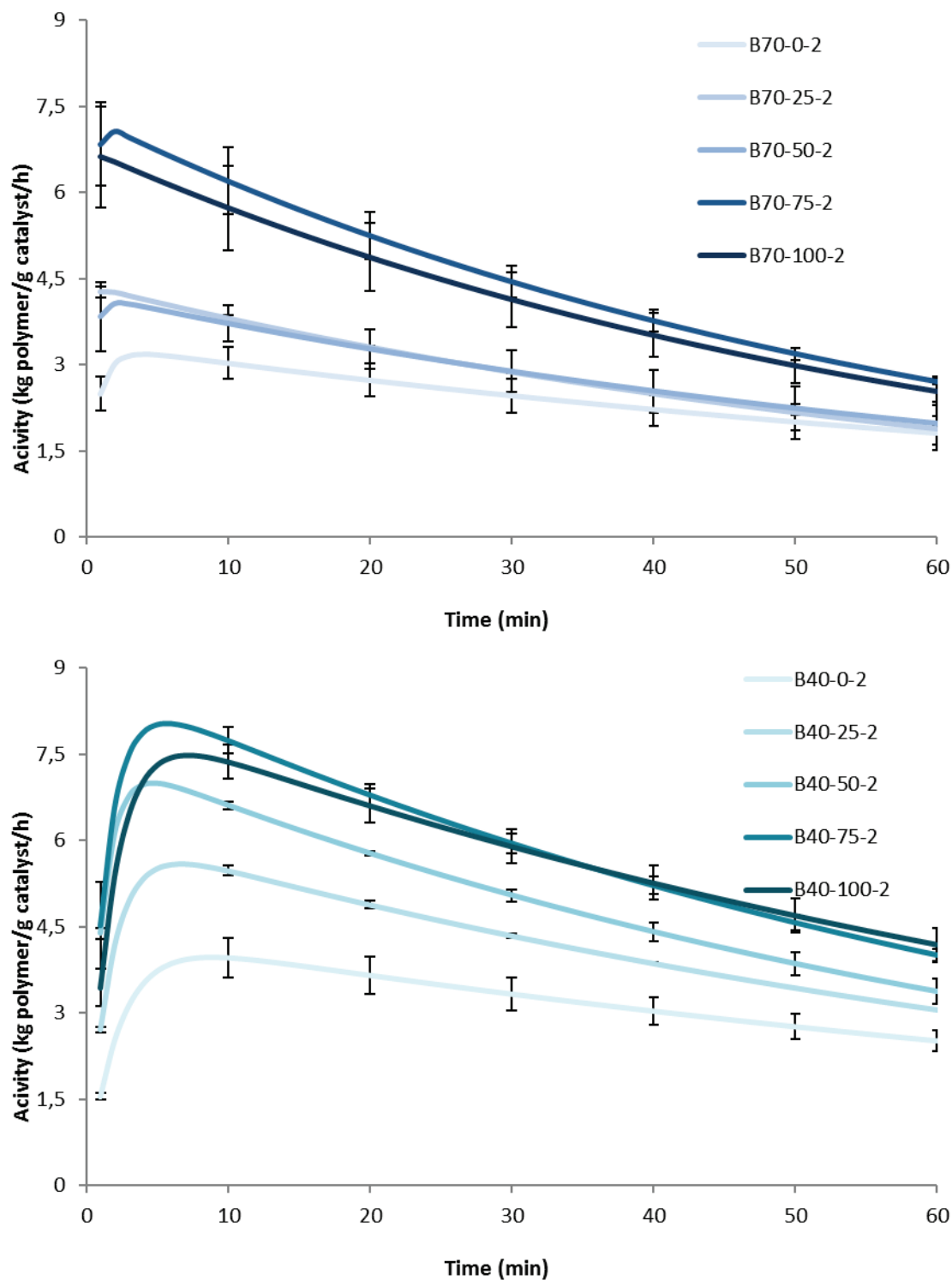


**Figure 3.3.** Instantaneous rate of propylene polymerization at 70 °C in the presence of 0.0, 0.33, 0.67, 1.00 and 1.33 bar of partial pressure of iso-hexane in the reaction environment with a non-prepolymerized supported catalyst and prepolymerized, corresponding to upper and lower graphs, respectively.

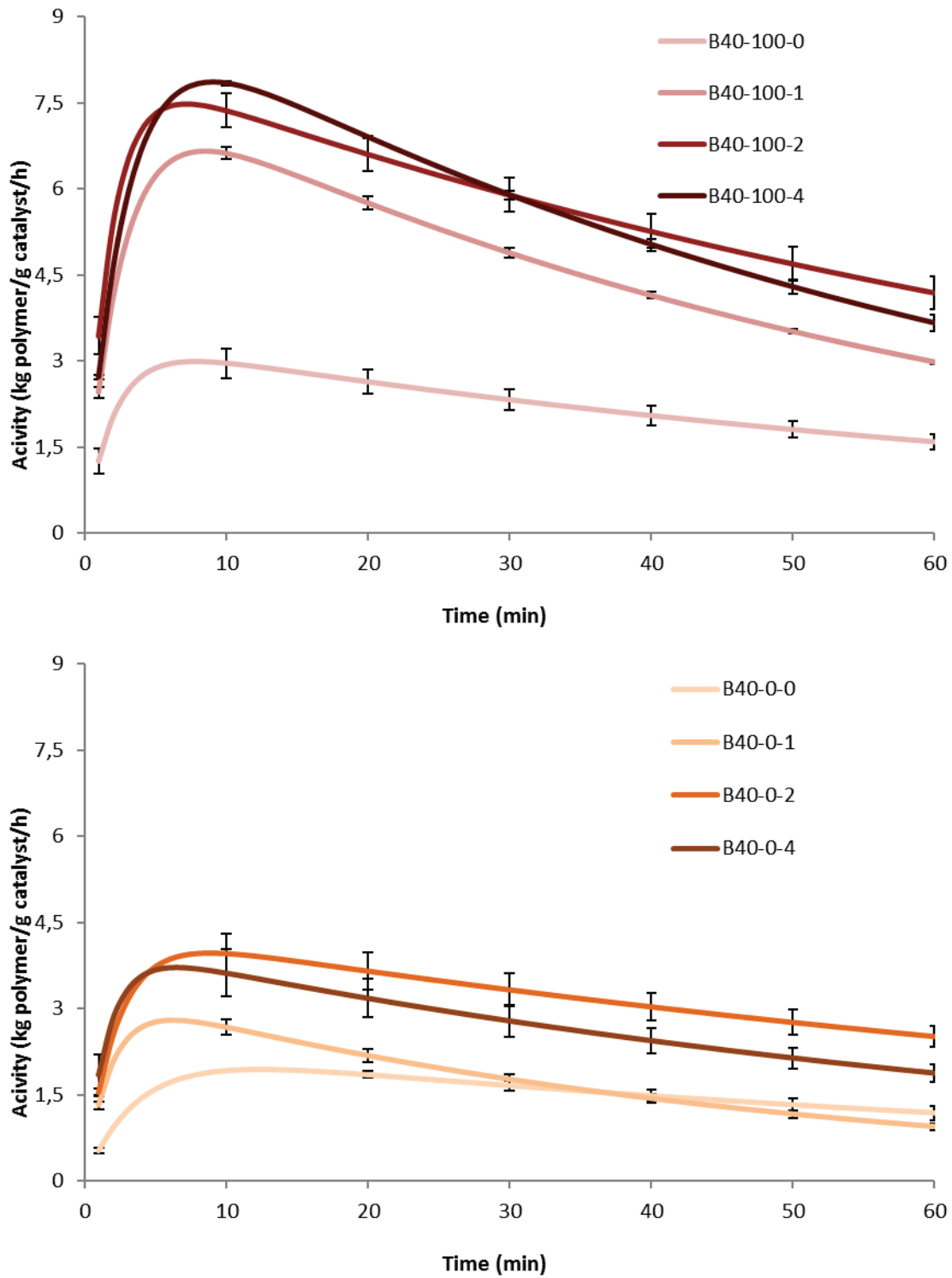


**Figure 3.4.** Instantaneous rate of propylene polymerization at 70 °C in the presence of 0, 1, 2 and 4 % of hydrogen in the reaction environment with a prepolymerized supported catalyst with 1.33 bar of iso-hexane (upper graph) and without iso-hexane (lower graph).

Increasing the concentration of hydrogen to a certain level can lead to an increase in the reaction rate.<sup>7-10</sup> As explained in the introduction, this effect is believed to be caused by the regeneration of the dormant sites following chain transfer with hydrogen. From Figure

3.4 it appears that, at least for the catalyst used in this study, the optimum hydrogen concentration in terms of activity for the conditions studied here is approximately 2% when no hexane is present in the gas phase. Before and beyond that point lower activities were obtained. However, the impact of adding iso-hexane to the reactor on the hydrogen effect seems quite limited. The ratio of the maximum rate of B40-100-2 to B40-100-0 is approximately 2.5 (i.e., the hexane increases the rate by about 2.5 times), and the same ratio of the maximum rates of B40-0-2 to B40-0-0 is also very close to 2.5. Thus, at the optimal concentration of around 2% hydrogen in the gas phase, adding hexane increases the rate but does not seem to change the hydrogen chemical effect on the catalyst. This is further reinforced by looking at the results of the molecular weight measurements shown in Table 3.4. Here we can see that changing the concentration of hexane for the wet mode of injection and fixed hydrogen concentration has no measurable influence on the average molecular weight for catalyst B. This suggests that the relative concentration of hydrogen to propylene in the active sites remains constant, independently of the alkane concentration in the gas phase. In addition, the absence of a prepolymerization step does not seem to have a major impact on the molecular weight distribution, even though it does enhance the rate via a co-solubility effect. The only time that the presence of hexane seems to influence the molecular weight is when the catalyst is injected dry.

**Table 3.4.** Number average molecular weight ( $M_n$ ), weight average molecular weight ( $M_w$ ) and polydispersity ( $M_w/M_n$ ) of every sample synthesized.

RUN	$M_n$ (kDa)	$M_w$ (kDa)	$M_w/M_n$
B40-0-2%	57 / 72	263 / 304	4,6 / 4,2
B40-25-2%	76 / 76	316 / 305	4,2 / 4
B40-50-2%	55 / 44	307 / 353	5,6 / 8
B40-75-2%	76 / 75	289 / 284	3,8 / 3,8
B40-100-2%	59 / 60	278 / 266	4,7 / 4,4
B70-0-2%	58 / 55	262 / 250	4,5 / 4,5
B70-25-2%	72 / 68	296 / 301	4,1 / 4,4
B70-50-2%	85 / 73	365 / 389	4,3 / 5,3
B70-75-2%	67 / 76	253 / 312	3,8 / 4,1
B70-100-2%	64 / 73	278 / 290	4,3 / 4,0
B40-0-0%	75 / 114	694 / 752	9,3 / 6,6
B40-100-0%	113 / 75	603 / 705	5,3 / 9,4
B40-0-1%	82 / 77	381 / 366	4,6 / 4,8
B40-100-1%	78 / 79	298 / 298	3,8 / 3,8
B40-0-4%	47 / 63	250 / 267	5,3 / 4,2

B40-100-4%	78 / 75	308 / 295	3,9 / 3,9
BDry-0-2%	35 / 44	201 / 211	5,7 / 4,8
BDry-100-2%	64 / 89	342 / 384	5,3 / 4,3

When iso-hexane was present in the reactor (BDry-100-2) the iPP chains were almost 2 times longer on average than polymers done without it (BDry-0-2). Definitely, wetting the precatalyst with mineral oil<sup>11</sup> prior to injection has a great effect not only in the morphology of the polymer, as shown in the previous chapter, but also on its intrinsic properties.

#### 3.1.4 Conclusions for Objective 1: Impact of alkanes and hydrogen

Propylene was polymerized in the gas phase with a supported Ziegler–Natta catalyst. The composition of the gas phase has been systematically varied to investigate its influence on the experimentally measured reaction rates, which were fitted with a kinetic model. The monomer concentration in the polymer was calculated with the Sanchez–Lacombe Equation of State.

In a propylene gas phase process, injection of heavier hydrocarbons leads to a more than twofold increase in the polymerization rate. This effect is quantified and attributed to the enhancement of the solubility of propylene in the active sites, caused by the co-solubility effect ascribed to the studied multicomponent gases/polymer mixture system. However, the relative concentration of hydrogen to propylene seems to be unaffected.

## 3.2 Solubility and Diffusivity of Propylene, Ethylene, and Propylene–Ethylene mixtures in Polypropylene

### 3.2.1 Introduction

Isotactic Polypropylene (iPP) homopolymers have higher stiffness than PE, but also limited toughness, especially at lower temperatures. This can be overcome incorporating an elastomeric copolymer of ethylene and propylene, resulting in high impact polypropylene (hiPP). This second step is always carried out in the vapor phase, where an ethylene-propylene mixture dissolves into the iPP particles and diffuses to the still active sites, to polymerize EPR (Ethylene Propylene Rubber). Thus, a multicomponent mixture of ethylene, propylene and iPP/hiPP (a ternary system) coexists in the reactor. To develop a full understanding of the kinetics of this process, and enhance the quality of the produced resins, precise knowledge of the concurrent solubility and diffusivity of ethylene and propylene in polymer (iPP and hiPP) phase is needed. Therefore, experimental data at industrially relevant conditions of mixtures of these monomers would be quite useful.

However, despite the industrial importance of phase equilibria of mixtures of these monomers, only Yoon *et al.*<sup>15</sup> have experimentally studied it. As shown in Table 3.5, they measured the co-solubility of ethylene/propylene mixture in poly(ethylene-co-propylene) copolymer containing 48.4 mol% of ethylene at 50, 70, and 90 °C temperatures in pressure range of 0.3 – 1.5 bar. They discovered that the mixture solubility was higher than the corresponding ethylene or propylene solubility in the polymer. While their results are interesting, these conditions are far from those employed industrially. As can be seen in Table 3.5, the range of working pressures used by Sato *et al.*<sup>13,16</sup> and Kröner and Bartke<sup>17</sup> was broader. Additionally, Sato *et al.*<sup>13,16</sup> used three types of polypropylenes: iPP, hiPP, and atactic polypropylene (aPP). However, they did not investigate ternary systems, and focused only on the phase equilibria of individual gases.

**Table 3.5.** Survey of experimental studies of sorption equilibria of ethylene, propylene, and ethylene-propylene gas mixtures in various kinds of polypropylene.

Authors		System	Conditions
Yoon <i>et al.</i> <sup>15</sup>	Ternary	Ethylene/Propylene - EP copolymer	50, 70, 90 °C; 0.3 - 1.5 bar
Sato <i>et al.</i> <sup>13</sup>	Binary	Propylene - iPP	50, 70, 90 °C; up to ~40 bar
	Binary	Ethylene - hiPP	50, 70, 90 °C; up to ~40 bar
	Binary	Propylene - hiPP	50, 70, 90 °C; up to ~40 bar
Sato <i>et al.</i> <sup>16</sup>	Binary	Propylene - aPP	50, 70, 90 °C; up to ~30 bar
	Binary	Propylene - iPP	50, 70, 90 °C; up to ~30 bar
Kröner <i>et al.</i> <sup>17</sup>	Binary	Propylene - iPP	70 °C; up to 25 bar
	Binary	Ethylene - iPP	70 °C; up to 25 bar

Solubility data of monomers in polymers at different conditions can be modelled using well-known equations of state (EoS). Among them, the lattice-fluid model of Sanchez and Lacombe (SL EoS),<sup>12</sup> has been shown to describe and predict the solubility of a gas phase (either as individual components or as a mixture of multiple) in amorphous polymer. For instance, Kanellopoulos *et al.*<sup>18</sup> fitted this theoretical model to available solubility measurements of different binary systems under various conditions of pressure and temperature with a single adjustable parameter,  $k_{ij}$ .

However, predicting behavior of multicomponent mixtures is more complex, partially because of the well-known co-solubility effect (i.e., for a mixture of solutes in polymer, the increase in the solubility of the lighter species due to the presence of the heavier one). Recently, Bashir *et al.*<sup>19</sup> extended the SL-EoS to successfully describe the solubility of two gas solute components in polyolefins, using two adjustable interaction parameters to account for the co-solubility phenomenon. The same approach will be used to describe the solubility of ethylene and propylene mixtures in iPP in the current work.

To the best of our knowledge, this is the first study investigating the equilibrium solubility of equimolar mixtures of ethylene-propylene in iPP close to industrially pertinent temperatures and pressures. SL-EoS was fitted to the experimentally obtained data of both binary systems studied (ethylene-iPP and propylene-iPP) using a single parameter,  $k_{ij}$  for each system. Subsequently, these two binary parameters were directly implemented in SL theoretical model for ternary systems and compared with the experimental results.

The diffusion of single gases and vapors in polymers has been the subject of a considerable number of studies.<sup>15,20–28</sup> However, those dealing with mixtures of gases or monomers are

scarce. For instance, Robeson and Smith<sup>29</sup> showed that the experimentally measured diffusivities of ethane–butane mixtures followed an exponential dependence with respect to the butane concentration. Pino *et al.*<sup>30</sup> studied the diffusion of mixtures of oxygen, carbon dioxide and nitrogen through films of polyethylene with different degrees and type of chain branching. Their results show that, in general, the presence of one gas can affect the diffusion and solubility of another. More recently, Freeman and co-workers,<sup>31</sup> investigated the diffusion of n-butane and methane mixtures in poly(dimethylsiloxane) (PDMS), and found that methane had a higher diffusivity and solubility in PDMS being mixed with n-butane than pure. Investigations of this kind are uncommon. In this sense, more experimental data dealing with the diffusion of mixtures of monomers in polymers would be useful, because of the importance of this subject for polyolefin industry. In this work, the sorption and desorption rates of ethylene/propylene mixtures in iPP are experimentally determined at appropriate conditions, and are compared to the respective diffusivities of the individual gases.

In the previous chapter, the influence of injecting the precatalyst suspended with coarse NaCl salt (dry) or with paraffinic oil (wet) over the resulting final iPP morphology was shown. The last objective of this section is to carry out sorption experiments of propylene in both homopolymer and heterophasic copolymers resulting from both injection methods, as an attempt to understand the impact that the initial iPP morphology has on the final hiPP powders.

### 3.2.2 Experimental Section

#### 3.2.2.1 Sorption Magnetic Balance

Solubility measurements were done in a high-pressure sorption magnetic balance (SMB). The setup is described in refs. [17,21,32] in more detail. A representation of its system is shown in Figure 3.5. The magnetic coupling of the balance allows an accuracy of 0.1 mg for weight measurements.

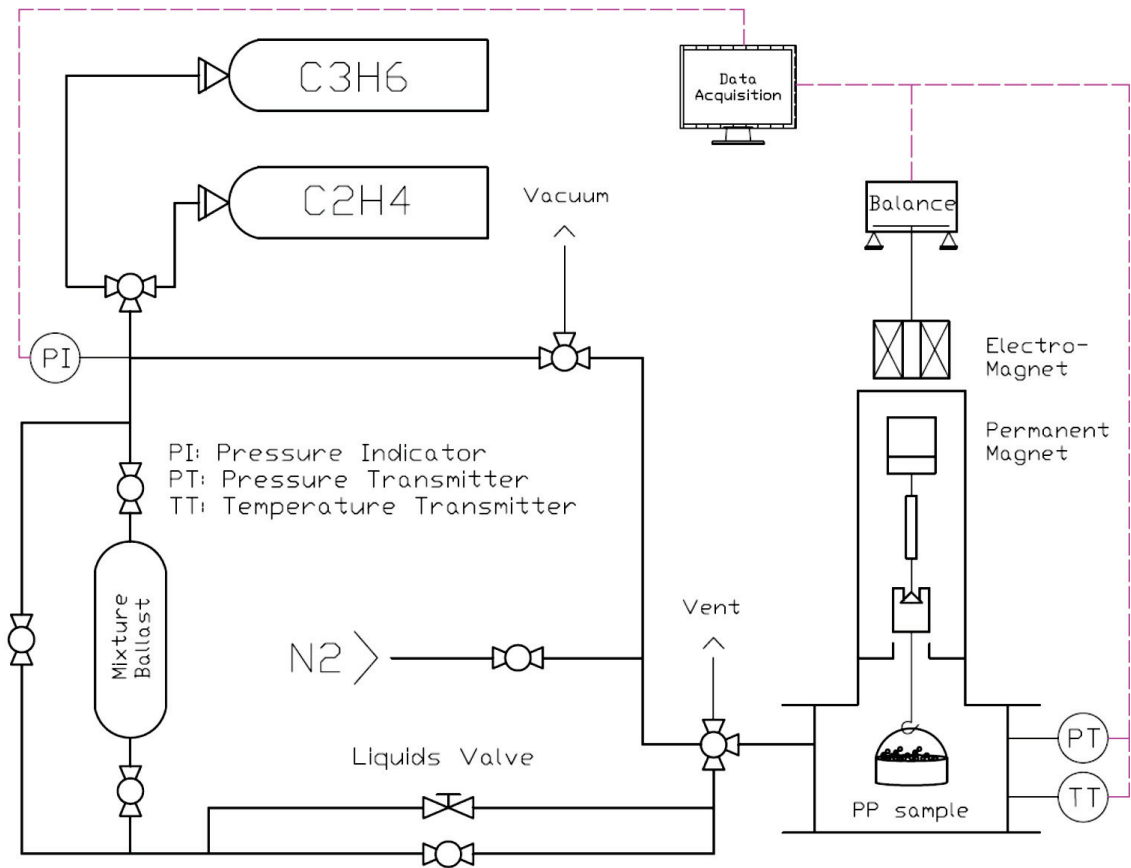


**Figure 3.5.** A schematic representation of the sorption magnetic balance system.

Between 1-2 grams of polymer particles are used for every sorption measurement. A sample is regenerated applying 39 mbar of vacuum for 20 minutes at the desired experimental temperature. The measurement is then started by increasing the pressure in the chamber with the monomer, or mixture of monomers, until the desired pressure is reached. The increase of gas densities results in greater buoyancy force acting on the sample and container. Therefore, weight readings were corrected following Equation 3.1.<sup>17</sup>

$$m_{corrected} = m_{reading} + \rho_{gas} \cdot (V_{container} + V_{polymer}) \quad 3.1$$

Gas densities of propylene, ethylene, and equimolar mixtures of ethylene and propylene at the temperatures and pressures of interest were described by a mathematical fit of a two parameter virial equation to literature data, for each time step. Weight readings include 1-2 g of polymer and mass of container (weighing basket and weighing hook), and as Equation 3.1 shows volume and mass of both should be precisely known. The volume of the container was determined by measuring its mass while increasing the pressure of N<sub>2</sub>, at constant temperature (e.g., at 50 °C). This results in a linear correlation between gas density

and measured mass with negative slope. The weight of the container decreases at higher gas densities because of the buoyancy effect, which is equal to the slope of the linear fit. The real mass is the y-intercept or the measured mass under vacuum.

However, the polymer volume was calculated with Equation 3.2 for each time step, since the volume of the polypropylene powder increases by the sorption process.

$$V_{polymer} = SW \cdot \left( \frac{\chi \cdot m_{polymer}}{\rho_c} + \frac{(1 - \chi) \cdot m_{polymer}}{\rho_a} \right) \quad 3.2$$

Where  $\rho_c$  and  $\rho_a$  are the densities of crystalline and amorphous iPP phases, considered equal to 0.95 and 0.85 g/cm<sup>3</sup>, respectively. <sup>35</sup>  $\chi$  is iPP crystallinity (assumed constant during solubility measurements), whose calculation is onwards explained.  $SW$  is the swelling behavior of polypropylene phase caused by the sorbed species, and it is calculated as a function of gas pressure, temperature and monomer using the SL EoS. The derivation of the model equations and solution methodology are described in detail in refs. [18,33,34] and in Appendix A. Table 3.6 shows the characteristic parameters used for theoretical calculations along their reference sources.

**Table 3.6.** Molecular characteristic parameters for Sanchez–Lacombe EoS

Substance	P* (Bar)	T* (K)	$\rho^*$ (Kg/m3)	Reference
Ethylene	3395	283	680	[18]
Propylene	3788	345,4	755	[16]
Polypropylene	3007	690,6	885,6	[16]

Bobak *et al.* <sup>36</sup> have measured iPP particles swelling by video microscopic techniques. They showed that swelling of polymer depends on the relative weight fraction of propylene sorbed in PP, and that it can be approximated by a simple linear expression (Equation 3.3). Our SL EoS calculations were compared to their experimental results. As figure shows for the conditions that prompted the highest degree of swelling (50 °C and propylene sorbed in iPP), both methods give similar swelling degrees.

$$SW = 1.7844 \cdot \frac{m_{sorbed}}{m_{polymer}} + 1 \quad 3.3$$

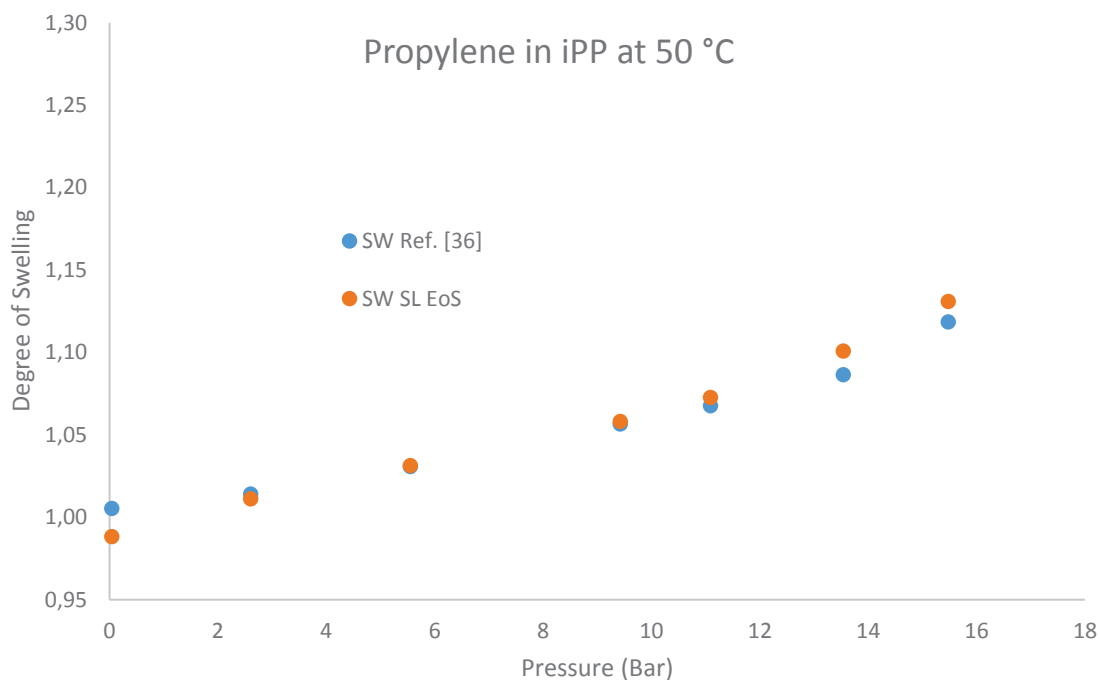


**Figure 3.6.** Degree of swelling as calculated with the SL EoS (binary interaction parameters were considered 0 for all calculations) and from the experimental correlation shown in ref. [36]

An example of the data obtained from the sorption magnetic balance is revealed in Figure 3.7. It shows the solubility of an equimolar mixture of ethylene and propylene in iPP particles at 50 °C as a function of time and pressure as this last one is lowered from 20 to 0 bar (a). The sorbed amounts displayed in this figure are already corrected for the buoyancy force. For every pressure studied, we can distinguish a transitional and an equilibrium state, dependent on (1) whether there is a differential of monomer concentration inside and outside polymer and on (2) the stabilization of temperature inside the chamber. Transitional data was used for diffusivity measurements (Page 105) and steady data for the solubility study. Every experimental point for the solubility study was calculated from the mean value of ~100 balance readings.

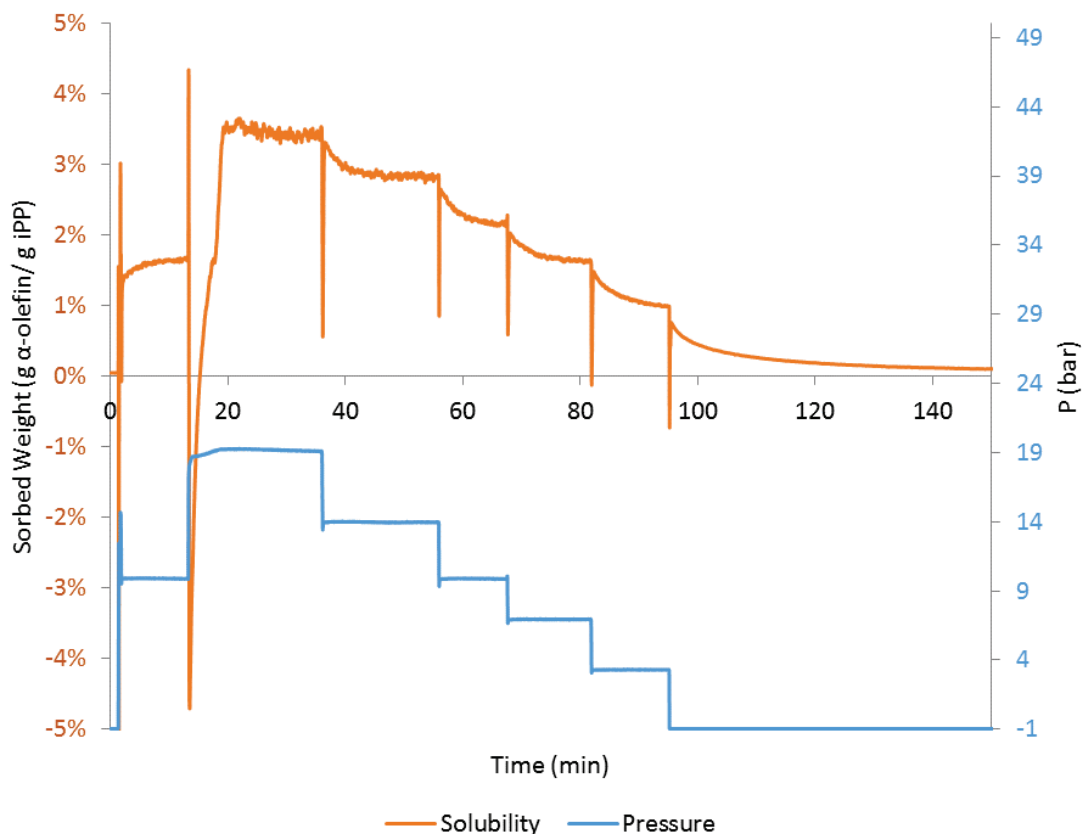


**Figure 3.7.** Solubility already corrected for buoyancy force (main y-axis) and chamber pressure (secondary y-axis) during a representative desorption measurement.

To verify our operative method, a sorption measurement was done in a sample impermeable to monomer, a 1-gram iron wire. Figure 3.8 confirms the reliability of our method, since propylene at 11 bar and 90 °C was not soluble in it.

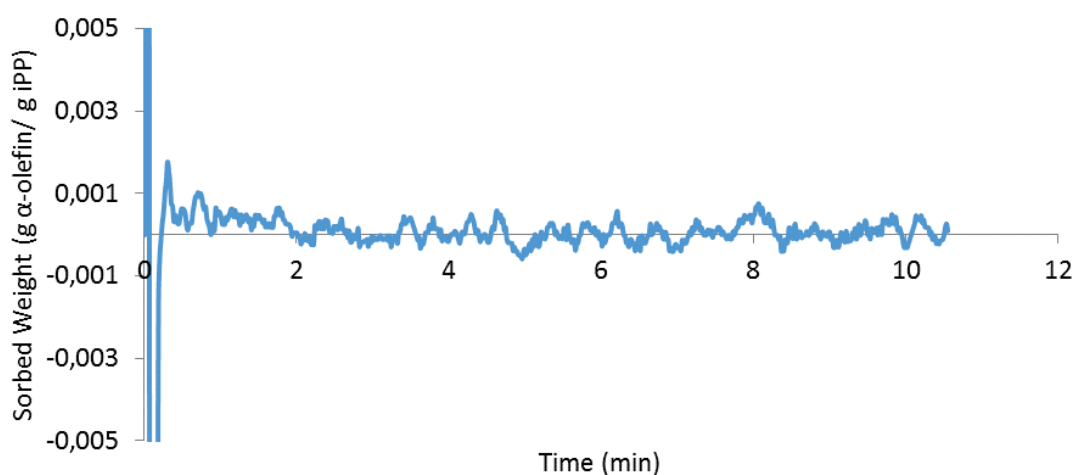


**Figure 3.8.** Sorption rate of propylene in 1 gram iron wire, at 90 °C and 11 bar of absolute pressure.

### 3.2.2.2 Chemicals

Propylene and ethylene with a least purity of 99.5 % were bought from Air Liquide (Germany). Isotactic polypropylene powder was polymerised in gas phase with a commercial ZN catalyst as described in previous publications,<sup>37,38</sup> and were used without any further treatment so their primary crystallinity could be conserved in solubility measurements. The main physical properties of this polymer are shown in Table 3.7.

**Table 3.7.** Main Properties of the iPP used in this work.

	Determined by	iPP
Mw (kDa)	HT-GPC	300
Mw/Mn	HT-GPC	5
Isotacticity (%)	<sup>13</sup> C NMR	98
Crystallinity (%)	DSC, 1 <sup>st</sup> and 2 <sup>nd</sup> Melting Curves	35/53
	Density Method	72

For evaluation of the solubility, Sato *et al.*<sup>16</sup> concluded that PP crystallinity obtained from a density method is more suitable than that from DSC. Therefore, in this study, PP crystallinity was obtained following Equation 3.4.

$$\rho_{PP} = \chi \cdot \rho_c + (1 - \chi) \cdot \rho_a \quad 3.4$$

Initially, PP density ( $\rho_{PP}$ ) was estimated measuring its weight while increasing N<sub>2</sub> pressure stepwise, as it was done to determine the container volume. Then, density data for crystalline and amorphous iPP phases was taken from literature,<sup>35</sup> and used to calculate the fraction of crystalline material. Table 3.7 shows that DSC results in a much lower crystallinity compared to the density method.

### 3.2.2.3 List of Experiments

Table 3.8 displays the solubility experiments performed in this study, executed at 50, 70 and 85 °C.

**Table 3.8.** Designed and performed solubility measurements in the current study.

Run	Temperature (°C)	Gas Phase Composition	
		Ethylene (mol%)	Propylene (mol%)
50-0	50	0	100
50-50	50	50	50
50-100	50	100	0
70-0	70	0	100
70-50	70	50	50
70-100	70	100	0
85-0	85	0	100
85-50	85	50	50
85-100	85	100	0

### 3.2.3 Results and Discussion

#### 3.2.3.1 Solubility Measurements

To prove the trustworthiness of the results of this work, the experimentally measured solubility at 70 °C of pure propylene and ethylene in iPP of this work was compared to both already published data in the literature and a measurement repeated in another sorption magnetic balance (University of Chemistry and Technology Prague). The aforementioned was done with the same iPP powder as that used in this study. Solubility in semicrystalline polymers is typically reported by amorphous content of the polymer, since the crystalline phase is supposed impermeable to the sorbed species in the polymer. Consequently, accurate measurement of the crystal content is crucial for the sorption process. Unfortunately, there is not a consensus for the determination of this parameter and different techniques are used in the literature (e.g. X-ray diffraction in Ref. [17], a density method in Ref. [13]), leading to discrepancies in the reported solubilities. Therefore, in Figure 3.9 and Figure 3.10 their reported solubility data was recalculated to take in account the full sample (both crystalline and amorphous phases). So, solubility is reported in g  $\alpha$ -olefin / g iPP powder.

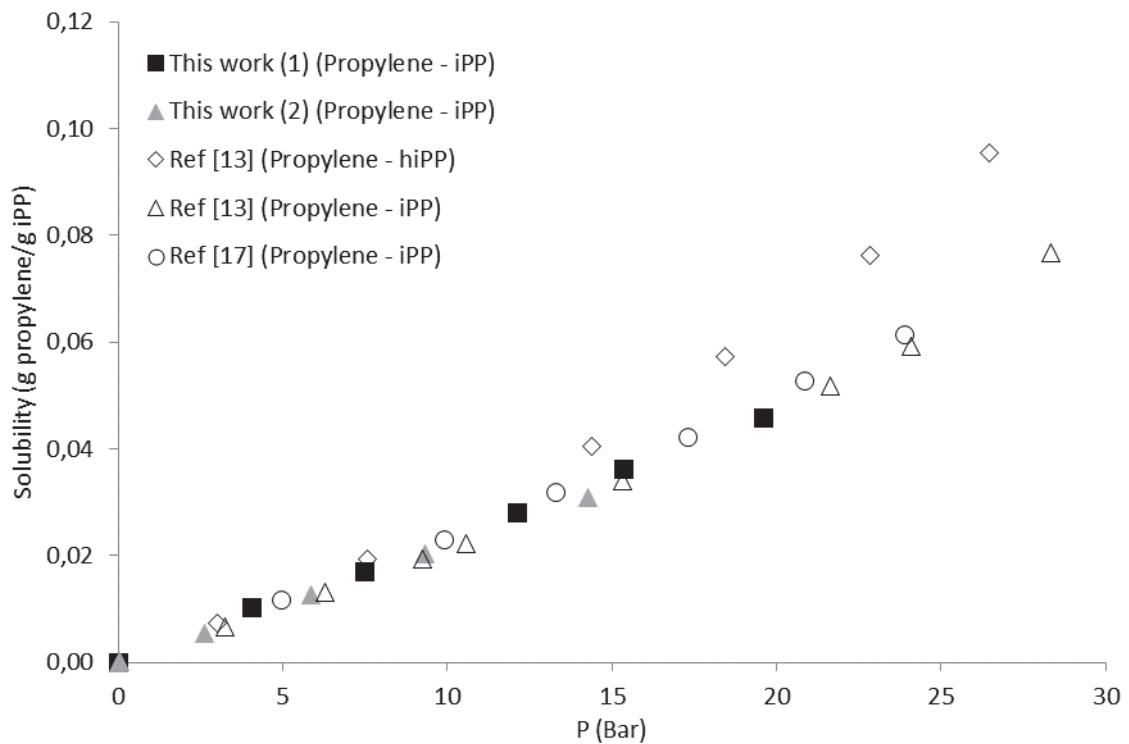


**Figure 3.9.** Comparison of the solubility of propylene in iPP at 70 °C from diverse sources: this work, Sato *et al.*<sup>13</sup> (please note that there is also a sorption thermogram of propylene in hiPP) and Kröner *et al.*<sup>17</sup>

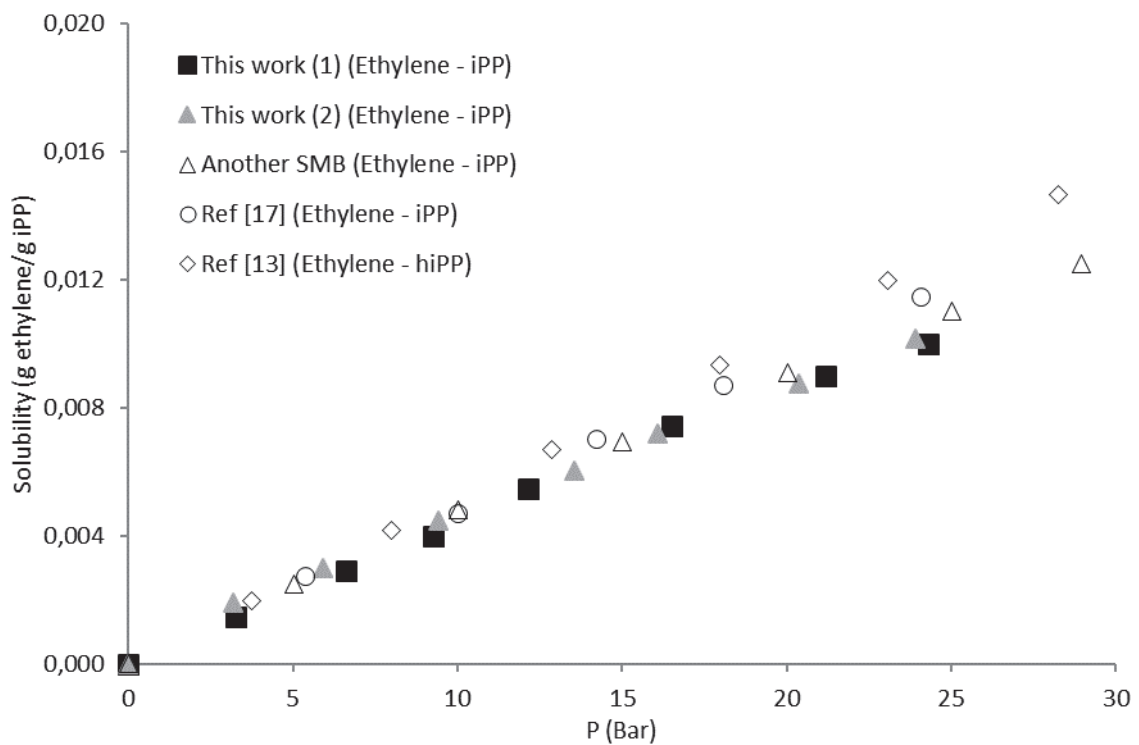
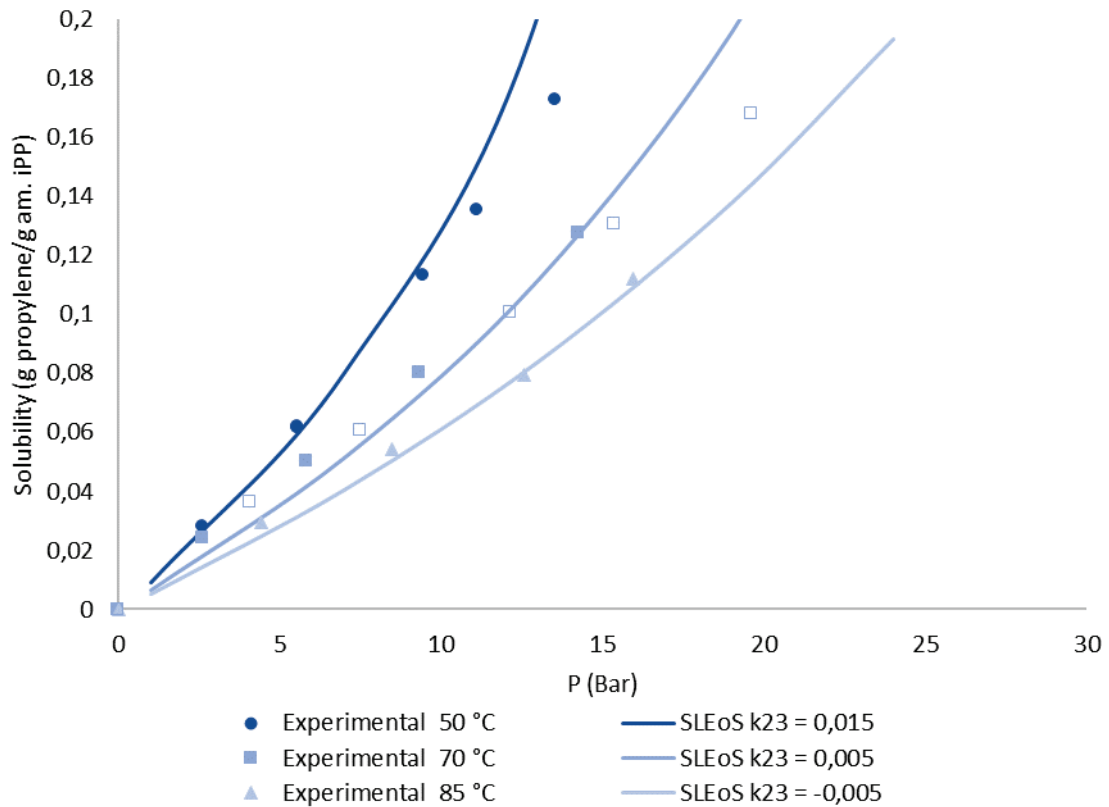


**Figure 3.10.** Comparison of the solubility of ethylene in iPP at 70 °C from diverse sources: this work, another SMB (kindly done by M. Podivinská and J. Kosek from the University of Chemistry and Technology Prague), Sato *et al.*<sup>13</sup> and Kröner *et al.*<sup>17</sup>

The similar gas solubilities of ethylene and propylene in iPP confirms the reliability of our results. In addition, they suggest that the crystallinity of our iPP powders are akin to those used by ref. [13] and [17]. However, Sato *et al.*<sup>13</sup> reported a crystallinity of 66.9 % (measured with a density method) and Kröner *et al.*<sup>17</sup> of 39% (via X-ray diffraction).

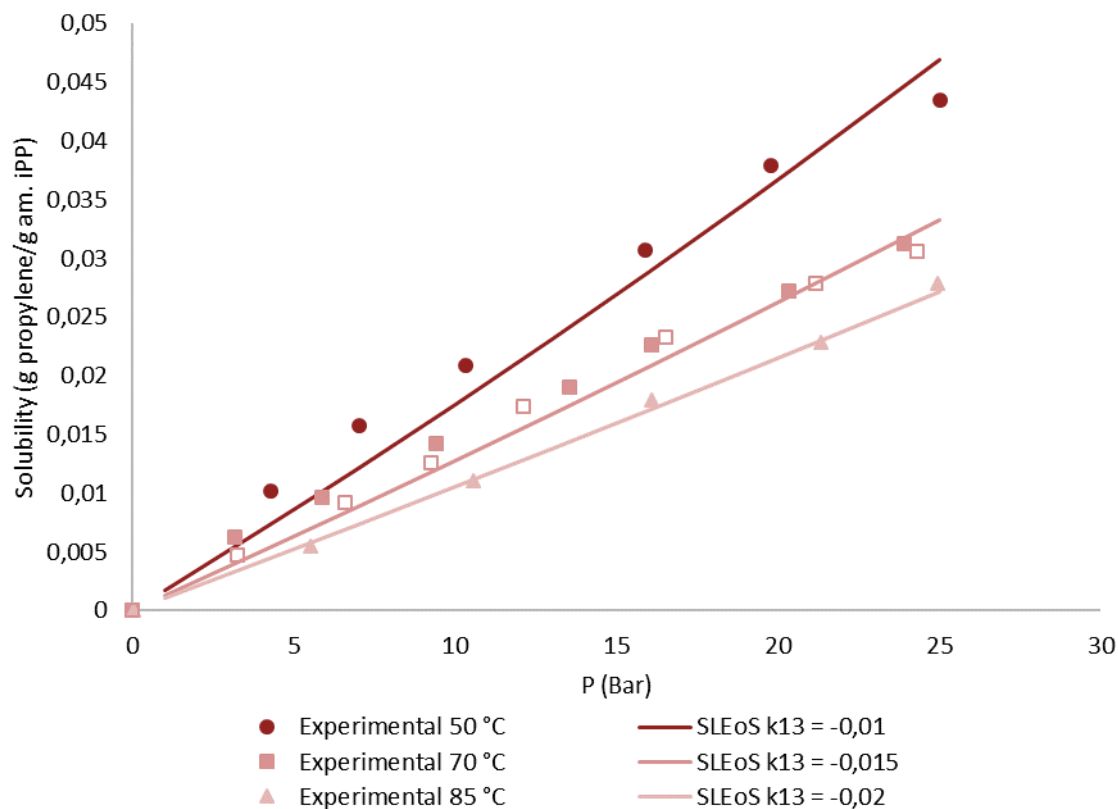
The experimentally obtained desorption isotherms for pure propylene, pure ethylene, and equimolar mixtures of both in iPP at 50, 70 and 85 °C are shown in Figure 3.11, Figure 3.12, and Figure 3.13, respectively. The experimentally measured solubilities were used to fit the gas-polymer interaction parameters of the SL-EoS. Appendix A briefly describes SL EoS. It can be seen from these figures that a good fit is obtained in the range of pressures studied. The characteristic parameters ( $P^*$ ,  $T^*$ ,  $\rho^*$ ) used here are shown in Table 3.6. As expected, solubilities of propylene, ethylene, and equimolar mixtures of both in iPP decrease with temperature and increase with pressure.

The desorption isotherms of propylene in iPP in Figure 3.11 are markedly nonlinear, especially at 50 °C. As the temperature increases, the non-linearity of both the experimental data and model predicts become less pronounced. Fitted binary interaction parameter  $k_{23}$  decreases with temperature. As Kanellopoulos *et al.*<sup>18</sup> pointed out, this fact suggests that the interaction activity between propylene and iPP increases with temperature.



**Figure 3.11.** Gas solubilities of propylene in amorphous iPP at 50, 70 and 85 °C, respectively. The points are desorption measurements and the curves are SL-EoS predictions.

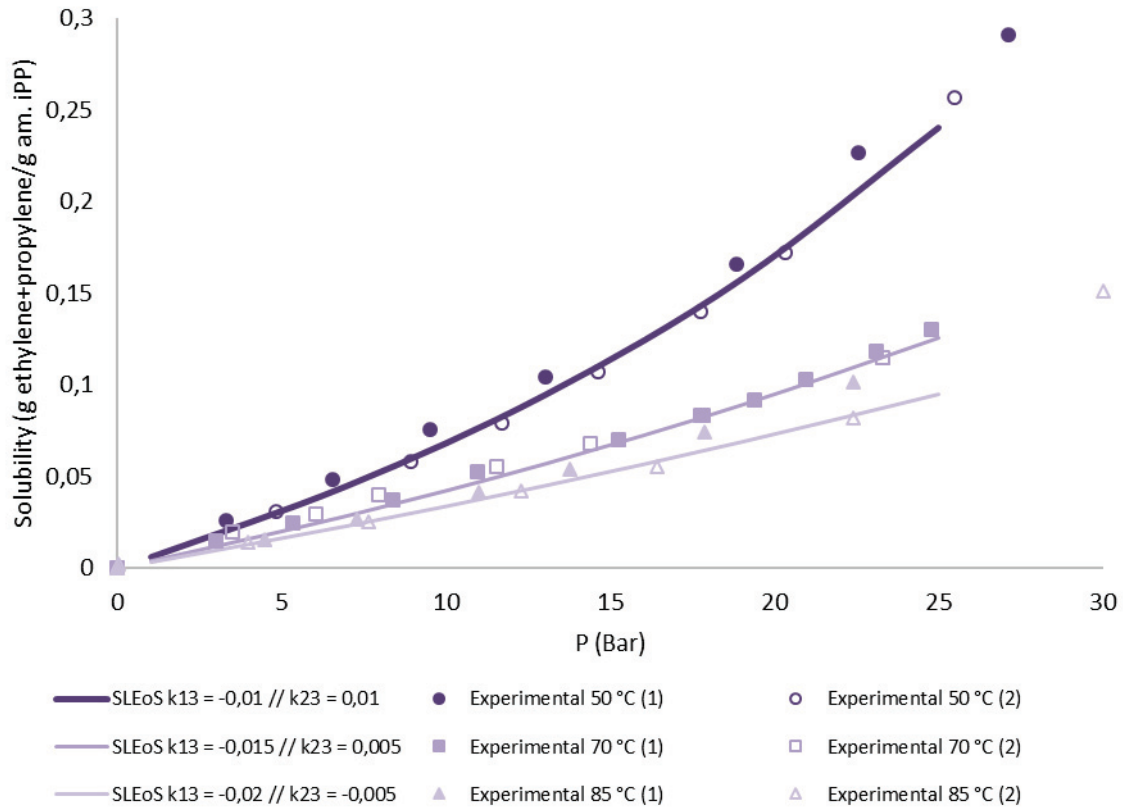
Figure 3.12 compares the experimental measurements of ethylene in iPP with SL model predictions. The SL model can be used to model the solubility with temperature dependent  $k_{13}$ . In a similar way to what was observed with the propylene-iPP system, the binary interaction parameter  $k_{13}$  decreases with temperature when ethylene is used as the process gas. Continuing with the previously exposed reasoning, this could be caused by the fact that the interaction activity between ethylene and iPP increases with temperature. Kanellopoulos *et al.*<sup>18</sup> used the experimental measurements of Sato *et al.*<sup>13</sup> on the solubilities of ethylene in hiPP to verify the predictive capabilities of the SL-EoS. In line with Figure 3.12, they saw that the binary interaction parameter decreases with temperature, even if they used hiPP instead of iPP.



**Figure 3.12.** Gas solubilities of ethylene in amorphous iPP at 50, 70 and 85 °C, respectively. The points are desorption measurements and the curves are SL-EoS predictions

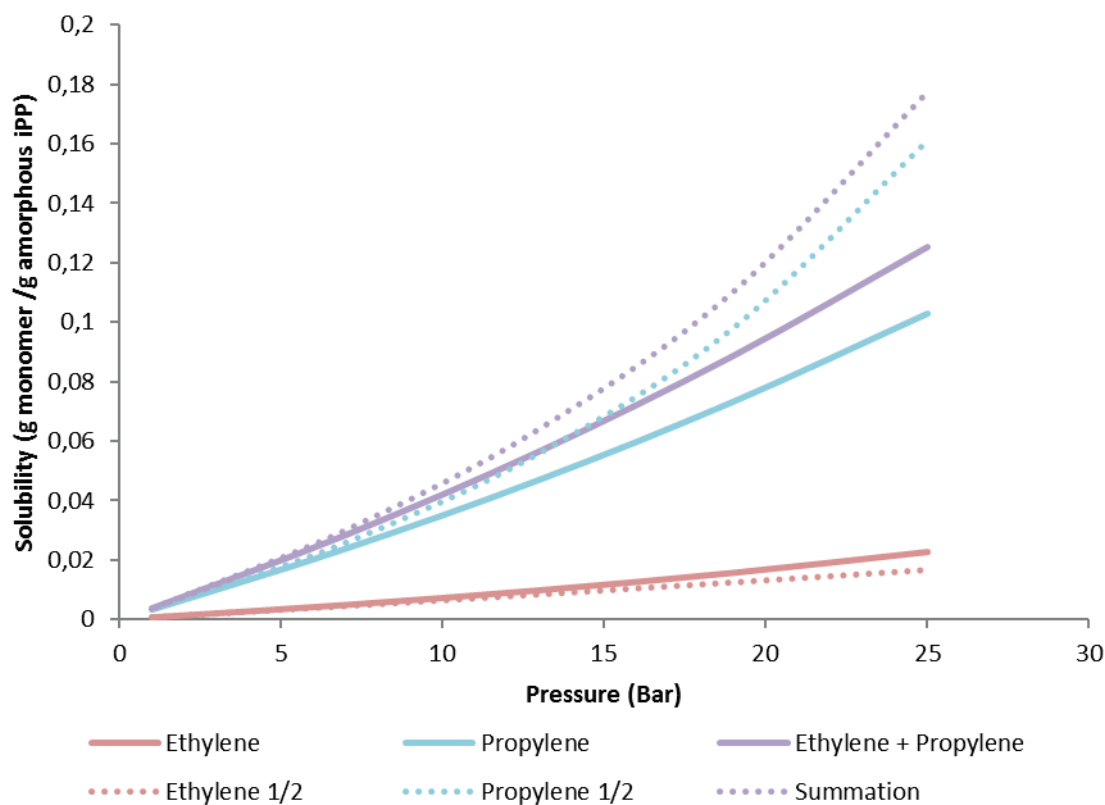
Based on the comparison of model and experimental results from Figure 3.13, it seems that fitted binary interaction parameters from Figure 3.11 and Figure 3.12 are suitable for the prediction of the solubility of equimolar ethylene-propylene mixtures in iPP, at 70 and 85 °C. However, for 50 °C, fitted binary interaction parameters are not suitable to predict the solubility of the ternary system—the solubility of the ternary system is higher—and a small readjustment of  $k_{23}$  is needed. After doing it, SL EoS can also be applied to forecast the solubility.

Figure 3.14 depicts SL calculations implemented to understand how mixing propylene and ethylene affected their solubility in iPP at 70 °C, as compared to being on their own in their respective binary systems. Solid lines stand for the overall solubility of ethylene-propylene mixture (purple) along the contribution of each single gas, (ethylene, red and propylene in blue) in the ternary system of ethylene-propylene/iPP. Dashed lines represent the solubility divided by 2 of each binary system (ethylene-iPP and propylene-iPP) at the same total pressure than that of the ternary system. Finally, purple dashed line is the summation of these last two.



**Figure 3.13.** Gas solubilities of an equimolar mixture of ethylene and propylene in amorphous iPP at 50, 70 and 85 °C, respectively. The points are desorption measurements and the curves are SL-EoS predictions.

Comparing the two red lines in Figure 3.14, we see that the solubility of ethylene in iPP is slightly higher if propylene is present. This is caused by the co-solubility effect, which is a term used to describe the fact that the concentration of ethylene in the polymer is higher in the presence of a heavier compound than it is just with ethylene (the heavier the alkene or alkane, the greater the effect). On the other hand, when blue lines are compared it is clear that ethylene acts as an antisolvent for propylene. Thus, solubility of propylene in iPP is lower if ethylene is present. Furthermore, comparison of purple lines in Figure 3.14 suggest that the overall solubility of ethylene/propylene gas equimolar mixture in iPP is lower than the corresponding individual solubilities of pure components. This is an indication that antisolvent effect of ethylene dominates over the co-solvent behaviour of propylene, since the presence of the two monomers reduces the overall solubility of the mixture in the polymer phase. However, at lower temperatures (at 50 °C) this trend changes completely, being the solubility higher when the two gases are dissolved simultaneously. Therefore, this indicates that for lower temperatures the co-solvent behaviour of propylene dominates over the antisolvent effect of ethylene, as opposed to temperatures greater than 70 °C



**Figure 3.14.** SL calculations with the experimentally obtained binary parameters at 70 °C. Solid lines stand for the solubilities of just ethylene (red) and propylene (blue) in the ternary system, and the sum of them (purple, overall solubility of an equimolar mixture of ethylene and propylene). Dashed lines are the solubility divided by 2 of each binary system at the same total pressure (being ethylene-iPP in red and propylene-iPP in blue). Dashed purple line represents the sum of these last two.

Calculations were run to understand how pressure and temperature impact the molar ratio of ethylene/propylene solubilized in amorphous iPP, which are shown in Figure 3.15. Once more, the previously obtained binary interaction parameters were used.

Even though the gas phase mixture of C2 and C3 is equimolar, Figure 3.15 shows that this ratio is altered when the mixture is sorbed into amorphous iPP, due to the different solubilities of propylene and ethylene in iPP. Roughly three moles of propylene are sorbed into iPP for each of ethylene. Nevertheless, temperature and pressure affect this proportion. The equilibrium molar ratio of C2 to C3 increases with temperature and pressure. However, based on Figure 3.15, it seems that temperature strongly loses its significance beyond 70 °C. While unexpected, these results are coherent with observations of experimental kinetic studies in hiPP by Kröner in his work.<sup>39</sup> During the second stage of hiPP production, he varied copolymerization pressure from 11 to 16 to 21 bar. Interestingly, a slight lower ethylene concentration ratio was needed in the gas phase to obtain a fixed copolymer

composition with increasing pressure. The lack of propylene at higher pressures may explain this outcome.

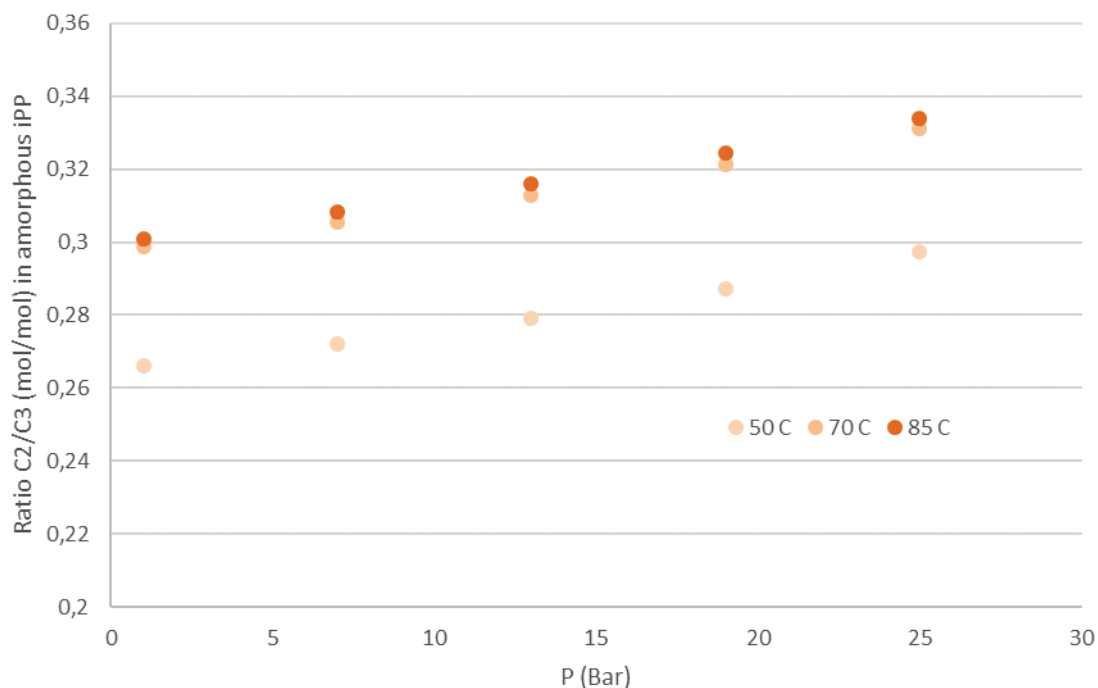


**Figure 3.15.** Equilibrium molar ratio of ethylene to propylene solubilized in amorphous iPP as calculated with SL EoS with the experimentally fitted binary interaction parameters, at 50 – 85 °C and 0 – 25 bar.

In general, during copolymerisation of hiPP, propylene is firstly sorbed into PP, and then ethylene. To reproduce the same conditions, in the experiments shown in Figure 3.13, gases were fed to the SMB chamber in this same order. However, to analyze the impact of sorption order, the opposite experiment was also conducted. Thus, first ethylene was let to get sorbed until its infinite dilution in PP (0 – 10 bar), and then propylene was added (10 – 20 bar). Note that actual pressures of each monomer to obtain an equimolar mixture were estimated with a real gas equation of state. Figure 3.16 exposes how this order of monomer injection didn't have any appreciable effect on the overall solubility of the equimolar gas mixture in iPP.

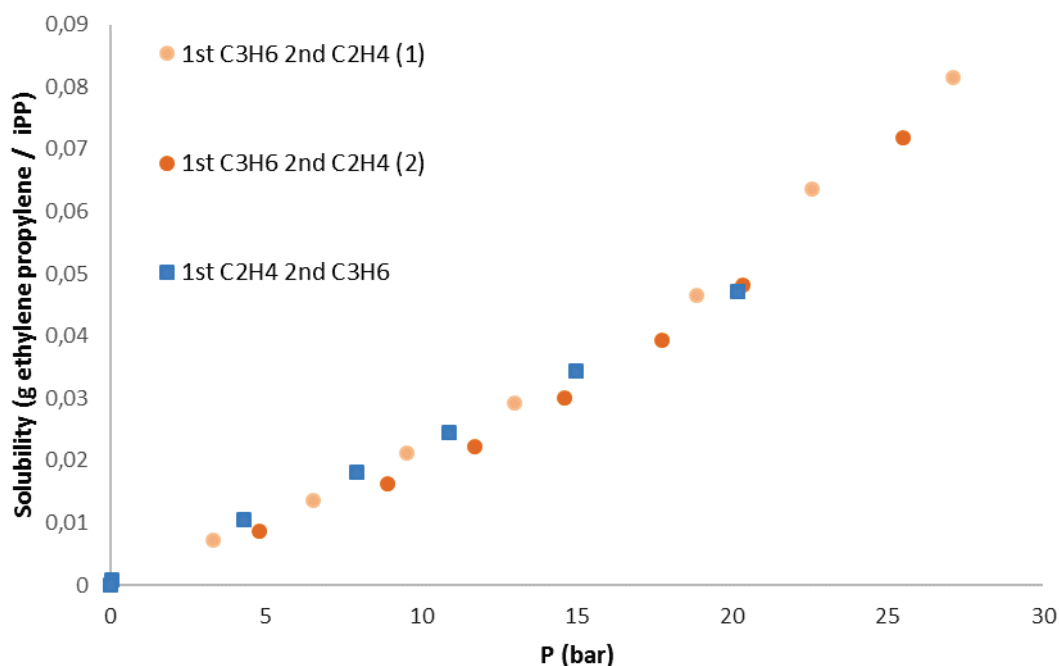


**Figure 3.16.** Comparison of experimental gas solubilities of equimolar mixtures of ethylene and propylene in full iPP at 50 °C, injecting ethylene first (blue, square points) or propylene (orange, circular points).

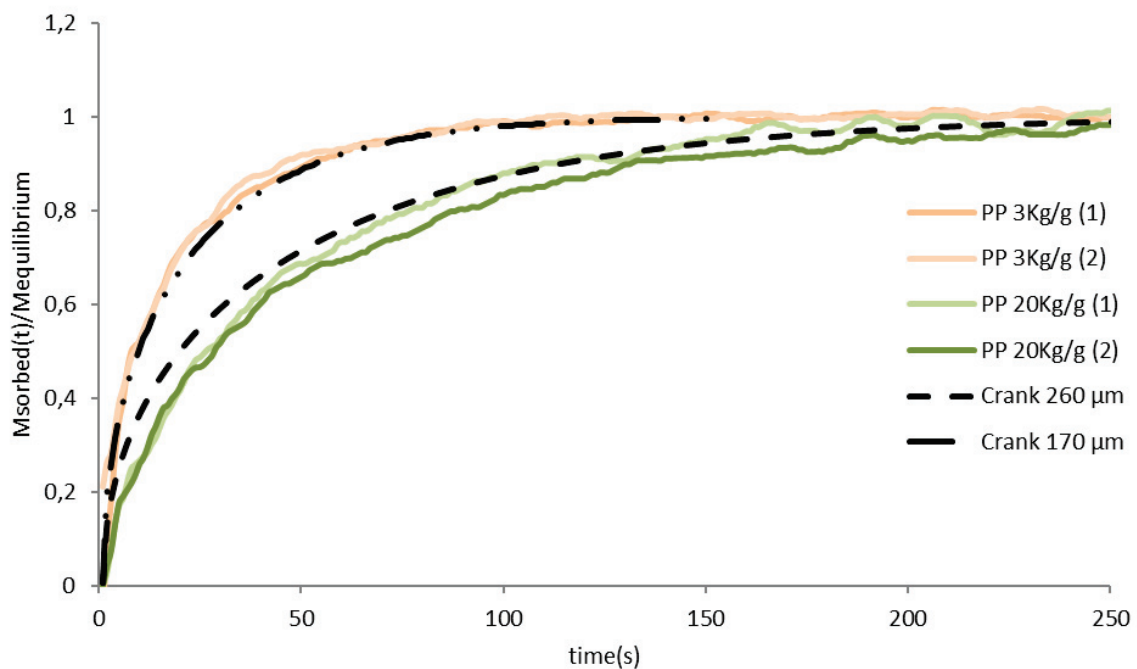
### 3.2.3.2 Sorption Measurements

For single particle modelling, description of the sorption of monomers during the course of polymerization is of great importance. Sorption rates were measured for ethylene, propylene and equimolar mixtures of ethylene/propylene in two additional polypropylene powders with different productivities, 3 and 20 Kg iPP / gram precatalyst, respectively. Rest of their properties were like those of the iPP powder used for desorption experiments and shown in Table 3.7. Particle morphology and diffusivity of the material influence sorption rates. Kroner and Bartke,<sup>17</sup> determined empirical constants for calculation of powder diffusion coefficients for propylene in polypropylene at 70 °C and 11 bar. Material properties of our PP are comparable to those studied by them. Equation 3.5 is the analytical solution of the diffusion equation for spheres, developed by Crank.<sup>40,41</sup>

$$\frac{M_t}{M_\infty} = 1 - \frac{6}{\pi^2} \sum_{n=1}^{\infty} \frac{1}{n^2} \exp\left\{-Dn^2\pi^2 \frac{t}{r^2}\right\} \quad 3.5$$

In Equation 3.5  $D$  is the effective diffusion coefficient and  $r$  is the effective diffusion length,

considered as the average radius of the clusters agglomeration that ultimately constitute the powders. First, Kröner and Bartke,<sup>17</sup> diffusion coefficients are implemented in Equation 3.5. Then, Equation 3.5 is fitted to the experimental powder sorption data done at 70°C and 11 bar, by readjusting the integral sorption length ( $r$ ). This is exemplarily shown in Figure 3.17, for both iPP powders used. Parameter “ $D$ ” was assumed to be  $10,05 \cdot 10^{-11}$  m<sup>2</sup>/s, in accordance to the empirical constants for calculation of powder diffusion coefficients reported by Kröner and Bartke.<sup>17</sup>

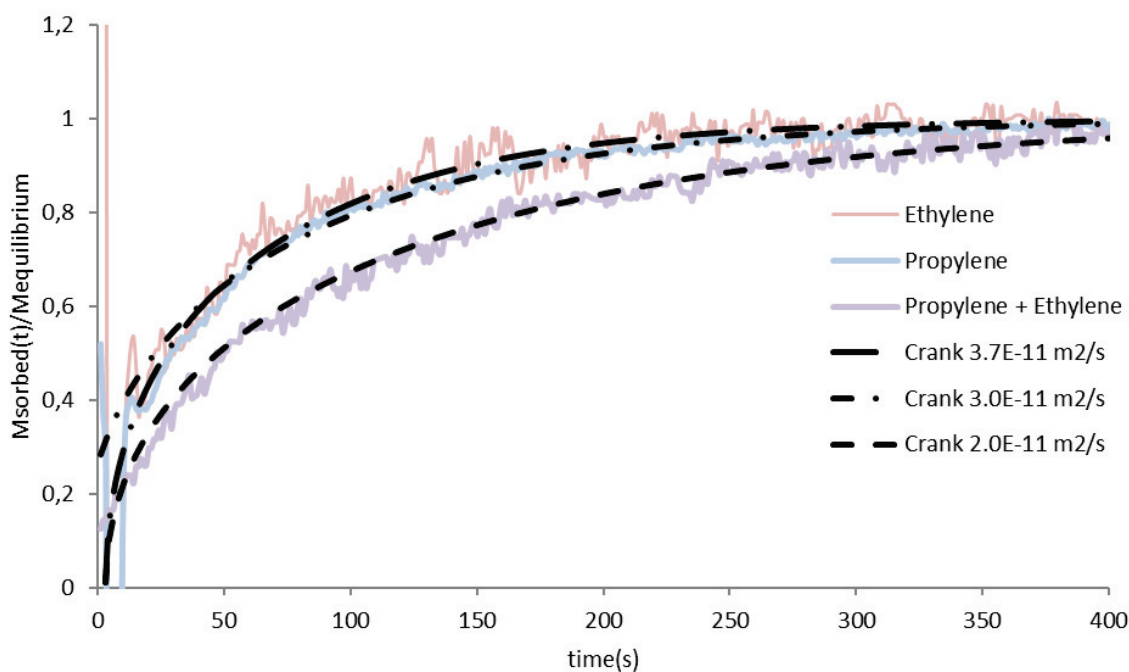


**Figure 3.17.** Determination of clusters radii in two polypropylenes powders. All the sorption rates were done at 70 °C and 11 absolute bar of propylene in the sorption magnetic balance

As predicted, the clusters' size of iPP with higher productivity are bigger. Once the clusters size is determined it is possible to do the inverse approach, i.e., implementing these experimentally determined sorption length (clusters radii,  $r$ ) in Equation 3.5 to evaluate quantitatively the diffusivity of the various gases under the several conditions here studied. Table 3.9 shows a summary of the powder diffusion coefficients resulting from sorption rates of propylene, ethylene, and an equimolar mixture of ethylene/propylene in iPP at the investigated conditions. It is important to note, that the ethylene/propylene equimolar mixture was already prepared in a separate ballast before feeding it to the sorption cell.

**Table 3.9.** Summary of the powder diffusion coefficients resulting from sorption rates at the various conditions studied.

iPP Kg/g	Temperature °C	Pressure Bar	Average $D \cdot 10^{11}$ (m <sup>2</sup> /s)		
			Propylene	Propylene+Ethylene	Ethylene
3	50	4	3	2,1	3,7
3	50	11	3,5	2,8	4,5
3	70	11	10	-	-
20	70	11	10	-	-
20	70	20	15	3,5	11
20	90	4	12	2	17
20	90	11	17	6	18,5
20	90	20	17	5	20

**Figure 3.18.** Sorption rates of propylene, ethylene, and an equimolar mixture of ethylene/propylene in iPP of 3Kg/g of productivity (clusters radii = 170  $\mu\text{m}$ ) at 4 bar and 50  $^{\circ}\text{C}$ .

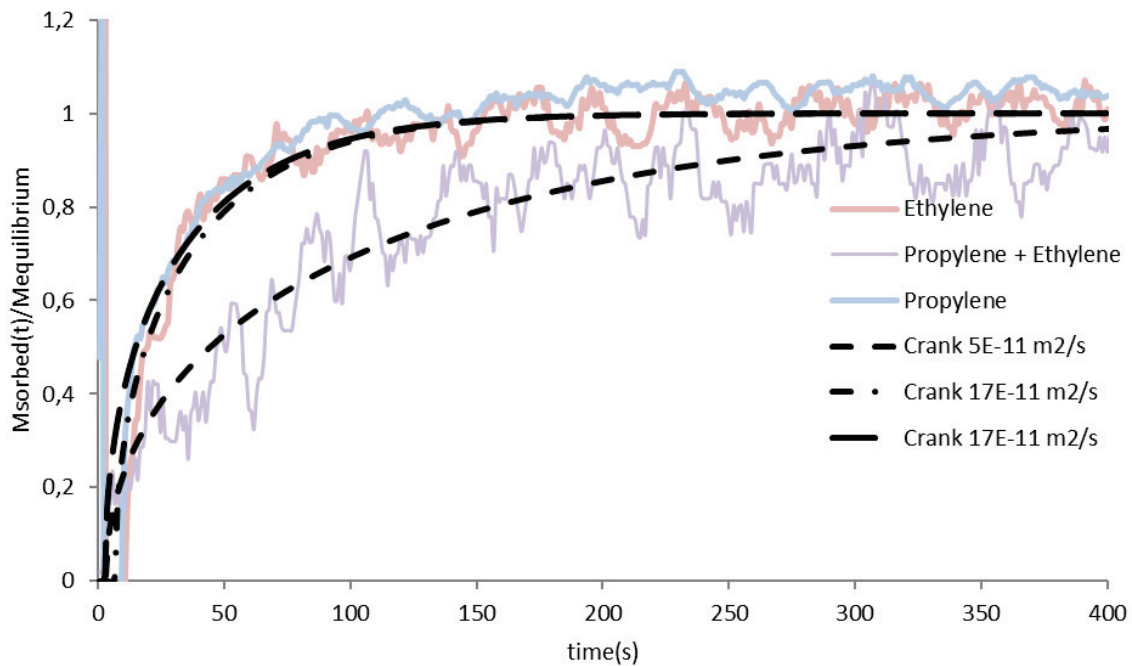


**Figure 3.19.** Sorption rates of propylene, ethylene, and an equimolar mixture of ethylene/propylene in iPP of 20Kg/g of productivity (clusters radii = 260  $\mu\text{m}$ ) at 20 bar and 90  $^{\circ}\text{C}$ .

Table 3.9 confirms as expected that the effective diffusion coefficient increases with pressure (or penetrant concentration in the polymer) and temperature. In addition, there are some unanticipated results. Firstly, in Table 3.9 is possible to appreciate a small tendency of ethylene having a higher diffusivity compared to propylene. However, looking at Figure 3.18 and Figure 3.19, the difference among them is minor compared to the accuracy of the measurement.

The most unexpected outcome is the lower diffusivity values shown by gas ethylene-propylene mixtures when diffusing into iPP, as compared to single gases. This is especially apparent in Figure 3.19, when the best conditions for a fast sorption are reunited (Highest temperature and pressure).

### 3.2.3.3 Desorption Measurements

All the desorption rates, resulting from previously shown solubility measurements, were fitted to Equation 3.6, as exemplarily shown in Figure 3.20. The clusters radii for this iPP powder was experimentally determined, as previously explained, to be 200  $\mu\text{m}$ . Table 3.10 displays the resultant effective diffusion coefficients

$$\frac{M_t}{M_\infty} = \frac{6}{\pi^2} \sum_{n=1}^{\infty} \frac{1}{n^2} \exp\left\{-Dn^2\pi^2 \frac{t}{r^2}\right\} \quad 3.6$$

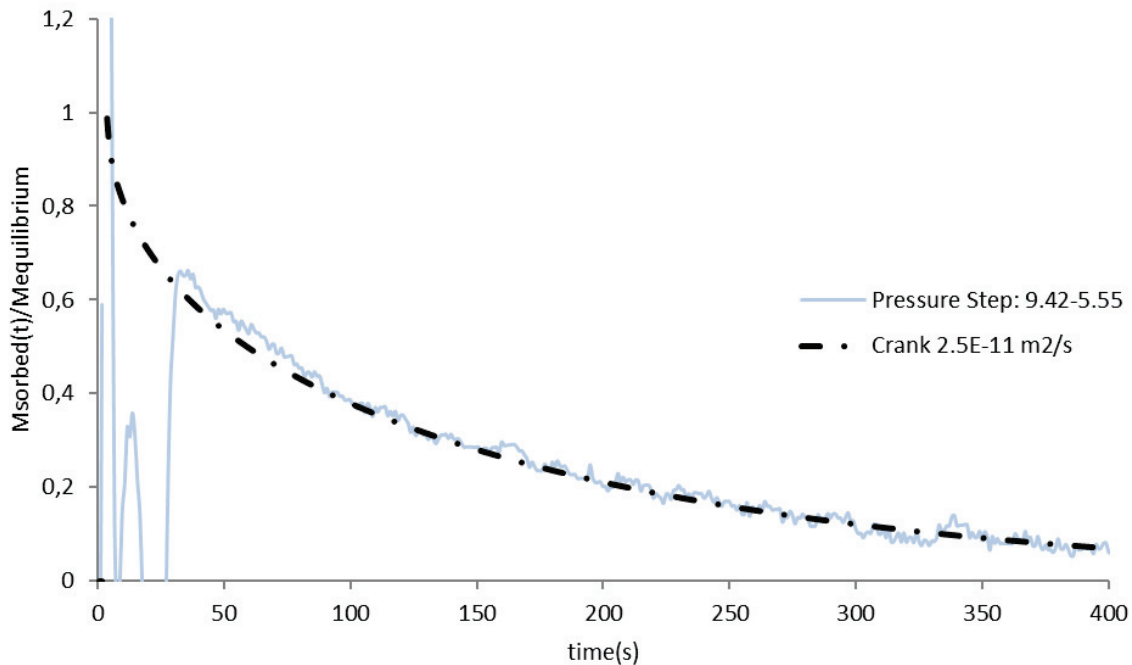


**Figure 3.20.** Desorption rate of propylene in iPP (clusters radii = 200  $\mu\text{m}$ ) from 9.42 to 5.55 bar at 50  $^{\circ}\text{C}$ .

**Table 3.10.** Summary of the powder diffusion coefficients resulting from desorption rates at the different conditions studied.

Temperature $^{\circ}\text{C}$	Approx. Pressure Range Bar	Effective Diffusion Coefficient [ $D \cdot 10^{11}$ ( $\text{m}^2/\text{s}$ )]			
		Propylene	Propylene 1 + Ethylene 2	Ethylene	Ethylene 1 + Propylene 2
50	17-13	3,5	2,7	1,8	2
50	13-9	2,5	2,2	-	2,1
50	9-5	2,2	2,2	-	1,8
50	5-2	1,8	2	-	1,6
50	2-0	-	-	0,8	0,6
70	13-8	4,5	3	2,5	-
70	8-5	4,5	3,2	3	-
70	5-0	4,5	2,7	3	-
90	15-12	7	-	-	-
90	12-7	6,5	6	-	-
90	7-4	7	6	-	-
90	4-0	-	6	3,5	-

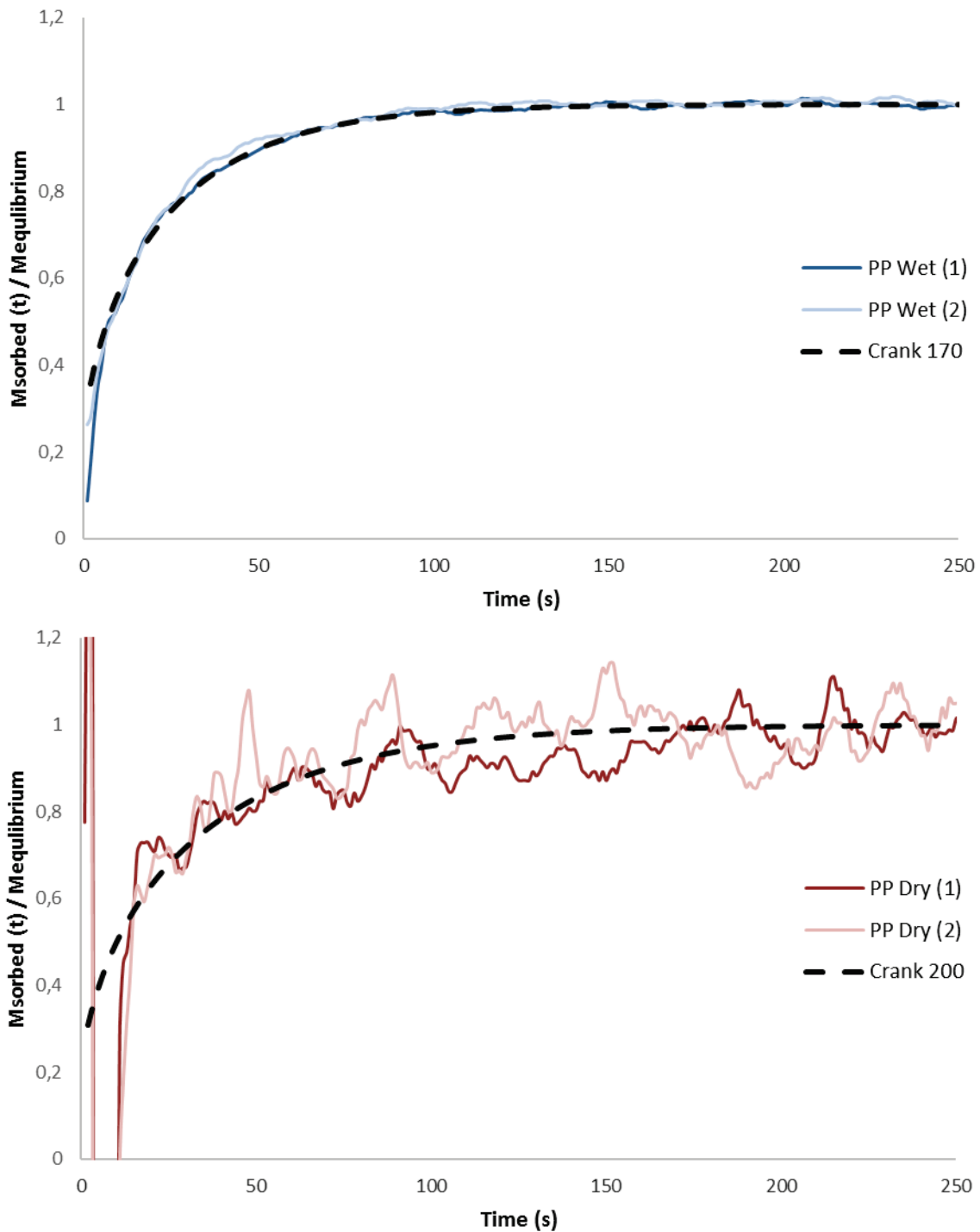
Once more, Table 3.10 confirms that the effective diffusion coefficient generally increases

with pressure and temperature. However, contrarily to sorption measurements, a straightforward conclusion is possible: The higher the solubility of the gas in iPP is, the greater its diffusion coefficient will be. Consequently, the fastest is propylene, then gas propylene ethylene mixtures, and the slowest ethylene. Despite of having studied the diffusion of ethylene and propylene into HDPE films, Kanellopoulos *et al.*<sup>28</sup> also found that diffusion coefficients were higher for propylene than for ethylene.

Besides, the order of gas addition for ethylene – propylene gases seems to have an impact on the desorption rate. As Table 3.10 exhibits, gas equimolar mixtures of ethylene propylene are faster evacuated from iPP if propylene is firstly dissolved into it. This may be related to the observation that propylene desorbs faster, when dissolved in iPP individually.

#### 3.2.3.4 Sorption Measurements of Dry and Wet Powders

In the previous chapter, the influence of injecting the precatalyst suspended with coarse NaCl salt (dry) or with paraffinic oil (wet) over the resulting iPP morphology was studied. In this subsection, sorption rates were used to further investigate the morphological differences of the final powders. The sorption rates of propylene at 70 °C and 11 bar in Dry PP (0.5 Kg iPP / g precatalyst of productivity) and in Wet PP (3 Kg iPP / gram precatalyst, same powder as the one used in subsection “3.2.3.2”) were measured. The effective diffusion coefficient “ $D$ ” used to determine the effective diffusion length “ $r$ ” is, once more,  $10,05 \cdot 10^{-11} \text{ m}^2/\text{s}$ , in accordance to the empirical constants for calculation of powder diffusion coefficients reported by Kröner and Bartke.<sup>17</sup> The fitting of Equation 3.5 to the experimental powder sorption data by readjusting the integral sorption length ( $r$ ) is shown in Figure 3.21.



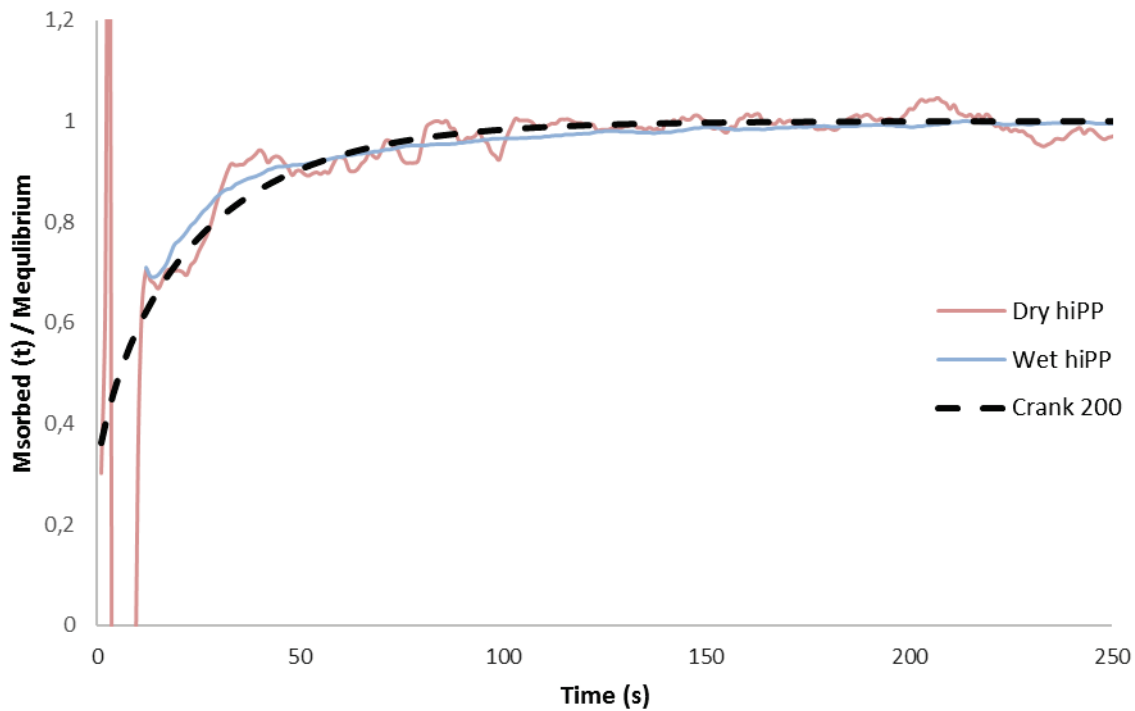
**Figure 3.21.** Determination of clusters radii in wet (blue) and dry (red) polypropylenes powders. Every sorption rate was done at 70 °C and 11 absolute bar of propylene in the sorption magnetic balance.

Figure 3.21 shows the sorption rates of dry and wet injection, where the different estimated clusters radii evidences the different morphologies, and that propylene diffuses faster into wet iPP than into dry iPP. This fact is in agreement with the higher activity observed for the wet injection protocol. Surprisingly, the average meso-particle that dry iPP particles are composed of ( $\sim 200 \mu\text{m}$ ) are bigger than those of wet polypropylenes ( $\sim 170 \mu\text{m}$ ). This

seems contradictory, since wet iPP powder has a bigger productivity, and thus, it seems logical that the particles would be composed of bigger clusters. However, this might be a consequence of agglomeration during particle formation, caused by the elevated temperatures that dry iPP particles undergo during its initial instants of reaction, as explained in the previous chapter.

To understand how the ethylene-propylene rubber impacts the iPP morphology and vice versa, two hiPP powders were made, namely Dry hiPP and Wet hiPP, and sorption measurements were done at the same conditions (70 °C and 11 bar of propylene). Both had an ethylene-propylene copolymer (EPC) content of 30%, estimated during reaction by the ballast pressure drop. The goal was to keep the iPP matrix constant compared to samples Dry iPP and Wet iPP, so iPP productivity of the heterophasic copolymers was correspondingly the same than these samples. The final productivities of samples Dry hiPP and Wet hiPP were 0,8 and 4 Kg iPP / g precatalyst, respectively.

However, because of the EPC content, the material properties of these two new samples are different from those of pure iPP (e.g., crystallinity). As sorption rates are affected by material properties, to correctly estimate the average size of the meso-particles “ $r$ ”, the diffusion coefficient “ $D$ ” to be implemented in Equation 3.5 should be adapted in accordance. Kröner and Bartke determined the empirical constants for calculation of powder diffusion coefficients for hiPP, in function of the EPC content.<sup>17</sup> Following their publication “ $D$ ” was found to be  $14,16 \cdot 10^{-11} \text{ m}^2/\text{s}$ .



**Figure 3.22.** Determination of clusters radii in wet (blue) and dry (red) high impact polypropylenes powders. Every sorption rate was done at 70 °C and 11 absolute bar of propylene in the sorption magnetic balance.

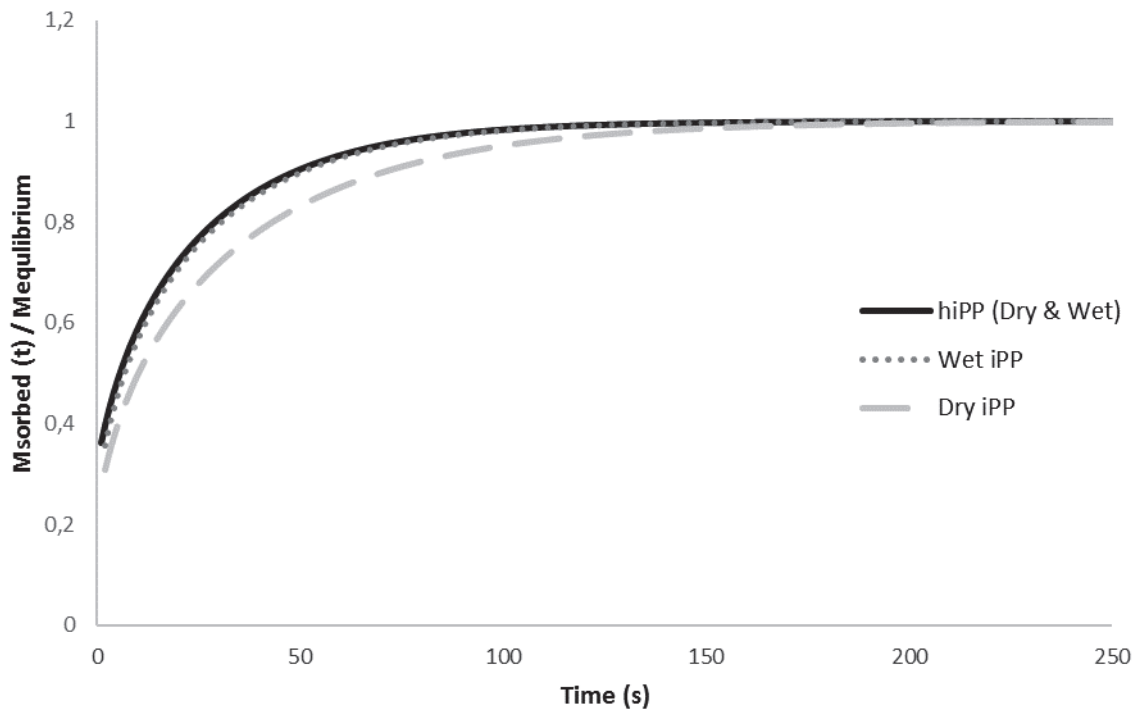


**Figure 3.23.** Comparison of the fitting curves obtained for each hiPP (Dry & Wet), Wet iPP and Dry iPP.

As Figure 3.22 shows, now the time that propylene needs to diffuse within both samples is similar, since the effective diffusion length is the same for both powders. This shows how the rubber, due to its amorphous nature, governs the mass transfer rate. However, if we

compare the absolute sorption rates of Dry iPP, Wet iPP and hiPP, as displayed in Figure 3.23, it can be seen a large enhancement in the sorption rate of the dry injection method when rubber is included. However, for the wet injection method this improvement is insignificant. This indicates that the initial morphology of iPP can have a substantial impact on the rubber production in-situ stage. It seems logical to think that the wet iPP powder is better suited to withstand the harsh conditions of copolymerization, which will probably result in a better rubber distribution.

### 3.2.4 Conclusions for Objective 2: Sorption

Equilibrium sorption isotherms of ethylene, propylene, and ethylene/propylene equimolar mixtures in a polypropylene (iPP) sample were determined gravimetrically at 50, 70 and 85 °C in the pressure range of 0-25 bar. Initially, the obtained experimental data from binary systems (ethylene-iPP and propylene-iPP) was used to find the binary interaction parameters of the Sanchez–Lacombe equation of state (SL EoS). Both binary interaction parameters of the systems ethylene in iPP and propylene in iPP decreased with temperature. A better interaction activity with temperature between molecules was expected as the main cause for this outcome. Fitted binary interaction parameters were suitable to predict the experimental solubility of the ternary system, (ethylene/propylene equimolar mixtures in iPP) for 70 and 80 °C. However, at 50 °C a small readjustment of the propylene iPP binary interaction parameter was needed. SL calculations with the fitted parameters showed that the anti-solvent effect of ethylene dominates over the co-solvent behaviour of propylene — except at 50 °C, where this trend changes—. This means, in practice, that the total solubility of the gas mixture is lower than the sum of the gas solubilities of the respective individual components. In addition, it was found that the concentration equilibrium molar ratio of ethylene to propylene dissolved in amorphous iPP increases with temperature and pressure. This is important for copolymerization kinetics and rubber properties during hiPP production.

For the diffusivities of the gases (individual or mixed) in iPP powders two straightforward conclusions are possible: First, for the desorption rates, the effective diffusion coefficient increases with pressure (or penetrant concentration in the polymer) and temperature. In the case of sorption experiments, the clearest effect which has been observed is the apparent lower diffusivity of gas ethylene-propylene equimolar mixtures as compared to that of each individual gas.

The significant impact that the method of catalyst injection (dry or wet) has on the final iPP morphology was confirmed by the major differences observed in the obtained sorption rates. However, similar sorption rates were measured in the corresponding hiPP powders resulting from both methods of injection, which indicates that mass transfer of monomers is governed by rubber, when it is present.

### 3.2.5 References

1. Kanellopoulos, V., Dompazis, G., Gustafsson, B. & Kiparissides, C. Comprehensive analysis of single-particle growth in heterogeneous olefin polymerization: the random-pore polymeric flow model. *Ind. Eng. Chem. Res.* **43**, 5166–5180 (2004).
2. Floyd, S., Choi, K. Y., Taylor, T. W. & Ray, W. H. Polymerization of olefins through heterogeneous catalysis. III. Polymer particle modelling with an analysis of intraparticle heat and mass transfer effects. *J. Appl. Polym. Sci.* **32**, 2935–2960 (1986).
3. Yiagopoulos, A., Yiannoulakis, H., Dimos, V. & Kiparissides, C. Heat and mass transfer phenomena during the early growth of a catalyst particle in gas-phase olefin polymerization : the effect of prepolymerization temperature and time. *Chem. Eng. Sci.* **56**, 3979–3995 (2001).
4. Petrochemical Analysis: Global Market Reports - Platts. Available at: <http://www.platts.com/products/petchem-analytics-global-polyolefins-outlook>. (Accessed: 28th October 2015)
5. Namkajorn, M., Alizadeh, A., Somsook, E. & McKenna, T. F. L. Condensed-Mode Cooling for Ethylene Polymerization: The Influence of Inert Condensing Agent on the Polymerization Rate. *Macromol. Chem. Phys.* **215**, 873–878 (2014).
6. Alizadeh, A., Namkajorn, M., Somsook, E. & McKenna, T. F. L. Condensed Mode Cooling for Ethylene Polymerization: Part II. The Effect of Different Condensable Comonomers and Hydrogen on Polymerization Rate. *Macromol. Chem. Phys.* **216**, 985–995 (2015).
7. Spitz, R., Bobichon, C. & Guyot, A. Synthesis of polypropylene with improved MgCl<sub>2</sub>-supported Ziegler-Natta catalysts, including silane compounds as external bases. *Makromol. Chem.* **190**, 707–716 (1989).

8. Guastalla, G. & Giannini, U. The influence of hydrogen on the polymerization of propylene and ethylene with an MgCl<sub>2</sub> supported catalyst. *Makromol. Chem. Rapid Commun.* **4**, 519–527 (1983).
9. Mori, H., Endo, M. & Terano, M. Deviation of hydrogen response during propylene polymerization with various Ziegler–Natta catalysts. *J. Mol. Catal. Chem.* **145**, 211–220 (1999).
10. Vizen, E. I. *et al.* Study of hydrogen effect in propylene polymerization on (with) the MgCl<sub>2</sub>-supported ziegler-natta catalyst—part 2. Effect of CS<sub>2</sub> on polymerization centres. *Eur. Polym. J.* **30**, 1315–1318 (1994).
11. Primol 352. Available at: [http://www.exxonmobil.com/Denmark-English/Specialties/PDS/GLXXENSPCEMPrimol\\_352.aspx](http://www.exxonmobil.com/Denmark-English/Specialties/PDS/GLXXENSPCEMPrimol_352.aspx). (Accessed: 30th July 2015)
12. Sanchez, I. C. & Lacombe, R. H. An elementary molecular theory of classical fluids. Pure fluids. *J. Phys. Chem.* **80**, 2352–2362 (1976).
13. Sato, Y. *et al.* Vapor–liquid equilibrium ratios for hexane at infinite dilution in ethylene+impact polypropylene copolymer and propylene+impact polypropylene copolymer. *Fluid Phase Equilibria* **170**, 49–67 (2000).
14. Bashir, M. A., Monteil, V., Kanellopoulos, V., Ali, M. A.-H. & McKenna, T. Partial Molar Volumes and Thermal Expansion Coefficients as an Explanation for Co-Solvent Effect of Penetrants in Multicomponent Polymer Mixtures. *Macromol. Chem. Phys.* **216**, 2129–2140 (2015).
15. Yoon, J.-S., Chung, C.-Y. & Lee, I.-H. Solubility and diffusion coefficient of gaseous ethylene and  $\alpha$ -olefin in ethylene/ $\alpha$ -olefin random copolymers. *Eur. Polym. J.* **30**, 1209–1214 (1994).
16. Sato, Y., Yurugi, M., Yamabiki, T., Takishima, S. & Masuoka, H. Solubility of propylene in semicrystalline polypropylene. *J. Appl. Polym. Sci.* **79**, 1134–1143 (2001).
17. Kröner, T. & Bartke, M. Sorption of Olefins in High Impact Polypropylene - Experimental Determination and Mass Transport Modeling: Sorption of Olefins in High Impact Polypropylene .... *Macromol. React. Eng.* **7**, 453–462 (2013).

18. Kanellopoulos, V., Mouratides, D., Pladis, P. & Kiparissides, C. Prediction of Solubility of  $\alpha$ -Olefins in Polyolefins Using a Combined Equation of StateMolecular Dynamics Approach. *Ind. Eng. Chem. Res.* **45**, 5870–5878 (2006).
19. Bashir, M. A., Al-haj Ali, M., Kanellopoulos, V. & Seppälä, J. Modelling of multicomponent olefins solubility in polyolefins using Sanchez–Lacombe equation of state. *Fluid Phase Equilibria* **358**, 83–90 (2013).
20. Patzlaff, M., Wittebrock, A. & Reichert, K.-H. Sorption studies of propylene in polypropylene. Diffusivity in polymer particles formed by different polymerization processes. *J. Appl. Polym. Sci.* **100**, 2642–2648 (2006).
21. Bartke, M. *et al.* Sorption and Diffusion of Propylene and Ethylene in Heterophasic Polypropylene Copolymers. *Macromol. Symp.* **259**, 327–336 (2007).
22. Gorval, E. G., Svejda, P. & Mutsers, S. M. P. Sorption and Desorption of *n*-Alkanes in Polypropylene Polymerized in the Gas Phase. *Ind. Eng. Chem. Res.* **40**, 814–825 (2001).
23. Sato, Y. *et al.* Solubility and Diffusion Coefficient of Carbon Dioxide in Biodegradable Polymers. *Ind. Eng. Chem. Res.* **39**, 4813–4819 (2000).
24. Sliepcevich, A., Storti, G. & Morbidelli, M. Measurement of diffusivity and solubility of olefins in polypropylene by gas chromatography. *J. Appl. Polym. Sci.* **78**, 464–473 (2000).
25. Dimos, V. & Kanellopoulos, N. Hybrid model for the diffusion of simple and complex penetrants in polymers. *J. Appl. Polym. Sci.* **104**, 2877–2885 (2007).
26. Kiparissides, C., Dimos, V., Boultouka, T., Anastasiadis, A. & Chasiotis, A. Experimental and theoretical investigation of solubility and diffusion of ethylene in semicrystalline PE at elevated pressures and temperatures. *J. Appl. Polym. Sci.* **87**, 953–966 (2003).
27. Chen, M., Wang, J., Jiang, B. & Yang, Y. Diffusion measurements of isopentane, 1-hexene, cyclohexane in polyethylene particles by the intelligent gravimetric analyzer. *J. Appl. Polym. Sci.* **127**, 1098–1104 (2013).
28. Kanellopoulos, V., Mouratides, D., Tsiliopoulou, E. & Kiparissides, C. An

Experimental and Theoretical Investigation into the Diffusion of Olefins in Semi-Crystalline Polymers: The Influence of Swelling in Polymer-Penetrant Systems. *Macromol. React. Eng.* **1**, 106–118 (2007).

29. Robeson, L. M. & Smith, T. G. Permeation of ethane–butane mixtures through polyethylene. *J. Appl. Polym. Sci.* **12**, 2083–2095 (1968).

30. Pino, M., Duckett, R. A. & Ward, I. M. Single and mixed gas diffusion through polyethylene films. *Polymer* **46**, 4882–4890 (2005).

31. Raharjo, R. D., Freeman, B. D., Paul, D. R., Sarti, G. C. & Sanders, E. S. Pure and mixed gas CH<sub>4</sub> and n-C<sub>4</sub>H<sub>10</sub> permeability and diffusivity in poly(dimethylsiloxane). *J. Membr. Sci.* **306**, 75–92 (2007).

32. Bartke, M. Gasphasenpolymerisation von Polybutadien. (TU-Berlin, 2002).

33. Alizadeh, A. Study of sorption, heat and mass transfer during condensed mode operation of gas phase ethylene polymerization on supported catalyst. (Université Claude Bernard-Lyon I; Queen's university at Kingston, 2014).

34. Bashir, M. A. *et al.* The Effect of Pure Component Characteristic Parameters on Sanchez-Lacombe Equation-of-State Predictive Capabilities. *Macromol. React. Eng.* **7**, 193–204 (2013).

35. Quynn, R. G., Riley, J. L., Young, D. A. & Noether, H. D. Density, crystallinity, and heptane insolubility in isotactic polypropylene. *J. Appl. Polym. Sci.* **2**, 166–173 (1959).

36. Bobak, M., Gregor, T., Bachman, B. & Kosek, J. Estimation of Morphology Characteristics of Porous Poly(propylene) Particles from Degassing Measurements. *Macromol. React. Eng.* **2**, 176–189 (2008).

37. Cancelas, A. J., Monteil, V. & McKenna, T. F. L. Influence of Activation Conditions on the Gas Phase Polymerisation of Propylene. *Macromol. Symp.* **360**, 133–141 (2016).

38. Martins, A. R., Cancelas, A. J. & McKenna, T. F. L. A Study of the Gas Phase Polymerization of Propylene: The Impact of Catalyst Treatment, Injection Conditions and the Presence of Alkanes on Polymerization and Polymer Properties. *Macromol. React. Eng.*

(2016). doi:10.1002/mren.201600011

39. Kröner, T. Mass Transport and Kinetics in the Heterophasic Copolymerization of Propylene. (Mensch & Buch, 2014).

40. Crank, J. The Mathematics of Diffusion. (Clarendon Press, 1979).

41. Frisch, H. L. “Diffusion in polymers” edited by J. Crank and G. S. Park, Academic Press, London and New York, 1968; 452 pg. J. Appl. Polym. Sci. **14**, 1657–1657 (1970).

## 4 The Effect of Reactor Conditions on High-Impact Polypropylene Properties and Gas Phase Polymerization Kinetics

*This chapter will be submitted for publication:*

Cancelas, A. J., Yang, L., Girod, R., de Heer, J., Kleppinger, R., Delsman, E., Wang, J., Gahleitner, M., Monteil, V. & McKenna, T. F. L. The Effect of Reactor Conditions on High-Impact Polypropylene Properties and Gas Phase Polymerization Kinetics. To be submitted. (2017).

### 4.1 Introduction

Isotactic Polypropylene (iPP) homopolymers have higher stiffness than PE, but also limited toughness, especially at lower temperatures. This can be overcome by incorporating an elastomeric copolymer of ethylene and propylene directly in the semi crystalline iPP matrix.<sup>1,2</sup> The resulting product is referred to as high impact polypropylene (hiPP). Such in situ reactor blends are well-known, and certain aspects of their production have been discussed in Chapter 1 (Page 17). Very briefly, an industrial process for hiPP products involves 2 reaction zones (each zone can be composed of one or more reactors). iPP is made in the first zone, the still active powders are then degassed and sent to a second zone in which usually a copolymer of propylene and ethylene (EPC) is made. The composition distribution of this copolymer is very broad, and includes amorphous ethylene-propylene copolymers (aEPC, also referred to as ethylene-propylene rubber, EPR) as well as crystallisable copolymers of ethylene and propylene (cEPC). The iPP homopolymer can be made in the gas phase or slurry phase, while the EPC must be made in a gas phase reactor, since aEPC is soluble in liquid hydrocarbons. In the current paper, our focus was on an “all gas phase” process.<sup>3</sup>

By varying the ratio EPC/iPP it is possible to control the property balance between toughness and stiffness of the final product. Thus, grades from low (5%) to super high (30-40%) impact product can be obtained. Concerning reactor performance and powder properties, several problems appear if the rubber is not well distributed in the iPP matrix. Considering a constant iPP matrix, how the EPC is distributed in the nascent hiPP particles will depend on the physical properties of the EPC itself, which in turn depend on the process engineering conditions, which will finally determine kinetics. For instance, too much rubber at the surface of the particles will affect powder flowability, causing stickiness and affecting reactor throughput.<sup>4,5</sup> This can finally lead to reactor fouling and blocking of

outlet valves, among other unfortunate incidents. As we can see, from a reaction engineering point of view it is important to fully understand this interconnected relationship among these three parameters: process engineering conditions, EPC properties, and copolymerization kinetics. Thus, in this study, we will investigate the systematic variation of rubber quantity, rubber properties and reaction conditions on the instantaneous rate of copolymerization and powder properties, keeping the initial PP matrix constant.

During polymerization, mass transport can become the reaction rate limiting factor if monomer does not diffuse from the gas phase through the polymer to the active sites as fast as it is converted into polymer. In the context of in situ rubber production in iPP, propylene is about 5 times more soluble in hiPP than ethylene,<sup>6</sup> and, for most Ziegler-Natta (ZN) catalyst systems, ethylene is roughly two times more active than propylene. Consequently, it seems reasonable to think that during the copolymerization step in hiPP production, ethylene might be subject to mass transfer resistance in certain cases, especially at elevated levels of EPC when the pore network of the iPP matrix powder is clogged with rubber, increasing the diffusion length. Model based analyses done by Kröner et al.<sup>7</sup> revealed significant diffusion limitations for ethylene, thus supporting this line of thought. Mass transfer limitations during the copolymerization of hiPP were experimentally investigated by a number of authors. Kittilsen and McKenna,<sup>8</sup> observed diffusion limitations for ethylene above 40% of EPC content. Hoel and Cozewith<sup>9</sup> polymerized ethylene-propylene copolymers with single-site metallocene catalysts, and saw differences between composition inside and out of the particles, being the change in composition greater for the large particles than for the small particles. They attributed this event to diffusion limitations. In contrast, experimental investigations of Debling and Ray<sup>10</sup> showed that if particles maintain sufficient porosity, any important mass transfer effects can be avoided for most situations, and they did not find hints for diffusion limitations until 70% of copolymer content, when they observed polymerization to take place only in the outer shell of the particles. As we can see, the experimental literature is inconclusive at this point. In this work, we will explore the relationship among kinetics, mass transfer limitations, physical properties, and chemical composition of the copolymers.

However, the previously mentioned disagreement present in the literature could also indicate that a way to improve EPC distribution and to diminish diffusion limitations is by modification of iPP morphology. This can be done by changing the precatalyst (as shown

by Smolná et al.<sup>11</sup>), or, if the same precatalyst is maintained, modifying its preparation and injection, as well as the phase in which the polymerization is carried out. The homopolymerization step can show different activities and lead to different morphologies depending on these factors, as shown in Chapter 2 and Appendix B. In this work, a different iPP morphology was obtained by varying the precontact procedure between precatalyst, alkyl aluminium and external lewis base, following the procedure shown in Appendix B. Keeping constant copolymerization conditions and ethylene/propylene ratio, the influence of iPP morphology on the EPC distribution was studied.

The objectives of the study are thus threefold: (1) to explore the relationship between process engineering conditions, EPC properties, and copolymerization kinetics; (2) to find evidence for mass transfer limitations of ethylene and their impact on EPC distribution; and (3) to explore the relationship between iPP morphology and EPC distribution.

## 4.2 Experimental Section

### 4.2.1 Chemicals

Two commercial MgCl<sub>2</sub> supported titanium fourth generation Ziegler Natta precatalyst were used. They are referred to as “A” and “C”. All heptane used was pre-treated on 3Å molecular sieves. Mineral oil Primol 352,<sup>12</sup> a medicinal grade white mineral oil, was purchased from Fisher Scientific. It is an inert and protective carrier commonly used industrially for polypropylene processes. Before use, it was degassed cold under vacuum to eliminate any trace of oxygen and then kept under argon atmosphere at room temperature. Propylene and propane with a minimum purity of 99.5 % and hydrogen with minimum purity of 99.99% were purchased from Air Liquide (France). Propylene was purified with a three-stage system of columns before use: a first one filled with BASF R3-16 catalyst (CuO on alumina), a second one filled with molecular sieves (13X, 3A, Sigma-Aldrich), and a last one filled with Selexsorb COS (Alcoa). Argon provided by Air Liquide, France, with a minimum purity of 99.5 %, was used to keep the reaction free of oxygen.

### 4.2.2 Semibatch Polymerization

The experimental set-up used in this section had some additional features as compared to the one shown in previous chapters and publications.<sup>13,14</sup> The first one, as displayed in Figure 4.1, is a 2.5L thermostated ballast which allowed us to run experiments at 20 bar of

gas propylene pressure. This was connected to the propylene reservoir and filled with liquid propylene when set to cooling. Once vapor liquid equilibrium was reached, the inner ballast temperature was raised to 49 °C and 20 bar of propylene pressure were obtained. A 0.5L volume was left without refrigeration to ensure that not all the volume was filled with liquid for safety considerations. Otherwise, uncontrolled fast rises of pressure could occur during temperature rise.

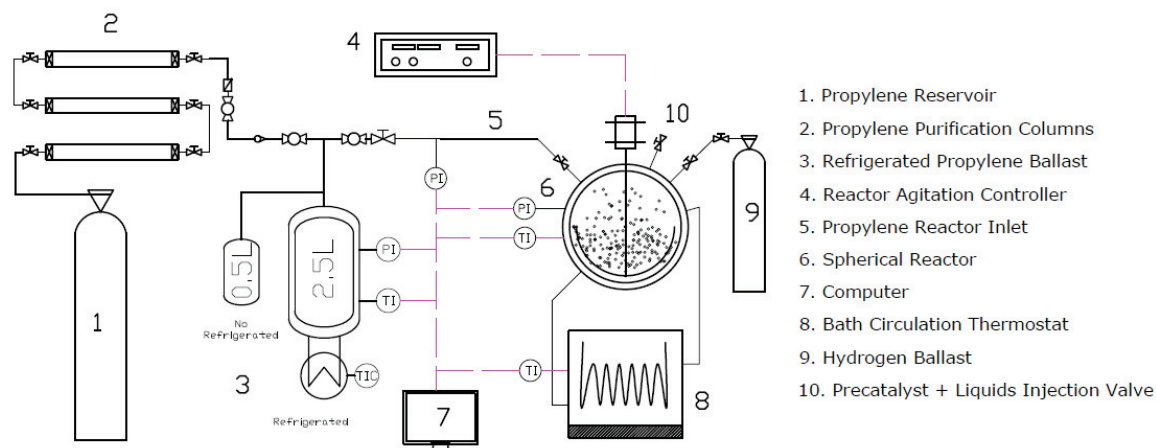


**Figure 4.1.** Turbosphere polymerization system. Thermostated ballast and thermostated reactor. Please note that this set-up was used for homopolymerization.

This set-up was used for the first stage of hiPP production, in this work, gas phase propylene homopolymerization. Before every experiment, the reactor was heated to 60 °C and kept under vacuum for 1 h. The reactor was further purged with argon before each experiment. Triethylaluminium (TEA, Witco, Germany) and Dicyclopentyldimethoxysilane (DCPDMS) were used as cocatalyst and external lewis base (ELB) respectively, with Al/Ti and Si/Ti ratios of 260 and 20. Once the reactor had reached the desired initial temperature, the required amount of 1M TEA/heptane mixture and the donor/heptane mixture (0,42 M) were injected under argon and agitation (~300 rpm) was started. A slurry precatalyst solution was used (60 mg/mL) with feed oil. About 5 minutes after TEA injection, 167  $\mu\text{L}$  of the precatalyst suspension (volume that corresponds to 10 mg of precatalyst) were injected. Injection could be done either under propylene (no precontacting) or argon (precontacting), as illustrated in Figure 4.2 **Figure 4.** If precontacting was done, TEA/ELB and precatalyst were stirred in the gas phase during 2 min, (difference in time of  $t_4$  and  $t_3$ ) and then propylene was injected.

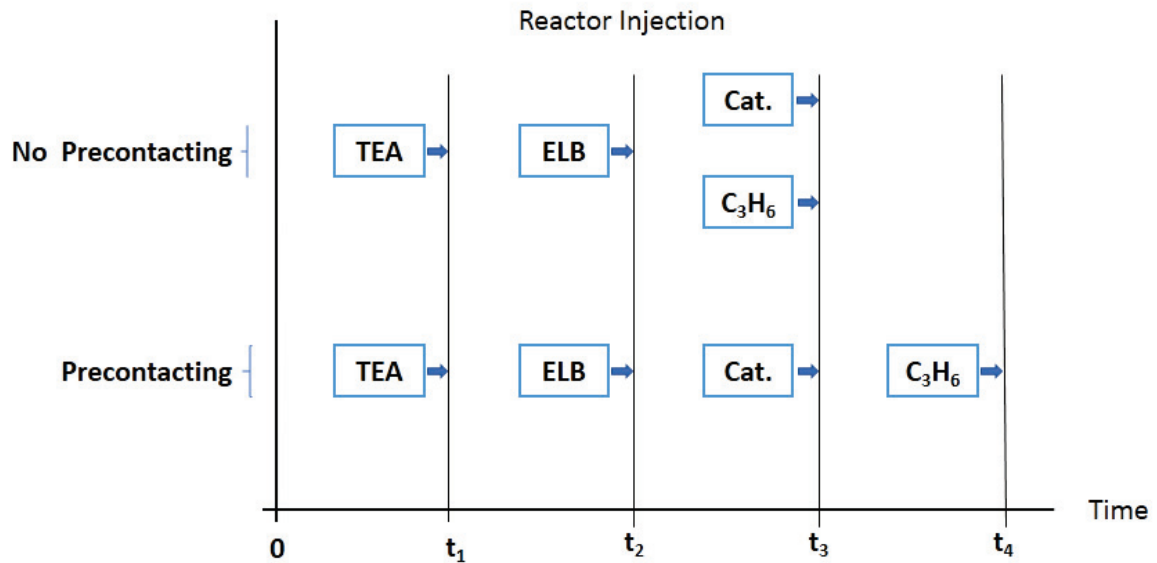


**Figure 4.2.** Schematic illustration of precontacting and no-precontacting procedures.

As explained in Appendix B (Page 177), precontacting the precatalyst, alkyl aluminium and ELB leads to PP particles with slightly larger meso-particles than one obtains if no precontacting is done. In turn, bigger meso-particles lead to slower monomer diffusion through the polymer particle. In other words, non precontacted polypropylenes display less resistance to the diffusion of monomers. No precontacting procedure was only applied to prepare one hiPP sample studied in the AFM section. The sample was A70-13-40-8.

#### 4.2.2.1 Homopolymerization

A gas phase prepolymerization was always performed for 10 min at 7 bars (gauge pressure) and 40°C without H<sub>2</sub>, then hydrogen was added (2% molar with respect to total pressure), and pressure and temperature were raised to 70°C and 20 bar. The reaction was stopped when a productivity of 10Kg/g was achieved. The activity was estimated by stopping the feed to the reactor and measuring the pressure drop over a fixed period. Pressure drop was interpreted using the Soave-Redlich-Kwong equation of state (SRK-EoS) to convert it to grams of PP. Then, the integral of the instantaneous reaction rate was fitted to the real obtained polymer yield. Finally, reaction rate was fitted to the kinetic model with lumped rate constants and 1st order deactivation shown in Chapter 2 (Equation 2.1) and in refs. [13,15]. Once the desired degree of homopolymer was obtained, the reactor was depressurized. If copolymerization had to be done without hydrogen, a brief period of vacuum was applied to remove the possible remaining traces from homopolymerization.

## 4.2.2.2 Copolymerization

Preliminary experiments were run with this catalyst to identify the gas phase compositions required to obtain some specific rubber compositions. This data is shown in Table 4.1.

**Table 4.1.** Experimentally found gas phase compositions needed to achieve the desired ethylene-propylene copolymer (EPC) compositions.

Equilibrium Gas Phase Composition (mol%)		EPC Composition (mol%)	
Ethylene	Propylene	Ethylene	Propylene
40	60	50	50
30	70	40	60
50	50	60	40

During copolymerization composition drift was avoided by starting with the same gas phase composition as it would end, according to Table 4.. If copolymerization was done at 8 bar, the reactor was pressurized up to 2.4 bar with pure propylene. Then, an ethylene-propylene gas mixture was fed continuously. The C2/C3 ratio of this mixture was the same as the one required in the rubber. Gas phase composition was evaluated with a gas micro-chromatograph ( $\mu$ PGC3000 from SRA instruments from France, Lyon). Every 15 min during reaction and then once more when reaction was stopped gas phase composition was measured. Each measurement was repeated 3 times for the sake of certainty. A scheme of the reaction configuration used during copolymerization is shown in Figure 4.3.

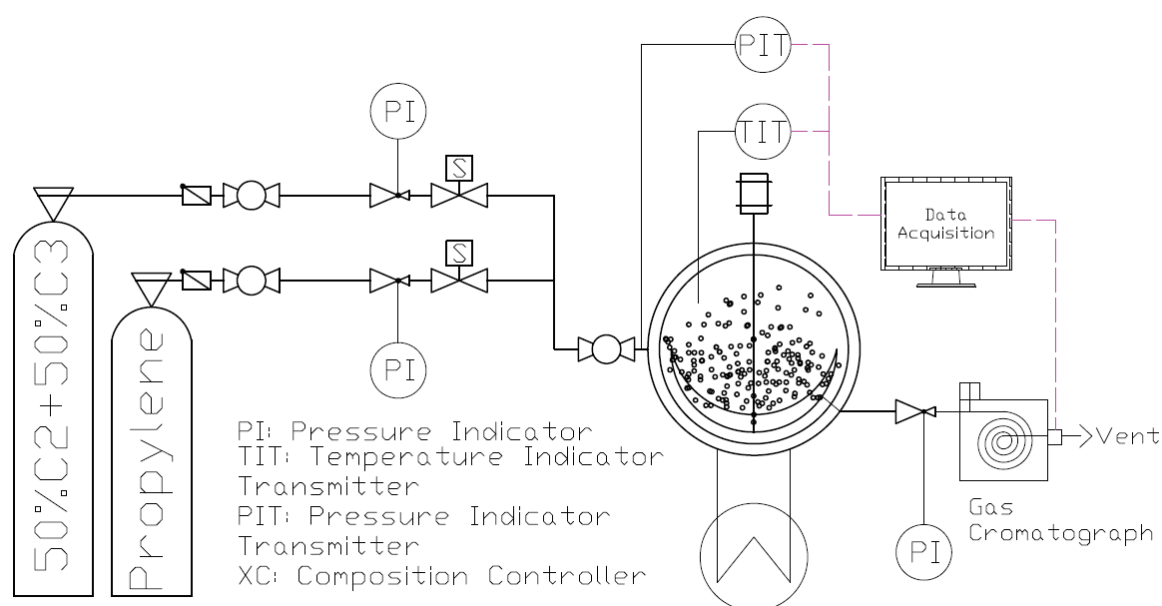


**Figure 4.3.** Experimental set-up of the gas phase reactor used during copolymerization.

Typical copolymerization conditions were 70 °C and 8 bars (gauge pressure). As an

illustration of the degree of control and the dynamics of a typical polymerization experiment, gas phase temperature (main axis) and reactor pressure (secondary axis) are shown in Figure 4.4.

The reaction was stopped when the desired degree of copolymerization was reached, this time calculated from ballast pressure drop. Then, the monomer inlet was closed and the reactor was cooled down rapidly.

Kinetic curves during the copolymerization step were obtained from the pressure drop of the propylene-ethylene ballast. Then, the fitted pressure curve was used to calculate the activity converting it to mass of propylene-ethylene present in the ballast at a certain time. SRK EoS was used for this calculation.<sup>16</sup> Molar mass, critical pressure ( $P_c$ ) and critical temperature ( $T_c$ ) were calculated via the pure values of ethylene and propylene depending on their ballast molar ratio.

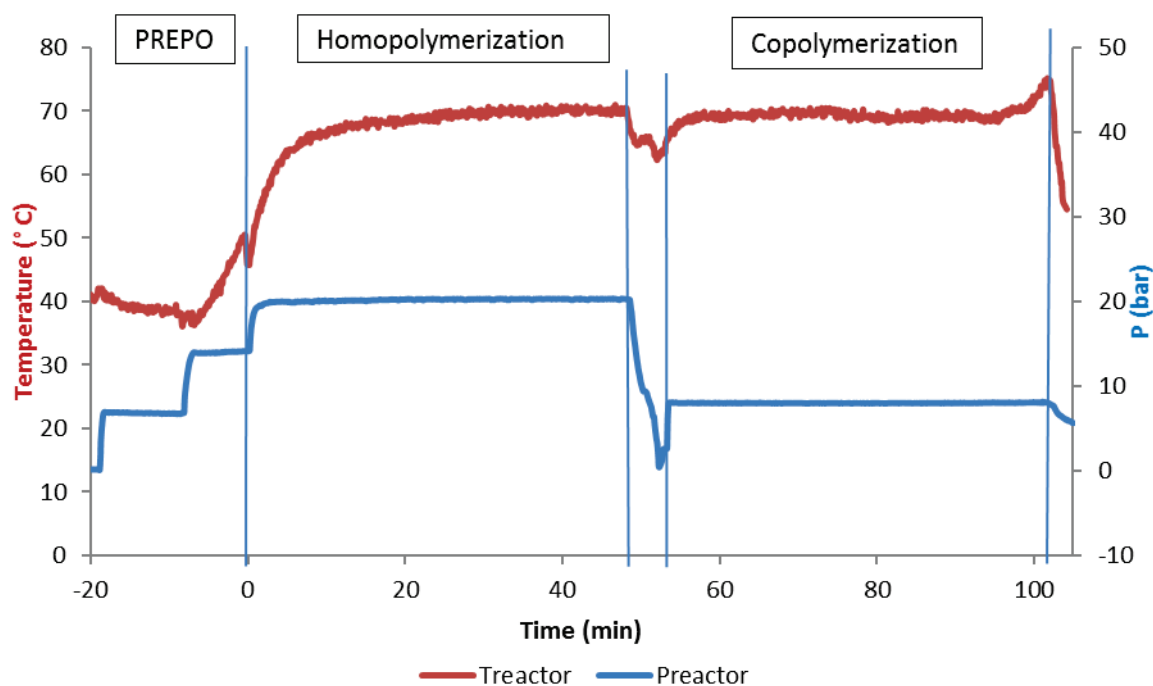


**Figure 4.4.** Gas phase temperatures (main axis) and reactor pressure (secondary axis) during a representative run with prepolymerization (A70-10-40-8).

### 4.2.3 Polymer Characterization

An analysis of the microstructure of the powders was done using  $^{13}\text{C}$  liquid NMR spectroscopy. Assignment of the peaks, quantification of the co-monomer fraction, analyses temperature and spectrometer specifications can be found in ref. [17].

Successive self-nucleation (SSA) differential scanning calorimetry (DSC) fractionation was also performed using the techniques applied in refs. [18,19]. This SSA method offers a practical way to evaluate chain heterogeneities in hiPP by using an easy to run thermal protocol in a Differential Scanning Calorimeter (DSC). The heating steps are shown in Figure 4.5. The crystallinity of the samples was calculated assuming enthalpy of fusion of  $207 \text{ J g}^{-1}$  for a fully crystalline polypropylene.<sup>20</sup> This value was also used for all other crystal populations that appeared in the DSC thermogram. This is not the correct value for those populations, but it is assumed for comparisons among hiPP samples since it is very difficult to correctly identify the chemical make-up of the polymer that corresponds to the additional crystalline peaks. We considered data of the thermogram obtained during the 52<sup>nd</sup> step (i.e. the last one).

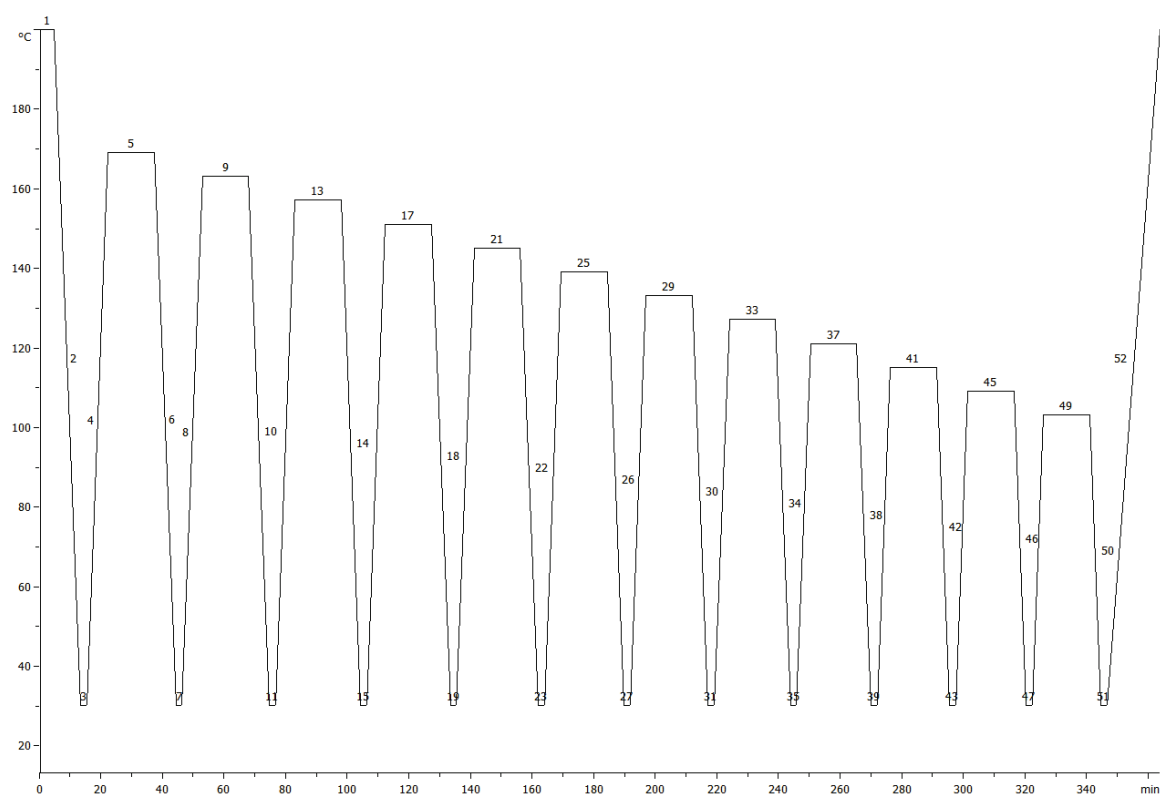


**Figure 4.5.** Temperature program of the applied SSA method to every hiPP sample of this study. (°C) for Y axis and (min) for X axis.

Before doing powder flowability (PF) tests, the powders were stabilized by solution spraying. 100 g of polymer powder were poured through a metallic funnel (to avoid possible electrostatic charges) at room  $T^\circ$ , and the time required was recorded (ISO 6186/1998).<sup>21</sup> Each measurement was repeated three times. When a different mass was used, results were normalized to 100 grams.

The crystalline and soluble fractions of the polypropylenes as well as the comonomer content and intrinsic viscosities of the respective fractions were analyzed by the CRYSTEX QC instrument, developed by and commercially available from Polymer Char (Valencia, Spain).<sup>22</sup>

Storage ( $G'$ ) and loss ( $G''$ ) moduli and their temperature dependence of hiPP samples were determined with Dynamic mechanical thermal analyses (DMTA). They were done according to standard ISO 6721-7 in torsion mode on specimens cut from compression moulded plates ( $40 \times 10 \times 1 \text{ mm}^3$ ) in an MCR301 instrument at a heating rate  $2 \text{ }^\circ\text{C}/\text{min}$  and at  $1 \text{ Hz}$  frequency, from  $-130$  to  $160 \text{ }^\circ\text{C}$ .

Determination of tensile properties, (tensile strength and tensile modulus) was conducted according to ISO 527-1, -2 at  $23 \text{ }^\circ\text{C}$ . The tests were performed with a test machine Zwick Z100-725333 and an extensometer Zwick MultiXtens-236190. Test speed was  $50 \text{ mm}/\text{min}$ . The specimens were of type 5A according to ISO 527-2 cut from a 2-mm thick compression moulded plaque.

Malvern Mastersizer 3000 was used for the measurement of particle size distribution (PSD) of polymer particles, with a specific dry module "Aero S Dry Powder Dispenser".

Porosity of selected polymer powders was measured via Mercury porosimetry. To prepare the mercury porosimetric measurement, the samples were dried for 1 hour, at  $80 \text{ }^\circ\text{C}$ . in a drying cabinet. The measurements were carried out on a QUANTACHROME POREMASTER 60-GT. Only the range from  $10 \text{ }\mu\text{m}$  to  $0.1 \text{ }\mu\text{m}$  was considered, since higher ranges represent the interstitial volume (between particles) and lower are due to material deformation. In addition, due to the uncertainties of the measurement, only results of total porosity (no pore size distributions) are used for discussion.

#### 4.2.3.1 Atomic Force Microscopy (AFM)

Particles were embedded in a resin and then sample cross section cryo-microtoming (LEICA EM UC7) was performed at constant temperature of  $-140 \text{ }^\circ\text{C}$  using a diamond knife (Diatome) mounted in a stainless-steel holder to obtain a flat cross section surface for AFM measurements. The multicomplex structure of hiPP can also include neat HDPE,<sup>2</sup> which has a glass transition temperature ( $T_g$ ) of around  $-120 \text{ }^\circ\text{C}$ . For this reason, such a low temperature was chosen for microtoming. To avoid rubber aging, which is the rubber

migration to the surface (see results and discussion for a deeper explanation about this phenomenon) samples were kept in a freezer at  $-21^{\circ}\text{C}$  right after being cut.<sup>23</sup> Then AFM measurements were performed over the obtained flat surfaces before rubber migration started to take place. An illustration of the procedure followed to prepare the samples for AFM measurements is shown in Figure 4.6.

AFM experiments were performed using a Dimension FastScan AFM system (Dimension FastScan, Bruker, Santa Barbara, USA). Software Nanoscope Analysis 1.5 from Bruker is used as computer interface for operation and analysis of AFM measurements. All AFM measurements were performed at ambient conditions and the experimental conditions for the measurements were dependent on the AFM mode. For rubber distribution characterization, AFM tapping mode in fast scan mode was used with a frequency of 5 Hz to further shorten the measurement time to avoid any rubber aging. Fastscan A tips (Bruker,  $f = 1400\text{kHz}$ ,  $K = 18\text{ N/m}$ ) was used for the Fastscan tapping mode imaging.

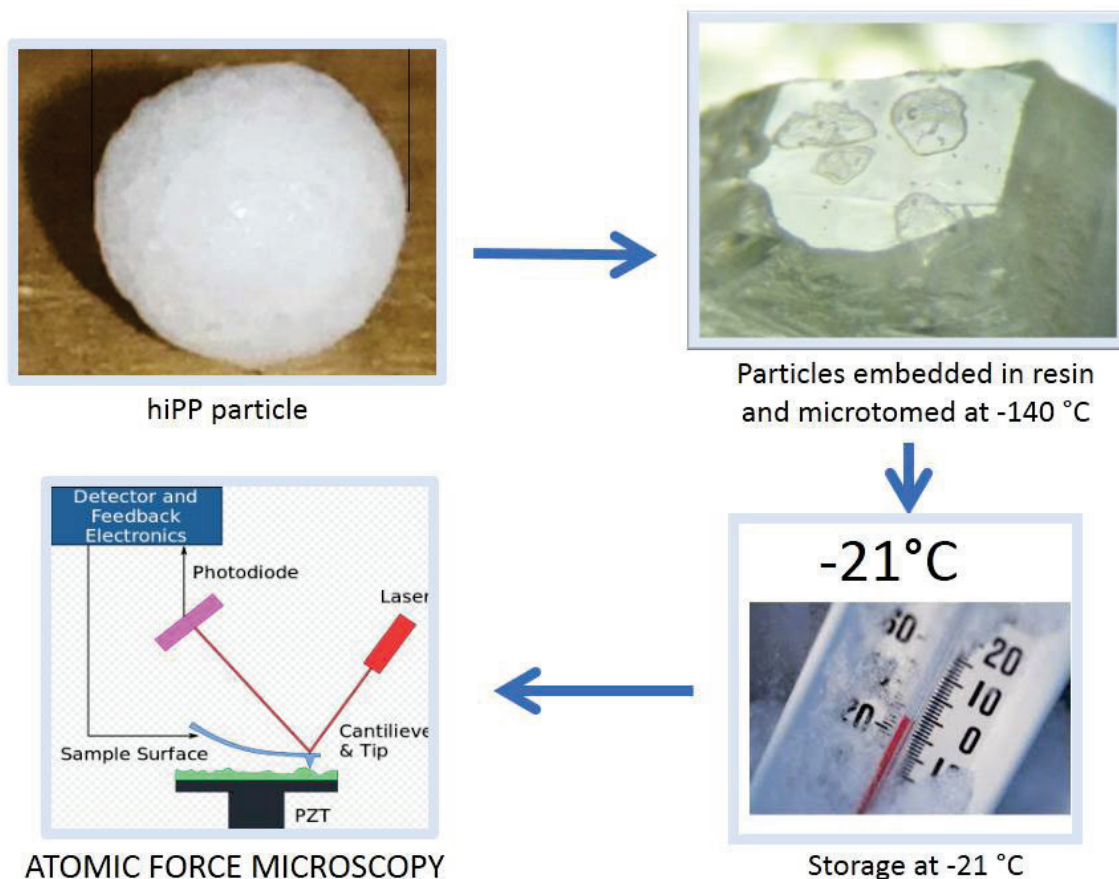


**Figure 4.6.** Block diagram illustration of the sample preparation procedure followed for AFM measurements.

To understand better the nano-mechanical properties with the hiPP particles, the stiffness

of rubber phase was characterized by AFM-QNM (Quantitative Nano-mechanical Mapping) mode with a frequency of 1 Hz using a AFM tip with a spring constant of 7 N/m (Bruker, RTESPA-150 Tip). Only for the samples that are left at room temperature for 7 days, a softer Scanasyst tip (Bruker) with spring constant of 0.5 N/m was used. QNM mode enables the quantitative measurements of nano-scale material mechanical properties by performing pixel-wise force curves in the scanned area. Analysis of the individual force curve data by the AFM Nanoscope software provides a map of material properties with the same resolution of topography image. Here the elastic modulus of the sample was fit from the force curve using the Derjaguin-Muller-Toropov model<sup>24</sup> and presented in the modulus mapping images. The spring constant of individual cantilever was calibrated using thermal noise spectrum method integrated in the Nanoscope software. Then the individual tip radii were estimated from the measurements on a PDMS calibration sample with known modulus of 2.5MPa (Bruker, PFQNM-SMPKIT-12M).

#### **4.2.4 List of Experiments**

The list of the experiments performed in the current study along with their conditions is summarized in Table 4.2. The name of the experiments is generally given by “AT<sup>o</sup>-XX-EPC-P”, where “A” is the catalyst used (A), “T<sup>o</sup>” is the temperature in °C at which copolymerization step is done at, “XX” can be (1) the estimated productivity during the homo-polymerization step through kinetics in Kg/g, (2) the presence of hydrogen during copolymer step, and (3) the predicted molar percentage of ethylene in the copolymer, if different from 50%. “EPC” is the wt% copolymer content estimated by pressure drop in the copolymerization ballast, and finally “P” is the pressure kept during copolymerization.

**Table 4.2.** Summary of the runs performed in this study <sup>a</sup>

Run	Homo-polymerization	Copolymerization			
	Productivity (kg/g)	EPC (wt%)	E/P mol ratio	P (bar)	T (°C)
A	10	-	-	-	-
A70-10-10-8	10	10%	50/50	8	70
A70-10-20-8	10	20%	50/50	8	70
A70-10-30-8	10	30%	50/50	8	70
A70-10-40-8	10	40%	50/50	8	70
A70-10-40-5	10	40%	50/50	5	70
A70-10-40-11	10	40%	50/50	11	70
A60-10-40-8	10	40%	50/50	8	60
A80-10-40-8	10	40%	50/50	8	80
A70-H <sub>2</sub> -40-8	10	40%	50/50 & H <sub>2</sub>	8	70
A70-0,4-40-8	10	40%	40/60	8	70
A70-0,6-40-8	10	40%	60/40	8	70

<sup>a</sup> Homopolymerization was done at 20 bar of propylene with 2% of H<sub>2</sub> at 70 °C

### 4.3 Results and Discussion

#### 4.3.1 Kinetic Profiles

The instantaneous rate of polymerization of the different runs displayed in Table 4.2 are shown in Figure 4.7, Figure 4.8, Figure 4.9, Figure 4.10, and Figure 4.11. Considered default conditions are those of run A70-10-40-8. Thus, the aforementioned kinetic curve is used as a reference and systematically compared to the others. Reproducibility of the kinetic curves was ensured by repeating only the most unexpected results, as those from runs A70-H<sub>2</sub>-40-8 and A80-10-40-8. Conditions during the homopolymerization step were kept constant, and therefore similar kinetic curves are obtained for all runs. Prepolymerization was done for every experiment. Time  $t = 0$  of the first step is the moment where the reactor temperature reached 50 °C (during the heat up from 40° to 70°) as exhibited in Figure 4.4. Experience showed that the reaction rate began to increase quickly

near this temperature for all runs. Therefore, at this point the pressure was increased to 20 bar and kinetic measurements were started. In this way, a similar amount of prepolymerization yield and the lowest possible level of catalyst deactivation were ensured for every run.

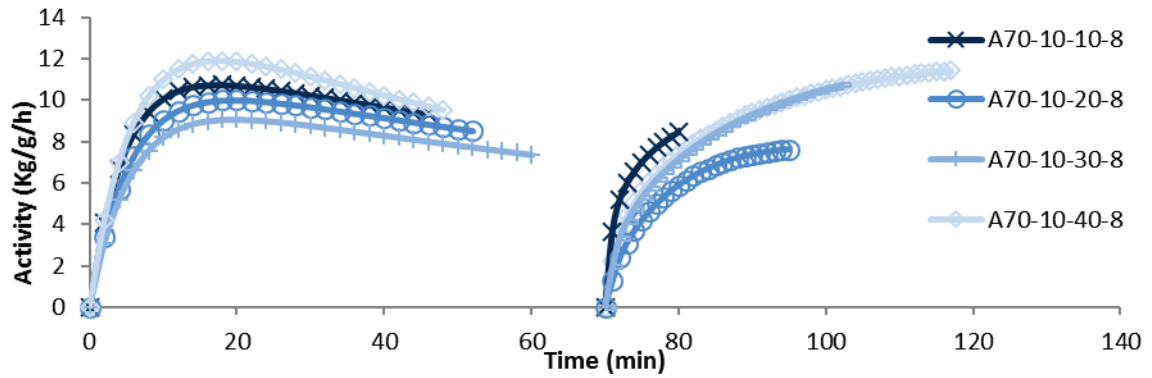


Figure 4.7. Kinetic profiles of runs with increasing EPC (10, 20, 30, and 40% EPC)

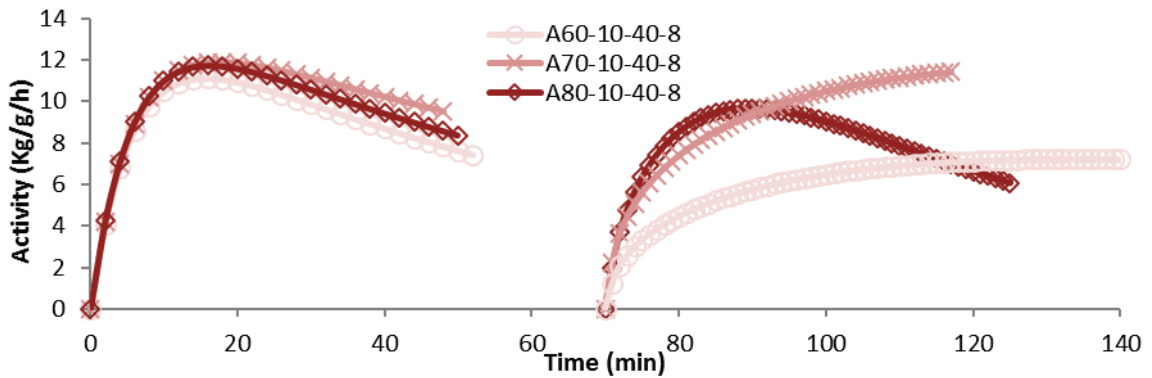


Figure 4.8. Kinetic profiles of runs with different  $T^\circ$  during copolymerization (60, 70 and 80 °C)

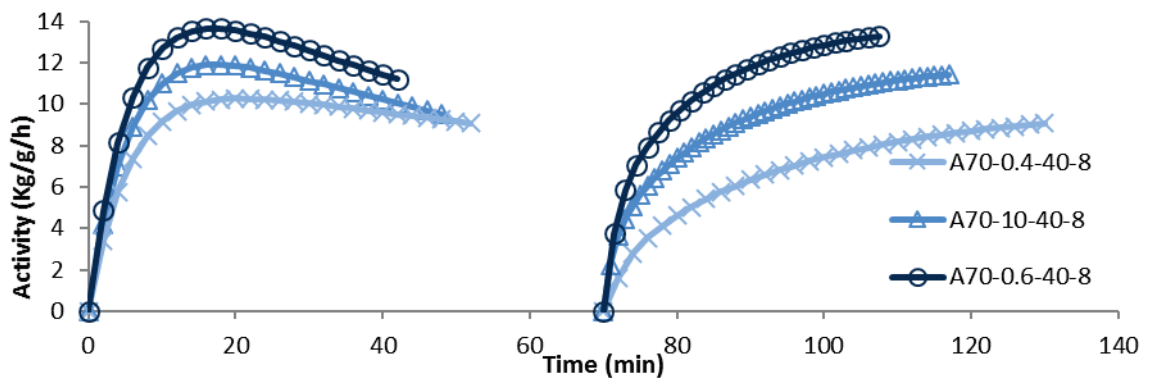
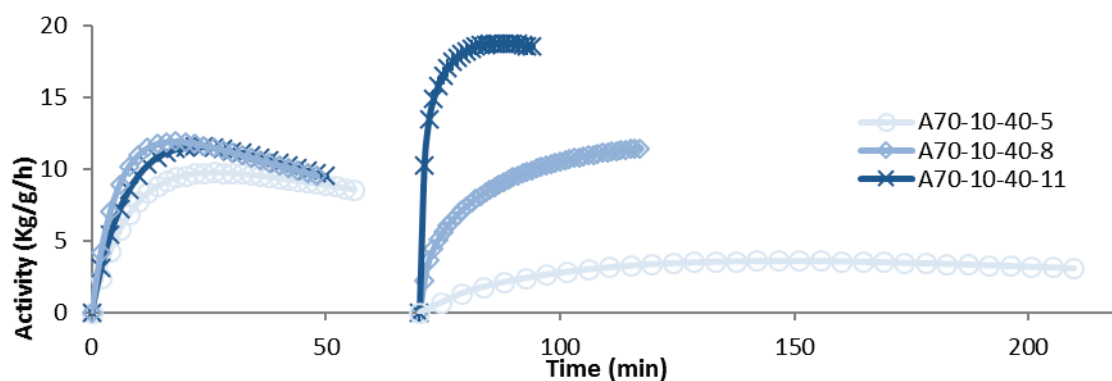
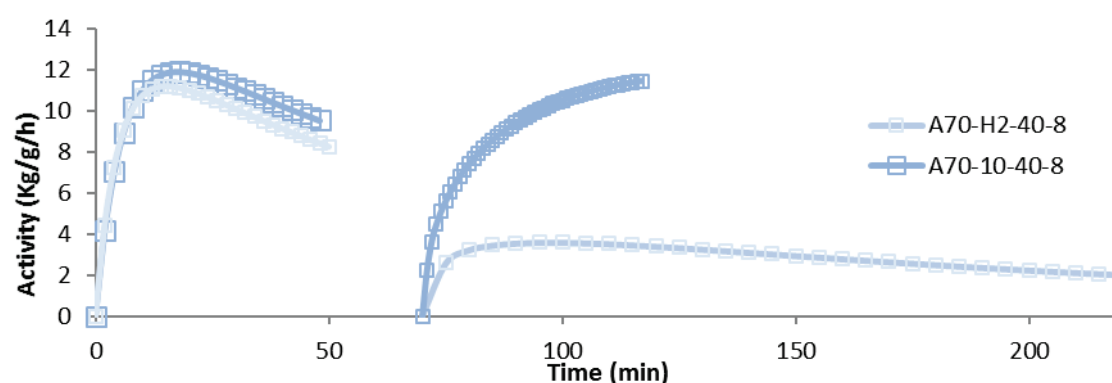


Figure 4.9. Kinetic profiles of runs with different % C2 in copolymer (40, 50 and 60%)



**Figure 4.10.** Kinetic profiles of runs with different pressure during copolymerization (5, 8 and 11 bar). Pay attention to the changes in Y and X scales as compared to earlier figures.



**Figure 4.11.** Kinetic profiles of runs with and without H<sub>2</sub> (2%) during copolymerization.

These figures show that all of the homopolymerization curves show rapid activation followed by a decay-type profile. A rise in activity is observed when copolymerization is started. This behavior is to be expected and has been observed elsewhere with Ziegler-Natta catalysts.<sup>7,10</sup>

The rates of the copolymerization experiments also show some predictable behaviours. The instantaneous reaction rate of the gas mixture of ethylene and propylene increases with pressure (Figure 4.10), and an enhancement in activity is also observed with the increase of the relative ethylene concentration in the gas phase (Figure 4.9), as ethylene is the more reactive monomer. Temperature also enhances activity, albeit up to a certain limit, probably set by catalyst thermal degradation (as discussed in Chapter 2).<sup>6-8,25,26</sup> Higher temperatures seem to faster activate the catalyst, although followed by faster deactivation.

Copolymerization kinetic profiles of runs with different copolymer content, as shown in Figure 4.7, give an idea of the good reproducibility during the 2<sup>nd</sup> step of our hiPP production protocol. It also seems that the curves tend to a maximum activity not yet reached during copolymerization. However, in Figure 4.8, Figure 4.10, and Figure 4.11 it

can be noticed that the activity peak (and the subsequent deactivation profile) is reached earlier if temperature, pressure or hydrogen concentration are increased, with respect to reference values. This effect of temperature on catalyst activity can be attributed to particle overheating in combination with the high sensitivity of polypropylene catalysts to elevated temperatures, as discussed in Chapter 2. Pressure may also contribute to a rise in the intraparticle temperature, caused by the higher activities and the bad heat transfer conditions of the gas phase.

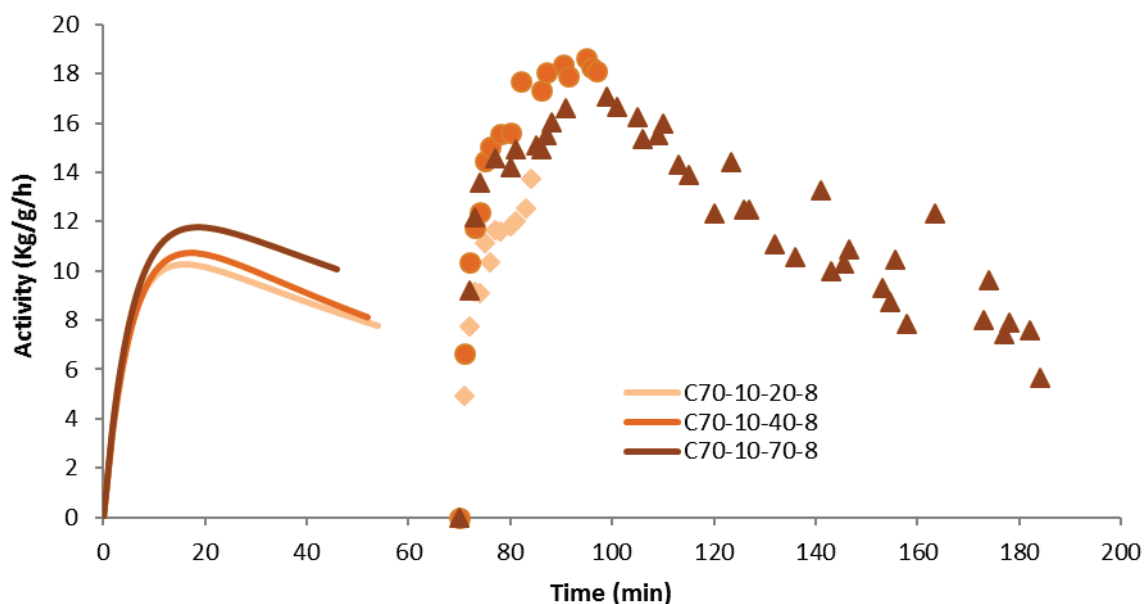
When only propylene is present in the reaction environment, hydrogen boosts activity of ZN catalyst systems, as it is well-known. Nevertheless, for the precatalyst used in this study it seems to have the opposite effect if ethylene is also present, as displayed in Figure 4.11. Therefore, a different ZN catalyst was used to investigate the influence of hydrogen in the copolymerization rate. Table 4.3 shows the experiments planned with C precatalyst, where the rest of conditions were kept equal as runs A70-10-40-8 and A70-H<sub>2</sub>-40-8. The resulting kinetic profiles are plotted in Figure 4.12 and Figure 4.13, for experiments without and with hydrogen during copolymerization, respectively. Note that the pressure drop in the ballast was not fitted to any function, in contrast to the runs of precatalyst A. Therefore, the obtained rate profiles show more noise.

Once more, kinetic profiles exhibit a high reproducibility both for homo- and copolymerization stages. Comparing these activity profiles with those resulting from precatalyst A, first it can be noticed that this catalyst system is more active, but only during the copolymerization, and second, the activity peak during copolymerization is reached earlier. In Figure 4.12 takes about 30 min while in Figure 4.7 activity peak didn't show up before 50 min of reaction, considering the same conditions. There is another clear difference with precatalyst A experiments: interestingly, in this case there was no appreciable difference in the copolymerization rate either with or without hydrogen in the gas phase. Therefore, the decrease in activity caused by the hydrogen presence in the gas phase is evidently subject to the catalyst system.

**Table 4.3.** Planning of the experiments for high impact polypropylene kinetics investigation with C precatalyst. <sup>a</sup>

Run	Homo-polymerization	Copolymerization			
	Productivity (kg/g)	EPC (%wt)	E/P mol ratio	P (bar)	T (°C)
C70-10-20-8	10	20%	50/50	8	70
C70-10-40-8	10	40%	50/50	8	70
C70-10-70-8	10	70%	50/50	8	70
C70-H <sub>2</sub> -40-8	10	40%	50/50 & H <sub>2</sub>	8	70

<sup>a</sup> Homopolymerization was done at 20 bar of propylene pressure with 2% of H<sub>2</sub> at 70 °C

**Figure 4.12.** Kinetic profiles of runs with increasing copolymer content (20, 40 and 70%)

To help in understanding the relationship between copolymerization kinetics and hiPP properties, the resulting powders of the experimental plan shown in Table 4.2 were characterized by different techniques, as detailed in the following subsections.

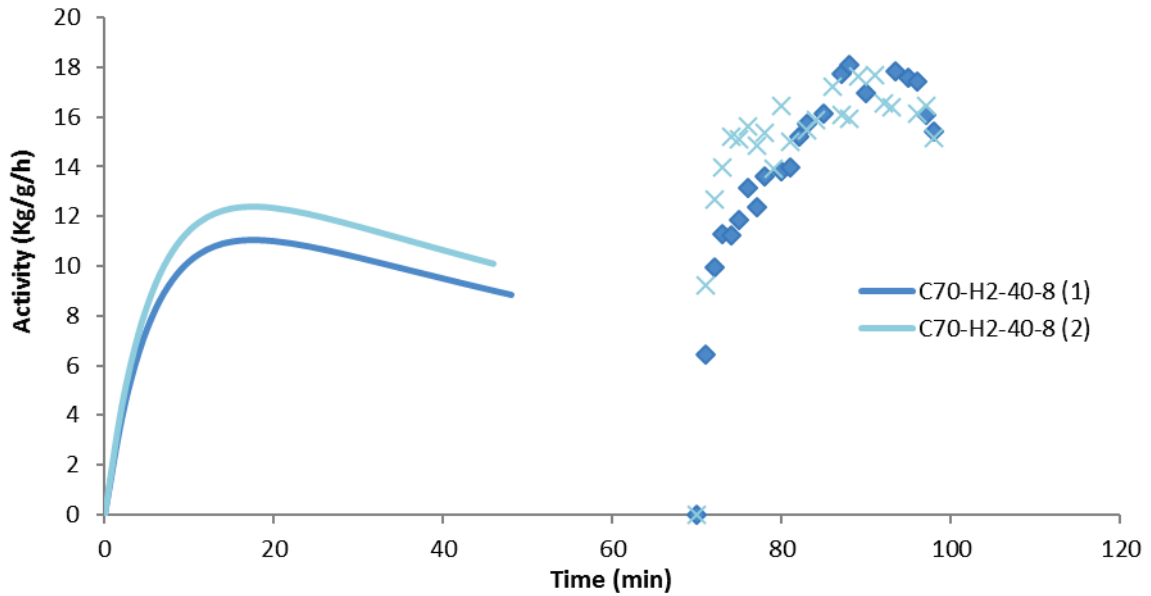


**Figure 4.13.** Kinetic profiles of runs with H<sub>2</sub> (2%) during copolymerization. Pay attention to the change in X axis as compared to the earlier figure.

### 4.3.2 Polymer Fractionation

**Table 4.4.** Crystex QC results of all hiPP samples planned in this study <sup>a</sup>

Sample	Fractionation (Crystex QC)							
	Sol. fract. wt%	C2 total wt%	C2 (SF) wt%	C2 (CF) wt%	IV total dl/g	IV (SF) dl/g	IV (CF) dl/g	IV ratio
A	3,2	0,0	6,9	0,8	3,3	0,1	3,2	0,0
A70-10-10-8	12,7	5,1	27,4	2,7	3,8	5,8	3,4	1,7
A70-10-20-8	19,3	8,3	30,1	4,0	5,1	8,9	3,9	2,3
A70-10-30-8	28,5	12,6	32,4	5,6	5,3	8,0	3,9	2,0
A70-10-40-8	39,1	18,7	34,6	10,0	7,2	9,2	5,0	1,8
A70-10-40-5	31,3	15,8	33,6	9,3	6,8	8,7	5,2	1,7
A70-10-40-11	34,5	16,1	33,7	7,9	6,3	8,4	4,5	1,9
A60-10-40-8	34,7	17,7	34,4	10,2	8,3	10,2	5,7	1,8
A80-10-40-8	35,2	16,4	34,7	8,7	3,6	3,9	3,4	1,2
A70-H2-40-8	35,1	17,1	34,4	8,8	3,6	4,0	3,3	1,2
A70-0,4-40-8	35,3	13,8	29,3	6,5	5,5	7,7	4,1	1,9
A70-0,6-40-8	36,3	20,9	41,6	10,7	6,2	8,1	4,5	1,8

<sup>a</sup> SF is soluble fraction, CF stands for crystalline fraction, and IV for intrinsic viscosity.

The crystalline and soluble fractions as well as the comonomer content and intrinsic

viscosities of the respective fractions of Table 4.2 polypropylenes are shown in Table 4.4. Samples were analyzed by the CRYSTEX QC technology.<sup>22</sup> CRYSTEX QC offers an automated determination of three crucial properties of heterophasic ethylene-propylene copolymers: (1) quantification of the soluble fraction (SF), which is equivalent to the xylene cold soluble (XCS) fraction and the crystalline fraction (CF), which is equivalent to the xylene cold insoluble (XCI) fraction, in line with ISO 6427,<sup>27</sup> (2) ethylene content (C2) of the full hiPP sample and its soluble and crystalline fractions, and (3) intrinsic viscosity (IV) of the full hiPP sample and its soluble and crystalline fractions.

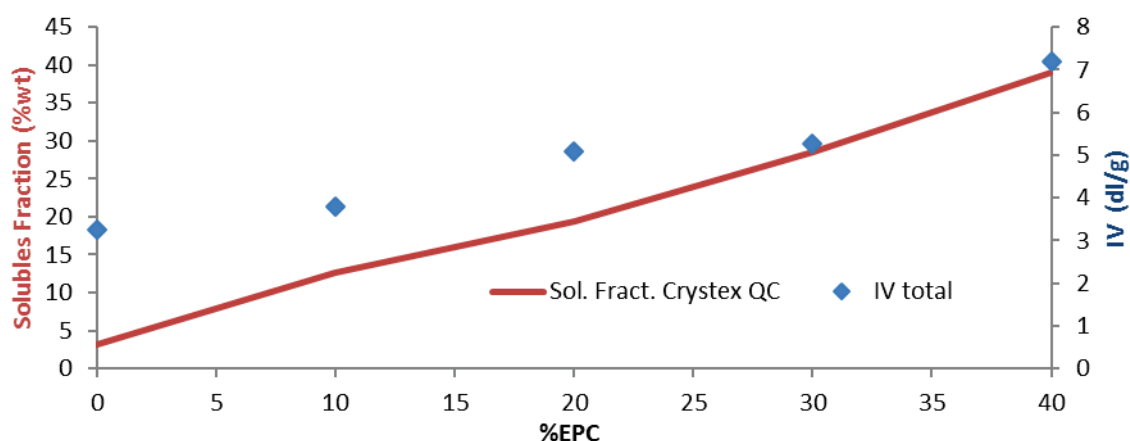


**Figure 4.14.** Solubles fraction in xylene at 40 °C and total intrinsic viscosity in function of copolymer content

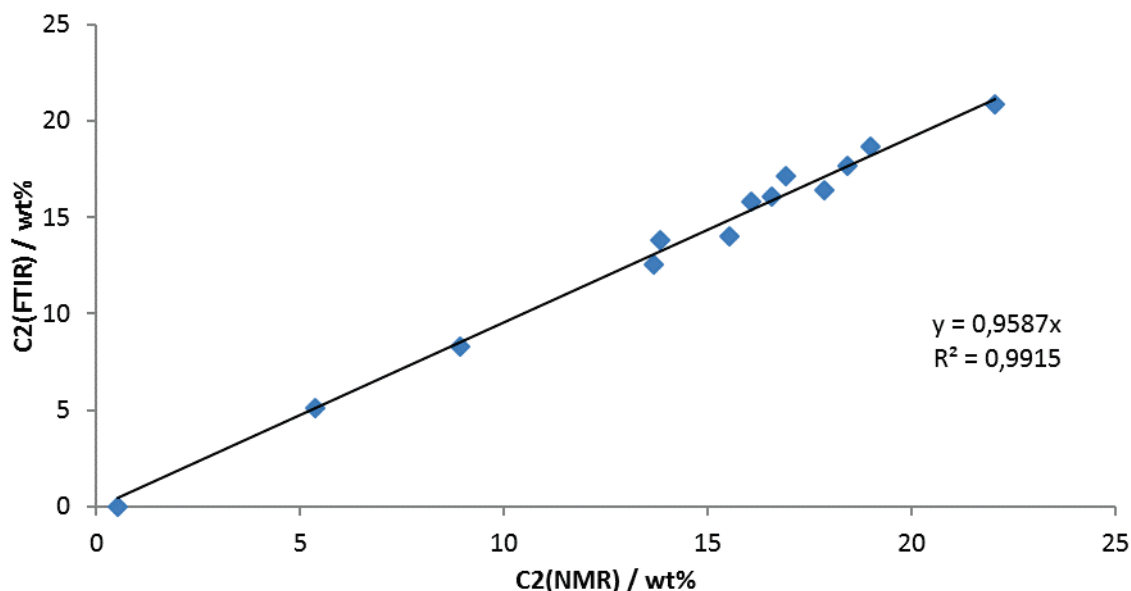


**Figure 4.15.** Correlation of ethylene content for every powder investigated among Crystex QC results and NMR results.

It can be seen here that the soluble fraction is in good agreement with the % of EPC estimated by pressure drop. It should also be noted that a small fraction of the copolymer

makes part of the crystalline fraction. Total IV increases with %EPC, as shown in Figure 4.14, since no hydrogen was used during copolymerization. In addition, the low IV of the SF of samples A80-10-40-8 and A70-H2-40-8 and the high IV of sample A60-10-40-8 evidence that temperature and hydrogen presence decrease the copolymer molecular weight, as expected.

NMR analyses were done for every polymer studied, and, as shown in Figure 4.15, results were quite consistent with those from Crystex QC, confirming their reliability.

These results shown in Table 4.4 will help us to elucidate the influence that the rubber (or copolymer) of different properties have on distinct features of final polymers, as powder flowability and mechanical properties.

### 4.3.3 Powder Flowability

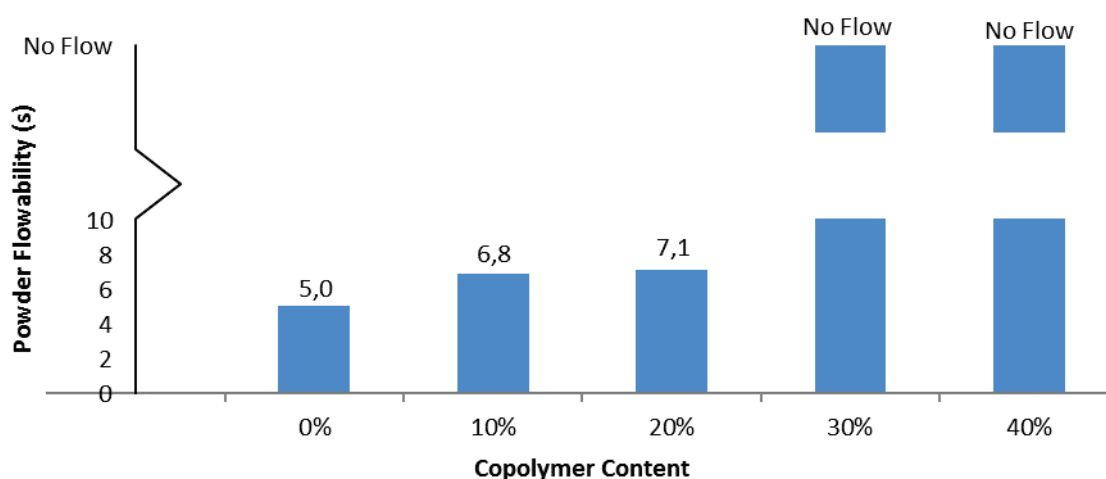
During the production of hiPP, the stickiness of the particles can cause lump formation, reactor fouling and many other unfortunate incidents. Their stickiness is due to two factors: (1) the rubber present on the surface and (2) the degree of stickiness of the rubber. This last one depends on the molar mass (lower molar mass rubber is stickier) and on the ethylene content of the rubber.<sup>28</sup> Flowability of the powder can be used as a measurement of the adhesiveness of the particles, which in practice has been found to be the key reason for process disturbances. Simple tests were conducted pouring the powder through a metallic funnel, as explained in the experimental section (ISO 6186/1998).<sup>21</sup> The resulting times are shown in

Table 4.5. There seems to be a correlation among copolymerization kinetic curves and flowability. When activity is higher or equal to that of run A70-10-40-8, resulting powders do not flow through the funnel. The higher the reaction rate, the more likely it is that we have concentration gradients inside the particles, and more rubber will be present at the surface. This irregular distribution causes stickiness, and so, A70-10-40-11 and A70-0,6-40-8 powders do not flow. On the other hand, powders with low activity during copolymerization do not get stuck while going through in the funnel.

**Table 4.5.** Flow analysis of hiPP powders

Sample	Flow analysis					
	Mass G	Times / s			Average s	norm./100g s
		1	2	3		
A	87	4,39	4,39	4,28	4,35	5,00
A70-10-10-8	73	5	4,98	4,95	4,98	6,82
A70-10-20-8	86	6,06	6,17	6,09	6,11	7,10
A70-10-30-8	76	n.d.	n.d.	n.d.	no flow	no flow
A70-10-40-8	108	n.d.	n.d.	n.d.	no flow	no flow
A70-10-40-5	110	7,37	7,48	7,46	7,44	6,76
A70-10-40-11	123	n.d.	n.d.	n.d.	no flow	no flow
A60-10-40-8	110	16,86	12,86	17,65	15,79	14,35
A80-10-40-8	114	9,53	11,84	10,09	10,49	9,20
A70-H2-40-8	107	6,76	6,73	6,67	6,72	6,28
A70-0,4-40-8	121	8,58	8,62	8,59	8,60	7,10
A70-0,6-40-8	137	n.d.	n.d.	n.d.	no flow	no flow

First, as predicted, we see a clear correlation among %EPC (Table 4.4) and flow-ability of the powders, represented in Figure 4.16. The particles become highly sticky with no flowability with 30% of EPC or more.



**Figure 4.16.** Flowability of powders with different %EPC: (A, A70-10-10-8, A70-10-20-8, A70-10-30-8, and A70-10-40-8)

Table 4.4 also shows the intrinsic viscosities of the soluble fraction (SF) and crystalline fraction (CF) components of the hiPP samples and the ratio of their viscosity. This data can

be used as an estimation of the molecular weights and their ratio of the SF and CF components. After compounding, it is well known that the more alike the viscosities of the SF and CF components, the better would be the distribution of the dispersed phase within the crystalline PP matrix.<sup>2,19</sup> However, chances are that this will also have an impact during the morphological evolution of hiPP. Therefore, the fact that sample A80-10-40-8 was able to flow through the funnel, despite its high activity during the second step and its low molecular weight rubber (low molecular weight rubber is stickier), can be attributed to its good viscosity ratio between SF and CF components. The good flowability of sample A70-H<sub>2</sub>-40-8 might be a result of the lower activity during copolymerization and the similar IVs among SF and CF. A60-10-40-8 has a high molecular weight rubber (not so sticky) probably not very well dispersed within the iPP matrix, due to the difference in IV. Consequently, it flows through the funnel, but slowly.

It is also known that propylene rich EPC, because of its lower interfacial tension against the PP matrix, results in a fine dispersion after compounding.<sup>2,29-31</sup> This could be the other reason for sample A70-0,4-40-8 having a good flowability.

#### 4.3.4 Crystallisable Copolymers of Ethylene and Propylene

Furthermore, it is noticeable in Table 4.4 that there is a small amount of ethylene in the crystalline fraction. This indicates the existence of crystallisable copolymers of ethylene-propylene, (cEPC), in addition to the PP matrix and the amorphous ethylene-propylene copolymers (EPR or aEPC). cEPC comprise crystalline copolymers having both PP and PE crystallisable segments and even neat HDPE.<sup>2</sup> It is known that they act as a compatibilizer between the two phases, and can improve the impact strength and stiffness in the PP impact copolymers. Ethylene in the crystalline fraction may have two sources: (1) from crystalline PP random copolymers (which are formed with a low ethylene content), and (2) crystalline PE (i.e. C3-LLDPE which formation is favored for EPC with high ethylene content).<sup>32</sup>

Crystex QC results allow us to quantitatively compare the amount of cEPC between our powders. To do this, the distribution of ethylene among crystalline and amorphous phases can be used as a reference, if the ratio of ethylene-propylene in the copolymer is kept constant. To determine the aforementioned, ethylene content in amorphous and crystalline fractions was multiplied by their xylene solubles percentage and “100-%XS” respectively. In this way Figure 4.17 is obtained, where the total percentage of ethylene of hiPP samples

with increasing copolymer content is represented along with the individual contributions of each fraction.

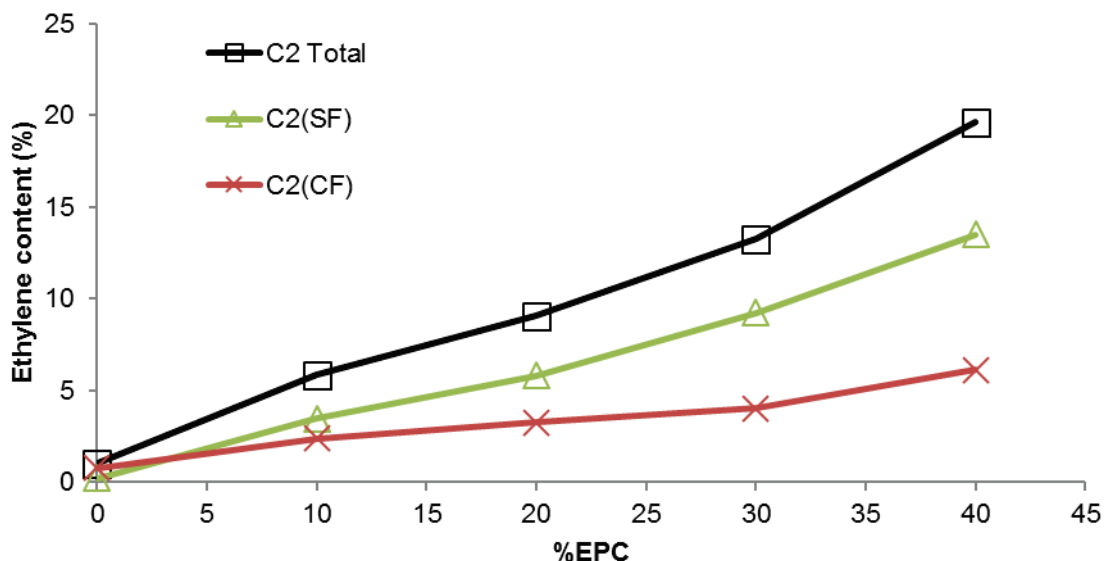


**Figure 4.17.** Weight percentage of ethylene content for the full sample (Black) with the contributions of amorphous and crystalline fractions.

Dividing amorphous and crystalline ethylene content by the total amount of ethylene allows to determine how ethylene is distributed among crystalline and amorphous phases, as shown in Figure 4.18.

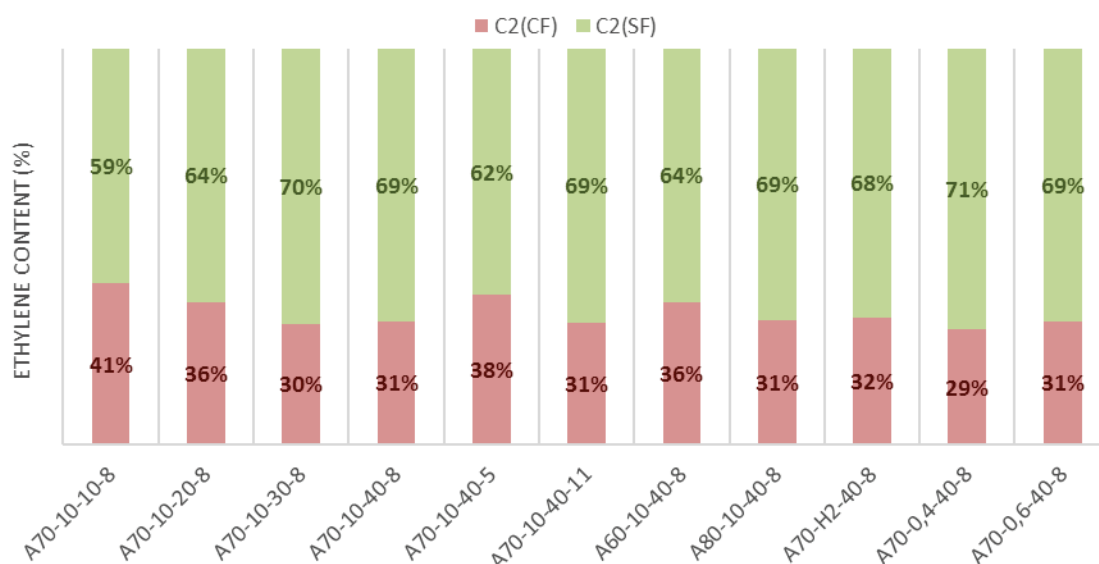


**Figure 4.18.** Distribution of ethylene among crystalline and rubbery phases of the powders planned in this study.

Concerning the distribution of ethylene among crystalline and amorphous phases along with copolymer content with constant composition (the first five powders starting from the

left in Figure 4.18) it seems that ethylene is rather incorporated in the crystalline fraction at the beginning of copolymerization than at the end. However, care must be taken when interpreting Figure 4.18 since the homopolymer atactic fraction is also part of the SF. Nevertheless, even taking in account its contribution (not shown here for the sake of brevity) the same trend is observed. This suggests that the relative amount of cEPC to aEPC decreases with time. Thus, a longer copolymerization time implies a lower cEPC/aEPC ratio at constant comonomer ratio in polymerization.

This change of the composition and crystallinity of copolymer over the course of the copolymerization was predicted by the simulation study done by Debling and Ray.<sup>10</sup> They proposed the resistance to the diffusion of ethylene as an explanation for this phenomenon. It seems logical to think that for each particle the resistance to mass transfer to monomers will increase with the amount of copolymer. Then, ethylene concentration in the active sites will be highest at the beginning of the copolymerization. At this point we are more likely to see long, crystallisable segments of C2 in the random copolymer chains. As the copolymerization proceeds, activity increases (as showed in kinetic rates in Figure 4.7) and ethylene starts to be scarce in the active sites, now mainly surrounded by EPC. On the contrary, propylene is less likely to suffer mass transfer resistance, because of its higher solubility in hiPP (~x5 that of ethylene), lower activity (half of that of ethylene), and higher availability in the gas phase (twice than ethylene). Therefore, as ethylene becomes scarcer (relative to propylene) the probability of polymerizing crystallisable sequences of ethylene is lower, and it may be rather assimilated in the particle combined with propylene as aEPC than as cEPC.

Comparing powders with constant composition and mass percentage of EPC (A70-10-40-8, A70-10-40-5, A70-10-40-11, A60-10-40-8, and A80-10-40-8) another observation can be made. It appears that powders that showed low activity during copolymerization have more cEPC polymers. To verify these outcomes, fractionation with DSC was done.

SSA fractionation as done by refs. [18,19] was performed on each hiPP sample. A comparison of two typical thermograms resulting from the 2<sup>nd</sup> melting curve from DSC and SSA method for sample A70-10-40-8 (40% of E/P copolymer with a ratio 1:1) is shown in Figure 4.19.

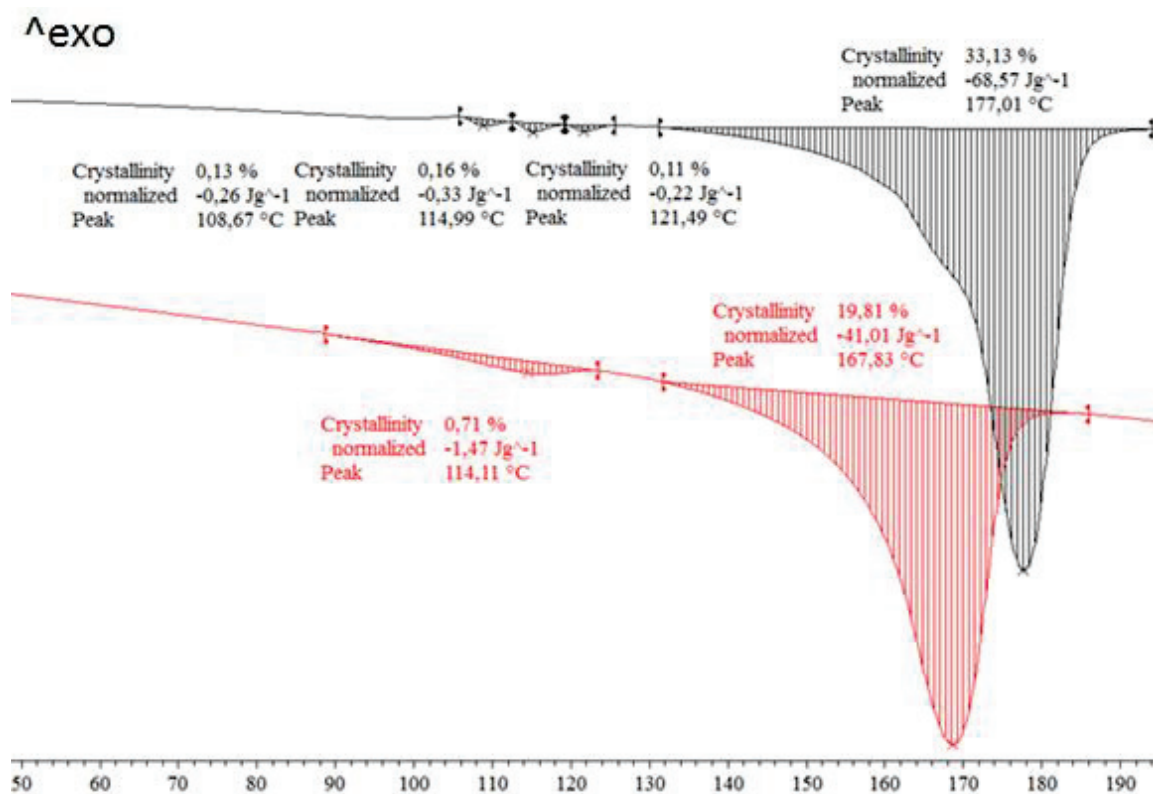


**Figure 4.19.** Comparison of a 2<sup>nd</sup> DSC melting curves and a SSA thermogram for sample A70-10-40-8. Note that melting peak of PP crystals is higher.

**Table 4.6.** Summary of the crystallinities of each crystal region along with their peak melting temperature

Run	Peak 1 (%)	Peak 2 (%)	Peak 3 (%)	Peak 4 (%)	Peak 5 (%)
	108 °C	114 °C	122 °C	128 °C	177 °C
A	-	-	-	-	68,87
A70-10-10-8	0,05	0,06	0,03	-	61,46
A70-10-20-8	0,07	0,09	0,05	-	49
A70-10-30-8	0,09	0,11	0,06	-	39,52
A70-10-40-8	0,13	0,16	0,11	-	32,85
A70-10-40-5	0,15	0,18	0,14	-	33,33
A70-10-40-11	0,13	0,16	0,09	-	33,13
A60-10-40-8	0,14	0,18	0,12	-	32,32
A80-10-40-8	0,10	0,12	0,08	-	31,82
A70-H2-40-8	0,15	0,21	0,28	0,10	36,41
A70-0,4-40-8	0,09	0,10	0,05	-	38,07
A70-0,6-40-8	0,16	0,23	0,20	-	34,37

As we can see, SSA method fractionates the different crystallisable polymers populations present in hiPP. In this way, minor differences in molecular structure are magnified and

samples can be quantitatively compared. This procedure was done for every powder. Results were treated and are summarized in Table 4.6.

In Figure 4.20 the crystallinity of melting peaks appearing at 108, 114, 122, and 128 °C was summed up for each powder.

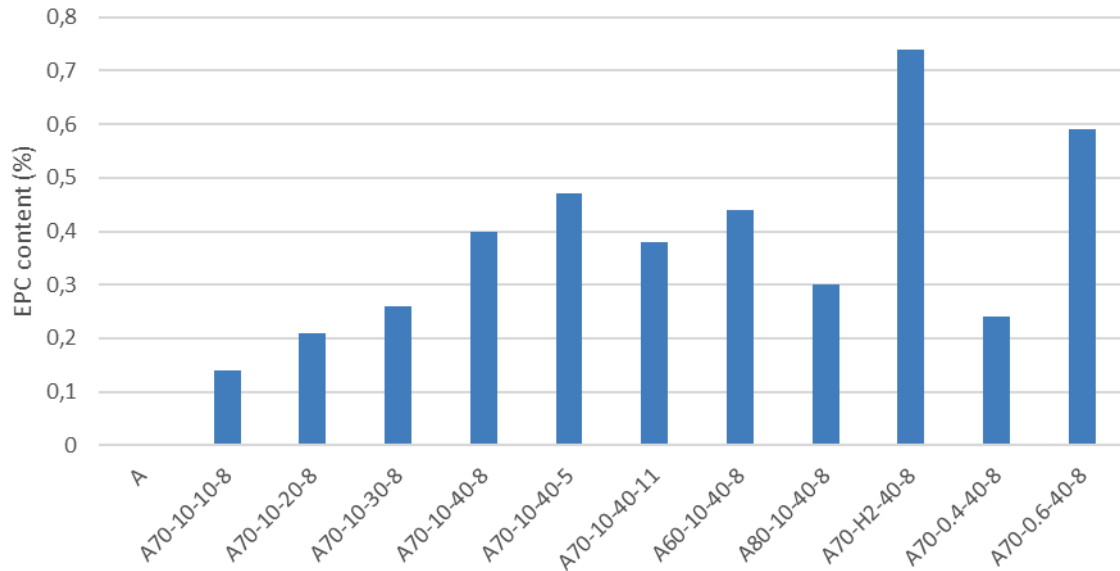


**Figure 4.20.** cEPC content estimated from the sum of peaks appearing at 108, 114, 122, and 128 °C in SSA treatment.

Based on Figure 4.20 results for sample A70-0,6-40-8, more ethylene in the gas phase during copolymerization enhances the polymerization of cEPC. The opposite effect is observed for powder A70-0,4-40-8, along with a higher crystallinity of iPP characteristic melting peak.

Furthermore, results shown in Figure 4.20 are consistent with the observed correlation in Figure 4.18. There were more cEPC polymers in those hiPP that showed a low copolymerization reaction rate (A60-10-40-8 (60 °C) and A70-10-40-5 (5 bar)). In contrast, hiPP powders with higher activity during copolymerization (A80-10-40-8 (80 °C) and A70-10-40-11 (11 bar)) had less cEPC polymer fraction. These results suggest that somehow higher activities during copolymerization induce ethylene incorporation as aEPC rather than cEPC. As previously stated, this fact might be consequence of mass transfer resistance to ethylene. At higher reaction rates C2 is scarcer in the reaction zone because of mass transfer problems (it is consumed faster so needs to diffuse faster than C3). As suggested above, higher concentrations of C2 might lead to more chains with higher C2 content and thus more easily crystallized.

Finally, based on the results for A70-H<sub>2</sub>-40-8, it seems that if hydrogen is present during copolymerization stage crystallinity is enhanced in general, both for cEPC (it is the only powder with a 4<sup>th</sup> peak for cEPC) and PP polymers. This can be attributed as a combination of its lower activity (which would not impose diffusion resistance to ethylene and would therefore ease the cEPC formation) and the resulting polymers with lower molecular weight. These shorter chains would easily rearrange themselves, because of their less probable entanglement among them.

#### 4.3.5 Mechanical Properties

To check the influence of the different conditions applied during copolymerization on the final mechanical properties of the produced powders, while keeping a constant iPP matrix, they were characterized by dynamic measurements (DMTA) and by tensile strength tests.

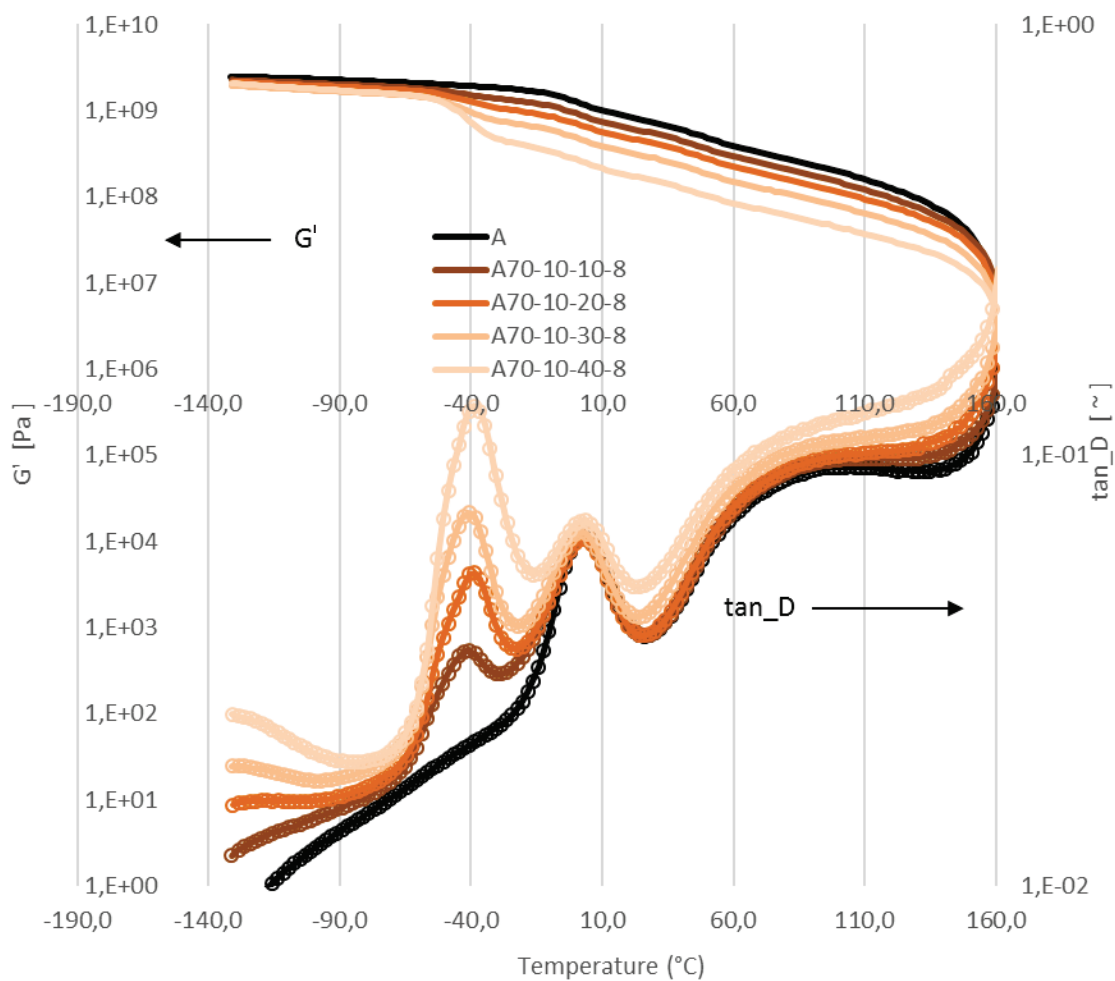


**Figure 4.21.** DMTA analyses of powders with increasing copolymer content.  $G'$  (left axis, in Pa) is the storage modulus, and  $\tan_D$  (right axis, adimensional) is tan delta, the ratio of the storage modulus to the loss modulus (the loss modulus is not shown here).

Figure 4.21 shows the storage modulus or elastic modulus ( $G'$ ) and the ratio of the storage modulus to the loss modulus, which is expressed by  $\tan(\delta)$  ( $\tan\_D$ ). Storage or elastic modulus is the ability of a determined material to storage energy for future use or to spring back when deformed (mainly provided by iPP matrix), and the loss modulus is the ability to dissipate energy applied to it (mostly the elastomer, plus the matrix above its  $T_g$ ).

The heterophasic nature of the copolymers can be clearly noticed in both  $G'$  and  $\tan\_D$  from Figure 4.21. The glass transition point of both components causes a sudden decrease of the storage modulus with temperature increase, and two peaks in  $\tan$  delta, at about  $-40$  and  $+2$  °C. The higher the copolymer content in the compounds the plainer is to see its glass transition phenomenon. For the sake of clarity, only powders with increasing copolymer content are shown in this figure. However, all powders were analyzed by DMTA, and the relevant data is shown in Table 4.7.

**Table 4.7.** Summarized data from DMTA analyses, along with tensile properties.

Sample	DMTA			Tensile ISO 527 -1,-2	
	$G'(23^\circ\text{C})$ MPa	$T_g(\text{PP})$ °C	$T_g(\text{aEPC})$ °C	Tensile Modulus MPa	Tensile Strength MPa
A	809	2,7	----	1885	39
A70-10-10-8	598	2,9	-41,2	1414	28
A70-10-20-8	460	2,6	-39,5	1064	23
A70-10-30-8	312	1,8	-40,8	646	13
A70-10-40-8	170	2,8	-38,8	288	9
A70-10-40-5	240	2,6	-36	486	15
A70-10-40-11	225	2,8	-40,5	451	9
A60-10-40-8	183	2,3	-37,7	375	12
A80-10-40-8	222	2,9	-40,1	385	10
A70-H2-40-8	314	2	-41,3	628	13
A70-0,4-40-8	267	2,5	-33,4	504	14
A70-0,6-40-8	198	3	-46,7	349	8

iPP matrix was kept constant for every powder. This is reflected on its constant  $T_g$  ( $\sim 2$  °C). Additionally, as expected,  $T_g$  of aEPC phase changes mostly with the comonomer content, being reduced with increasing  $C_2(\text{SF})$ . This can be very nicely seen for the series A70-0,4-40-8 / A70-10-40-8 / A70-0,6-40-8, with the corresponding  $T_g$  of  $-33.4$  /  $-38.8$  /  $-46.7$ , and, as shown in Table 4.4,  $C_2(\text{SF})$  of  $29.3$  /  $34.6$  /  $41.6$ , respectively. Interestingly,  $T_g$  varies with  $M_w$  /  $IV$  of the aEPC phase at constant comonomer content, as it can be seen for

samples A60-10-40-8 / A70-10-40-8 / A80-10-40-8 having IV(SF) 10.2 / 9.2 / 3.9 and Tg -37.7 / -38.8 / -40.1, respectively. Therefore, this suggests that Tg increases with IV of the aEPC phase.

Storage modulus, tensile modulus and tensile strength, decrease with the copolymer content in the hiPP in-reactor alloys. These properties were normalized for each sample with the respective one for pure iPP (sample A) as shown in Figure 4.22.

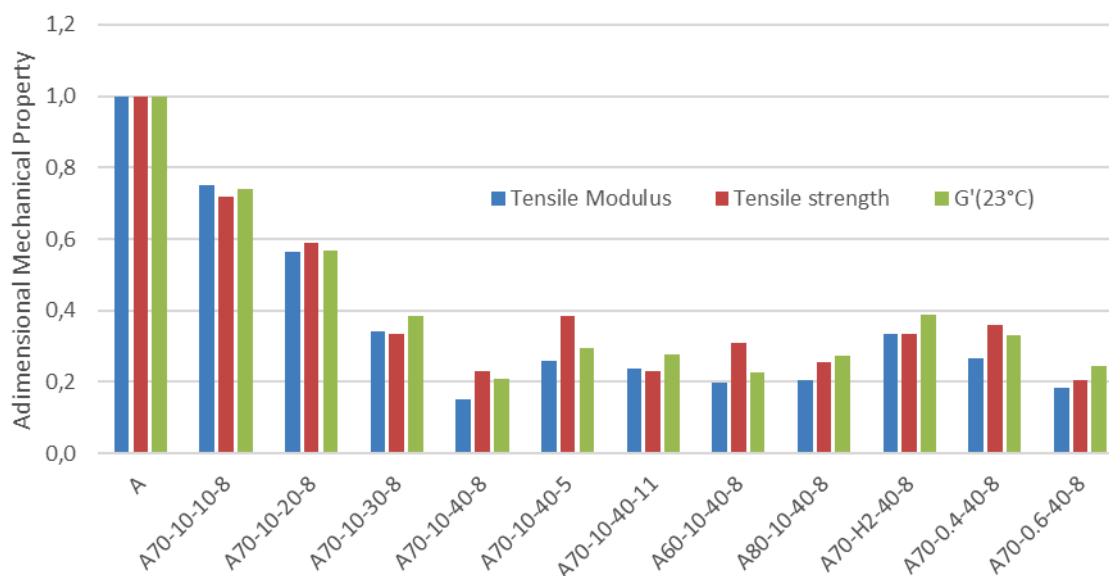


**Figure 4.22.** Tensile modulus, tensile strength and storage modulus of every powder studied normalized by the same mechanical property for pure PP (Sample A), correspondingly.

First, in Figure 4.22 it is observed how the three mechanical tests performed are pretty much in agreement among them. However, based these results, combined with the complexity of this kind of materials, the withdrawal of a straightforward general conclusion for all the powders is not easy. Nevertheless, comparing samples with a constant matrix and similar EPC content, the most striking effect observed is the good mechanical properties of sample A70-H<sub>2</sub>-40-8. This outcome might be consequence of two key reasons: its higher amount of cEPC, which acts as a compatibilizer between the aEPC and the matrix, combined with the good matrix/dispersed-phase compatibility, caused by their similar IV (However, please note that AFM on the compressed samples was not done. These would show the typical core-shell morphology.). These two factors lead to a stronger adhesion of the rubber phase to the stiff matrix. None of the rest of the powders with similar EPC composition meet these two criteria. While sample A80-10-40-8 has a similar IV among both phases, it had not as much as cEPC content. On the other hand, samples A70-10-40-5

and A60-10-40-8 had a relatively big amount of cEPC polymers, but their two phases are not as compatible, as it can be seen in their unlike IV.

Doshev et al.<sup>2,32</sup> observed that the tensile modulus and yield stress had a big dependence on the EPC composition for PP impact copolymers with constant matrix and EPC content. We also see this dependence on EPC composition, namely, the comonomer content of the disperse phase. While sample A70-0,4-40-8 (40 mol% of ethylene content in EPC) displays relatively good mechanical properties for its rubber content, those of A70-10-40-8 and A70-0,6-40-8 (50 and 60 mol% of ethylene content in EPC, respectively) are quite poor. As shown by Grein et al.,<sup>31</sup> in melted hiPP the particle size of the EPC phase is smaller if comonomer content is lower (i.e. ethylene), which results, as mentioned earlier, in a rather fine dispersion of the EPC within the iPP matrix. This might be the principal cause for the observed good mechanical properties of sample A70-0,4-40-8. On the contrary, more ethylene in the rubber increases the interfacial tension leading to poor compatibility in the multiphase system, even if a high amount of cEPC crystals is present.

However, it should be noted that the purpose of hiPP polymers is to obtain a good balance among toughness and the mechanical properties here studied. While having done impact strength tests of these samples would have been desirable, it is well-known that the higher the IV of the disperse phase the tougher the iPP/EPC blends.<sup>33</sup> Therefore, we can expect that the toughest samples to be A60-10-40-8.

#### **4.3.6 Powder Morphology with Increasing Copolymer Content.**

Particle size distribution (PSD) of the 5 powders with increasing copolymer content was analyzed as explained in the experimental section and it is represented in Figure 4.23.

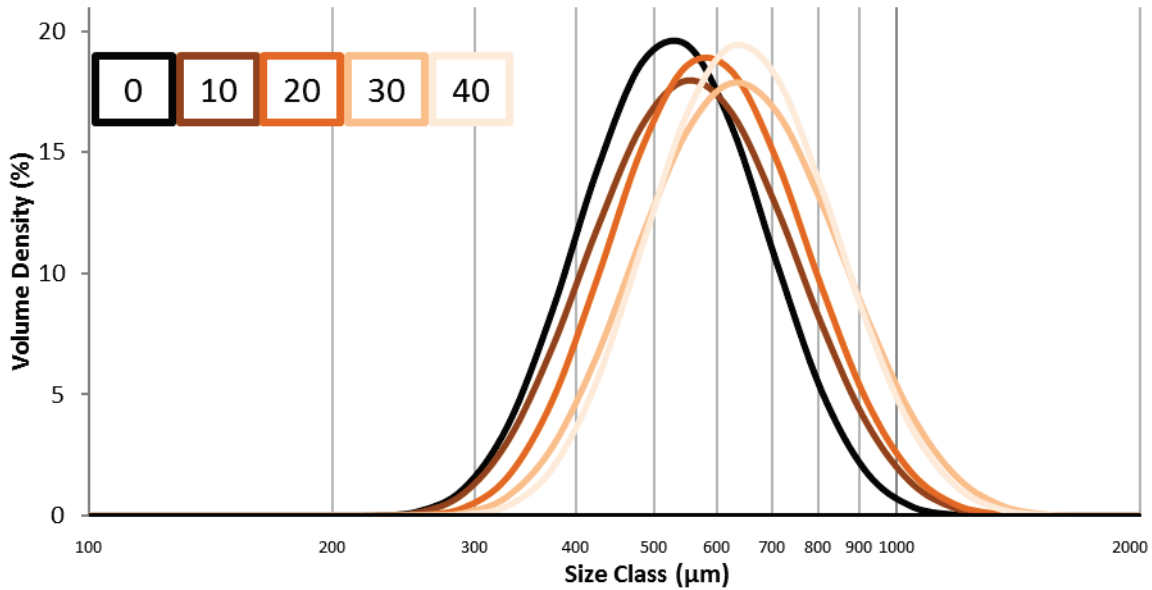


**Figure 4.23.** PSD of PP and hiPP powders with increasing copolymer content up to 40%.  $D_x(50)$  are 527, 557, 584, 639 and 644  $\mu\text{m}$  for powders A, A70-10-10-8, A70-10-20-8, A70-10-30-8, A70-10-40-8 respectively.

It can be seen how PSD shifts to the right with productivity increase, as expected. Unexpectedly, however, similar PSDs are obtained for 30 and 40 wt% PP impact copolymers. An explanation for this phenomenon can be given as follows: A 50 wt% copolymer content hiPP implies that each particle weights the double as the original PP matrix. Following this line of thought, hiPP of 10, 20, 30 and 40% copolymer content should weight 1.11, 1.25, 1.43 and 1.66 times more than the original PP matrix, respectively. As an approximation, if we assume the same density for rubber and PP matrix, when copolymer content rises each particle should increase its volume proportionally to its weight. Thus, a hiPP particle with 40% of EPC content would have seen its diameter to increase 1.18 times:

$$r_{hiPP\ 40\%} = \sqrt[3]{1,66} \cdot r_{PP} = 1,18 \quad 1$$

Now we can calculate an expected average diameter for our hiPP particles. Table 4.8 exhibits the difference among the expected diameter resulting by our fast calculations and the real diameter, along with the estimated copolymer content for each powder. Additionally, Figure 4.24 shows the porosity of iPP and hiPP samples with increasing copolymer content.

**Table 4.8.** Real Dx50 of PSD from Figure 4.23 and calculated diameters of those particles, considering the same density of rubber and PP and similar distribution in space.

EPC (%)	Expected Weight&Volume Increase	Expected Diameter Increase	Expected Final Diameter (µm)	Real Dx50 (µm)
0	1	1	527	527
10	1,11	1,04	546	557
20	1,25	1,08	568	584
30	1,43	1,13	594	639
40	1,66	1,18	624	644

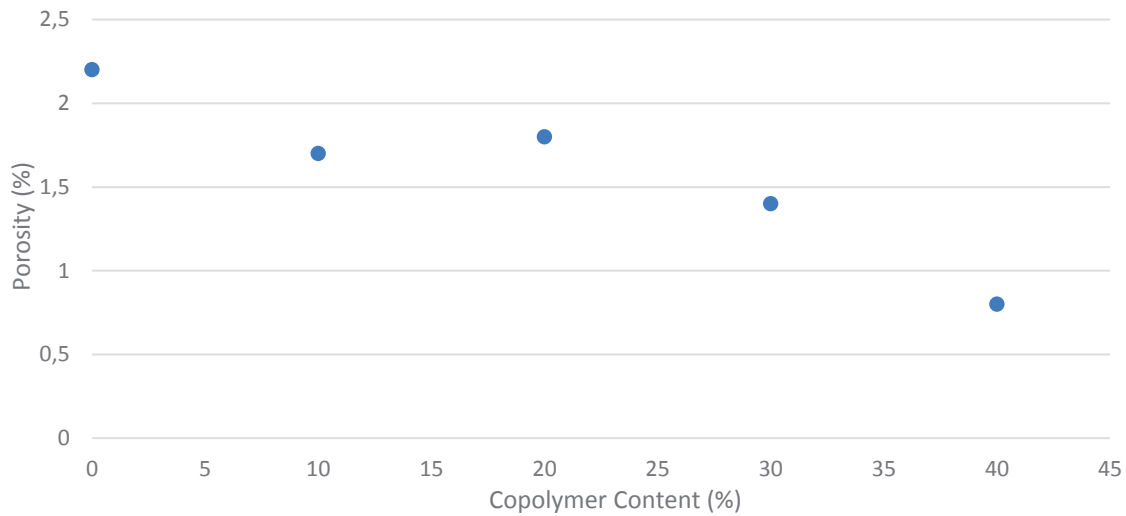


**Figure 4.24.** Porosity of iPP and hiPP samples (A, A70-10-10-8, A70-10-20-8, A70-10-30-8, and A70-10-40-8)

Table 4.8 shows that particle size rises along with copolymer content. Figure 4.24 illustrates the low porosity of our samples, and its decrease with copolymer content. Up to 20 wt% porosity is rather constant, and the increase of the real Dx50 diameter coincides closely with the estimated one. Based on these results, it seems that at low EPC content, particle morphology is like that of the PP matrix, as long ago proposed by Kakugo et al.<sup>34</sup>, since pores and cavities are not filled. This suggests that EPC is formed in the iPP primary particles.

However, the particles become highly sticky with no flowability at 30 wt% of EPC content, as Figure 16 illustrates. Furthermore, at this point particle volume doesn't increase anymore along with EPC content, and porosity decreases pronouncedly. These morphological changes can be attributed to the flow of the already formed aEPC into the pore space of the homo-polymer matrix and to the surface. This hypothesis is in accordance with already proposed theories, which describe the flow of rubbery phase from the place of its origin in

the iPP meso-particles to the pores and subsequently to the particle surface.<sup>10,35,36</sup> Other authors have observed similar morphological changes when increasing EPC content as in this work, despite having worked with different ZN systems.<sup>6–8,25,26</sup> This suggests that these facts might be common to ZN systems.

In addition, these morphological changes can help to justify the earlier claim of mass transfer resistance to ethylene which would cause the drop of relative amount of cEPC with increasing copolymer content. To react, the monomer in the bulk must diffuse through the particle to the active sites. The length scale characterizing this process will increase if less pores are available, as it will occur when they start to be filled with aEPC. In fact, Kröner and Bartke have shown that at higher copolymer contents the effective diffusion length of hiPP powders increases.<sup>6</sup> As a result, the mass transfer resistance to both monomers will also increase, especially for ethylene, for the reasons exposed above.

#### 4.3.7 AFM analyses

To further investigate if the resistance to the mass transfer of ethylene was taking place, three hiPP powders from the list of experiments shown in Table 4.2 were selected for AFM analyses (A70-10-40-8, A70-0,4-40-8, and A70-0,6-40-8). The reason for this choice was the fact that they were copolymerized with different partial pressures of ethylene in the gas phase, while having a constant iPP matrix. Comparison of the resulting polymers can offer a valuable insight about the ethylene diffusion within the particle. Contrarily to these three samples, the 4<sup>th</sup> sample (A70-13-40-8) had an outstanding iPP matrix made of smaller meso-particles, easing monomer diffusion, but the same copolymer composition as one of the earlier three samples. This singular iPP matrix is originated varying its precontacting procedure, as explained in the experimental section. The influence of precatalyst and cocatalyst/external electron donor precontacting in the gas phase polymerization of propylene was investigated in Appendix B (Page 177). Additionally, the PP matrix has a slightly higher productivity. The four powders analyzed in this subsection along with their properties are shown in Table 4.9.

**Table 4.9.** Summary of the polymerization conditions of the analyzed samples

Run	Homopolymerization		Copolymerization			
	Pre-contact	PP-Product kg/g	Copo wt%	C2/C3* mol/mol	P bar	T °C
A70-10-40-8	Yes	10	40	50/50	8	70
A70-13-40-8	No	13	40	50/50	8	70
A70-0,4-40-8	Yes	10	40	40/60	8	70
A70-0,6-40-8	Yes	10	40	60/40	8	70

\*Expected composition of the copolymer (not in the gas phase)

The soluble fraction and the ethylene/propylene content of the four hiPP analyzed in this part of the study are shown in Table 4.10. Contrarily to the other samples, sample A70-13-40-8 was not analyzed with Crystex QC. However, its solubles fraction can be estimated with the crystallinity peak corresponding to PP as obtained from DSC SSA method. The correlation among PP crystallinity and soluble fractions for powders with different copolymer content but identical copolymer composition is exhibited in Figure 4.25, along with the estimation for sample A70-13-40-8.

**Table 4.10.** Soluble fraction and ethylene content of the soluble fraction of hiPP powders

Run	Tg Inflect. Pt. (°C)	C2/C3 in XS fraction (NMR) mol %	Crystallinity PP peak (DSC SSA) wt %	Sol. Fract wt %
A70-10-40-8	-42,4	44/56	32,6	39
A70-13-40-8	-42,4	(44/56)*	35,9	(34,5)*
A70-0,4-40-8	-37,1	38/62	38,1	35
A70-0,6-40-8	-53,3	52/48	34,4	36

\* These values were estimated from Tg and Crystallinity PP peak resulted from the second melting curve from -80 to 200 °C and SSA fractionation, respectively.

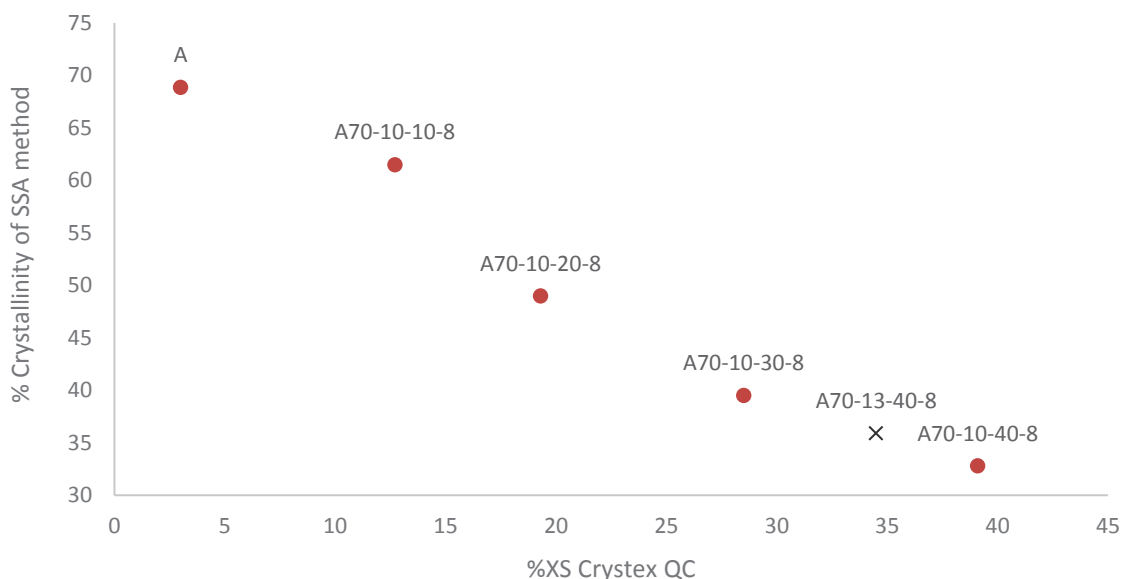


**Figure 4.25.** Estimation of % of xylene solubles at 40 °C (as evaluated by Crystex QC) for sample A70-13-40-8 from its PP crystallinity evaluated with SSA method.

As can be seen in Table 4.10 sample A70-10-40-8 and A70-13-40-8 exhibited the same  $T_g$  for the rubber fraction. Thus, it was considered that they had the same or very similar copolymer composition.

It is interesting to note that despite the different PP morphologies of A70-10-40-8 and A70-13-40-8, the same gas phase composition leads to the same rubber composition. This shows that PP morphology has a limited impact in the overall aEPC composition.

As said before, the ethylene/propylene ratio in SF is different from that of the whole copolymer, since cEPC corresponds to the insoluble fraction, and some atactic PP is filtered along with the soluble fraction. However, Table 4.10 allows us to conclude that our goals in terms of soluble fraction and its ethylene/propylene content for the four powders were achieved.

#### 4.3.7.1 Rubber Migration

Figure 4.26 shows phase and height images from AFM scanning of the cross-sections of sample A70-10-40-8 at different times after being cryo-sectioned (right after re-cutting, one, and two days later). The sample was stored at room temperature. The AFM scanning was done approximately in the same area.

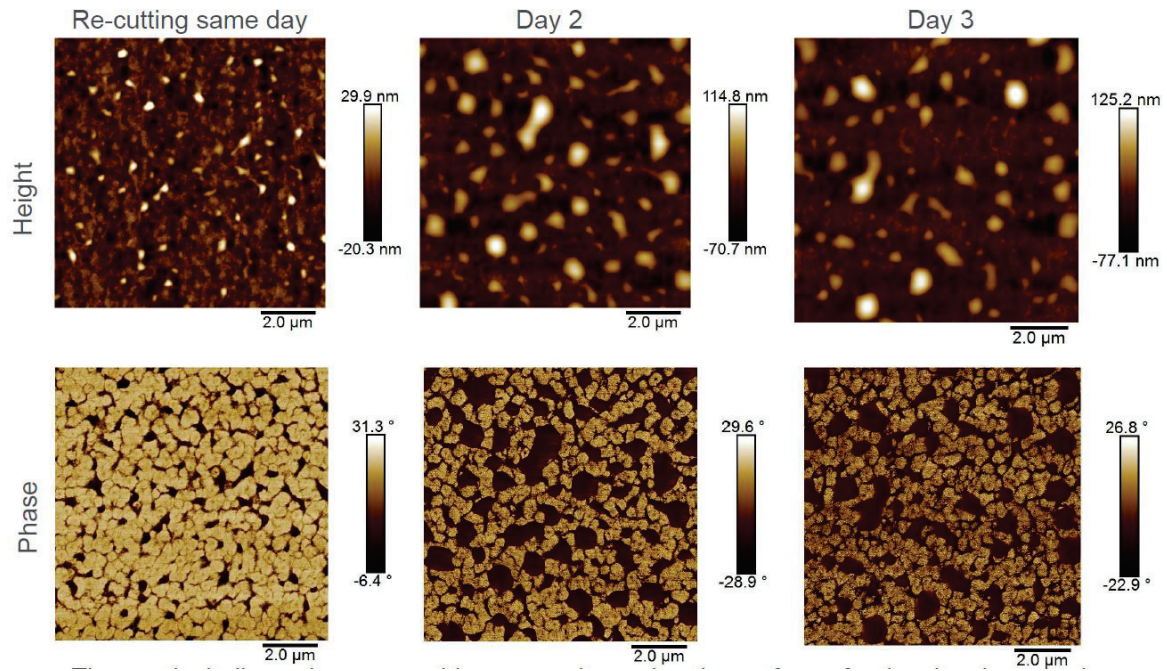


**Figure 4.26.** Rubber migration from PP matrix with time when stored at room temperature ( $\sim 25\text{ }^{\circ}\text{C}$ ) for sample A70-10-40-8. AFM measurements were done at the edge, where rubber was more abundant as compared to the center.

In the phase images, the darker zones correspond to the rubber phase. The image on the left corresponds to an AFM scan conducted right after re-cutting the sample. Here, a well dispersed network structure of rubber phase among the PP matrix is observed, in addition to some rubber domains (larger dark zones). In the corresponding height image, it can be observed that the rubber domains are a bit higher in topography than the PP matrix (please note that now the darker zones correspond to the matrix/stiff phase). In addition, this topographical difference grows over time. From a difference of 50 nm, observed in the height image of the freshly microtomed particle, to a maximum difference of 185 nm after one day of sample storage at room temperature. Simultaneously, as can be seen in the respective phase image, the rubber domains start to be more common at the surface. In fact, they seem to be the result of multiple droplets coalescing, a fact that can explain the topography difference to PP matrix. What was initially a well dispersed network structure is slowly moving to be the most abundant phase in the surface. These droplet features are probably related to the “liquid-like” nature of aEPC phase (note that aEPC can be a very high viscosity liquid; at  $iV = 9$  the room temperature viscosity will be in the order of  $10^{14}$  Pa.s). Smolná *et al.*<sup>23</sup> also observed and studied this phenomenon. They explained it as the squeezing of aEPC caused by the recrystallization of the PP matrix, which would provoke the flow of the aEPC towards the cross-sectioned surface. This is not an established fact, and it could also be that the cooling which the powder undergoes once it is removed from

the reactor, builds up stresses in the particle, and then the rubber flows when the sample is cut. In any case, Smolná *et al.*<sup>23</sup> showed that this phenomenon can be prevented or slowed down by storing the sample at low temperature. Therefore, in our study the hiPP samples were stored in the freezer at -21 °C after being cryo-microtomed, as explained in the experimental section. As can be seen in Figure 4.27, by freezer-storing samples, morphology is blocked and sample aging is halted. Indeed, the images at day 2 and day 8 do not show significant differences. Morphology seems to be more “area” dependent than “time” dependent.

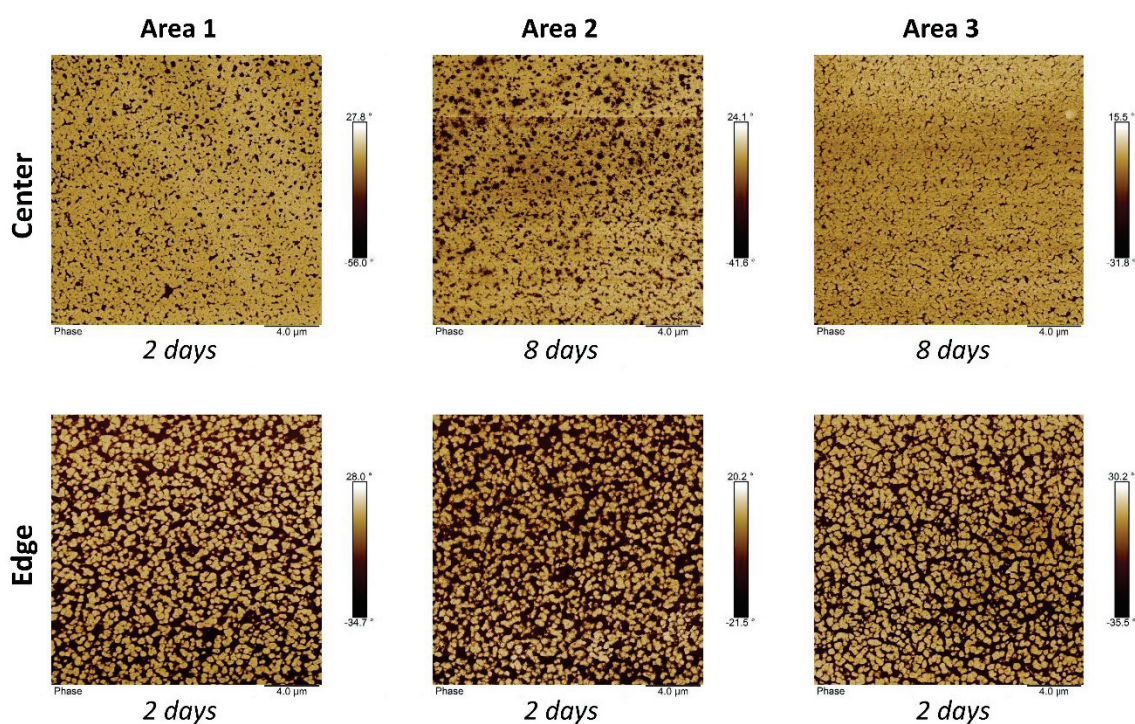


**Figure 4.27.** Phase images of six different areas of sample A70-10-40-8. The day after cutting is shown under each image.

#### 4.3.7.2 Rubber Distribution

Rubber phase distribution for the four hiPP samples was studied by tapping mode AFM phase images. Two different zones which can be well recognized by the integrated light microscopy (LM) in AFM were compared: The center and the edge of the meso-particles. The LM images from Figure 4.28 reveal the reason for considering the meso-particles and not the whole section of the particle as the determining structure for aEPC distribution. A couple of works in the literature reveal similar findings. Electron microscopy images convincingly illustrating the presence of large compact zones in hiPP particles have been provided by Kroner and Bartke<sup>6</sup> and by Kittilsen and McKenna.<sup>8</sup> These compact zones

are believed to be the relevant length scale for mass transfer in the polymer particles.

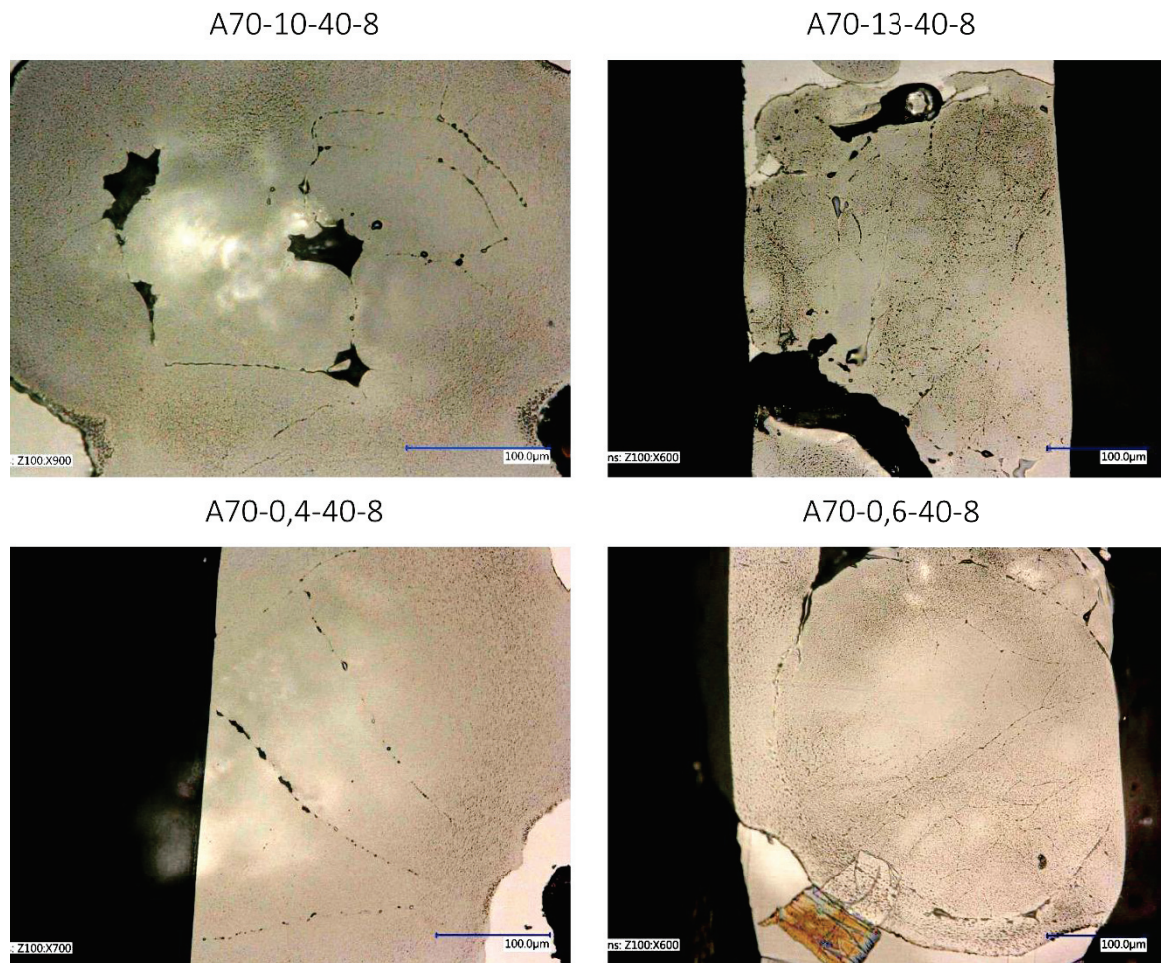


**Figure 4.28.** Light microscopy image of the four resin-embedded and cryo-microtomed hiPP particles, where it is possible to appreciate the meso-particles which have a much higher rubber concentration in the edges than in the center (clearer zones).

It is worth recalling that during the production of sample A70-13-40-8 precontacting procedure was avoided. In Appendix B (Page 177), it is concluded that samples which didn't undergo this procedure presented smaller meso-particles. Indeed, this seems to be the case when comparing the meso-particles size of sample A70-13-40-8 in Figure 4.28 to the others. However, it must be noted that this imaging was just done to one particle so our interpretation remains to be confirmed.

The average rubber percentage in the center and at the edge of the four samples is estimated from three phase images of 20x20 µm scan size for each particle, treated with an AFM software. Results are summarized in Table 4.11. Figure 4.29 helps to picture the differences in rubber distribution among every particle.

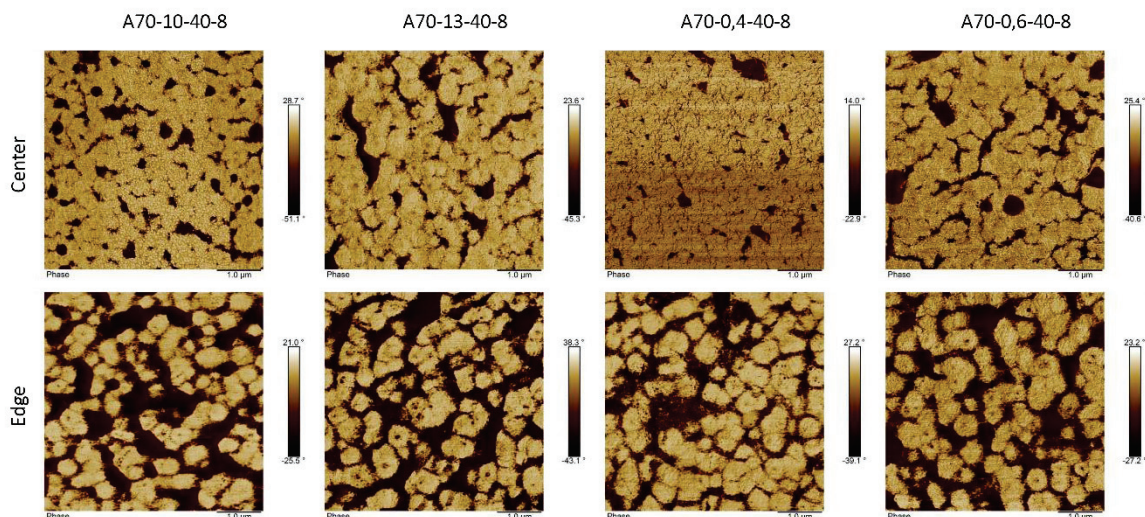


**Figure 4.29.** AFM phase images for comparison of 5  $\mu\text{m}$  of scan size on different samples. There are differences in rubber distribution in the edge and center of the four samples.

**Table 4.11.** Average rubber content based on three areas 20 x 20  $\mu\text{m}$  analyzed by AFM

Sample	Precontact	C2/C3	Center	Edge
A70-10-40-8	Yes	50/50	10%	42%
A70-13-40-8	No	50/50	15%	40%
A70-0,4-40-8	Yes	40/60	9%	35%
A70-0,6-40-8	Yes	60/40	18%	40%

According to Table 4.11, there is a substantial difference in aEPC content between the center and the edge of meso-particles for each sample. The lack of ethylene in the center of meso-particles due to diffusion limitations to this molecule may be the cause for having less rubber content in the center. As said in the introduction, the simulation study done by Kröner et al. <sup>7</sup> points in this direction, since they predicted diffusion limitations for both monomers, but mainly for ethylene.

Additionally, samples A70-13-40-8 and A70-0,6-40-8 had around 50 and 80% more aEPC in the respective centers of meso-particles as compared to samples A70-10-40-8 and A70-0,4-40-8. The higher aEPC in the center of A70-13-40-8 powders may be caused by its PP matrix with improved mass transfer, which eases the arrival of ethylene to the most hidden active sites. On the other hand, the high aEPC content in the center of A70-0,6-40-8 particles can be explained by the higher partial pressure of ethylene in the bulk during its copolymerization. As it has been recently shown in Chapter 3, a higher partial pressure improves solubility and diffusivity which results in an enhanced penetration of ethylene in

the particle.

#### 4.3.7.3 Rubber Stiffness Homogeneity Study by AFM-QNM

Every sample was imaged by AFM quantitative nano-mechanical mapping (AFM-QNM) mode, to study the modulus of the rubbers. For each sample two images in the edge region and the center of different meso-particles were captured. In Figure 4.30 the data gained for sample A70-10-40-8 regarding this new AFM mode is exhibited. A very similar contrast and resolution as in tapping mode can be noticed. However, in this case quantitative values of rubber stiffness are provided, in (MPa).

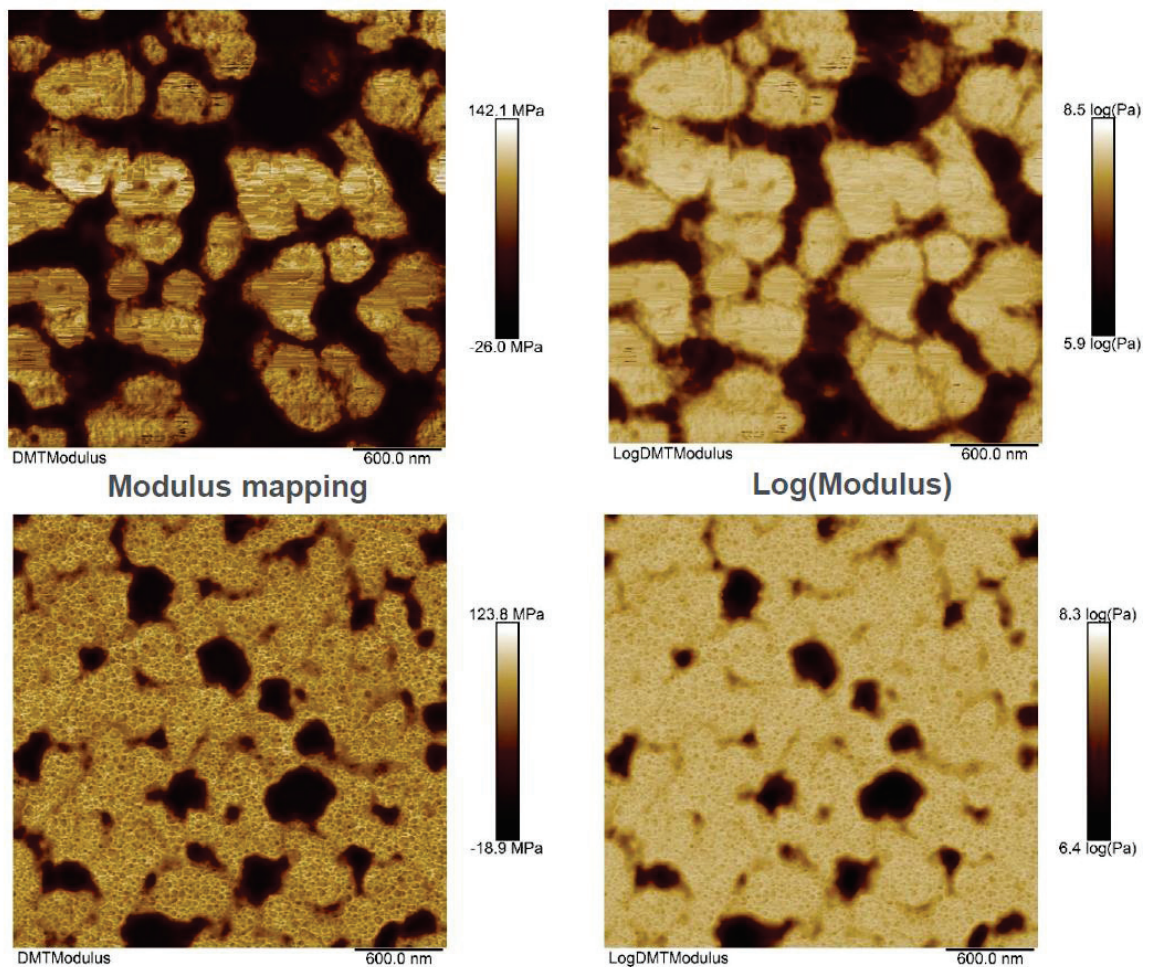
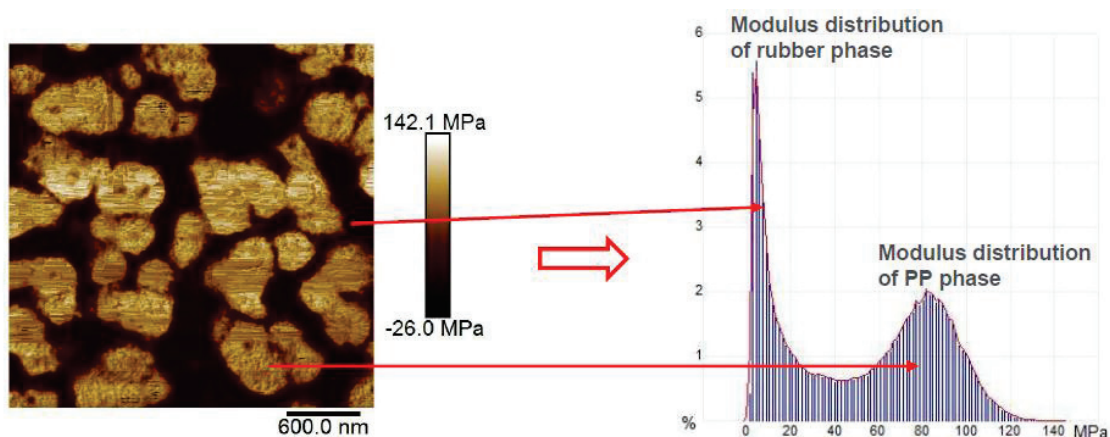


**Figure 4.30.** AFM-QNM modulus mapping in MPa (left) and LogPa (right) for sample A70-10-40-8 in the edge (upper images) and in the center of meso-particles (lower images)

The modulus mapping image is based on 512 x 512 points of individual force measurements from the scanned area. The modulus distribution can be derived from the modulus mapping raw data and the histogram shows clearly modulus distribution from different phases in the polymer. Figure 4.31 displays the normalized distribution. Note that

two distinct peaks appear in the bimodal distribution (local maxima). They correspond to the two phases, PP and aEPC. This procedure was done for every powder in the central and edge regions. For each region of every particle we have two distributions (from two different meso-particles modulus mapping) each one with two local maxima. The average of every local maxima is shown in Table 4.12.



Modulus distribution based on 512\*512 points of individual force measurements.

**Figure 4.31.** Representation of how the modulus distribution data of rubber phase and of PP phase from Modulus mapping images was gained.

**Table 4.12.** Average mechanical properties of rubber domains <sup>a</sup>

Sample	Precontact	C2/C3	Average Modulus (MPa)	
			Center	Edge
A70-10-40-8	Yes	50/50	5,4	3,9
A70-13-40-8	No	50/50	4,1	4
A70-0,4-40-8	Yes	40/60	8,95	4,2
A70-0,6-40-8	Yes	60/40	4,5	3,5

<sup>a</sup> Average rubber domains modulus (from the peak value) based on 2 modulus mapping images from 2 area measurements.

Concerning these results, it seems that in the center area the rubbers are a bit stiffer for all the samples. This could be due to rubbers with a higher amount of propylene. This finding is coherent with a recent publication of Cheruthazhekatt and Pasch.<sup>37</sup> They performed a sequential xylene extraction method in ZN based hiPP particles, and found that EPRs richer in propylene at the centre region of the particles. Additionally, it is interesting to note, regarding samples where PP matrix was kept constant (A70-0,4-40-8, A70-10-40-8, and A70-0,6-40-8), that every estimated modulus either in the center or in the edge is coherent with their C2/C3 ratio. However, the difference among central and edge region increases

with the lack of ethylene. Therefore, these two events can be attributed to an existing mass transfer resistance to ethylene which is enhanced (as expected) with its deficit, or diminished with its surplus.

On the other hand, there is almost no difference of the rubber properties in the edge and center of the rubber particles of sample A70-13-40-8. This could indicate that there is practically no mass transfer resistance for sample A70-13-40-8. However, this is not coherent with the difference in rubber concentration noticed in the previous subdivision of this paper. Right now, there is no clear explanation for this phenomenon. It could be that sample A70-13-40-8 doesn't present mass transfer resistance to ethylene and that there is a higher concentration of active sites in the edge than in the center of meso-particles. A second possible explanation is that the edge region is more porous, and rubber tends to flow into these areas, although formed elsewhere.

Cross-sectioned samples were left at room temperature for 7 days, to allow the forming of rubber concentrated regions. Then, stiffness analyses were done in these regions, which mainly appeared in the edges, as depicted in Figure 4.32. In this way, the lowest modulus value of every powder was found. Measurements were not performed in the center since the morphology did not change much there.

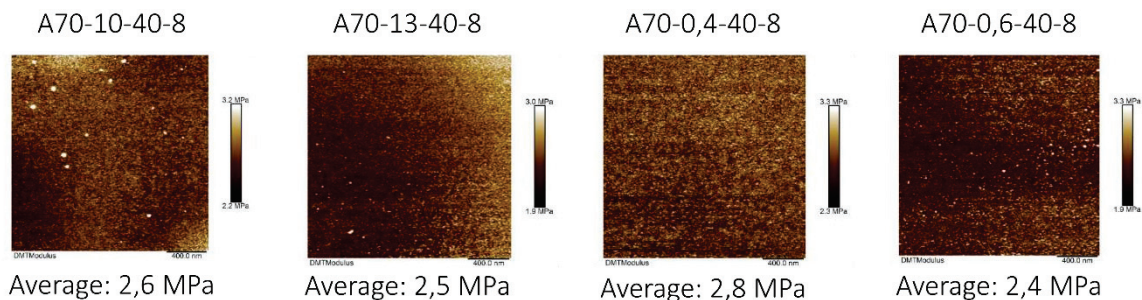


**Figure 4.32.** Average stiffness of the rubber droplets appearing in the edge of every sample after aging for 7 days at room temperature.

These modulus values are lower than those of Table 4.12, probably because of the higher concentration of the segregated rubber. In addition, they seem consistent with the ethylene/propylene content and their respective  $T_g$  shown in Table 4.10.

#### 4.4 Conclusions

Several high impact polypropylene (hiPP) powders were polymerized in a 2.5L gas phase reactor with a supported Ziegler-Natta catalyst. Conditions during copolymerization such

as amount of copolymer, temperature, pressure, relative amount of ethylene to propylene and the presence of hydrogen were systematically varied to study their impact on the experimentally measured reaction rates, powders stickiness, chemical composition of the polymers, mechanical properties and powders morphology. The isotactic Polypropylene (iPP) matrix was kept constant.

Some predictable results were observed in terms of copolymerization activity. For instance, it was enhanced with the increase of temperature, pressure and ethylene concentration in the gas phase. Nevertheless, there were also some unexpected ones. Decay-type profiles were noticed with temperature increase, which can be attributed to catalyst thermal degradation. In addition, presence of hydrogen greatly reduced copolymerization activity. This last event is subject to the catalyst system.

Comparison of powders with the same copolymer composition led to some interesting facts. Ratio of crystalline ethylene-propylene (cEPC) copolymers to amorphous ones (aEPC) decreases with copolymerization content. In a similar vein, lower activity during the second step seems to lead to a higher cEPC fraction. Although now there is no a clear explanation to these phenomena, they were attributed to mass transfer resistance to ethylene diffusion within the iPP/hiPP particle.

Two factors seem to improve the studied mechanical properties (tensile strength, tensile modulus, and storage modulus) if copolymer composition is kept constant: (1) A higher amount of cEPC, which acts as a compatibilizer between the aEPC and the matrix, and (2) a similar intrinsic viscosity (IV) among the matrix/dispersed-phase, which enhanced their compatibility. In addition, these same mechanical properties were enhanced if copolymer had a higher propylene content, due to the improved affinity among EPC and iPP phases. Factors that caused better mechanical properties also ameliorated powder flowability.

Size of polymer particles increased more than estimated based on their productivity when increasing copolymer content. In addition, porosity of the iPP particles was very low (~2%) but only decreased to its half when a 40% of copolymer was incorporated. This combination of morphological factors probably indicate that the rubber is formed in the iPP primary particles, to be after pushed to the pores and to the surface. This pore-filling could be the cause of the mass transfer resistance to ethylene. To investigate whether this limitation was happening or not, 4 hiPP samples were studied by AFM. 3 of them had equal iPP matrix

but different copolymer compositions, in terms of ethylene/propylene ratios. Contrarily, the 4th sample had a singular iPP matrix made of smaller meso-particles, easing monomer diffusion, but the same copolymer composition as one of the previous three samples. After cryo-microtomed, the hiPP were stored at  $-21^{\circ}\text{C}$  to avoid rubber migration to the surface, preserving the original morphology. AFM analyses showed that every particle had less rubber in the center of meso-particles than in the edges. Additionally, it was revealed that powders with more ethylene in the copolymer had more rubber in the center of the meso-particles. The singular iPP matrix had also more rubber in the center. This indicates that mass transfer limitations for ethylene can occur in the center of meso-particles.

In the literature, several authors have observed similar morphological changes when increasing rubber content in hiPP as those described in this work. This suggests that they are common to most ZN systems. However, in this work it is shown that the catalyst preparation method can significantly ameliorate this expected morphology development.

#### 4.5 References

1. Gahleitner, M. & Paulik, C. Polypropylene. in *Ullmann's Encyclopedia of Industrial Chemistry* (Wiley-VCH Verlag GmbH & Co. KGaA, 2000). doi:10.1002/14356007.o21\_o04.pub2
2. Gahleitner, M., Tranninger, C. & Doshev, P. Heterophasic copolymers of polypropylene: Development, design principles, and future challenges. *J. Appl. Polym. Sci.* **130**, 3028–3037 (2013).
3. *Polypropylene handbook*. (Hanser, 2005).
4. Bouzid, D., Gaboriaud, F. & McKenna, T. F. Atomic Force Microscopy as a Tool to Study the Distribution of Rubber in High Impact Poly(propylene) Particles. *Macromol. Mater. Eng.* **290**, 565–572 (2005).
5. Bouzid, D. & McKenna, T. F. L. Improving Impact Poly(propylene) Morphology and Production: Selective Poisoning of Catalyst Surface Sites and the Use of Antistatic Agents. *Macromol. Chem. Phys.* **207**, 13–19 (2006).
6. Kröner, T. & Bartke, M. Sorption of Olefins in High Impact Polypropylene - Experimental Determination and Mass Transport Modeling: Sorption of Olefins in High

- Impact Polypropylene .... *Macromol. React. Eng.* **7**, 453–462 (2013).
7. Kröner, T. *Mass Transport and Kinetics in the Heterophasic Copolymerization of Propylene*. (Mensch & Buch, 2014).
  8. Kittilsen, P. & McKenna, T. F. Study of the kinetics, mass transfer, and particle morphology in the production of high-impact polypropylene. *J. Appl. Polym. Sci.* **82**, 1047–1060 (2001).
  9. Hoel, E. L., Cozewith, C. & Byrne, G. D. Effect of diffusion on heterogeneous ethylene propylene copolymerization. *AIChE J.* **40**, 1669–1684 (1994).
  10. Debling, J. A. & Ray, W. H. Morphological development of impact polypropylene produced in gas phase with a TiCl<sub>4</sub>/MgCl<sub>2</sub> catalyst. *J. Appl. Polym. Sci.* **81**, 3085–3106 (2001).
  11. Smolná, K., Gregor, T., Buráň, Z. & Kosek, J. Formation and Distribution of Rubbery Phase in High Impact Poly(propylene) Particles. *Macromol. Mater. Eng.* **301**, 390–400 (2016).
  12. Primol 352. Available at: [http://www.exxonmobil.com/Denmark-English/Specialties/PDS/GLXXENSPCEMPrimol\\_352.aspx](http://www.exxonmobil.com/Denmark-English/Specialties/PDS/GLXXENSPCEMPrimol_352.aspx). (Accessed: 30th July 2015)
  13. Martins, A. R., Cancelas, A. J. & McKenna, T. F. L. A Study of the Gas Phase Polymerization of Propylene: The Impact of Catalyst Treatment, Injection Conditions and the Presence of Alkanes on Polymerization and Polymer Properties. *Macromol. React. Eng.* (2016). doi:10.1002/mren.201600011
  14. Cancelas, A. J., Monteil, V. & McKenna, T. F. L. Influence of Activation Conditions on the Gas Phase Polymerisation of Propylene. *Macromol. Symp.* **360**, 133–141 (2016).
  15. Cancelas, A. J. *et al.* A Comparison of the Influence of Temperature During Slurry and Gas Phase Propylene Polymerization on Ziegler-Natta Catalyst. *Macromol. Symp.* **370**, 41–51 (2016).
  16. Redlich, O. & Kwong, J. N. S. On the Thermodynamics of Solutions. V. An Equation of State. Fugacities of Gaseous Solutions. *Chem. Rev.* **44**, 233–244 (1949).

17. Aarnio-Winterhof, M., Doshev, P., Seppala, J. & Gahleitner, M. Structure-property relations of heterophasic ethylene-propylene copolymers based on a single-site catalyst. *Express Polym. Lett.* **11**, 152–161 (2017).
18. Müller, A. J. & Arnal, M. L. Thermal fractionation of polymers. *Prog. Polym. Sci.* **30**, 559–603 (2005).
19. Chen, J. *et al.* Controlled properties of high-impact polypropylene in-reactor alloys by tailoring chemical structure and morphology. *J. Polym. Res.* **22**, (2015).
20. Bu, H.-S., Cheng, S. Z. D. & Wunderlich, B. Addendum to the thermal properties of polypropylene. *Makromol. Chem. Rapid Commun.* **9**, 75–77 (1988).
21. ISO 6186:1998 - Plastics -- Determination of pourability. Available at: <https://www.iso.org/standard/25202.html>. (Accessed: 12th July 2017)
22. Polymer Char | CRYSTEX QC: Soluble Fraction for QC Polypropylene Plants. Available at: [http://www.polymerchar.com/CRYSTEX\\_QC\\_video](http://www.polymerchar.com/CRYSTEX_QC_video). (Accessed: 10th November 2016)
23. Smolná, K., Gregor, T. & Kosek, J. Morphological analysis of high-impact polypropylene using X-ray microCT and AFM. *Eur. Polym. J.* **49**, 3966–3976 (2013).
24. Derjaguin, B. V., Muller, V. M. & Toporov, Y. P. Effect of contact deformations on the adhesion of particles. *J. Colloid Interface Sci.* **53**, 314–326 (1975).
25. Bouzid, D. *Interaction between the polymerisation process and particle morphology*. (Lyon 1, 2004).
26. Bouzid, D., Gaboriaud, F. & McKenna, T. F. L. Study and Control of the Distribution of Elastomer in High Impact Polypropylene. *Macromol. Symp.* **243**, 215–224 (2006).
27. ISO 6427:2013 - Plastics -- Determination of matter extractable by organic solvents (conventional methods). Available at: [http://www.iso.org/iso/iso\\_catalogue/catalogue\\_tc/catalogue\\_detail.htm?csnumber=62009](http://www.iso.org/iso/iso_catalogue/catalogue_tc/catalogue_detail.htm?csnumber=62009). (Accessed: 27th August 2015)

28. Vestberg, T., Denifl, P. & Wilén, C.-E. Increased rubber content in high impact polypropylene via a sirius ziegler-natta catalyst containing nanoparticles. *J. Polym. Sci. Part Polym. Chem.* **51**, 2040–2048 (2013).
29. D’Orazio, L., Mancarella, C., Martuscelli, E. & Sticotti, G. Polypropylene/ethylene-co-propylene blends: influence of molecular structure of EPR and composition on phase structure of isothermally crystallized samples. *J. Mater. Sci.* **26**, 4033–4047 (1991).
30. Nomura, T. *et al.* Compatibility and tensile behavior of polypropylene/ethylene-propylene rubber blends. *Polym. Eng. Sci.* **35**, 1261–1271 (1995).
31. Grein, C., Gahleitner, M., Knogler, B. & Nestelberger, S. Melt viscosity effects in ethylene–propylene copolymers. *Rheol. Acta* **46**, 1083–1089 (2007).
32. Doshev, P. *et al.* Phase interactions and structure evolution of heterophasic ethylene–propylene copolymers as a function of system composition. *J. Appl. Polym. Sci.* **101**, 2825–2837 (2006).
33. Grein, C., Bernreitner, K., Hauer, A., Gahleitner, M. & Neißl, W. Impact modified isotactic polypropylene with controlled rubber intrinsic viscosities: Some new aspects about morphology and fracture. *J. Appl. Polym. Sci.* **87**, 1702–1712 (2003).
34. Keii, T. & Soga, K. *Catalytic Olefin Polymerization*. (Elsevier, 1990).
35. Zhou, Y. *et al.* Probing into the pristine basic morphology of high impact polypropylene particles. *Polymer* **50**, 4690–4695 (2009).
36. Urdampilleta, I., González, A., Irui, J. J., de la Cal, J. C. & Asua, J. M. Morphology of High Impact Polypropylene Particles †. *Macromolecules* **38**, 2795–2801 (2005).
37. Cheruthazhekatt, S. & Pasch, H. Defining the distribution of ethylene-propylene copolymer phases in heterophasic ethylene-propylene copolymers by a sequential xylene extraction method: Chemical and morphological analysis. *Polymer* **55**, 5358–5369 (2014).

## 5 Conclusions and Perspectives

### 5.1 Conclusions

From a reaction engineering perspective, the current Ph.D. dissertation shows a combination of experimental and modelling efforts intended to develop a global understanding about the production of hiPP in the gas phase. It is investigated the effects that the gas phase reactor conditions have on the morphology of the initial isotactic polypropylene (iPP) matrix and on the properties and localization of the rubber on it, which in turn will impact the evolution of the final properties of high impact polypropylene (hiPP). Three different commercially available supported Ziegler Natta (ZN) precatalysts were used for the polymerizations, so general conclusions to the various systems can be withdrawn. Such an extensive study is divided in three inter-connected chapters that reflect the progress made against our goals. Each of the chapters is focused on distinct aspects of the production of hiPP in the gas phase.

The morphology and reaction rates of hiPP will depend on those of the intermediate iPP, which in turn, will be subject to the precatalyst. However, the same precatalyst can lead to different polymerization rates and iPP morphologies, depending on the injection protocol followed, among other factors. Therefore, to carry out the previously described wide-ranging aim, first it is needed to understand the impact of catalyst injection conditions on several aspects of the propylene homopolymerization, which is the goal of Chapter 1. The experimental studies in the lab-scale reactors shown that the use of a gas phase prepolymerization step enhanced polymerization activity by 30%. It was argued that prepolymerization avoids thermal deactivation during in the initial instants of reaction. A series of runs where the precatalyst was heated at different temperatures clearly demonstrated that overheating the catalyst leads to thermal deactivation.

In addition, a further, more significant enhancement of the polymerization rate was obtained when the catalyst was injected wet, i.e., suspended in mineral oil, than when it was injected dry. This was still the case even when thermal degradation was avoided through prepolymerization in both cases. Furthermore, the original shape of the precatalyst was only well replicated by the polymer wet-injected, while dry injection yielded in general a very bad morphology, either with or without prepolymerisation. Since morphology and activity are determined during catalyst fragmentation, which takes place during the first

instants of reaction, a stopped flow reactor was used to study primary overheating and morphology evolution. It is discovered that dry particles overheat more while wet particles show a steadier, slower increase of temperature. This is explained because the slower monomer diffusion in the oil blocked pores, and the better particle temperature control provided by oil. DSC analysis of the resulting polymers (both from stopped flow and semi-batch reactors) reveals that mineral oil provokes a decrease in crystallization temperature of iPP, as low as 70 °C. This absence of crystallinity during initial instants of life of the particles explains the better morphology observed by different patents and in ‘typical’ semibatch polymerizations when mineral oil is present. Another consequence is that the solubility of propylene is enhanced due to polymer swelling, a higher amorphous fraction and the co-solubility effect due to mineral oil. This provokes a further enhancement of the polymerization rate in the gas phase polymerization of propylene.

The third chapter is divided in two parts, since its goal is twofold. The first one is to investigate how different gas phase compositions affect kinetics and MWD during propylene homopolymerization. Thus, propylene was polymerized in the gas phase with a supported ZN catalyst. The composition of the gas phase has been systematically varied to investigate its influence on the experimentally measured reaction rates, which were fitted with a kinetic model. The monomer concentration in the polymer was calculated with the Sanchez–Lacombe Equation of State (SL EoS). In a propylene gas phase process, injection of heavier hydrocarbons leads to a more than twofold increase in the polymerization rate. This effect is quantified and attributed to the enhancement of the solubility of propylene in the active sites, caused by the co-solubility effect ascribed to the studied multicomponent gases/polymer mixture system. However, the relative concentration of hydrogen to propylene seems to be unaffected.

The second objective of the third chapter is to study the solubility of propylene, ethylene and ethylene/propylene mixtures in iPP, and how they diffuse into the polymer powder. Thus, the measured gas solubilities for propylene, ethylene, and propylene-ethylene equimolar mixtures in isotactic polypropylene (iPP) obtained with a high-pressure sorption balance at different temperatures and pressures are shown. The resulting experimental sorption isotherms of both binary systems (propylene-iPP and ethylene-iPP) were fitted with the Sanchez-Lacombe Equation of State (SL EoS). Fitted binary interaction parameters were suitable to predict the experimental solubility of the ternary system,

(ethylene/propylene equimolar mixtures in iPP) except for 50 °C where a small readjustment was needed. Diffusivities of the gases (individual or mixed) in iPP powders were also studied. For the desorption rates, the effective diffusion coefficient increases with pressure (or penetrant concentration in the polymer) and temperature. In the case of sorption experiments, diffusion of gas ethylene-propylene mixtures has always been lower as compared to both individual gases, which diffused into the polymer at similar rates.

In Chapter 4 several hiPP powders were made in the gas phase, initially keeping the iPP matrix constant. Conditions during copolymerization such as amount of copolymer, temperature, pressure, relative amount of ethylene to propylene and the presence of hydrogen were systematically varied to study their impact on the experimentally measured reaction rates, powders stickiness, chemical composition of the polymers, mechanical properties and powders morphology. Along with other discoveries, evidence for a resistance to the mass transfer of ethylene during copolymerization was found. To understand this phenomenon 4 selected hiPP samples were microtomed and analyzed by atomic microscopy techniques (AFM). 3 of them had equal iPP matrix but different copolymer compositions, in terms of ethylene/propylene ratios. Contrarily, the 4th sample had a singular iPP matrix with a smaller effective diffusion length, (obtained by varying the catalyst preparation method, as shown in Appendix B) but the same copolymer composition as one of the previous three samples. After cryo-microtomed, the hiPP samples were stored at -21°C to avoid rubber migration to the surface, preserving the original morphology. AFM analyses showed that all hiPP samples had less rubber in the center of meso-particles than in the edges, being this difference smaller for the sample with the singular iPP matrix. This suggests that mass transfer limitations for ethylene can occur in the center of meso-particles, fact also observed by other authors in the literature which worked with different ZN catalyst systems. However, it is shown how catalyst preparation method can significantly alter this predicted morphology development.

Finally, other investigations not fitting with the body of the thesis were also done. For instance, Appendix B depicts the importance that (1) precontacting the precatalyst and cocatalyst/External electron donor and (2) the hydrocarbon injected along the precatalyst have on the gas phase polymerization of propylene, in terms of activity and morphology. It was seen that when the precatalyst was not precontacted the overall activity of the polymerizations was higher, and that iPP matrix was composed of smaller meso-particles,

easing monomer diffusion, as compared to powders obtained when precontacting occurred. Finally, in appendix C it is investigated the incorporation of ethylene during semibatch copolymerization of hiPP in the smallest and biggest particle populations. It was seen that resistance to the diffusion of ethylene is more probable to happen in the bigger particles.

## 5.2 Perspectives

In Chapter 2 the impact of a gas phase prepolymerization over activity and morphology during the gas phase polymerization of propylene was studied. However, the effect of diverse kinds of prepolymerizations was not investigated, which would be of high industrial interest. A couple of examples are: (1) Atactic gas phase prepolymerization. Since the atactic fraction might help in catalyst fragmentation, an atactic gas phase prepolymerization can be done. To do so, the external electron donor can be injected right after prepolymerization. (2) 1-butene – propylene prepolymerization: The rubbery elastomer might also help in catalyst fragmentation. Once prepolymerization is finished 1-butene is evacuated and homopolymerization is continued with just propylene.

In Appendix B precatalyst precontacting with TEA/ELB before propylene feeding and the type of feed hydrocarbon injected along the precatalyst have been systematically varied to investigate their influence on the experimentally measured reaction rates and powders morphology. However, it would be of great interest to extend this investigation to dry injection gas phase and slurry phase polymerizations. It is expected that precontacting will have an enormous impact if the precatalyst is injected in a dry manner in the gas phase, and an insignificant one if the polymerization is done in slurry phase, over morphology and kinetics. This will probably show the protective role that liquid hydrocarbons play in morphology and kinetics of propylene homopolymerization. These differences might be reflected in the MWD of the distinct powders. In this context, another investigation of high concern would be the influence that precatalyst precontacting time with TEA/ELB before propylene feeding has on morphology and kinetics. In this work precontacting time was fixed in two 2 minutes. It is expected to obtain worse morphologies and lower activities with longer precontacting times.

In Chapter 2 evidence of heat transfer limitations during the initial moments of polymerization was found. The prediction of this experimental results with a model would be of great interest to fully understand catalyst fragmentation.

Chapter 2 showed that paraffinic oils are miscible with iPP in a wide concentration range and affect the crystallinity of the polymer significantly. It would be of high interest to further understand the effect that this feed oil has on the distinct aspects of crystallization and rheology of iPP-homopolymers.

In Chapter 3 the solubility and diffusivity of the ternary system ethylene/propylene in iPP are studied. A future investigation could include different ethylene/propylene ratios besides equimolar mixtures, such as 1:3 molar ratio ethylene propylene. This can elucidate how different gas phase compositions affect the copolymerization of hiPP. Extending this study to different mixed-gas getting sorbed into iPP is another possibility, for instance, linear alkanes (e.g., iso-butane or hexane) and propylene.

It can be noticed, if the proper calculations with the SL EoS are run, that temperature and pressure affect the molar solubility ratio of ethylene/propylene in iPP and hiPP. Therefore, it is reasonable to think that during the copolymerization of ethylene-propylene (2<sup>nd</sup> stage of hiPP production) this physical factor will play a key role in the comonomer incorporation and copolymer properties.

Typically, an ethylene-propylene rubber is used to toughen iPP. It would be useful to understand the effect that other elastomers, such as propylene-1-hexene or propylene-1-butene, would have over the final properties of hiPP.

AFM was a valuable tool to reveal differences in rubber distribution, as shown in Chapter 4. While the impact of different concentrations of ethylene in the gas phase composition and iPP morphology over the final rubber distribution was elucidated, extending the AFM analyses to the rest of the samples with a constant iPP matrix can further shed light on the relationship among copolymerization conditions and rubber distribution.



## A. Sanchez-Lacombe equation of state (SL EoS)

First, the Sanchez-Lacombe equation of state is briefly described. Then, an example of a vapor liquid system in equilibrium is solved step by step.

### A.1. Description of SL EoS model

SL EoS is one of the simplest statistical thermodynamics models able to describe the phase behaviour of monomer(s)/polymer binary and multicomponent systems. According to the original Sanchez and Lacombe publication,<sup>1</sup> for a determined system the equation of the state would be:

$$\bar{\rho}^2 + \bar{P} + \bar{T} \left[ \ln(1 - \bar{\rho}) + \left(1 - \frac{1}{r}\right) \bar{\rho} \right] = 0 \quad \text{A-1}$$

where  $\bar{\rho}$ ,  $\bar{P}$  and  $\bar{T}$  are the reduced density, the reduced pressure and the reduced temperature of a pure component, respectively. These reduced properties are related to the corresponding absolute properties as follows:

$$\bar{\rho} = \frac{\rho}{\rho^*}, \quad \bar{P} = \frac{P}{P^*}, \quad \bar{T} = \frac{T}{T^*} \quad \text{A-2}$$

$T$ ,  $P$ , and  $\rho$  are the absolute temperature (K), pressure (Pa), and density ( $\text{g}/\text{m}^3$ ).  $\rho^*$ ,  $P^*$  and  $T^*$  are the characteristic density, characteristic pressure, and characteristic temperature, respectively, for each pure component in the mixture. In the current thesis, they were taken from refs. [2,3]. They are used to obtain  $r$ , (the number of lattice sites a fluid molecule occupies in the lattice, adimensional),  $v^*$ , (the molar volume of those lattice sites, in  $\text{m}^3 \cdot \text{mol}^{-1}$ ), and  $\varepsilon^*$  (the interaction energy per mole in  $\text{J} \cdot \text{mol}^{-1}$ ) as follows:

$$\varepsilon^* = R \cdot T^*, \quad v^* = \frac{\varepsilon^*}{P^*}, \quad r = \frac{MW}{\rho^* \cdot v^*} \quad \text{A-3}$$

Where  $R$  is the universal gas constant ( $\text{J} \cdot \text{mol}^{-1} \cdot \text{K}^{-1}$ ) and  $MW$  is the molecular weight ( $\text{g}/\text{mol}$ ). Now is possible to calculate the reduced density, finding the possible solutions (maximum three, depending on the conditions) for Equation A-1. This can be done using a

non-linear algebraic equation solver (e.g., Solver from Excel). The correct solution will be that one that provides the minimal chemical potential for each component in the phase of interest. The chemical potential of each component present in one of the phases of the system (gas or liquid) is calculated as follows:

$$\begin{aligned} \mu_i = RT & \left[ \ln \phi_i + \left( 1 - \frac{r_i}{r_{mix}} \right) \right. \\ & + r_i \left[ -\bar{\rho}_{mix} \left[ \frac{2}{v_{mix}^*} \left( \sum_{j=1}^{N_c} \phi_j v_{ij}^* \varepsilon_{ij}^* - \varepsilon_{mix}^* \sum_{j=1}^{N_c} \phi_j v_{ij}^* \right) + \varepsilon_{mix}^* \right] \right. \\ & + r_i \left[ \frac{RT}{\bar{\rho}_{mix}} \left[ (1 - \bar{\rho}_{mix}) \ln(1 - \bar{\rho}_{mix}) + \frac{\bar{\rho}_{mix}}{r_i} \ln \bar{\rho}_{mix} \right] \right. \\ & \left. \left. \left. + \frac{P}{\bar{\rho}_{mix}} \left( 2 \sum_{j=1}^{N_c} \phi_j v_{ij}^* - v_{mix}^* \right) \right] \right] \right] \end{aligned} \quad A-4$$

Where  $\phi$  is the volume fraction of the  $i$ th and the  $j$ th component in the mixture. Therefore, the sum of all the components volume fractions is 1. Note that, when a single component is the only present in one phase  $\phi$  is 1, which tremendously simplifies Equation A-4.  $N_c$  denotes the number of components in the mixture.  $r_{mix}$ ,  $v_{mix}^*$ ,  $v_{ij}^*$  and  $\varepsilon_{mix}^*$  are calculated as follows:

$$v_{ij}^* = \frac{v_{ii}^* + v_{jj}^*}{2} (1 - n_{ij}), \quad v_{mix}^* = \sum_{i=1}^{N_c} \sum_{j=1}^{N_c} \phi_i \phi_j v_{ij}^*, \quad A-5$$

$$\varepsilon_{mix}^* = \frac{1}{v_{mix}^*} \sum_{i=1}^{N_c} \sum_{j=1}^{N_c} \phi_i \phi_j \left( (\varepsilon_{ii}^* \varepsilon_{jj}^*)^{0.5} (1 - k_{ij}) \right) v_{ij}^*, \quad \frac{1}{r_{mix}} = \sum_{j=1}^{N_c} \frac{\phi_j}{r_j}$$

where  $n_{ij}$  corrects the deviation from the arithmetic mean and  $k_{ij}$  is a mixture parameter that accounts for specific binary interactions between components  $i$  and  $j$ . In a vapor-liquid system at equilibrium (e.g., a closed bottle of a mixture of hexane isomers at room temperature, or the solubility experiments of ethylene-propylene in iPP done in Chapter 3) the chemical potential of each component should be equal in every phase

$$\mu_i^{liquid} = \mu_i^{gas} \quad A-6$$

However, because of its characteristic parameters the polymer (considered as a “liquid phase”) has a practically non-existent vapor pressure. Therefore, while gases are present in the gas and liquid phases, polymer is only present in the liquid one.

For a phase in equilibrium, closed packed molar volume of each component is related to the mass fraction of every component in the mixture as follows:

$$\phi_i = \frac{\omega_i}{\rho_i^* v_i^*} \left( \sum_{j=1}^{N_c} \frac{\omega_j}{\rho_j^* v_j^*} \right) \quad \text{A-7}$$

Where  $\omega_i$  is the mass fraction of component  $i$  in the mixture and in the phase of interest. All the properties of interest related to the sorption phenomena are consequently calculated from this parameter as explained in Appendix A from ref. [4].

Example shown in subsection A.2 explains the solution methodology for a vapor-liquid system at equilibrium with SL EoS. Once this example is understood, reader should easily solve binary and ternary polymer systems composed of a gas phase (single or mixed gases) and a liquid phase (amorphous polymer plus the dissolved gases within).

## A.2. Example: Solution methodology for a vapor-liquid system at equilibrium with SL-EoS

**Example.** Consider a closed vapor-liquid system at equilibrium where the gas phase is composed of an equimolar mixture of n-hexane and n-heptane. Determine the exact molar composition of the liquid phase with SL EoS.  $T=373.15$  K,  $P = 1.57$  bar.  $k_{ij}$  and  $n_{ij}$  are considered 0.

**Table A.1.** Molecular weight and Characteristic parameters for n-hexane and n-heptane taken from ref. [1]

Component	1 (n-hexane)	2 (n-heptane)
MW (g/mol)	86.18	100
$T^*$ (K)	476	487
$P^*$ (Pa)	294000000	305000000
$\rho^*$ (g/m <sup>3</sup> )	775000	800000

### A.2.1. Gas phase

First, the mass fraction of both components is calculated for the gas phase, with the gas phase molar composition ( $x_i$ ) and the molar mass of every component, according to Equation A-8:

$$\omega_i = \frac{MW_i \cdot x_i}{\sum_{i=1}^{Nc} MW_i \cdot x_i} \quad \text{A-8}$$

With the molar mass fraction and equation A-7 the closed packed molar volume of each component is calculated. Then,  $r$ ,  $v^*$ , and  $\varepsilon^*$  are obtained for both single components, with Equation A-3. Characteristic parameters for hexane and heptane can be found in ref. [1]. Then,  $r_{mix}$ ,  $v^*_{mix}$  and  $\varepsilon^*_{mix}$  are found with the equations shown in A-5. Henceforward is possible to calculate  $\overline{P}$  and  $\overline{T}$  of the gas mixture, which included in Equation A-1 provide the reduced density of the gas mixture.

To obtain the reduced density a non-linear solver is needed. Please take in account that there are three possible solutions and two of them are correct, which correspond to gas and liquid phases, respectively. Thus, it is useful to estimate consequently the chemical potential of both components ( $\mu_{Hexane}^{gas}$   $\mu_{Heptane}^{gas}$ ) to identify the correct reduced density. The correct solution would be (1) the minimal (the greatest value corresponds to the liquid phase) and (2) the one of the two that minimize both  $\mu_{Hexane}^{gas}$  and  $\mu_{Heptane}^{gas}$ , correspondingly. The possible solutions of the reduced density are exemplarily shown in Figure A.1, extracted from the original publication of Sanchez and Lacombe. <sup>1</sup>

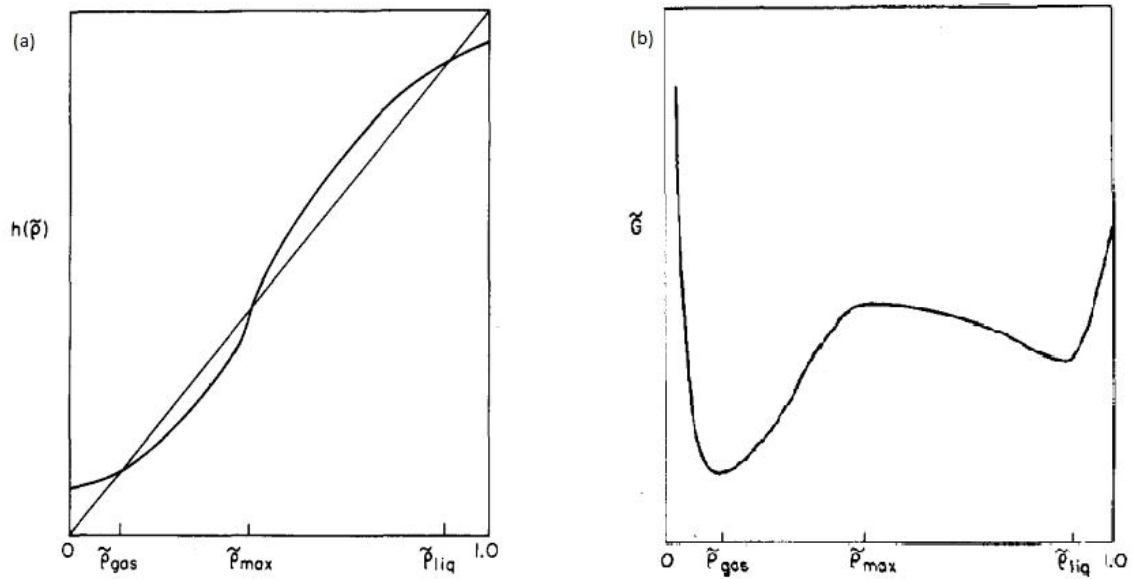


**Figure A.1.** (a) Schematic representation of the solutions of the SL EoS. Solutions at the lowest and highest values of reduced density correspond to minima in the Gibbs free energy (or in the chemical potential); the intermediate solution corresponds to a maximum. (b) Schema of the variation of the reduced Gibbs free energy (similar for the chemical potential), with reduced density at a pressure and temperature where a liquid phase is metastable with respect to the vapor phase. Adapted with permission from ref. <sup>1</sup> Copyright 2017 American Chemical Society.

In this example, the reduced density and chemical potential of each component present in the gas phase as calculated with SL EoS are:

$$\bar{\rho} = 0.00625, \quad \mu_{hexane}^{gas} = -40862.13 \text{ J} \cdot \text{mol}^{-1},$$

$$\mu_{heptane}^{gas} = -44120.95 \text{ J} \cdot \text{mol}^{-1} \quad \text{A-2}$$

While not necessary for the goal of this example, at this point is possible to calculate the density of the gas equimolar mixture. To do that  $\rho^*$  of the gas mixture is needed, and can be estimated as follows:

$$\rho_{gas\ mixture}^* = \frac{1}{\frac{\omega_{hexane}^{gas}}{\rho_{hexane}^*} + \frac{\omega_{heptane}^{gas}}{\rho_{heptane}^*}} \quad \text{A-3}$$

### A.2.2. Liquid phase

To solve the liquid phase, the inverse approach as taken for the gas phase should be done.

Starting from the known chemical potentials of both components (remember Equation A-6) the goal is to obtain  $\phi_{Hexane}^{liquid}$ . (Think of  $\phi_{Heptane}^{liquid} = 1 - \phi_{Hexane}^{liquid}$ ). The simultaneous solution of Equations A-1 and A-4 is done, where two unknowns are present: (a) the reduced density of the liquid phase ( $\bar{\rho}_{liquid}$ ) and (b) the closed packed molar volume ( $\phi_{Hexane}^{liquid}$ ) of n-hexane. Again, a non-linear solver is needed, and giving approximate initial guesses of both values is crucial for correctly solving the system of equations. Understanding the physical meaning of each parameter greatly helps in this process. As exposed in Figure A.1, a good range for  $\bar{\rho}_{liquid}$  initial guess is [0.6-1]. N-hexane is more volatile than n-heptane. If the gas phase composition is equimolar,  $\phi_{Hexane}^{liquid}$  should be smaller than  $\phi_{Heptane}^{liquid}$ . Therefore, a good starting point for  $\phi_{Hexane}^{liquid}$  would be 0.3.

After resolution of the system of equations by iteration, the values of the reduced density of the liquid mixture and the closed packed molar volume of n-hexane in the liquid mixture are:

$$\bar{\rho} = 0.759, \quad \phi_{hexane}^{liquid} = 0.283 \quad \text{A-4}$$

With these parameters, both mass fractions are deduced with Equation A-7. Then, through Equation A-8 molar fractions of every component in the liquid phase are subsequently obtained:

$$x_{n-hexane} = 0.3106, \quad x_{n-heptane} = 0.6893 \quad \text{A-5}$$

### A.3. References

1. Sanchez, I. C. & Lacombe, R. H. An elementary molecular theory of classical fluids. Pure fluids. *J. Phys. Chem.* **80**, 2352–2362 (1976).
2. Kanellopoulos, V., Mouratides, D., Pladis, P. & Kiparissides, C. Prediction of Solubility of  $\alpha$ -Olefins in Polyolefins Using a Combined Equation of StateMolecular Dynamics Approach. *Ind. Eng. Chem. Res.* **45**, 5870–5878 (2006).
3. Sato, Y., Yurugi, M., Yamabiki, T., Takishima, S. & Masuoka, H. Solubility of propylene in semicrystalline polypropylene. *J. Appl. Polym. Sci.* **79**, 1134–1143 (2001).

4. Alizadeh, A. Study of sorption, heat and mass transfer during condensed mode operation of gas phase ethylene polymerization on supported catalyst. (Université Claude Bernard-Lyon I; Queen's university at Kingston, 2014).



## B. Impact of Precatalyst and Cocatalyst/External Electron Donor Precontacting in the Gas Phase Polymerization of Propylene

*This appendix will be submitted for publication:*

Cancelas, A. J., Monteil, V. & McKenna, T. F. L. Impact of Precatalyst and Cocatalyst/External Electron Donor Precontacting in the Gas Phase Polymerization of Propylene. To be submitted. (2017).

### B.1. Introduction

In addition to a precatalyst, Ziegler-Natta catalyst systems for propylene polymerization comprise an organo-aluminum compound as co-catalyst and an external electron-donor (EED). The way in which the precatalyst, the co-catalyst, the EED and the monomer are brought into contact can have some importance. For instance, if the three components of the catalyst system are added to the reactor in the presence of propylene without being previously mixed (or precontacted), the initial phase of the polymerization (and catalyst activation) will be different than if the components are premixed then fed to the reactor. Industrially, some process employ precontacting (e.g. Borstar and Spheripol)<sup>1,2</sup> and others do not (e.g. Innovene, Unipol PP).<sup>3</sup> At the risk of oversimplifying, it appears that the catalyst components are not precontacted in major gas phase iPP processes, but are in the case of slurry processes. Given the results in the Chapter 2 (Figure 2.14, Page 53), where we demonstrated that overheating during the initial instants of polymerization can indeed be a problem in gas phase systems, it is possible that this choice of feeding the components separately in gas phase reactors allows the users to control the initial rate of polymerization, thereby avoiding overheating.

The very few studies dealing with the importance of precontacting the catalyst components in the literature suggest that it is of profound significance in terms of catalyst kinetics. Tan *et al.*<sup>4</sup> observed that the polymerization reaction rate curves with and without catalyst precontacting are similar in shape, but that overall the activity was higher with precontacting than it was without precontacting. On the other hand, in terms of morphology, Raisi *et al.*<sup>5</sup> did not observe any difference between powders obtained with and without catalyst pre-contact.

This study presents a series of experiments of the gas phase polymerization of propylene in a stirred bed reactor using a Ziegler-Natta catalyst that is added to the reactor in different

manners. The influence of precontacting and precatalyst suspension (mineral oil/heptane) on reaction kinetics and polymer morphology was systematically studied for an industrial Ziegler-Natta catalyst.

## B.2. Experimental Conditions

### B.2.1. Chemicals

In this work precatalyst “A” as described in the experimental section of Chapter 2 (Page 36), was used. Rest of chemicals used in this section are essentially the same and therefore, the relevant details can be found there.

### B.2.2. Semi-batch Polymerization

The experimental set-up and gas propylene homopolymerization conditions used in this Appendix are the same as those described in Chapter 4. However, an additional slurry precatalyst suspension (in addition that done with feed oil) was prepared with heptane (60mg/mL). Injection of the catalyst formulation was done either under propylene (no precontacting) or argon (precontacting), as illustrated in Figure B.1. If precontacting was done, TEA/ELB and precatalyst were stirred in the gas phase during 2 min, and then propylene was injected.

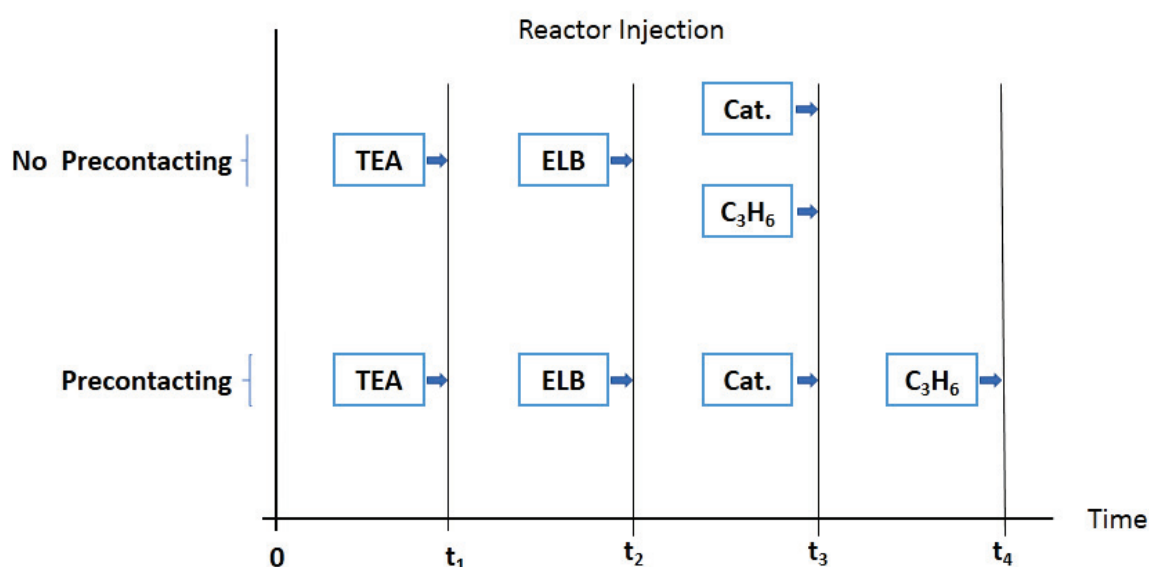
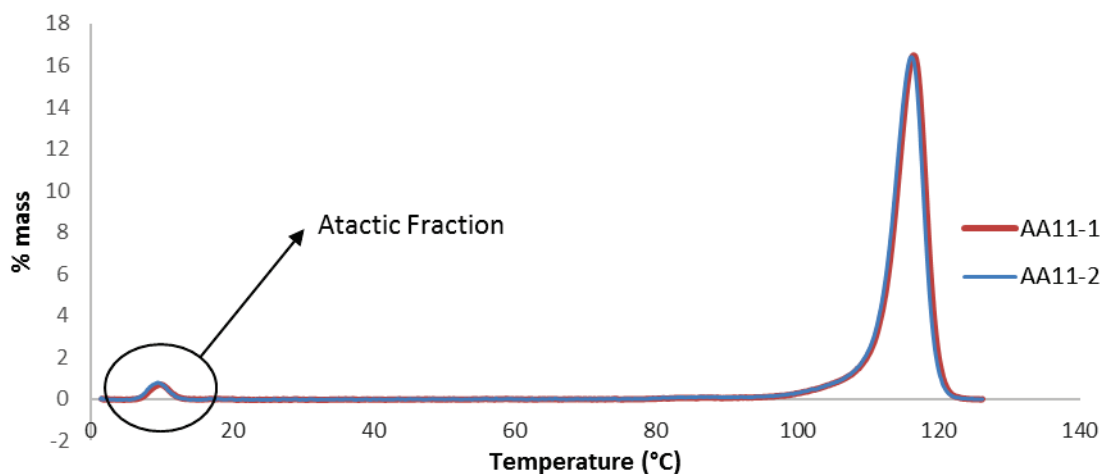


Figure B.1. Schematic illustration of precontacting procedure

### B.2.3. Polymer Characterization

Sorption rates of propylene in 1-2 grams of isotactic polypropylene (iPP) particles were measured in the sorption magnetic balance described in Chapter 3 (Figure 3.5) at 50 °C and 11 bar of propylene pressure.

Crystallization Elution Fractionation (CEF) analysis were performed using a TGIC/CEF Polymer Char instrument. Samples were dissolved in TCB at a concentration of 2 mg·mL<sup>-1</sup> during 60 minutes at 160 °C. 200 μL of the sample solution were loaded in the column at high temperature (150°C). Then a cooling ramp was applied at a rate of 2.0 °C·min<sup>-1</sup>, with a crystallization flow of 0.05 mL·min<sup>-1</sup>. After the crystallization step, an elution flow was applied at 1.00 mL·min<sup>-1</sup>, and the temperature was increased up to 130 °C via a heating ramp of 4.0 °C·min<sup>-1</sup>. Eluted fractions were analysed with a dual integrated infrared IR5 MCT spectrometer coupled to a viscometer detector to measure the chemical composition distribution (CCD). Atacticity was estimated from the area of the eluted fraction at ~8 °C. An example of the differential elution for sample A11 along with its atacticity estimation is shown in Figure B.22.



**Figure B.2.** CEF profile: Differential eluted fraction of an iPP sample (AA11) in function of temperature.

The bulk density was determined by weighing a known volume of loosely packed polypropylene powder. A recipient with a precisely known volume was filled with a known mass of polymer powder. Filling was done pouring the powder through a metallic funnel to avoid electrostatic charges, which could impact the measurement. The bulk density is indicated in grams of polymer per milliliter volume, and every measurement was repeated

at least twice.

### B.3. Results and Discussion

#### B.3.1. Kinetic Study

Table B.1 shows the polymerizations done in this study, along with the determined kinetic parameters. These were determined fitting the described kinetic model in Chapter 2 (Equation 2.1) by minimizing the deviations between the experimental and model curves. Activation constant  $K_a$  was not shown since the first period of the activity profile curves are affected by prepolymerization. Monomer concentration in the amorphous polypropylene was considered to 95 g/L, based on the data of Sato *et al.*<sup>6</sup> data. Every polymerization run was done twice, to ensure reproducibility of kinetics and morphology. Finally, to ensure that the particles were of a similar degree of growth, and thus comparable in terms of the development of morphology for the sorption studies and bulk density, all of the principle runs were designed to attain a productivity of 10 Kg/g.

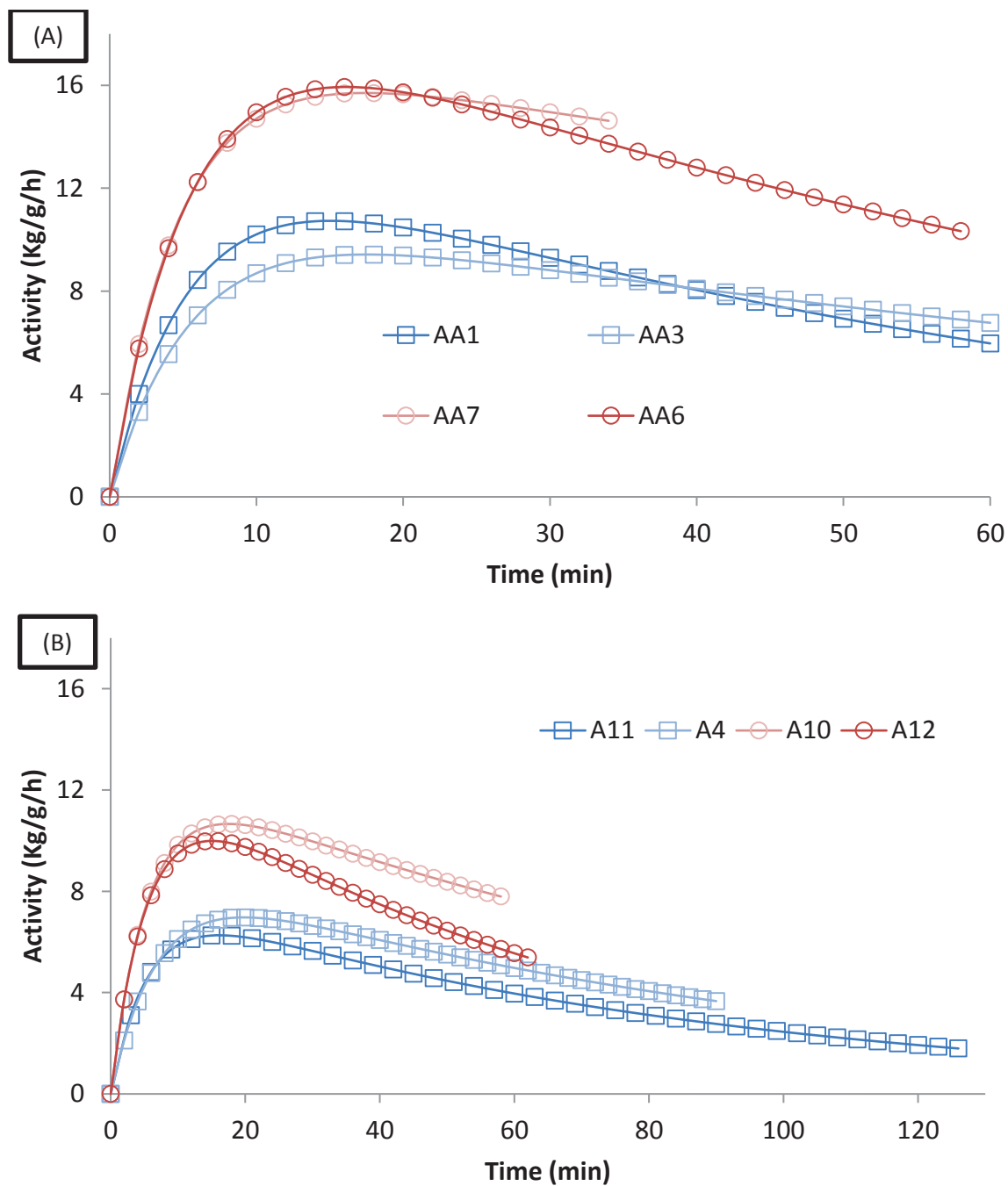


Figure B.3. Kinetic curves of propylene homo-polymerization with precontacting (blue) and without (red) for precatalyst injected suspended in mineral oil (A) and heptane (B).

**Table B.1.** Propylene homopolymerization conditions and resulting kinetic parameters <sup>a</sup>

Run	Precontacting	Wet Suspension	$k_p \cdot C_0$ (L·gcat <sup>-1</sup> h <sup>-1</sup> )	$k_d 10^4$ (s <sup>-1</sup> )	Productivity (Kg/g)
AA4	Yes	Heptane	90	1,7	9
AA11	Yes	Heptane	80	2	9,5
AA3	Yes	Oil	116	1,5	10
AA1	Yes	Oil	140	2,5	10
AA10	No	Heptane	131	1,5	10,2
AA12	No	Heptane	132	2,5	10,5
AA7	No	Oil	183	1	9,2
AA6	No	Oil	203	2	12,7

<sup>a</sup> All gas phase polymerizations were done at 20 bar of propylene with 2% of H<sub>2</sub> at 70 °C

The results shown in Table B.1 and Figure B.3, suggest 2 very clear conclusions. First, a greater activity is observed when the precatalyst was injected in mineral oil than when it was injected with heptane, independently of whether or not the components were precontacted. It is possible that an enhanced co-solubility effect due to the higher molecular weight of the mineral oil (its properties can be consulted in ref. [7] or Chapter 2 (Table 2.1) of this thesis), as compared to that of heptane can explain this observation. In addition, the plasticisation of the nascent PP will be more persistent, thereby enhancing diffusion to the active sites. Finally, the oil has a much higher boiling point than heptane, which will evaporate rapidly if the particles heat up slightly.

Secondly, avoiding the precontact of the catalyst components lead to a highly activity and greater productivity in the gas phase systems. This can be seen in the estimated values of  $k_p \cdot C_0$ . On the other hand, precontact of the catalyst components did not seem to have a noticeable impact on the deactivation rate, as  $k_d$  appears similar for all experiments. These results are coherent with the sorption rates shown in the next section.

Figure B.4 shows that non-precontacted PP powders also were more active during copolymerization with ethylene when a two-step procedure was used to make high impact polypropylene. A faster activation during copolymerization was observed for the non-precontacted catalyst.

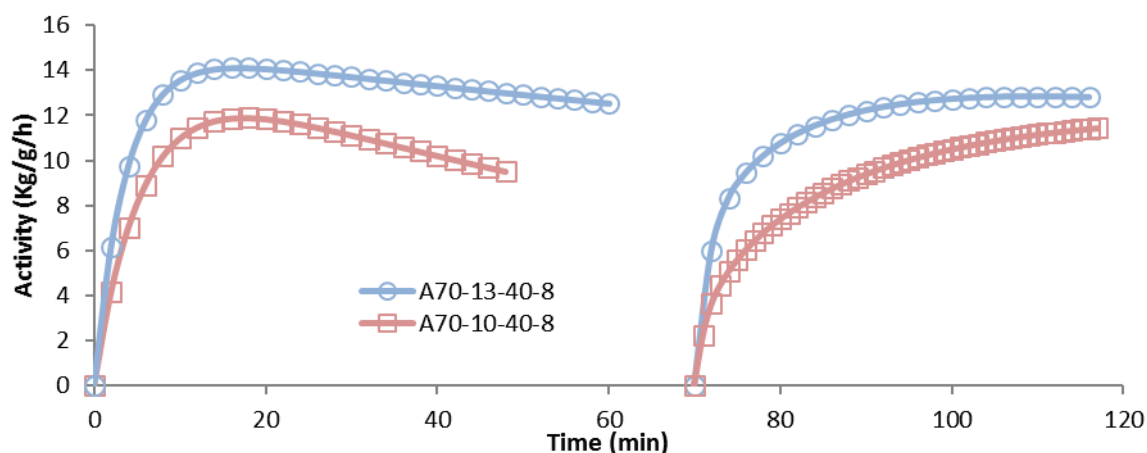


**Figure B.4.** Kinetic profiles of runs with/without catalyst precontacting, being A70-10-40-8 and A70-13-40-8, respectively. Left curves are resulting from homopolymerization and right ones from copolymerization.

### B.3.2. Sorption measurements

Sorption measurements were done in samples A11 (heptane and precatalyst slurry injection + precontacting), A3 (oil slurry injection + precontacting), A10 (heptane slurry injection + no-precontacting) and sample A6 (oil slurry injection + no-precontacting). Empirical values for the diffusion coefficients for propylene in polypropylene powder at 50 °C and 11 bar were determined in Chapter 3 (Page 102), and found to be  $3.5 \cdot 10^{-11} \text{ m}^2/\text{s}$ . Since the material properties of the iPP produced in these experiments are comparable to those studied in Chapter 3 (Page 93), we can use the same diffusion coefficient in the analytical solution of the diffusion equation for spheres (Chapter 3, Equation 3.5, Page 102), to determine the effective diffusion length for the powders presented in this study. This effective diffusion length can be considered as the average radius of the clusters agglomeration that ultimately constitute the powders.

In Figure B.5 propylene mass transfer rate appears to be (slightly) faster in iPP powders where precontacting was not done, but does not appear to depend on whether the catalyst was injected in heptane or in mineral oil. As shown in Table B.2 the isotacticity (and therefore amorphous fraction) of the four powders was very similar, indicating that the differences in mass transfer rate can be solely attributed to the structure of the particles, and not to any differences in the value of the diffusivity (i.e. all powders have the same amount of amorphous material). Thus, a smaller effective length diffusion indicates that a powder is composed by smaller meso-particles (or clusters). For productivities of 10Kg/g, clusters size is around 200 when precontacting procedure was applied vs 175  $\mu\text{m}$  when it

was not. This difference is not very high certainly, and the limited population of samples makes it difficult to assess the statistical validity of these values, but the tendency is very clear. Also, as we shall see below, there appear to be other trends linked to the morphology that support the idea that precontacting can influence the structure of the particles.

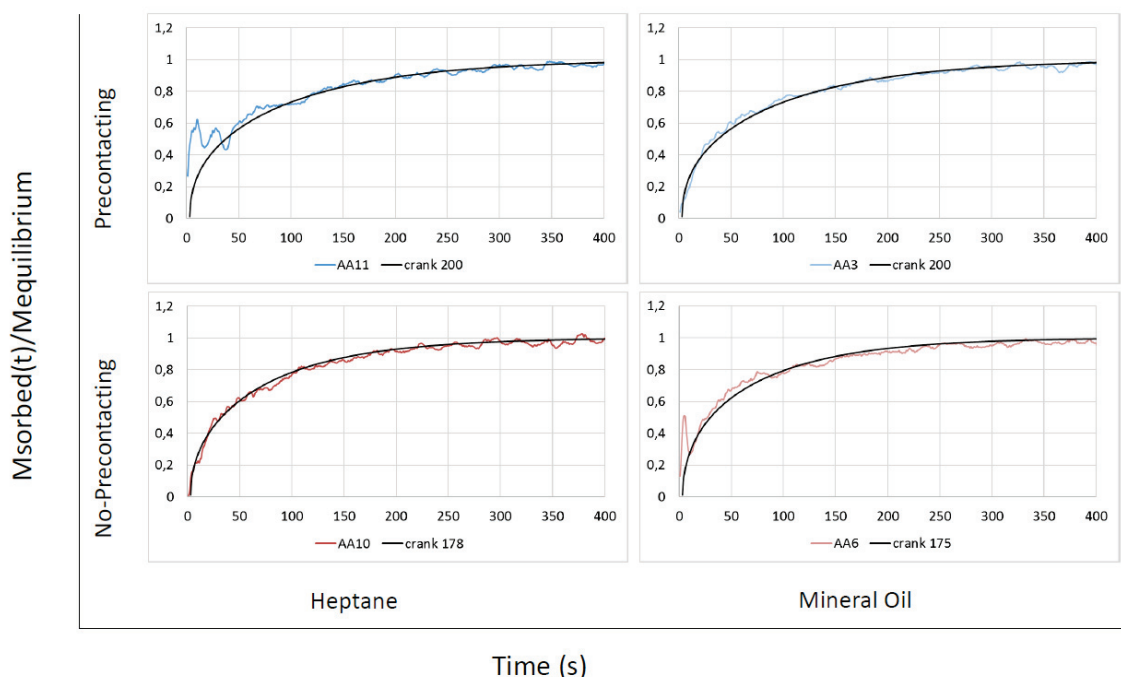


**Figure B.5.** Determination of clusters radii in four polypropylenes powders. All the sorption rates were done at 50 °C and 11 absolute bar of propylene in the sorption magnetic balance.

**Table B.2.** Determined clusters radii and atacticity of four iPP powders. <sup>a</sup>

Run	Precontacting	Wet Suspension	Clusters Radii (μm)	Atacticity	
				Average	Deviation
AA11	Yes	Heptane	200	2,42%	0,17%
AA3	Yes	Oil	200	2,36%	0,21%
AA10	No	Heptane	178	2,44%	0,27%
AA6	No	Oil	175	2,28%	0,19%

<sup>a</sup> Atacticity was determined by CEF, as explained in the experimental section.

Bulk density was measured for every powder, twice, always filling the known volume with a metallic funnel to avoid electric charges in the powder, which could affect the measurements. Results are shown in Figure B.6.

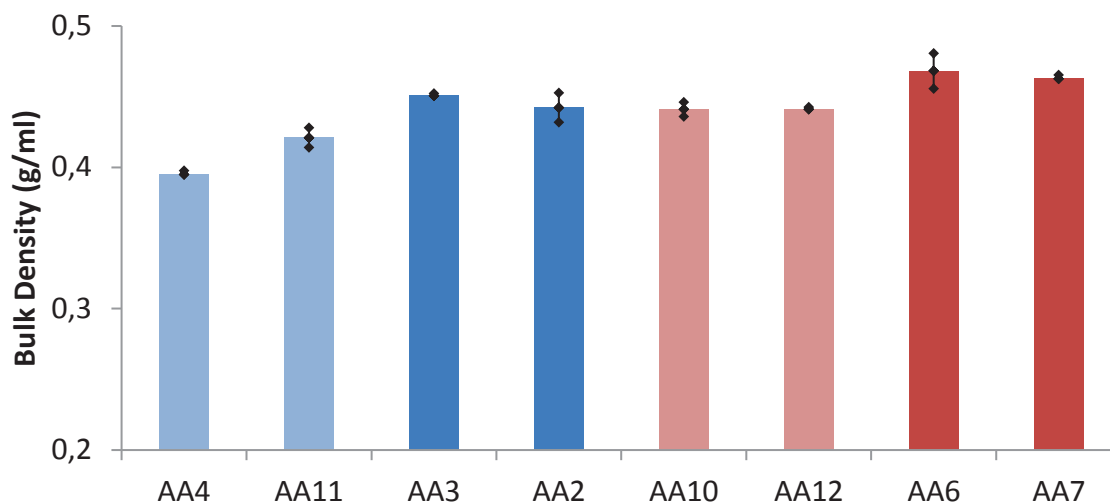


**Figure B.6.** Bulk density of the obtained powders from the runs shown in Table B.1.

Figure B.6 indicates that bulk density (BD) increased with the molecular weight of the feed hydrocarbon, and when there was no precontacting of the precatalyst with TEA/ELB. In addition, we see that higher BD results from powders that showed higher activities. As mentioned and demonstrated in Chapter 2, and by Pater et al.<sup>10</sup> in the literature, it is known that BD depends on the initial reaction rate. Higher initial reaction rates lead to lower activities, possibly due to thermal degradation of the catalyst, which lead to lower BD. This seems coherent with the observed outcomes in Figure B.3 and Figure B.6.

Scanning electron microscopy imaging of powders injected with mineral oil with and without precontacting was done. However, they were not found any significant differences in the external or internal morphology depending on precontacting procedure.

#### B.4. Conclusions

Propylene was polymerized in the gas phase with a supported Ziegler-Natta catalyst. Precatalyst precontacting with TEA/ELB before propylene feeding and the type of feed hydrocarbon injected along the precatalyst have been systematically varied to investigate their influence on the experimentally measured reaction rates and powders morphology.

When the precatalyst was not precontacted with TEA/ELB prior to injection in the reactor, the overall activity and productivity of the polymerizations were higher than when precontacting occurred. It is possible that a precontacted ZN catalyst has higher initial activity than a non-precontacted one, since all the “Ti” sites are already activated. Thus, the polymerization could start quickly as soon as the activated catalyst enters into contact with

propylene. However, when the precatalyst must mix with TEA and ELB before it can react, then the polymerization would start in a more gradual fashion. As a result, the temperature will increase more slowly during the initial instants in this second case. Since we have shown that thermal deactivation is important for PP catalyst activity, even at very short times it is likely that the slower activation during the first seconds or minutes of polymerization would be important in determining the long-term activity of the catalyst system. In addition, depending on the diffusion of TEA/ELB and propylene reaction start could even be much more delayed. In this context, it seems evident that mineral oil would offer more resistance to both, as compared to heptane (which will be rapidly vaporized due to its high vapor pressure).

The catalyst preparation method (like the injection method) also appears to have an impact on particle morphology in the sense that things that favour a slower immediate activation of the catalyst (even for a few seconds or minutes) lead to higher long-term activities and more compact iPP particles.

## B.5. References

1. Murzin, D. Y. *Chemical Reaction Technology*. (Walter de Gruyter GmbH & Co KG, 2015).
2. Cavalieri, C., Pantaleoni, R., Fujiishi, H. & Otsubo, A. Propylene-ethylene copolymers and process for their preparation. (2011).
3. Jezl, J. L. & Peters, E. F. Horizontal reactor for the vapor phase polymerization of monomers. (1978).
4. Tan, N., Yu, L., Tan, Z. & Mao, B. Kinetics of the propylene polymerization with prepolymerization at high temperature using Ziegler-Natta catalyst. *J. Appl. Polym. Sci.* **132**, (2015).
5. Bahareh Raisi. EFFECTS OF CATALYST PRE-CONTACT PROCEDURE ON KINETICS, PROPERTIES AND MORPHOLOGY OF PROPYLENE POLYMERIZATION. Available at: [http://www.civilica.com/Printable-ICHEC06\\_503=EFFECTS-OF-CATALYST-PRE-CONTACT-PROCEDURE-ON-KINETICS-PROPERTIES-AND-MORPHOLOGY-OF-PROPYLENE-](http://www.civilica.com/Printable-ICHEC06_503=EFFECTS-OF-CATALYST-PRE-CONTACT-PROCEDURE-ON-KINETICS-PROPERTIES-AND-MORPHOLOGY-OF-PROPYLENE-)

POLYMERIZATION.html. (Accessed: 24th October 2016)

6. Sato, Y. *et al.* Vapor–liquid equilibrium ratios for hexane at infinite dilution in ethylene+impact polypropylene copolymer and propylene+impact polypropylene copolymer. *Fluid Phase Equilibria* **170**, 49–67 (2000).
7. Primol 352. Available at: [http://www.exxonmobil.com/Denmark-English/Specialties/PDS/GLXXENSPCEMPrimol\\_352.aspx](http://www.exxonmobil.com/Denmark-English/Specialties/PDS/GLXXENSPCEMPrimol_352.aspx). (Accessed: 30th July 2015)
8. Bartke, M. *et al.* Sorption and Diffusion of Propylene and Ethylene in Heterophasic Polypropylene Copolymers. *Macromol. Symp.* **259**, 327–336 (2007).
9. Kröner, T. & Bartke, M. Sorption of Olefins in High Impact Polypropylene - Experimental Determination and Mass Transport Modeling: Sorption of Olefins in High Impact Polypropylene .... *Macromol. React. Eng.* **7**, 453–462 (2013).
10. Pater, J. T. M., Weickert, G. & Swaij, W. P. M. V. Polymerization of liquid propylene with a fourth-generation Ziegler–Natta catalyst: Influence of temperature, hydrogen, monomer concentration, and prepolymerization method on powder morphology. *J. Appl. Polym. Sci.* **87**, 1421–1435 (2003).
11. Yu, Y. Molecular Kinetics of Catalytic Olefin Polymerization: an Integrated Quenched-Flow and High-Temperature Cryoprobe NMR Approach. (2015).



## C. Mass Transfer Resistance to Ethylene in Very High Impact Polypropylene

### C.1. Introduction

In the second stage of hiPP production, a multicomponent mixture of ethylene, propylene, and iPP/hiPP coexists in the reactor. Since ethylene is the more reactive monomer, but its equilibrium gas solubility is very low, mass transfer restrictions are a probable intrinsic consequence, as explained in the introduction of this thesis. In the DPI project #711,<sup>1</sup> model-based analyses of reaction and mass-transfer revealed severe mass-transfer restrictions for ethylene. This is also further supported by the results shown in Chapter 4, where it was seen that rubber amount was less and with less ethylene in the center of the meso-particles (Figure 4.29).

On the other hand, different authors have observed that the diffusion coefficients of propylene and ethylene in polypropylene homopolymer increase with increasing polymer particle size.<sup>2-4</sup> If this is the case and mass transfer resistance to ethylene occurs, it seems logical to think that hiPP particles with assorted sizes will show differences in copolymer content (or rubber) and composition. In this work, a hiPP powder with 70% of RC was polymerized and then sieved into three fractions: <1mm, >1mm & <2mm, and >2mm. Difference scanning calorimetry (DSC) analyses were done to the biggest and smallest fractions.

### C.2. Experimental Section

#### C.2.1. Chemicals

Commercial fourth generation  $\text{MgCl}_2$  supported titanium Ziegler-Natta with titanium content of 2.0 wt% was used for polymerization. It is a different ZN precatalyst from “A” and “B” previously mentioned throughout this thesis. It had an average particle size of 55  $\mu\text{m}$ . Triethylaluminium (TEA, from Witco, Germany) and Dicyclopentyldimethoxysilane (DCPDMS) were used as cocatalyst and external electron donor, respectively. All heptane used was pre-treated on 3Å molecular sieves. Propylene and ethylene with minimum purity of 99.5 % and hydrogen with minimum purity of 99.99 % were purchased from Air Liquide (France). Propylene was purified with a three-stage system of columns before use: a first

one filled with BASF R3-16 catalyst (CuO on alumina), a second one filled with molecular sieves (13X, 3A, Sigma- Aldrich), and a last one filled with Selexsorb COS (Alcoa). Argon provided by Air Liquide, France, with minimum purity of 99.5 %, was used in order to keep the reaction free of oxygen.

### C.2.2. Semibatch Polymerisation Methods

Experimental set-up, homopolymerization and copolymerization were done exactly as described in Chapter 4 of this thesis, and reader is referred there for further information.

### C.2.3. Polymer Characterization

The DSC characterization of polymer samples was done as explained in Chapter 4 (Figure 4.5). SSA method was used.<sup>5,6</sup>

## C.3. Results and Discussion

### C.3.1. Resistance to the mass transfer of ethylene in very hiPP

The hiPP powder C70-10-70-8, shown in Chapter 4 (Table 4.3), had a 70% of copolymer content and it was sieved into three fractions: <1mm, >1mm & <2mm, and >2mm. Then, SSA fractionation, as explained in Chapter 4 (Figure 4.5), was performed to the smallest (<1mm) and the biggest (>2mm) sieved fractions. SSA fractionation is a practical way to determine differences in copolymer content, which may be caused by mass transfer limitations which in turn are dependent on particle size.

Furthermore, xylene solubles (XS) of the 2 particle populations was extracted and analyzed in DSC at different heating rates, as shown in Table C.1 and represented in Figure C.2.

It is observed how results from Table C.1 and Figure C.1 are consistent. Figure C.1 indicates that there was more ethylene propylene rubber (EPR) in smaller particles, since the crystallinity relative to iPP is lower. Besides of having more EPR or aEPC, its composition was different. These particles presented a EPR with a lower T<sub>g</sub>, which is a sign that had incorporated more ethylene. In conclusion, these results are consistent and suggest that smaller particles have a higher ability to incorporate ethylene.

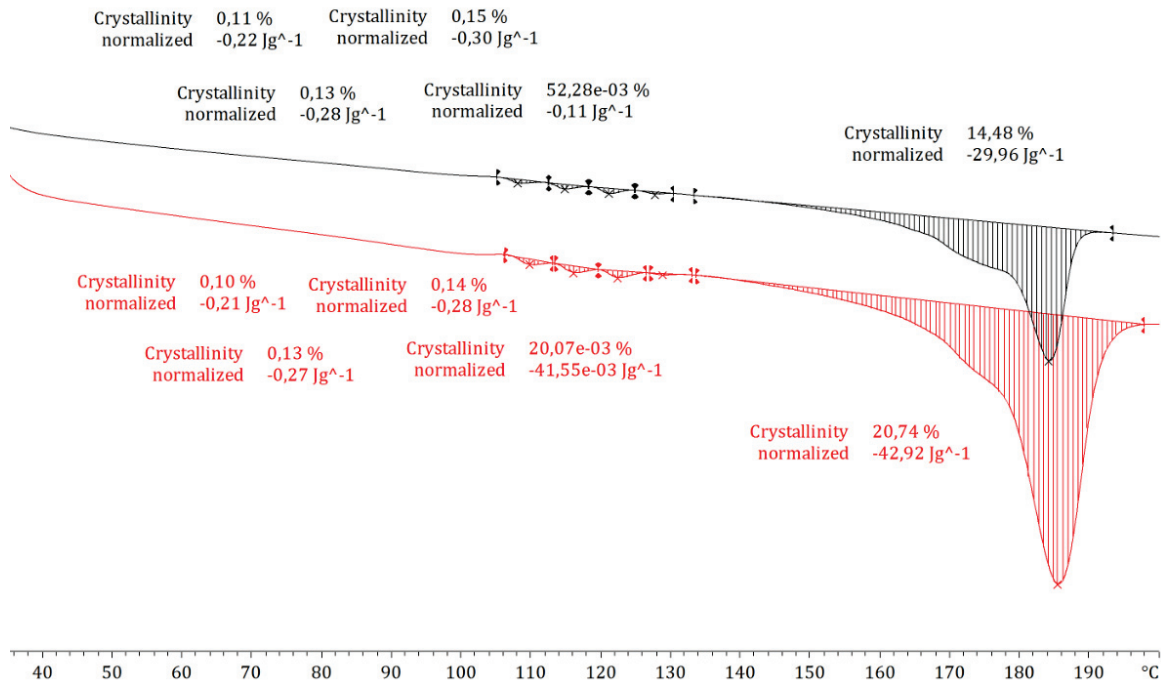


**Figure C.1.** DSC endotherms of two sieved fractions from C70-10-70-8 hiPP sample: >2mm (red) <1mm (black) after SSA treatment.

**Table C.1.** Temperature glass transition evaluated by DSC at different heating rates of the (XS) of hiPP particles smaller than 1mm sieve and bigger than 2mm sieve from run C70-10-70-8

Heating Speed °C/s	B70-10-70-8 MidPoint ISO			
	>2 mm		<1 mm	
	Tg	Deviation	Tg	Deviation
5	-45,4	0,1	-47,7	0,4
10	-40,8	1,0	-44,1	0,1
20	-40,3	0,1	-41,5	0,4

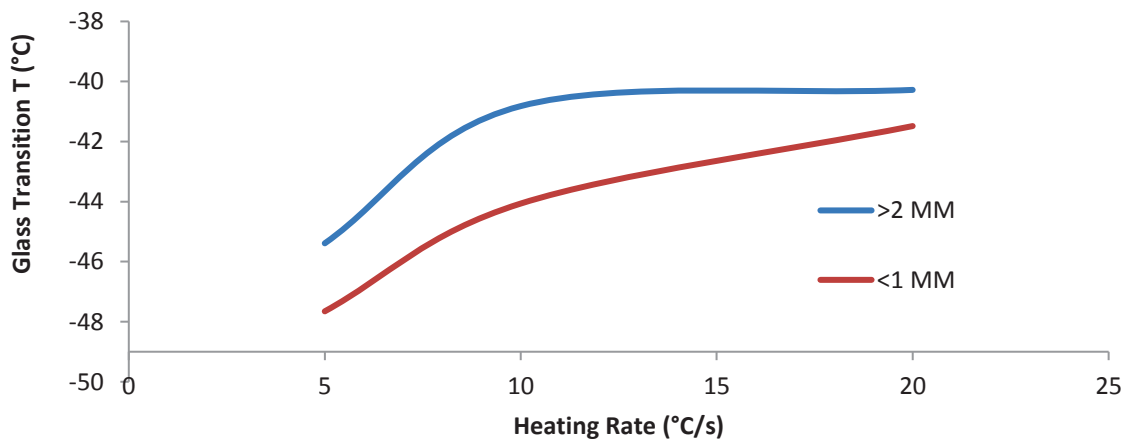


**Figure C.2.** Graphic representation of Table C.1.

**C.4. Conclusions**

A high impact polypropylene (hiPP) powder with 70% of copolymer content was made in

a 2.5L gas phase reactor with a supported Ziegler-Natta catalyst. Then it was sieved, and smallest (<1mm) and biggest (>2mm) fractions were analyzed by SSA method (as explained in Chapter 4). In addition, xylene solubles were extracted and analyzed by DSC to compare qualitatively which sieved fraction had more ethylene. Lower PP crystallinity and lower glass transition temperatures of the rubber phase were observed for the smaller sieved fraction. This indicates that there was more rubber in smaller particles which, in turn, had incorporated more ethylene during reaction in the rubber phase. These results suggest that mass transfer resistance to ethylene is more likely to occur in bigger particles.

### C.5. References

1. Kröner, T. *Mass Transport and Kinetics in the Heterophasic Copolymerization of Propylene*. (Mensch & Buch, 2014).
2. Patzlaff, M., Wittebrock, A. & Reichert, K.-H. Sorption studies of propylene in polypropylene. Diffusivity in polymer particles formed by different polymerization processes. *J. Appl. Polym. Sci.* **100**, 2642–2648 (2006).
3. Patzlaff, M., Wittebrock, A. & Reichert, K.-H. Sorption Studies of Propylene in Polypropylene Polymerized with Novel Ziegler-Natta-Catalysts in Liquid and Gas Phase. *Macromol. Symp.* **236**, 235–240 (2006).
4. Gonzalez, A., Eceolaza, S., Etxeberria, A. & Irui, J. J. Diffusivity of ethylene and propylene in atactic and isotactic polypropylene: Morphology effects and free-volume simulations. *J. Appl. Polym. Sci.* **104**, 3871–3878 (2007).
5. Müller, A. J. & Arnal, M. L. Thermal fractionation of polymers. *Prog. Polym. Sci.* **30**, 559–603 (2005).
6. Chen, J. *et al.* Controlled properties of high-impact polypropylene in-reactor alloys by tailoring chemical structure and morphology. *J. Polym. Res.* **22**, (2015).